

NELSON MANDELA METROPOLITAN UNIVERSITY

**CHARACTERISATION OF  
DISSIMILAR FRICTION STIR WELDS  
BETWEEN 5754 ALUMINIUM ALLOY  
AND C11000 COPPER**

---

**AKINLABI, Esther Titilayo**

## **COPYRIGHT STATEMENT**

The copy of this thesis has been supplied on condition that anyone who consults it is understood to recognise that its copyright rests with the Nelson Mandela Metropolitan University, and that no information derived from it may be published without the author's prior consent, unless correctly referenced.

***CHARACTERISATION OF DISSIMILAR FRICTION STIR  
WELDS BETWEEN 5754 ALUMINIUM ALLOY AND C11000  
COPPER***

A thesis submitted in compliance with the full requirements for the  
degree of

**Doctor Technologiae: Engineering: Mechanical**

Akinlabi, Esther Titilayo

Submitted to the

Faculty of Engineering,  
The Built Environment and Information Technology  
Nelson Mandela Metropolitan University  
Port Elizabeth,  
South Africa

December, 2010

Promoters

Prof. Annelize Els-Botes

Prof. Patrick McGrath

## **AUTHOR'S DECLARATION**

I, Akinlabi Esther Titilayo hereby declare that:

- The work done in this thesis is my own;
- All sources used or referred to have been documented and recognized; and
- This thesis has not been previously submitted in full or partial fulfilment of the requirements for an equivalent qualification at any other educational institution.



Author's Signature

Date: December, 2010

## **ACKNOWLEDGEMENT**

Unto the Lord be the glory, honour, and adoration for his infinite mercies and favour upon my life.

Sincere gratitude and appreciation goes to my promoter, Prof Annelize Els-Botes, for her guidance and support throughout the period of study. I am grateful to Prof Andre Venter of the Physics Department for his assistance with the electrical resistance measurements; Dr Ernst Ferg of the Chemistry Department for his assistance with the X-Ray Diffraction analysis; Dr Petersen Jacques for the statistical analysis; and Mr G. C. Erasmus for his assistance in the Metallurgy lab. In addition, I would like to express my appreciation to Dr T. Hua and Mr L. Von Wielligh for operating the Friction Stir Welding platform; and to members of the staff of the Mechanical Engineering workshop for their ceaseless support in the use of equipment. Furthermore, the input of the Head Of Department and my Co-Promoter - Prof P. J. McGrath, Director of Automotive Components Technology Station (ACTS) Prof D. G. Hattingh, and members of staff. These people are all noted and appreciated. Special thanks must go to Dr H. Lombard for her input at the preliminary stages of the research work, and to Dr S. Krishnan for her technical advice. I would also like to thank my fellow researchers – the currently registered Masters' and Doctoral students for their moral support.

Special gratitude also goes to my parents, Chief Dare Olorunfemi (1945-2006), who was a source of inspiration to me in my academic career. You encouraged me to be an engineer like you, I miss you dad. To my mum – Mrs Felicia Olorunfemi and my parents-in-law - Mr and Mrs S.O. Akinlabi, I say a big “Thank you”, for your support and prayers. Also, my appreciation goes to my uncle Barr J. F. Olorunfemi, my siblings and their spouses, - Dr and Mrs Gbenga Olorunfemi, Mr and Mrs Peter Oloba and Mr and Mrs Abraham Ilugbuhi- for their moral support.

As anticipated, my spiritual mentors Rev and Pastor Mrs Alfred Oladapo and Pastor and Mrs Kunle Oyeniyi of the Divine Grace Baptist Church Woji, Port Harcourt

Nigeria, and Pastors Vic and Lathicia Klackers of Church on the Way, Summerstrand. My humble thanks for your prayers and support.

I remain grateful to family friends – Dr and Mrs K. A. Olowu, Dr and Mrs A. A. Ogungbire, Dr and Mrs Oluwatobi Oluwafemi, Mr and Mrs F. A. Emuze, Prof and Dr (Mrs) A. A. Olufayo, Dr and Mrs P. A. Olubambi, Dr and Mrs Kutu, Engr and Mrs E. I. Obieje, Mr and Mrs D. R. Pienaar, Mr and Mrs Toba Dada, Mr and Mrs A. O. Aiyetan, Mr and Mrs A. B. Taiwo, Mr and Mrs E.A Taiwo, Mr and Mrs O.F. Inegbedion, Mr and Mrs A. Adelakun, Mr and Mrs R.A. Jimoh, Oluwole Olufayo, Bukola Makinwa, Seun Oshoniyi, Kayode Oyedemi, and Manka Kariuki for supporting me whenever the need has arisen.

I would like to thank the National Research Foundation (NRF) of South Africa, Research Capacity Development (RCD) unit and the Automotive Components Technology Station (ACTS) of NMMU for their financial support.

Finally, and most importantly, to the most significant adviser, supporter, and financier in my life, my love and husband, Mr Stephen Akinlabi, who is always there to encourage and shower me with love when the going gets tough. I sincerely appreciate you for all your financial support to enable me attend the 8<sup>th</sup> International Conference on Trends in Welding Research organized by ASM International at Georgia, the United States of America; between June 1-6, 2008; and the 8<sup>th</sup> International Friction Stir Welding Symposium organized by The Welding Institute (TWI) at Hamburg, Germany between May 18-20, 2010.

To my lovely kids - Stephen Akinkunmi and Stephanie Omolabake, I thank you for your understanding. From the very depth of my heart, I say that I am truly fortunate to have you, I am highly humbled by your co-operation; and you remain my pride and joy. I love you all.

# **ABSTRACT**

## ***Characterisation of Dissimilar Friction Stir Welds Between 5754 Aluminium Alloy and C11000 Copper***

Akinlabi, E.T.

Faculty of Engineering, the Built Environment and Information Technology

P.O. Box 77000, Nelson Mandela Metropolitan University,

Port Elizabeth, South Africa

December, 2010

Friction Stir Welding (FSW) is a solid state welding process invented and patented by The Welding Institute (TWI) in 1991, for joining ferrous and non-ferrous materials<sup>1</sup>. The FSW of Aluminium and its alloys has been commercialised; and recent interest is focused on joining dissimilar materials. However, in order to commercialise the process, research studies are required to characterise and establish process windows.

This research work through material characterisation of the welded joints establishes a process window for the Friction Stir welding of 5754 Aluminium Alloy and C11000 Copper. Furthermore, preliminary studies<sup>83,85</sup> on the FSW of aluminium and copper have revealed the presence of intermetallic compounds which are detrimental to the weld qualities. This research work is also aimed at establishing process parameters that will result in limited or no intermetallic formation in the weld. The joint integrity of the resulting welds will also be correlated with the input process parameters.

Based on the preliminary investigations conducted, a final weld matrix consisting of twenty seven welds was produced by varying the rotational speed between 600 and 1200 rpm, and the feed rate between 50 and 300 mm/min using three different shoulder diameter tools – 15, 18 and 25 mm to compare the heat input into the welds and to achieve the best results. The welds were characterised through microstructural evaluation, tensile testing, microhardness profiling, X-Ray Diffraction analysis, electrical resistivity and statistical analysis – in order to establish the inter-relationship between the process parameters and the weld qualities.

Microstructural evaluation of the weld samples revealed that the interfacial regions are characterised by mixture layers of aluminium and copper; while 33 % of the tensile samples are within the acceptable range (> 75 % joint efficiency). High Vickers microhardness values were measured at the joint interfaces, which corresponded with the intermetallic compounds. The Energy Dispersive Spectroscopy analysis revealed the presence of thin layers of intermetallics in nanoscale at the interfacial regions. The diffractograms of the X-Ray Diffraction analysis showed small peaks for intermetallics in some of the welds. Low electrical resistivities were measured at the joint interfaces. The statistical analysis showed that the downward vertical force, ( $F_z$ ) can significantly influence the resulting weld qualities.

An overall summary of the analysis of the weld qualities - with respect to the shoulder diameter tools employed showed that the 18 mm shoulder diameter tool is most appropriate among the three shoulder diameters considered, and a process window of medium spindle speed of 950 rpm and low-to-medium feed rate between 50 and 150 mm/min is established for FSW of Aluminium and Copper. Welds produced at 1200 rpm and 300 mm/min with low heat input did not have intermetallics formed at the joint interface.

# TABLE OF CONTENTS

Copyright Statement	ii
Author's Declaration	iv
Acknowledgement	v
Abstract	vii
Abbreviations	xiii
Nomenclature	xiv
List of Figures	xv
List of Tables	xxi
Glossary of Terms	xxiii
CHAPTER 1      INTRODUCTION	1
1.1      Introduction.....	1
1.2      Problem Statement.....	2
1.3      Aim.....	2
1.4      Objectives.....	3
1.5      The Hypothesis Statement.....	3
1.6      Research Methods.....	3
1.7      Delimitation.....	4
1.8      Significance of the Research.....	5
1.9      Project Layout.....	5
CHAPTER 2      FACTORS AFFECTING THE FRICTION STIR WELDING PROCESS	7
2.1      Introduction.....	7
2.1.1      Fusion welding.....	7
2.1.2      Solid-state welding.....	8
2.2      The FSW Process.....	9
2.3      FSW process parameters.....	12
2.3.1      Tool Design.....	12

2.3.1.1	Tool Pin.....	15
2.3.1.2	Tool shoulder .....	16
2.3.2	Welding Parameters.....	17
2.3.2.1	Feed rate and Rotational speed.....	17
2.3.2.2	Tool tilt angle.....	18
2.3.3	Joint Configuration .....	18
2.3.4	Forces acting on the tool during the FSW process.....	19
2.3.5	Heat input during the FSW process .....	21
2.4	Friction Stir Weld Microstructures .....	21
2.5	X-Ray Diffraction (XRD) Analysis of FSW Joints .....	23
2.6	Mechanical and electrical properties of FSW Joints .....	23
2.6.1	Defects.....	23
2.6.2	Grain Size and Microhardness.....	25
2.6.3	Tensile Properties .....	25
2.6.4	Electrical Properties .....	26
2.7	Weldability .....	27
2.7.1	Aluminium Alloys.....	27
2.7.2	Copper Alloys.....	28
2.7.3	Metallurgy of Aluminium-Copper system.....	28
2.8	Dissimilar metal joining .....	30
2.8.1	Friction Stir Welding of dissimilar materials.....	31
2.8.2	Friction Stir Welding of Aluminium Alloys and Copper .....	31
2.9	Summary .....	34

CHAPTER 3	EXPERIMENTAL TECHNIQUES AND TEST MATRIX	
DETERMINATION		36
3.1	Introduction.....	36
3.2	The FSW Platform .....	36
3.3	Backing plate and clamping system.....	37
3.4	The Welding Process.....	38
3.5	Tool designs for the FSW of Al / Cu.....	39

3.5.1	Initial weld .....	40
3.5.2	The use of Magnesium Oxide (MgO) as a refractory layer.....	42
3.6	The position of the work pieces during the FSW process .....	43
3.7	Optimisation of the FSW process parameters .....	44
3.7.1	Spindle speed .....	44
3.7.2	Traverse speed .....	45
3.7.3	Tool displacement .....	45
3.7.4	Dwell time.....	47
3.7.5	Tool tilt.....	47
3.7.6	Plunge depth.....	48
3.8	Final Weld Matrix.....	49
3.9	Parent Materials.....	50
3.9.1	Chemical analysis .....	51
3.9.2	Microstructure .....	51
3.10	Specimen Layout .....	51
3.11	Material Characterisation.....	53
3.11.1	Optical Microscopy .....	53
3.11.2	X-Ray Diffraction Analysis.....	53
3.11.3	Mechanical Characterisation.....	54
3.11.4	Electrical Resistivity Determination .....	55
3.12	Summary .....	55
 CHAPTER 4 RESULTS AND DISCUSSION		 57
4.1	Introduction.....	57
4.2	Inter-relationship between input and output FSW process parameters .....	57
4.3	Macro appearances of the welds.....	60
4.3.1	The effect of input process parameters on resulting macrostructures .....	60
4.3.2	Weld defects .....	63

4.3.3	FSW force feed back.....	66
4.4	Tensile Results .....	68
4.4.1	Tensile data of the welds.....	68
4.4.2	Percentage elongation data .....	73
4.4.3	Joint efficiency of the welds.....	77
4.4.4	Tensile fracture location characterisations .....	79
4.5	Microstructural evaluation.....	82
4.5.1	Weld microstructure zones.....	82
4.5.2	Grain size determination of microstructure zones .....	84
4.5.3	Scanning Electron Microscopy .....	86
4.5.4	Measurement of the thickness of intermetallic particles .....	88
4.6	Microhardness Profiling results of the welds.....	89
4.7	X-Ray Diffraction Analysis .....	93
4.8	Electrical Resistivity measurement .....	98
4.9	Statistical Analysis .....	101
4.9.1	Regression analysis.....	102
4.9.2	Analysis of scatter plots .....	104
4.9.3	Analysis of surface plots .....	106
4.10	Summary .....	113
CHAPTER 5 CONCLUSIONS AND FUTURE WORK		115
5.1	Introduction.....	115
5.1.1	Conclusions.....	116
6.1.1	Final Conclusions.....	119
5.2	Future work.....	120
REFERENCES		121
APPENDIX A		142
APPENDIX B		143
APPENDIX C		170
APPENDIX D – PUBLICATIONS		265

## ABBREVIATIONS

AA	- Aluminium Alloy
Al	- Aluminium
AS	- Advancing side
ASTM	- American Society for Testing and Materials
Cu	- Copper
EDS	- Energy Dispersive Spectroscopy
FSW	- Friction Stir Welding
FSWeld	- Friction stir weld
HAZ	- Heat Affected Zone
HRC	- Rockwell hardness
HV	- Vickers hardness
MPa	- Mega Pascal
mm/min	- Millimetre per minute
NMMU	- Nelson Mandela Metropolitan University
rpm	- Revolutions per minute
RS	- Retreating Side
SEM	- Scanning Electron Microscope
SiC	- Silicon Carbide
TMAZ	- Thermo-Mechanical Affected Zone
TWI	- The Welding Institute
UTS	- Ultimate Tensile Strength
WJE	- Weld Joint Efficiency
XRD	- X-Ray Diffraction

## NOMENCLATURE

$(F_x)$	- advancing force in the direction of welding (N).
$(F_y)$	- uniaxial force perpendicular to the $F_x$ during the welding process (N).
$(F_z)$	- vertical downward force on the tool (N).
$Q$	- heat input (J/min).
$\eta$	- efficiency factor.
$\omega$	- rotational speed (rev/min).
$T$	- torque (Nm).
$f$	- feedrate (mm/min).
$\phi$	- diameter.

# LIST OF FIGURES

## CHAPTER 1

Figure 1.1: Flow diagram of project activities .....	5
--	---

## CHAPTER 2

Figure 2.1: Schematic diagram of the Friction Stir Welding process <sup>25</sup> .....	10
Figure 2.2: Joint configurations for Friction Stir Welding: (a) Square butt, (b) Edge butt, (c) T-Butt joint, (d) Lap joint, (e) Multiple lap joint, (f) T-Lap joint, and (g) Fillet joint <sup>25</sup> .....	19
Figure 2.3: Typical force feedback plot of vertical downward force ( $F_z$ ) with respect to time.....	20
Figure 2.4: Typical FS weld of aluminium showing microstructural zones <sup>82</sup> .....	22
Figure 2.5: Weld defects in FSW <sup>22</sup> .....	24
Figure 2.6: The Aluminium-Copper (Al-Cu) Binary phase diagram <sup>114</sup> .....	29

## CHAPTER 3

Figure 3.1: The I-Stir PDS FSW Platform .....	36
Figure 3.2: The backing plate and clamping system.....	37
Figure 3.3: Bead-on-Plate (a) AA (b) Cu .....	40
Figure 3.4: First trial FSW of Al / Cu produced at 800 rpm and 100 mm/min .....	41
Figure 3.5: FSW Al / Cu with tool design 'A' at (a) 950 rpm and 100 mm/min (b) 1200 rpm and 100 mm/min .....	41

Figure 3.6: FSW Al/Cu with tool design B at (a) 800 rpm and 100 mm/min (b) 1200 rpm and 100 mm/min .....	41
Figure 3.7: FSW Al/Cu with tool design 'C' at (a) 800 rpm and 100 mm/min (b) 1200 rpm and 100 mm/min (c) 950 rpm and 100 mm/in (d) 950 rpm and 300 mm/min .....	42
Figure 3.8: Joint interface of FSW Al / Cu produced at 1200 rpm and 150 mm/min and EDS analysis result .....	43
Figure 3.9: FSW Al/Cu at 600 rpm and 150 mm/min (a) Cu on the advancing side (b) Cu on the retreating Side .....	44
Figure 3.10: Welds produced at 1200 rpm and 150 mm/min with the tool pin plunged in (a) Cu (b) at centreline (c) in AA .....	46
Figure 3.11: Macro and micro-graphs of welds produced at 1200 rpm and 150 mm/min with the tool pin plunged in (a) and (d) Cu, (b) and (e) at centreline (c) and (f) in AA .....	46
Figure 3.12: Welds produced at 950 rpm and 100 mm/min with (a) 1° tool tilt (b) 2° tool tilt (c) 3° tool tilt .....	48
Figure 3.13: Shoulder plunge in FSW <sup>23</sup> .....	48
Figure 3.14: Research test coupon .....	50
Figure 3.15: Microstructure of the parent materials (a) 5754 AA and (b) C11000 Cu .....	51
Figure 3.16: Layout of specimens .....	52
Figure 3.17 Circuit diagram of the electrical resistance measurement .....	55

## CHAPTER 4

Figure 4.2 (a): Macro appearance of weld produced with the 15 mm shoulder diameter tool at 950 rpm and 50 mm/min .....	60
--	----

Figure 4.2 (b): Macro appearance of weld produced with the 18mm shoulder diameter tool at 950 rpm and 50 mm/min .....	61
Figure 4.2 (c): Macro appearance of weld produced with the 25mm shoulder diameter tool at 950 rpm and 50 mm/min .....	61
Figure 4.3: Macro appearance of weld produced with the 18mm shoulder diameter tool at 950 rpm and 300 mm/min .....	62
Figure 4.4: Macro appearance of weld produced with the 18 mm shoulder diameter tool at 950 rpm and 50 mm/min .....	62
Figure 4.5: Macro appearance of weld produced with the 18mm shoulder diameter tool at 600 rpm and 50 mm/min .....	62
Figure 4.6 (a): Macro appearance of weld produced with the 15mm shoulder diameter tool at 600 rpm and 50 mm/min with a wormhole defect .....	64
Figure 4.6 (b): Macro appearance of weld produced with the 15mm shoulder diameter tool at 950 rpm and 300 mm/min showing root defect.....	64
Figure 4.7 (a): Force feedback plot for weld produced at 950 rpm and 50 mm/min with 18mm shoulder diameter tool (Figure 4.4 shows the macro appearance through the cross section of the weld) .....	67
Figure 4.7 (b): Force feedback plot for weld produced at 1200 rpm and 150 mm/min with 25 mm shoulder diameter tool (Macro appearance is shown in Appendix C1, Figure h (S25_08, p.167)).....	67
Figure 4.8: Tensile behaviour of FSW Al / Cu produced at 950 rpm and 50 mm/min .....	70

Figure 4.9 (a): Average UTS versus Weld Pitch of all the welds produced with the 15 mm shoulder diameter tool.....	71
Figure 4.9 (b): Average UTS versus Weld Pitch of all the welds produced with the 18 mm shoulder diameter tool.....	72
Figure 4.9 (c): Average UTS versus Weld Pitch of all the welds produced with the 25 mm shoulder diameter tool.....	73
Figure 4.10 (a): Average % Elongation versus Weld Pitch of all the welds produced with the 15 mm shoulder diameter tool.....	76
Figure 4.10 (b): Average % Elongation versus Weld Pitch of all the welds produced with the 18 mm shoulder diameter tool.....	76
Figure 4.10 (c): Average % Elongation versus Weld Pitch of all the welds produced with the 25 mm shoulder diameter tool.....	77
Figure 4.11: Photo montage of fracture location of weld produced at 950 rpm and 300 mm/min with the 18 mm shoulder $\phi$ due to weld defect.....	80
Figure 4.13 (a) to (e): Typical Microstructures of the various weld zones.....	83
Figure 4.14: Average grain sizes of the PM and microstructure zones .....	86
Figure 4.15 (a): Joint interface of S15_02 produced at 600 rpm and 150 mm/min with 15 mm shoulder diameter tool.....	87
Figure 4.15 (b): Joint interface of S18_04 (produced at 950 rpm and 50 mm/min with 18 mm shoulder diameter tool.....	87

Figure 4.15 (c): Joint interface of S25_01 produced at 600 rpm and 50 mm/min shoulder diameter tool.....	88
Figure 4.16: Measurements of the thicknesses of intermetallics.....	89
Figure 4.17: Typical microhardness profile of FS weld of aluminium .....	90
Figure 4.18 (a): Microhardness profiles of welds produced at a constant spindle speed of 950 rpm with the 15 mm $\phi$ .....	91
Figure 4.18 (b): Microhardness profiles of welds produced at a constant spindle speed of 950 rpm with the 18 mm $\phi$ .....	91
Figure 4.18 (c): Microhardness profiles of welds produced at a constant spindle speed of 950 rpm with the 25 mm $\phi$ .....	92
Figure 4.19: Microhardness indentations at the interfacial region of S18_04 produced at 950 rpm and 50 mm/min .....	93
Figure 4.20: PDF Diffractogram of Al and Cu up to 55 $2\theta$ .....	94
Figure 4.21: PDF Diffractogram of a weld produced with the 15 mm shoulder diameter tool at 950 rpm and 150 mm/min .....	97
Figure 4.22: PDF Diffractogram of S15_09 produced at 1200 rpm and 300 mm/min.....	98
Figure 4.23 (a): Electrical Resistivity versus Heat input of welds produced at constant rotational speed with the 15 mm shoulder diameter tool .....	100
Figure 4.23 (b): Electrical Resistivity versus Heat input of welds produced at constant rotational speed with the 18 mm shoulder diameter tool .....	100

Figure 4.23 (c): Electrical Resistivity versus Heat input of welds produced at constant rotational speed with the 25 mm shoulder diameter tool .....	101
Figure 4.24 (a): Scatter plot of percentage elongation versus maximum force for all the welds .....	105
Figure 4.24 (b): Scatter plot of Electrical resistivity versus heat input for all the welds .....	105
Figure 4.25 (a): Surface plot relating horizontal force ( $F_x$ ), spindle speed and feed rate for all the welds.....	107
Figure 4.25 (b): Surface plot relating horizontal force $F_y$ , spindle speed and feed rate for all the welds.....	108
Figure 4.25 (c): Surface plot relating vertical force ( $F_z$ ), spindle speed and feed rate for all the welds.....	109
Figure 4.25 (d): Surface plot relating torque ( $T$ ), spindle speed and feed rate for all the welds .....	110
Figure 4.25 (e): Surface plot relating heat input, spindle speed and feed rate for all the welds .....	111
Figure 4.25 (f): Surface plot relating UTS, spindle speed and feed rate for all the welds.....	112
Figure 4.25 (g): Surface plot relating percentage elongation, spindle speed and feed rate for all the welds.....	113

# LIST OF TABLES

## CHAPTER 2

Table 2.1: Benefits of the FSW process <sup>24</sup> .....	12
Table 2.2: A selection of tools designed at TWI <sup>57</sup> .....	14
Table 2.3: Al-Cu Intermetallic Phases and their Properties <sup>114-</sup> 119 .....	30

## CHAPTER 3

Table 3.1: FSW Tool designs, dimensions and features .....	39
Table 3.2: FSW tool designs, dimensions and features.....	42
Table 3.3: Final weld matrix using the 15, 18 and 25 mm shoulder diameter tools .....	50
Table 3.4: Tensile test results of the parent materials .....	54

## CHAPTER 4

Table 4.1: Input process parameters of the welds.....	58
Table 4.2: FSW output data obtained .....	59
Table 4.3: Data obtained for microstructure zones .....	63
Table 4.4: Weld defects characterisation of welds produced with the 15, 18 and 25 mm shoulder diameter tool .....	65
Table 4.5 (a): Tensile test results of the welds produced with 15 mm shoulder diameter tool .....	69
Table 4.5 (b): Tensile test results of the welds produced with the 18 mm shoulder diameter tool .....	69
Table 4.5 (c): Tensile test results of the welds produced with the 25 mm shoulder diameter tool .....	70
Table 4.6 (a): Percentage Elongation data of the parent materials .....	73

Table 4.6 (b): Percentage Elongation data of the welds produced with the 15 mm shoulder diameter tool .....	74
Table 4.6 (c): Percentage Elongation data of the welds produced with the 18 mm shoulder diameter tool .....	74
Table 4.6 (d): Percentage Elongation data of the welds produced with the 25 mm shoulder diameter tool .....	75
Table 4.7 (a): Weld Joint Efficiency ( $\eta$ ) of welds produced with the 15 mm shoulder diameter tool .....	78
Table 4.7 (b): Welded Joint Efficiency ( $\eta$ ) of welds produced with the 18 mm shoulder diameter tool .....	78
Table 4.7 (c): Weld Joint Efficiency ( $\eta$ ) of welds produced with the 25 mm shoulder diameter tool .....	79
Table 4.8: Fracture location characterization of the tensile samples .....	79
Table 4.9: Average grain size determination for Al microstructure zones .....	84
Table 4.10: Average grain size determination for Cu microstructure zones .....	85
Table 4.11: Percentage decrease in grain size of microstructure zones .....	85
Table 4.12: EDS analysis of representative weld samples .....	88
Table 4.13: Peaks, intermetallic compounds and the estimated heat input into the welds.....	95
Table 4.14: Peaks and the corresponding intermetallic compounds of aluminium and copper .....	96
Table 4.15: Summary of joint electrical resistivity and heat input into the welds .....	99

## GLOSSARY OF TERMS

### A

- **Advancing side** – the advancing side is the side of the weld where the local direction of the rotating tool is in the same direction of traverse.
- **Alloy** – A substance having metallic properties and being composed of two or more chemical elements, of which at least one is a metal.
- **Alloying element** – An element added to and remaining in metal, which changes its structure and properties.
- **Arc Welding** -A group of welding processes wherein coalescence or complete fusion is produced by heating with an electric arc.

### B

- **Backing plate** – A layer of material that is placed below the joint interfaces of the materials to be welded. It provides a surface to oppose the vertical downward force on the material, and protects the machine bed.
- **Body Centred Cube**-The body centred cube unit is a cube with an atom at each corner of the unit cell, and an atom in the centre of the unit cell.
- **Breaking load** – the load at which fracture occurs.
- **Brittleness** – the tendency of a material to fracture without first undergoing significant plastic deformation.
- **Brittle fracture** – rapid fracture preceded by little or no plastic deformation.
- **Butt weld** – A welded joint formed between the squared ends of the two joining pieces, which come together but do not overlap.

### C

- **Clamping System** – the device used to hold, locate and prevent the work piece from moving during the large forces involved in the FSW process.
- **Coalescence** –the merging of two or more materials (metals) into one.

## D

- **Defect** - A discontinuity or discontinuities that accumulate to render a weld or part unable to meet minimum acceptance standards or criteria of the design specifications.
- **Deformation** – is a change in the form of a body due to stress, thermal, or other causes.
- **Diffraction** – the scattering of electrons by any crystalline material, through discrete angles depending only on the lattice spacing of the material and the velocity of the electrons.
- **Ductility** – the ability of a material to deform plastically before fracture.
- **Dwell time** – the period of time after the rotating tool has been plunged into the work and for which it remains stationary, generating frictional heat and plasticizing the materials, before commencing the traverse along the joint (seconds).

## E

- **Elastic region** – a material is said to be stressed within the elastic region when the working stress does not exceed the elastic limit.
- **Elastic deformation** – is the deformation of the material that is recovered when force is applied.
- **Elastic limit** – the greatest stress which a material is capable of sustaining without any permanent strain remaining upon complete release of the stress.
- **Elongation** – the increase in gauge length of a body subjected to a tension force, referenced to a gauge length of a body. Usually expressed as a percentage of the original gauge length.
- **% Elongation** – the total percent increase in the gauge length of a specimen after a tensile test.
- **Engineering strain** – this is a dimensionless value that is the change in length ( $\Delta L$ ) per unit length of the original linear dimension ( $L_0$ ) along the loading axis of the specimen; that is  $e = \Delta L / L_0$  the amount that a material deforms per unit length in a tensile test.

- **Engineering stress** – it is the normal stress, expressed in units of applied force,  $F$ , per unit of original cross-sectional area,  $A_0$ ; that is,  $S = F/A_0$ .
- **Equilibrium** – a state of dynamic balance between the opposing actions, reactions, or velocities of a reversible process.
- **Etchant** – a chemical solution used to etch a metal to reveal structural details.
- **Etching** – subjecting the surface of a metal to preferential chemical or electrolytic attack to reveal structural details for metallographic examination.
- **Extrusion** – the process where a material is shaped by force or squeezed through a die or nozzle.
- **Exit hole** – a hole left at the end of the weld when the FSW tool is withdrawn, resulting from displacement of material during the plunge. Some special techniques are in-use to fill or prevent the occurrence of this hole.

## F

- **Face Centred Cube**- this is a crystal system where atoms are arranged at the corners and centre of each cube face of the cell.
- **Filler Metal** - Metal added in making a welded, brazed, or soldered joint.
- **Force control** – a mode in the Friction Stir Welding process in which a known force from previous welds is added to other input process parameters to produce a weld.
- **Fusion** – the melting together of filler metal and base metal, or of base metal only, which results in coalescence.
- **Fusion welding** – any welding process that uses fusion of the base metal to make the weld.
- **Friction** – the force required to cause one body in contact with another to begin to move.
- **Friction Stir Welding** – Is a process developed at The Welding Institute (TWI) that utilizes local friction heating to produce continuous solid-state seams. It allows butt and lap joints to be made without the use of filler metals. The solid-state low distortion welds produced are achieved with relatively low costs, using simple and energy-efficient mechanical equipment.

## G

- **Grain** – an individual crystallite in metals.
- **Grain growth** – this is a phenomenon which occurs when the temperature of a metal is raised, the grains begin to grow and their size may eventually exceed the original grain size.
- **Grain size** – a measure of the areas or volumes of grains in a polycrystalline metal or alloy, usually expressed as an average when the individual sizes are fairly uniform. Grain size is reported in terms of number of grains per unit area or volume, average diameter, or as a number derived from area measurements.
- **Grain boundary** –an interface separating two grains, where the orientation of the lattice changes from that of one grain to that of the other. When the orientation change is very small, the boundary is sometimes referred to as a sub-boundary structure.
- **Grinding** – removing material from the surface of a work piece by using a grinding wheel or abrasive grinding papers.

## H

- **Hardness** –a term used for describing the resistance of a material to plastic deformation.
- **Hardness test** – measures the resistance of a material to penetration by a sharp object.
- **Hardening** – increasing hardness by suitable treatment.
- **Heat-Affected Zone** - The portion of the base metal which has not been melted, but whose mechanical properties have been altered by the heat of welding or cutting.
- **Homogeneous** – a chemical composition and physical state of any physical small portion, and that is the same as that of any other portion.
- **Hot working** – deformation under conditions that result in recrystallization.

## I

- **Indentation hardness** – this is the hardness, as evaluated from the measurements of an area of an indentation made by pressing a specified indenter into the surface of a material under specified static loading conditions.
- **Intensity** (X-rays) – the energy per unit time of a beam per unit area perpendicular to the direction of propagation.
- **Interfacial region** –weld joint boundary of the workpieces indicating the positions of the pin and shoulder diameters during the welding process.
- **Intermetallic compounds** –this are any solid materials, composed of two or more metal atoms in a definite proportion, which have a definite structure which differs from those of its constituent metals.

## J

- **Joint efficiency** - The ratio of the strength of a joint to the strength of the base metal, expressed as a percentage.

## L

- **Lap Joint** - A welded joint in which two overlapping metal parts are joined by means of a fillet, plug or slot weld.

## M

- **Macrograph** –a graphic reproduction of a prepared surface of a specimen at a magnification not exceeding 25x.
- **Macrostructure** – the structure of metals as revealed by macroscopic examination of the etched surface of a polished specimen.
- **Magnification** – the ratio of the length of a line in the image plane to the length of a line on the imaged material.
- **Material Test Report (MTR)** - A document on which the material manufacturer records the results of test examinations or treatments required by the material specification.

- **Mechanical properties** – the properties of a material that reveal its elastic or inelastic behaviour when force is applied, indicating the suitable mechanical applications.
- **Mechanical testing** – the determination of mechanical properties.
- **Metallurgy** – The science and technology of metals and their alloys including methods of extraction and use.
- **Microstructure** – The structure of a prepared surface of a metal, as revealed by a microscope at a particular magnification.

## O

- **Onion-skin flow pattern** – a characteristic weld pattern featuring a cyclic ring or onion skin-like profile.
- **Oxidation** – the addition of oxygen to a compound.

## P

- **Parameter** – The minimum and maximum parameters that will describe the operating range of a variable.
- **Parent material** – this is the sheet-metal plate in its as manufactured form, as supplied.
- **Plastic deformation** –this is the distortion of material continuously and permanently in any direction. The deformation that remains or will remain permanent after the release of the stress that caused it.
- **Plasticity**– capacity of a metal to deform non-elastically without rupturing.
- **Polished surface** – a surface that reflects a large proportion of the incident light in a peculiar manner.
- **Position control** – a mode in FSW in which the machine automatically adjusts the forces acting during the welding process.
- **Plunge depth** – the plunge depth is the maximum depth that the tool shoulder penetrates into the weld plates.
- **Plunge force** – during the plunging stage of the tool pin in FSW, the vertical force in the direction of the Z-axis movement is normally referred to as the plunging force.

- **Porosity** - A rounded or elongated cavity formed by gas entrapment during cool-down or solidification.

## R

- **Recrystallization** – a change from one crystal structure to another, such as that occurring upon heating and / or cooling through a critical temperature.
- **Residual stress** – stress in a body which is at rest, in equilibrium, and at uniform temperature in the absence of any external force.
- **Retreating side** – the retreating side of the tool is where the local direction of the weld surface due to tool rotation and the direction of the traverse are in the opposite direction.
- **Rolling direction** – refers to the direction in which the billet was rolled during the sheet-metal plate manufacture.
- **Rotational speed** – the tool rotation speed is the rate of angular rotation (usually specified in rpm) of the tool about its rotational axis.

## S

- **Scanning Electron Microscope** – an electron microscope in which the image is formed by a beam operating simultaneously with an electron probe scanning the object.
- **Side flash** – in FSW, a build-up of weld material, normally on the retreating side of the rotating tool, which has a ‘peel-like’ effect; this is termed side flash.
- **Solid-phase** – A physically homogeneous and distinct portion of a material system in the solid state.
- **Spindle speed** – also referred to as the rotational speed, is the speed of the work holding device (chuck), measured in revolutions per minute.
- **Spindle torque** – the spindle torque required to rotate the FSW tool when plunging into and traversing through the work piece along the joint (Nm).

## T

- **Tensile strength** – the maximum tensile stress which a material is capable of sustaining. Tensile strength is calculated from the maximum load during a tension test carried out to rupture, and the original cross-sectional area of the specimen.
- **Tensile test** – measures the response of a material to a slowly applied axial force. The yield strength, tensile strength, modulus of elasticity and ductility are obtained.
- **Tool displacement**- to offset the tool at a certain distance from the weld centre line.
- **Tool shoulder** – part of the welding tool which rotates and is normally disk-shaped.
- **Tool pin** – the part of the tool that rotates in contact with the surface of the work piece.
- **Tool plunge** – the process of forcing the tool into the material at the start of the weld.
- **Tool tilt angle** – the angle at which the FSW tool is positioned relative to the work piece surface; that is, zero tilt tools are positioned perpendicular to the work piece surface (degrees).
- **Traverse speed** – also referred to as feed rate; it is the speed at which the rotating FSW tool is translated along the joint line (mm/min).

## V

- **Vickers hardness number** – a number related to the applied load and the surface area of the permanent impression made by a square-based pyramid diamond indenter.
- **Void** – the space that exist between particles or grains. Normally in welding, voids are associated with defects.

## U

- **Unaffected material** – the bulk of material which is not affected by either heat or deformation during the welding process.

## **W**

- **Welding** – the process of joining, in which materials are enabled to form metallurgical bonds under the combined action of heat and pressure.
- **Weld nugget or stir zone** – the recrystallized central area of the joint interface.
- **Weld root** – the part of the joint profile opposite the shoulder is designated the root of the weld.
- **Welding speed** – also known as the traverse speed; this is the speed (usually specified in mm/min) of the tool traversing along the work piece per specified time.
- **Work piece** – the component to be welded.
- **Worm holes** – a defect in a FS weld, usually on the advancing side of the rotating tool, due to lack of mixing and re-bonding of the plasticized material.

## **X**

- **x-axis** – relating to a specific axis (horizontal) or a fixed line determining the direction of movement or placement in a 2-Dimensional or 3-Dimensional co-ordinate system.

## **Y**

- **y-axis** – relating to a specific axis (perpendicular to x-axis) or a fixed line determining the direction of movement or placement in a 2-D or 3-D co-ordinate system.

## **Z**

- **z-axis** – relating to a specific axis (vertical) or a fixed line determining the direction of movement or placement in a 3-D co-ordinate system.

## CHAPTER 1 INTRODUCTION

### 1.1 Introduction

Friction Stir Welding (FSW) is a solid–state joining technique invented and patented by The Welding Institute (TWI) in 1991 for butt and lap welding of ferrous and non–ferrous metals and plastics<sup>1</sup>. Since its invention, the process has been continually improved and its scope of application expanded.

FSW is a continuous process that involves plunging a portion of a specially shaped rotating tool between the butting faces of the joint. The relative motion between the tool and the substrate generates frictional heat that creates a plasticised region around the immersed portion of the tool. The shoulder prevents the plasticised material from being expelled from the weld. The tool is moved relatively along the joint line, forcing the plasticised material to coalesce behind the tool to form a solid–phase joint<sup>1</sup>.

The benefits of this technology include: low distortion, greater weld strength compared to the fusion welding process, little or no porosity, no filler metals, little or no post-weld repair, no solidification cracking, no welding fumes or gases, improved corrosion resistance, and lower cost in production applications<sup>2-5</sup>. Because of the many demonstrated advantages of FSW over fusion welding techniques, the commercialisation of FSW is proceeding at a rapid pace. In fact, it is currently being applied in production activities that involve both large and small-scale products<sup>5</sup>.

Furthermore, most of the work done to bring FSW to production applications has not only been practical in nature, but has also been driven primarily by the pressing need of industries. However, the information generated through previous work is often hidden from the public for proprietary reasons. FSW of low melting temperature materials, such as aluminium and its alloys, and other similar material joining have now been commercialised in the aerospace, marine, and transportation industries<sup>6-10</sup> and in recent years, considerable interest has been generated in joining dissimilar materials<sup>11-16</sup>.

The need for joints between dissimilar materials often arises in industrial applications which are experiencing complex loading conditions. This provides the platform for the need / or the availability of a sound joining technique for dissimilar materials, because of the requirements, such as light weight and high performance. High quality joints between

Aluminium (Al) and Copper (Cu) will promote the use of such joints in industrial applications especially in the field of electrical components. Aluminium (Al) and Copper (Cu) are widely applied in engineering structures due to their unique properties, such as high electric conductivity, heat conductivity, corrosion resistance and mechanical properties<sup>17</sup>. Al and Cu are used in the production of bus-bars.

A bus-bar is an electrical conductor that makes a common connection between several circuits; and it is found in the interconnection of the incoming and outgoing transmission lines and transformers at an electrical substation. Bus-bars are also used to connect generators and the main transformers in a power plant<sup>17-18</sup>. However, due to the inherently different chemical, mechanical and thermal properties of the materials being joined, a dissimilar joining process presents more challenges than a similar materials joining process.

## 1.2 Problem Statement

Aluminium and Copper are difficult to weld with conventional welding processes because of their high affinity for each other; and they are not very soluble in one another in the solid state. Currently, a typical joint between Aluminium and Copper, like bus-bars, is made with the use of mechanical fasteners. It is expected that if FSW is used, it will give better contact, better current flow, less resistance, and thereby save energy. Conserving energy is a global issue and every effort geared towards it is worthwhile, especially with respect to climate change and from global warming perspectives.

Attempts to join both metals through solid-state processes have resulted in the formation of hard and brittle intermetallic phases at the joint interface. These intermetallic phases lead to cracks during and/or after welding, lower the toughness of the weld, and increase the resistivity of the joint<sup>16</sup>.

## 1.3 Aim

The aim of this research work is to successfully join 5754 Aluminium Alloy (AA) and commercially pure Copper (Cu), by using the FSW process. Weld quality and joint integrity will be quantified through metallurgical evaluation, mechanical testing, X-Ray Diffraction analysis and electrical resistance measurements. The main focus will be on producing welds with limited or no intermetallics at certain parameter combinations.

## 1.4 Objectives

The research objectives include:

- Carry out a study on FSW to be used as a process for joining dissimilar metals.
- Establish the properties of the materials used in the research work; material evaluations will be conducted on each of the parent materials. These will include:
  - Chemical analysis
  - Microstructure, and
  - Microhardness
- Design and develop an appropriate FSW tool with features and dimensions suitable to weld 3.175 mm thick plates.
- Carry out analyses and material characterisation on the welded samples. These analyses will include microstructural evaluation, X-ray diffraction analysis, tensile testing, microhardness profiling and electrical resistivity - in order to establish a process window for the FSW of Al / Cu.

## 1.5 The Hypothesis Statement

It is envisaged that material characterisation used in this study will determine optimum process parameters to join 5754 Aluminium Alloy and C11000 Copper using FSW. During FSW, it is expected that the risk of segregation and formation of excessive brittle intermetallic phases will be significantly reduced due to the high cooling rates and lower fusion temperature.

## 1.6 Research Methods

The base materials to be used in the research work are 5754AA and C11000 Cu of dimensions 600 mm x 120 mm x 3.175 mm and the type of joint considered is a butt joint.

The research procedure is as follows:

A comprehensive literature survey was conducted to gain insight relative to the FSW process. The literature survey entails information including tool materials and the geometry to FS weld alloys of Al and Cu; the availability of the parent materials and the experimental equipment needed to effectively carry out the characterisation of the weld properties. All these issues were considered.

After the survey of the related literature, attention was given to the actual experimental set-up. This includes preliminary laboratory tests on the parent material - Al and Cu, microstructure, and microhardness. The research work was conducted on the actual FSW of the weld coupons and the weld analysis, as well as the characterisation thereof.

Many FSW process parameters are variables and they influence each other during the process; only the rotational speed and the feedrate will be varied, as these parameters are known to greatly influence the heat input during the welding process<sup>19-20</sup>. A series of preliminary welds were produced to determine the optimum weld settings used for the final test matrix.

The rationale behind the methodology used in analysing and characterising the welded samples is as follows:

- Microstructural evaluation was conducted to determine precipitate formation, intermetallic compounds and the level of mixing in the welded samples.
- X-Ray Diffraction analysis was carried out to identify the intermetallic phases at the joint interfaces.
- Microhardness profiling – this is an important physical-mechanical characteristic that governs the wear resistance of materials. Microhardness profiling in this research was used to characterise the formation of precipitates in the weld. It was also used to characterise the hardness of the different weld zones.
- Tensile testing was conducted to measure and compare the strength and ductility of the welded samples to the base material (weld joint efficiency).
- Electrical resistivity measurements were carried out to compare the electrical resistance of the friction stir welded sample to the average joint resistance of the base materials.

All the mechanical and electrical tests and the metallographic sample preparations were done in accordance to ASTM standards.

## 1.7 Delimitation

The research project will only focus on joining 5754 Aluminium Alloy and commercially pure Copper. In addition, only plates of 3.175 mm thickness of both metals will be used at the experimental stage. The welds will be produced using the position control on the FSW platform and no temperature studies will be considered.

## 1.8 Significance of the Research

The importance of the study is multi-faceted. In the academic context, the study will expand on the research undertakings relative to the FSW of dissimilar materials at the Nelson Mandela Metropolitan University. And in terms of its significance to other applications, FSW of 5754 Aluminium Alloy and C11000 Copper will expand the industrial application of FSW within the South African manufacturing industries - especially in the field of electrical engineering.

## 1.9 Project Layout

The flow diagram of the project activities is presented in Figure 1.1.

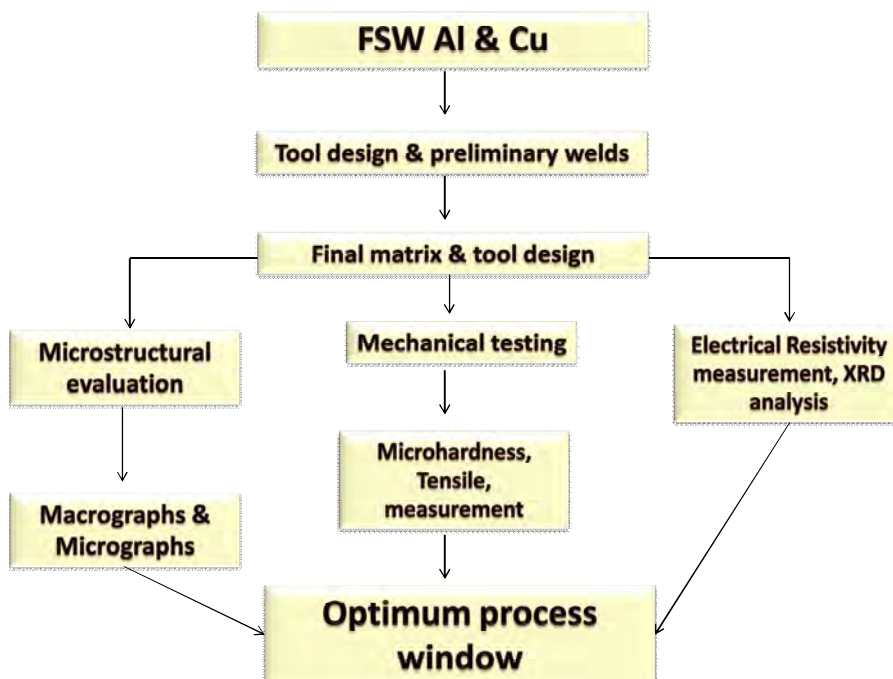


Figure 1.1: Flow diagram of project activities

The organisation of the thesis is as follows:

Chapter One briefly introduces the aims and objectives, the research hypothesis, the methods, the delimitations and the significance of the research project.

Chapter Two presents a review of the related literature and it is focused on the FSW process, the significance of the essential process parameters, the weldability of aluminium

and copper alloys, dissimilar metal joining, FSW of dissimilar materials, and a critical look at the few available literature sources on the FSW of aluminium and copper alloys.

Chapter Three describes the overall experimental set-up and preliminary investigation conducted. This includes tool designs, positions of the work pieces during welding, optimisation of the process parameters, resulting weld defects and the decision on the final weld matrix.

Chapter Four presents the results and discussions of the research welds and;

Chapter Five is the conclusion; this includes a discussion on possible future work and development.

## **CHAPTER 2 FACTORS AFFECTING THE FRICTION STIR WELDING PROCESS**

### **2.1 Introduction**

Welding is a material joining process achieved by the application of heat, with or without pressure, and the addition of filler material. The applications of welding are varied and extensive from small-scale industry to large-scale industry and from small machines to large machineries. Prior to the development of Friction Stir Welding (FSW), many different welding techniques were used to join metals. These techniques range from the conventional oxy-acetylene torch welding to laser welding. Fusion and solid-state welding are basically the two general categories of welding types.

The review of related literature in this research work is focused on:

- The FSW process;
- Significance of the essential process parameters – tool design, welding parameters, joint configuration, forces acting on the tool during the welding procedure, and heat input during the FSW process;
- FSW microstructure;
- X-Ray Diffraction analysis of FSW joints;
- Mechanical and electrical properties of FS welded joints;
- Weldability of aluminium and copper alloys;
- Dissimilar metal joining;
- FSW of dissimilar materials; and
- A critical look at the available literature sources on FSW of aluminium and copper alloys.

#### **2.1.1 Fusion welding**

The fusion welding process involves chemical bonding of the metal in the molten stage; and it may need a filler material, such as a consumable electrode or a spool of wire of the filler materials. Examples of the fusion welding processes are Metal Inert Gas welding (MIG), Tungsten Inert Gas welding (TIG) and Laser Beam Welding (LBW). The process may also need an inert ambience in order to avoid oxidation of the molten metal. This could be

achieved by a flux material, or with the use of an inert gas shield in the weld zone. There could also be a need for adequate surface preparations.

There are many disadvantages to fusion welding techniques. The process requires that the metals to be joined are heated to their melting temperatures; and then allowed to solidify to form the joint. The melting and solidification processes lead to the deterioration of the mechanical properties of the joint - such as low tensile strength, fatigue strength and ductility<sup>21</sup>.

Fusion welding processes are not readily used for welding aluminium to copper, because both materials are incompatible. However, they can be welded by solid state processes that do not heat the materials to melting temperatures; although similar aluminium alloys and copper alloys can be welded separately by using fusion welding processes.

### 2.1.2 Solid-state welding

Solid-state welding is the process whereby coalescence is produced at temperatures below the melting point of the base metal without the use of any filler metal. Examples of solid-state welding processes include friction welding, Friction Stir Welding (FSW), ultrasonic welding, resistance welding, explosive welding and diffusion welding. There are fewer defects in solid-state welding because the metals do not reach their melting temperatures. However, the base metals being joined retain their original properties, and the Heat Affected Zone (HAZ) is small when compared with the fusion welding techniques<sup>22</sup>.

FSW is a variant of friction welding that produces a weld between two or more work pieces by the heating and plastic material displacement caused by a rapidly rotating tool that traverses the weld joint<sup>1</sup>. FSW has been successfully used to weld similar and dissimilar materials. Moriera *et al.*<sup>9</sup> and Larsson *et al.*<sup>10</sup> conducted a research study on butt FS welds of similar aluminium alloys. Successful welds were produced; and they found that the nugget zone was characterised by recrystallized grains and lower Vickers microhardness was measured at the nugget zone, due to the stirring effect of the tool pin. Research studies on dissimilar metal friction stir welds conducted by Yoshikawa<sup>11</sup>, Fukumoto *et al.*<sup>12</sup>, Uzun *et al.*<sup>13</sup>, Zettler *et al.*<sup>14</sup> and Watanabe *et al.*<sup>15</sup> revealed that potential exists to successfully join dissimilar materials using the FSW process. Yoshikawa<sup>11</sup> established a joining criterion for lap welding of dissimilar aluminium and stainless steel and Fukumoto *et*

al<sup>12</sup> achieved good weld joint efficiency in dissimilar joints between normal carbon steel (S45C) and 6063 aluminium alloy. Replacement of fastened joints with friction stir welded lap joints has been observed to lead to significant weight reduction and cost savings for many industries. The weight savings can be achieved as a result of the elimination of the fasteners. The cost savings can be realised by a decrease in design, manufacturing, assembly and maintenance times, and improved corrosion performance by eliminating the fasteners as a source of dissimilar metal contact<sup>23</sup>.

## 2.2 The FSW Process

In 1991, FSW was invented at The Welding Institute (TWI) in the United Kingdom as a solid-state joining technique, and it was initially applied to aluminium alloys<sup>1</sup>. The basic concept of FSW is remarkably simple: a non-consumable rotating tool with a specially designed pin and shoulder is inserted into the abutting edges of the sheets and plates to be joined; and subsequently, it is traversed along the joint line. Figure 2.1 illustrates the process definitions for the tool and work piece. The advancing side is on the right, where the tool rotation direction is the same as the tool travel direction (opposite the direction of metal flow), while the retreating side is on the left, where the tool rotation is opposite the tool travel direction (parallel to the direction of the metal flow).

The tool serves three primary functions, namely: the heating of the work piece, the movement of material to produce the joint and the containment of the hot metal beneath the tool shoulder. Furthermore, heating is created within the work piece by both friction between the rotating tool pin and shoulder, and severe plastic deformation of the work piece. The localized heating softens the material around the pin; and combined with the tool rotation and translation, this leads to movement of the material from the front to the back of the pin, thus filling the hole in the tool wake as the tool moves forward. The tool shoulder restricts metal flow to a level equivalent to the shoulder position<sup>24</sup>.

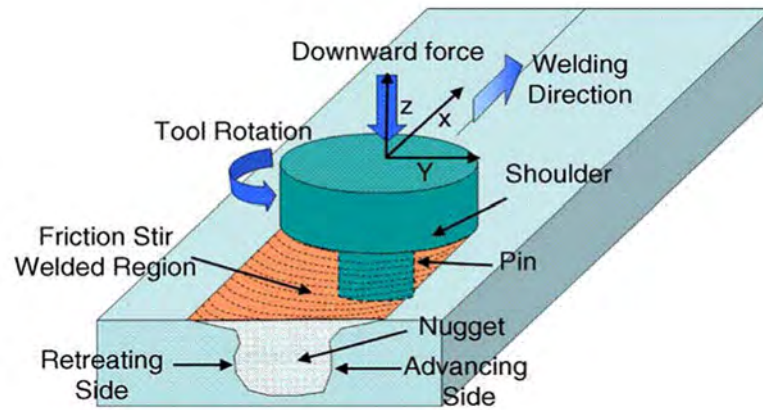


Figure 2.1: Schematic diagram of the Friction Stir Welding process<sup>25</sup>

The three distinct stages in a typical FSW process cycle include<sup>4</sup>:

1. Tool plunge – the process of forcing the tool pin into the work pieces that are being joined.
2. Dwell period – after the plunge, a certain time period elapses where the tool rotates in contact with the plates, but with no traverse. This generates the initial heat to plasticise the material before the traverse is started.
3. Welding – the traverse is then started and the tool moves along the joint line, welding the materials together.

As a result of the tool action and influence on the work piece, when performed properly, a solid-state joint is produced. Because of various geometrical features on the tool, material movement around the pin can be complex, with gradients in strain, temperature, and strain rate<sup>26</sup>.

Accordingly, the resulting nugget zone microstructure reflects these different thermo-mechanical histories that are not homogeneous. In spite of the local microstructural inhomogeneity, one of the significant benefits of this process is the fully recrystallized, equiaxed, fine grain microstructure created in the nugget by the intense plastic deformation at an elevated temperature. The fine grain microstructure produces excellent mechanical properties, fatigue properties, enhanced formability, and exceptional superplasticity<sup>27-29</sup>.

FSW is considered to be the most significant development in metal joining techniques in decades; and it is, in addition, a “green technology” due to its energy efficiency, environmental friendliness and versatility. When compared with the conventional welding

methods, FSW consumes considerably less energy and no harmful emissions are created during the welding process<sup>6</sup>. Furthermore, because FSW does not involve the use of filler material; and the absence of melting makes it possible to join all aluminium alloys, without any concern for compatibility of composition or solidification cracking issues normally associated with fusion welding.

FSW can be applied to most geometric structural shapes and to various types of joints, such as butt, lap, T-butt, and fillet shapes<sup>30</sup>. For butt and lap joints, it is advisable to use a backing plate. This prevents the abutting joint faces from being forced apart, while the backing plate is required to resist the normal forces associated with FSW and the work piece. During the initial tool plunge, the lateral forces are also fairly large, and extra care is required to ensure that the plates in the butt configuration do not separate.

FSW is becoming the choice of industry for structurally demanding applications, because the process is devoid of severe distortion and residual stresses, compared with the conventional welding processes. This result is supported by authors who have observed that severe distortions and the generated residual stresses are very low in the FSW process compared with the conventional welding processes<sup>31-35</sup>. Comparing the residual stresses of the FS weld interfacial region to the parent material using a synchrotron X-ray diffractometer, Steuer *et al.*<sup>32</sup> reported that the parent material used in their investigation has a peak width of about 2.5 times greater than that seen in the weld zone. The peak width  $\beta$ , measured in radians is inversely proportional to the crystallite size and it is a qualitative indicator of the size of crystals present.

Currently, FSW is being used for joining similar and dissimilar alloys in ship building, marine industries, aerospace, rail industries, container and fuel tank industries. Furthermore, the technology provides significant advantage to the aluminium industry; and automotive suppliers are already using the technique for wheel rims and suspension arms. Compared with conventional fusion welding methods, FSW offers a number of advantages: the benefits of the process are presented in Table 2.1.

Table 2.1: Benefits of the FSW process<sup>24</sup>

Metallurgical benefits	Environmental benefits	Energy benefits
<ol style="list-style-type: none"> <li>1. Solid– phase process.</li> <li>2. Low distortion.</li> <li>3. Good dimensional stability and repeatability.</li> <li>4. No loss of alloying elements.</li> <li>5. Excellent mechanical properties in the joint area.</li> <li>6. Fine recrystallized microstructure.</li> <li>7. Absence of solidification cracking.</li> <li>8. Replaces multiple parts joined by fasteners.</li> </ol>	<ol style="list-style-type: none"> <li>1. No shielding gas required for materials with low melting temperature.</li> <li>2. Minimal surface cleaning required.</li> <li>3. Eliminates grinding wastes.</li> <li>4. Eliminates solvents required for degreasing.</li> <li>5. Consumable materials saving.</li> <li>6. No harmful emissions.</li> </ol>	<ol style="list-style-type: none"> <li>1. Improved materials use (e.g. joining different thickness) allows reduction in weight.</li> <li>2. Only 2.5% of the energy needed for a laser weld.</li> <li>3. Decreased fuel consumption in lightweight aircraft, automotive, and ship applications.</li> </ol>

## 2.3 FSW process parameters

Although FSW gives high quality welds, proper execution of the process and control of a number of parameters is required for a successful outcome. Recent experimental and computational works have provided insight into how process parameters influence material flow in FSW. Most of the material flow occurs through the retreating side and the transport of plasticised material behind the tool forms the welded joint<sup>6</sup>. Process parameters, such as tool design, welding parameters, joint configuration, forces acting on the tool during welding and the heat input during the process, are found to exert significant effects on the material flow and the temperature distribution and by implication these factors inevitably influence the microstructural evolution and mechanical properties of the materials being joined<sup>19, 36-42</sup>. The effect of these process parameters will now be discussed in more detail.

### 2.3.1 Tool Design

FSW tool design, which includes material selection and geometry, is one of the most important factors that influence heat generation, plastic flow, joint integrity, the resulting microstructure and the mechanical properties. Tool materials, apart from having to satisfactorily endure the welding process, affect friction coefficients and heat generation. Tool configuration influences joint size and profile<sup>6, 23</sup>.

Selecting the correct tool material requires the knowledge of material characteristics that are important for each friction stir application. In addition to the physical properties of a material, some practical considerations such as wear resistance, reactivity and machineability are properties that may also dictate the tool material selection<sup>43</sup>. Hot-worked tool steel, such as AISI H13 has proven acceptable for welding a wide range of materials because it provides sufficient hardness, is easily available, has good machineability, is relatively cheap and has high abrasion resistance<sup>44-52</sup>. Other types of materials that are commonly used in the manufacture of tools include: nickel alloys, tungsten alloys, and Polycrystalline Cubic Boron Nitride (PCBN)<sup>53</sup>.

The tool geometry is concerned with the shape and size of the pin and shoulder. From the heating aspect, the relative sizes of the pin and shoulder are important; the shoulder also provides confinement for the heated volume of material. A concave shoulder profile is usually employed; it acts as an escape volume for the material displaced by cylindrical pins, and prevents material from extruding out of the sides of the shoulder.

The diameter of the tool's shoulder is proportional to the torque at a constant rotational speed. As the tool shoulder diameter increases, so does the torque during welding. Different pin diameters have virtually no effect on torque values. Increasing the diameter of the shoulder has practical limitations, and tends to produce side flash on the weld surface<sup>20</sup>.

With increasing experience and improvement in understanding material flow, the tool geometry has evolved significantly. The pin length is typically slightly shorter than the thickness of the work piece, and its diameter is typically slightly larger than the thickness of the work piece<sup>54-56</sup>. Table 2.2 gives a selection of tools designed at TWI with their corresponding applications.

Table 2.2: A selection of tools designed at TWI<sup>57</sup>

Tool	Cylindrical	Whorl™	MX triflute™	Flared triflute™	A-skew™	Re-stir™
Schematics						
Tool pin shape	Cylindrical with threads	Tapered with threads	Threaded, tapered with three flutes	Tri-flute with flute ends flared out	Inclined cylindrical with threads	Tapered with threads
Ratio of pin volume to cylindrical pin volume	1	0.4	0.3	0.3	1	0.4
Swept volume to pin volume ratio	1.1	1.8	2.6	2.6	Depends on pin angle	1.8
Rotary reversal	No	No	No	No	No	Yes
Application	Butt welding: fails in lap welding	Butt welding with lower welding torque	Butt welding with further lower welding torque	Lap welding with lower thinning of upper plate	Lap welding with lower thinning of upper plate	When minimum asymmetry in weld property is desired

When welding thin sheets, the main source of heat is from the shoulder of the tool. As the material thickness increases, more heat must be supplied by the friction between the rotating pin and the material. In addition, the main function of the pin is to ensure sufficient working of the material at the weld joint, and to control the flow of the material around the tool, in order to form a quality weld<sup>58</sup>.

For proprietary reasons, the tool geometries employed in research studies are not reported. However, the importance of tool geometry was illustrated in an FSW lap joint of 6 mm 5083 aluminium alloy sheet by Thomas *et al.*<sup>59</sup>. A conventional cylindrical threaded pin tool was used, which gave a good as-welded appearance. Bend testing showed the weld to be weak, however, due to excessive thinning of the top sheet and thickening of the bottom sheet, as a result of differential pressure during welding. This problem arises from the inappropriate use of the tool in lap welds. The tool employed gave satisfactory butt welds. This further confirmed that good welded joints can only be achieved by the use of a tool appropriate to the application<sup>60</sup>.

A study that addressed the effect of tool pin design on the weldability and mechanical properties of welded 2014 aluminium plates, where unthreaded cylindrical and tapered tool pins were used, reported that effective mixing in the vertical direction was not achieved and

this, subsequently, led to the formation of wormholes at the base of the TMAZ<sup>61</sup>. However, when tapered tools with threads were used, defect-free welds were obtained. Other studies have also confirmed that tools with screw threads generate more heat and improve the flow of the softer material by exerting a downward force. Since the material flows mainly on the retreating side, insufficient plasticity and material flow results in wormholes on the advancing side<sup>55</sup>.

The role of an FSW tool on material flow and weld formation was conducted by Kumar *et al.*<sup>62</sup> in similar material joining of 7020 aluminium alloy. An attempt was made to understand the mechanism of material flow in friction stir welded plates. Their results showed that there are two different modes of material flow regimes involved in the friction stir weld formation; namely, “pin-driven flow” and the “shoulder-driven flow”, caused by the rotation of the pin and shoulder respectively. They concluded that it is important that the design of the pin be such that the maximum amount of transferred material is retained in the weld cavity, and the shoulder-driven material flow can be described as the effectiveness of the shoulder in keeping the material in the weld cavity. Thus, the tool shoulder should be designed in such a way that the maximum amount of the ejected material from the weld cavity by the pin is forced back into the weld cavity.

A further study on the effect of shoulder geometry on material flow in FSW of thin aluminium sheets was conducted by Leal *et al.*<sup>63</sup>. Two types of tool shoulders were used: a shoulder with a conical cavity and one with a scrolled shoulder. They observed that pin-driven flow predominates in welds produced with the conical cavity shoulder. These are characterised by an onion ring structure. The scrolled shoulder gave a shoulder-driven flow, and there was some mixing of the base materials.

Improvements in tool design have been shown to cause substantial enhancements in productivity and quality. The majority of tools have a concave shoulder profile with threaded pin, the shoulder-to-pin ratio ranges between 2.5:1 and 3.0:1 for thin sheets<sup>6</sup>. The tool pin and shoulder are hereafter discussed in detail.

### 2.3.1.1 Tool Pin

Friction stirring pins play significant roles in material flow during the FSW process. The pin is designed to disrupt the fraying surface of the workpiece. Research work on fundamental characterisation of friction stir welding process parameters was conducted by Record *et al.*<sup>19</sup>. The tool used was made from heat-treated H13 tool steel with a threaded pin and a

concave shoulder. They used statistical experimentation to study important process parameters and the sensitivity of the operating conditions applicable to these process parameters. It was confirmed that the most significant input parameters in FSW are spindle speed, feed rate and tool depth. They also observed that other important variables to consider are weld location (proximity of weld to edge of the plate) and pin length.

Most of the papers cited that gave reports on their tool designs used threaded pins<sup>60-63</sup>. However, Clark *et al.*<sup>64</sup> in their research, reported on tool design in friction stir processing: dynamic forces and material flow with unthreaded pins. Two types of tools: cylindrical and tapered pins were used. They observed that welds made with the cylindrical pin had severe wormhole defects. In an effort to quantify and remedy this problem, the forces were analysed across the matrix. It was apparent that faster spindle speeds and slower travel speeds reduced the wormhole, whereas welds made with the tapered pin were more successful in minimizing the wormhole defect, and some defect-free welds were made.

Fujii *et al.*<sup>65</sup> also used unthreaded pins in their research work on the effect of tool shape on mechanical properties and on the microstructure of friction stir welded aluminium alloys. Three different types of pins were used: column without threads, column with threads and the triangular prism shape. It was reported that the unthreaded pin produced the weld with the best mechanical properties.

### **2.3.1.2 Tool shoulder**

Tool shoulders are designed to produce heat through friction and material deformation to the surface and subsurface of the workpiece. Also, the shoulder produces the downward forging action necessary for weld consolidation. Rodrigues *et al.*<sup>66</sup> studied the influence of FSW parameters on the microstructural and mechanical properties of AA6016-T4 thin sheets. Two different tool designs were used: conical and scrolled shoulders; it was observed that the differences in tool geometry and welding parameters induced significant changes in the material flow path during welding, as well as in the microstructure of the weld nugget. The weld produced with the conical shoulder displayed a larger nugget grain size with fewer coarsened precipitates, as opposed to the welds done with the scrolled shoulder, which showed a smaller grain size containing many coarsened precipitates.

Research work on the effects of rotation speed and welding speed on material flow and stir zone formation during FSW was also conducted by Cui and Chen<sup>67</sup>. The FS tools used

were made from H13 tool steel with threaded pin and a concave shoulder. They concluded that rotational speed and welding speed affected the shoulder-induced and pin-induced flow quite differently. Rotational speed affected the relative flow significantly, but affected the overall stir flow volume only slightly. At low rotational speeds, shoulder-induced flow dominated, but such flow reduced substantially in volume when the speed was higher than 500rpm.

### 2.3.2 Welding Parameters

In FSW, the inter-relationship between the process parameters is complex; the two most important welding parameters being the tool rotational speed in a clockwise or anti-clockwise direction, and the tool traverse speed along the joint line<sup>25</sup>. The rotation of the tool results in the stirring and mixing of material around the rotating pin, while the translation of the tool moves the stirred material from the front to the back of the pin and finishes the welding process<sup>25, 68</sup>.

The choices of feed rate and rotational speed are crucial for heat generation, in order to create good flow of the material around the tool, while minimizing the forces on the tool. The ratio of feed rate to rotational speed is usually reduced to a single parameter referred to as pitch. The properties of the welds are usually related to the pitch, which is believed to be an important parameter in FSW<sup>69-70</sup>.

#### 2.3.2.1 Feed rate and Rotational speed

A study concerning the effect of welding parameters on mechanical and microstructural properties of AA6056 joints produced by FSW was conducted by Cavaliere *et al.*<sup>71</sup>. They reported that when high rotating and welding speeds are used, the hardness of the material reaches higher values compared with the base metal, and the profiles become less uniform across the weld centre. The microstructure of the joint appears as fine and equi-axed grains in all the welding conditions. Further work by Cavaliere *et al.*<sup>72</sup> on the effect of welding parameters on mechanical and microstructural properties of dissimilar AA6082-AA2024 joints produced by FSW observed that the vertical force increases as the travel speed for all the produced joints increases. The joints were produced with different aluminium alloys positioned on the advancing side of the tool. They concluded that different vortex-like structures resulted in the centre of the joints in all the different configurations. The tool used was made from C40 tool steel with a threaded pin and a conical shoulder.

### 2.3.2.2 Tool tilt angle

In addition to the tool rotation rate and traverse speed, another important process parameter is the angle of the spindle or tool tilt angle with respect to the work piece surface. A suitable tilt of the spindle towards the trailing direction ensures that the shoulder of the tool holds the stirred material by the pin and moves the material efficiently from the front to the back of the pin<sup>25</sup>. Not much literature exists on the effect of tool tilt angle on the FSW process.

Research work on the effects of tool tilt angle on metal flow phenomenon in friction stir welds of A5005 aluminium alloy and A1100 pure aluminium was conducted by Shinoda<sup>73</sup>. It was reported by him that metallurgical observation revealed that the angle of stir tool affects the metal flow patterns in two directions: bottom flow and surface flow. Microhardness values across the weld revealed that the values are almost equivalent to the base material. This meant that joint efficiency is quite close to base metal values, more than 95%. However, he reported that lower tensile strength appeared at low rotational speed and low travel speed combination.

Arici and Selale<sup>74</sup> also studied the effect of tool tilt angle on the tensile strength and fracture locations of friction stir welding of polyethylene. It was observed that the tensile strength of the material decreased with increasing tool tilt angles and that the thickness of the welding zone decreased with increasing tool tilt angle. This affects the tensile strength of the joint.

The relationship between the welding speeds and the heat input during welding is complex, but in general, it can be said that increasing the rotational speed or decreasing the traverse speed will result in a hotter weld. In order to produce a successful weld, it is necessary that the material surrounding the tool be hot enough to facilitate the extensive plastic flow required, and to minimise the forces acting on the tool.

### 2.3.3 Joint Configuration

FSW can be applied to most geometric structural shapes and to various types of joints, such as butt, lap, T-butt, and fillet shapes<sup>30, 75</sup>. The most convenient joint configurations for FSW are butt and lap joints. A simple square butt joint is shown in Figure 2.2(a). Two plates or sheets of the same thickness are placed on a backing plate, and clamped firmly to prevent the abutting joint faces from being forced apart. The backing plate is required to resist the normal forces associated with FSW and the work piece.

During the initial tool plunge, the lateral forces are also fairly large, and extra care is required to ensure that the plates in the butt configuration do not separate. Tool position and penetration depth during welding are maintained by either position control or control of the applied normal force. On the other hand, for a lap joint configuration, two lapped plates or sheets are clamped, and a backing plate may or may not be needed, depending on the thickness of the lower plate (Figure 2.2(d)).

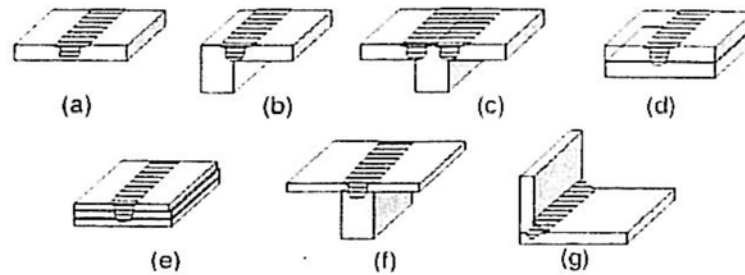


**Figure 2.2: Joint configurations for Friction Stir Welding: (a) Square butt, (b) Edge butt, (c) T-Butt joint, (d) Lap joint, (e) Multiple lap joint, (f) T-Lap joint, and (g) Fillet joint<sup>25</sup>**

### 2.3.4 Forces acting on the tool during the FSW process

During welding, a number of forces act on the tool<sup>4</sup>:

- A downward force, ( $F_z$ ), is necessary to maintain the position of the tool at or below the material surface.
- The traverse force, ( $F_x$ ), acts parallel to the tool motion and is positive in the traverse direction. Since this force arises as a result of the resistance of the material to the motion of the tool, it might be expected that this force will decrease as the temperature of the material around the tool is increased<sup>4</sup>.
- The lateral force, ( $F_y$ ), may act perpendicularly to the tool traverse direction, and is defined here, as a positive force acting towards the advancing side of the weld.
- Torque is required to rotate the tool, the amount of which will depend on the down force and friction coefficient and or the flow strength of the material in the surrounding region.

The stages in FSW viz the tool plunge, dwell time, shoulder contact, welding and pin retraction as discussed in section 2.2 are presented in Figure 2.3.

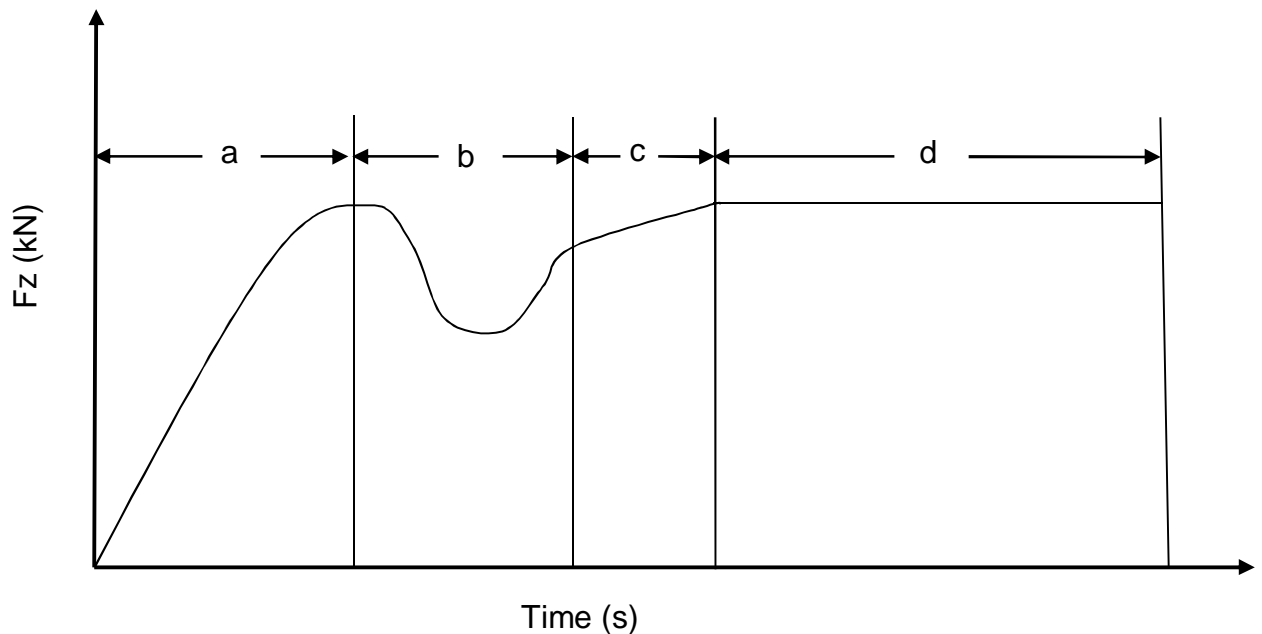


**Figure 2.3: Typical force feedback plot of vertical downward force ( $F_z$ ) with respect to time**

Where,

a = tool plunge

b = dwell time

c = ramp up

d = steady state weld region.

Figure 2.3 shows a typical force feedback plot of the downward vertical force versus time in an FS weld. At the beginning of the weld phase, as the rotating tool is plunged into the workpieces, the  $F_z$  rises while the tool drills a hole in the workpieces forming a region of severely deformed material due to the tool/material interaction. The first spike shown is caused by overly fast plummet of the tool into the workpieces; this is referred to as the tool plunge. After the plunge, a certain time period elapses, referred to as the dwell time where the tool rotates in the workpieces, but with no traverse. This generates the initial heat to plasticise the material before the traverse is started. At the end of the dwell time, the tool traverses and a ramp up occurs due to forging resulting in an increase in the downward vertical force. It should be noted that the grain deformation and heat transfer process in the entire weld is transient and normally not considered to be in steady state due to vibration of the equipment and variation of the parameters with time and x position. Then, a stable vertical downward force is achieved in the welding where all welding parameters are nearly

constant. This period can be referred to as the steady state of the welding process, i.e., the period during which the force, torque and heat reach a near equilibrium state<sup>71</sup>.

### 2.3.5 Heat input during the FSW process

The heat input into the weld in the FSW process is an important quantity, due to its influence on the resulting properties of the weld. Heat generation during FSW arises from two sources: friction at the surface of the tool, and the deformation of the material around the tool. The heat generated is often assumed to occur predominantly under the shoulder, due to its greater surface, and to be equal to the power required to overcome the contact forces between the tool and the work piece<sup>76</sup>.

Average heat input in FSW has been proposed by many authors in the context of simple energy models<sup>70,77</sup>. Although, this is only an estimate of the heat input since there may be losses that depend on the input parameters. For example, the rate of heat loss through radiation or by conduction from the anvil and the tool, may change based on the weld parameters. Hence, the heat input (J/mm) from the shoulder of the tool in FSW is determined through the spindle torque measurements. These are constant, once the thermal equilibrium has been reached. This is given by<sup>70</sup>:

$$Q = \eta \frac{2\pi\omega T}{f} \quad 2.1$$

Where,

Q= heat input (J/mm)

$\eta$ = efficiency factor = 0.9 for Al and Cu

$\omega$ = rotational speed (rev/min)

T= torque (Nm)

f= feed rate (mm/min)

## 2.4 Friction Stir Weld Microstructures

The resulting microstructure and subsequent property distributions produced during FSW of similar and dissimilar materials are dependent on several factors. The contributing factors include alloy composition, welding parameters, thickness of the welded material and other geometric factors. Alloy composition determines the available strengthening mechanisms and how the material will be affected by the temperature and strain history associated with FSW. Welding parameters determine, for a given tool geometry, the temperature and strain history of the material being welded. Plate thickness and other geometric factors (clamping

device and backing plate) may affect the temperature distribution within the weld zone, and in particular, through the thickness of the welded plates<sup>78</sup>.

As with many new technologies, a new nomenclature is required to accurately describe observations. In FSW, new terms were necessary to adequately describe the post-weld microstructures. The first attempt at classifying friction stir welded microstructures was made by Threadgill<sup>79-81</sup>. Figure 2.4 identifies the different microstructural zones after FSW. A brief description of the different zones/regions is presented as follows:

- Unaffected material or base metal (BM): This is material remote from the weld that has not been deformed and that, although it may have experienced a thermal cycle from the weld, is not affected by the heat in terms of microstructure or mechanical properties.
- Heat-affected zone (HAZ): In this region, which lies closer to the weld-centre, the material has experienced a thermal cycle that has modified the microstructure and/or the mechanical properties. However, no plastic deformation occurs in this area.
- Thermo-mechanically affected zone (TMAZ): In this region, the FSW tool has plastically deformed the material, and the heat from the process would also have exerted some influence on the material. In the case of aluminium, it is possible to obtain significant plastic strain without recrystallization in this region; and there is generally a distinct boundary between the recrystallized zone (weld nugget) and the deformed zones of the TMAZ.
- Weld nugget: The fully recrystallized area, sometimes called the Stir Zone (SZ) or Stir Nugget (SN), refers to the zone previously occupied by the tool pin. The term stir zone is commonly used in friction stir processing, where large volumes of materials are processed.

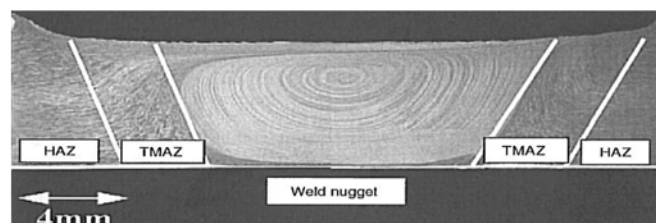


Figure 2.4: Typical FS weld of aluminium showing microstructural zones<sup>82</sup>

## 2.5 X-Ray Diffraction (XRD) Analysis of FSW Joints

During the FSW process, plastic deformation and dynamic recrystallization of the weld metal occurs as a result of stir action and frictional heat. These may lead to a change of phase constituents and crystal structure of the weld nugget zone. However, in FSW of dissimilar materials, an intermetallic compound which has a definite structure different from those of its constituent metals may be formed at the joint interface<sup>16</sup>. X-Ray Diffraction (XRD) analysis which has been used for materials characterisation and as an analysis technique can be used to identify the phases at the joint interface and compare them with the base materials<sup>83</sup>.

An XRD analysis was conducted by Venkateswaran *et al.*<sup>84</sup> to determine the composition in and around the joint interface of dissimilar Al-Mg friction stir welds. These authors reported that the spectra are similar on both sides of the weld indicating good mixing. Also, Liu *et al.*<sup>83</sup> in a research study on microstructure and XRD analysis of FSW copper T2/aluminium 5A06 dissimilar materials reported that deviation of diffraction peaks existed between the weld nugget zone and the base materials due to the presence of intermetallics. They concluded that the structure of the weld zone was characterised by a plastic diffusion combination of aluminium and copper.

However, Lee *et al.*<sup>85</sup> in a study on the effects of intermetallic compounds on the electrical and mechanical properties of friction welded Cu/Al bimetallic joints during annealing reported that XRD analysis was used to identify the layers of intermetallic compounds formed at the Al/Cu joint interface.

## 2.6 Mechanical and electrical properties of FSW Joints

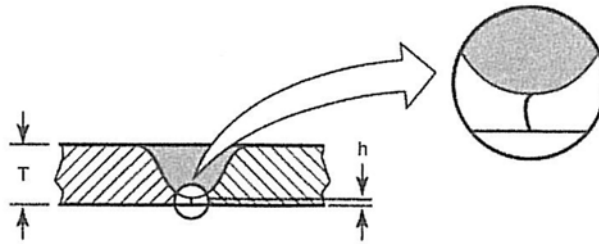
The resulting mechanical and electrical properties of the welded joint are greatly influenced by the tool design and the choice of process parameters<sup>86-87</sup>. Weld properties, such as defects; mechanical properties such as tensile strength, grain size and microhardness values; and electrical properties, such as electrical resistance measurement of joints will be discussed in this section.

### 2.6.1 Defects

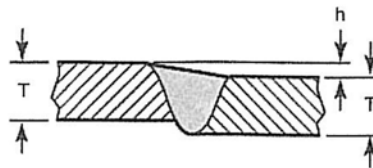
The quality of joints produced in FSW is affected by the choice of tool profile, rotational speed, feed rate, tilt angle, plunge depth and variation in plate thickness. Inappropriate

combinations of these parameters result in weld defects in FSW joints<sup>88</sup>. Common defects associated with FSW are shown in Figure 2.5 below.

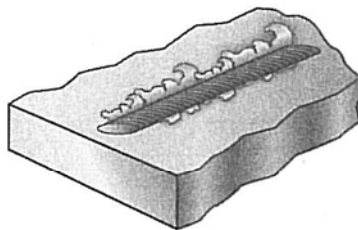
- a. Incomplete Penetration - Root defect



- b. Joint Mismatch



- c. Excess Weld Flash



- d. Cavity

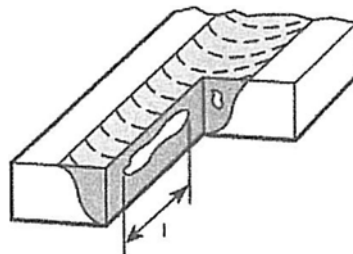


Figure 2.5: Weld defects in FSW<sup>22</sup>

The weld defects shown in Figure 2.5 are explained briefly as follows:

- Incomplete root penetration, also referred to as root defect, results from insufficient pin length of the tool or insufficient plunge depth.
- Joint mismatch, can occur if fixturing is not properly made or if clamping pressures are too low.
- Excess weld flash occurs if the plunge depth is too high or the shoulder diameter is too small.
- Wormholes, sometimes called voids or cavities, are caused by incomplete bonding that stems from insufficient forging pressure or incorrect tool design<sup>22, 89-92</sup>.

Further studies revealed that wormholes are formed in welds, as a result of insufficient material flow towards the bottom of the weld, and also because of inadequate heat under the tool shoulder<sup>69,93</sup>. According to Crawford<sup>94</sup>, at a constant rotational speed, an increase in the travel speed leads to wormhole initiation near the bottom of the weld, and a high weld pitch ratio. This is the ratio of the traverse speed to the rotational speed; is also known to cause wormholes in welds<sup>6,89,95</sup>.

### 2.6.2 Grain Size and Microhardness

It is well established that the dynamic recrystallization during the FSW process results in the generation of fine and equi-axed grains in the nugget zone<sup>96-104</sup>. It is reported that the grain size decreases from the parent material towards the nugget zone<sup>105-106</sup>. FSW process parameters, tool design, forge force and active cooling, all exert significant influences on the size of the recrystallized grains in the FS welded materials<sup>107-108</sup>. Sato *et al.*<sup>101</sup> studied the effect of process parameters on microstructure in FSW process, and reported that recrystallized grain size can be reduced by decreasing the tool rotation rate, as well as the overall heat input.

Many investigators use hardness data for an initial evaluation of the variation in mechanical properties across the weld zone. They have reported changes in hardness in the friction stir weld zones compared with the parent material; and this varies from one material to another. It is expected that mechanical properties would increase in a corresponding manner with the increase in hardness<sup>82</sup>.

### 2.6.3 Tensile Properties

Yield and tensile strength in FS welded samples are usually assessed to compare the strength and ductility of the welded sample to the base material. This is often related to hardness. Many investigators have reported tensile strengths of FS welded joints as a percentage relative to that of the parent material; and some have studied its relationship to the process parameters<sup>109-110</sup>.

Research work on tensile behaviour of friction stir welded Al 6061-T651 was conducted by Lim *et al.*<sup>110</sup> who reported that the tensile elongation of friction stir welded Al 6061-T651 decreased with decreasing welding speed or increasing rotating speed. Ceschini *et al.*<sup>111</sup> also studied the effect of friction stir welding on microstructure, tensile and fatigue

properties of the AA7005/10% vol. %Al<sub>2</sub>O<sub>3</sub>P composite, and found that the tensile test results of the FS welded samples showed a high efficiency of about 80% of the ultimate tensile strength of the parent material.

#### 2.6.4 Electrical Properties

Electrical properties, such as resistivity measurement of FS Welds is only applicable to similar and dissimilar joining of materials used in the electrical industries. Examples include Silver, Gold, Aluminium and Copper. Electrical resistivity, sometimes referred to as electrical resistance, is a measure of how strongly a material opposes the flow of electric current. A low resistivity indicates a material that readily allows the movement of electrical charge<sup>112</sup>. Resistivity is usually determined by calculating from the measurement of electrical resistance of samples having a known length and uniform cross-section, according to the following equation:

$$\rho = R \frac{A}{l} \quad 2.2$$

Where,

- ρ= Electrical resistivity
- R= Resistance
- A= Cross-sectional area
- l= Length of the sample

There are different methods used in measuring electrical resistance, the Four-Point probe meter was used in this research work, and the resistivity calculated using expression 2.3.

$$\rho = 2\pi s \left( \frac{V}{I} \right) \quad 2.3$$

Where,

- ρ = Electrical resistivity
- s= Probe spacing
- V= voltage drop
- I= Current
- $\left( \frac{V}{I} \right)$  = Resistance

The probe spacing, 's' is a constant and is equal to 1.6 mm; the 2πs becomes unity, and ρ becomes simply:

$$\rho = \left( \frac{V}{I} \right) = R \quad 2.4$$

Limited information exists on resistivity measurement of weld cross-sections in FSW. The only report being that conducted by Savolainen *et al.*<sup>112</sup> in a preliminary study on friction stir

welding of dissimilar metal joints of copper and aluminium in which the electrical resistivity of the joint was measured and found to be relatively low compared with that of the base material. However, this is a pilot study as no process window was established; hence, only a limited range of parameters was considered.

## **2.7 Weldability**

The weldability of a material is its capacity to be welded into a specific structure that has certain properties and characteristics and will satisfactorily meet the service requirements. The weldability of aluminium and copper and their alloys are hereafter discussed.

### **2.7.1 Aluminium Alloys**

The most important characteristics of aluminium and its alloys which make them suitable for a wide variety of applications are their weight, appearance, ease of fabrication, strength and resistance to corrosion. The primary welding methods used are the gas-shielded arc welding processes. The selection method depends on many factors, such as geometry and the material of the parts to be joined, the required strength of the joint, permanent or dismountable joint, number of parts to be joined, the aesthetic appeal of the joint, and finally, the service conditions, such as moisture, temperature, inert atmosphere and corrosion.

Aluminium and its alloys have several chemical and physical properties that need to be understood when using the various joining processes. These include oxide formation, the solubility of hydrogen in molten aluminium; its thermal, electrical, and non-magnetic characteristics; its lack of colour change when heated; and its wide range of mechanical properties and melting temperatures that result when alloying it with other metals.

The weldability of some aluminium alloys can be an issue with the fusion welding processes. The 2000, 5000, 6000 and 7000 series of aluminium alloys all have different degrees of weldability. The 2000 series of aluminium alloys have poor weldability generally because of the copper content. This causes hot cracking and poor solidification microstructure, as well as porosity in the fusion zone.

The 5000 series of aluminium alloys with more than 3% Magnesium content are susceptible to cracking due to stress concentration in corrosive environments at high temperatures. All

the 6000 series of aluminium are readily weldable, but are sometimes susceptible to hot cracking under certain conditions. The 7000 series of aluminium is both weldable and non-weldable, depending on the chemical composition of the alloy. Alloys with Zn-Mg and Cu content are readily weldable; and they have the special ability of recovering the strength lost in the HAZ after some weeks of storage subsequent to the weld. All these problems associated with the welding of these different alloys of aluminium have led to the development of solid-state welding processes like the Friction Stir Welding technique. FSW can weld a variety of aluminium alloys, some of which are difficult to weld by any of the fusion welding processes<sup>21</sup>.

### 2.7.2 Copper Alloys

Copper and copper alloys offer a unique combination of material properties that make them advantageous for many manufacturing environments. They are widely used because of their excellent electrical and thermal conductivities, outstanding resistance to corrosion, ease of fabrication, and good strength and fatigue resistance, low-permeability properties, and distinctive colour. Copper and copper alloys find their greatest use in electrical conductors and in the manufacture of electrical components. The electrical conductivity reference standard of engineering materials is copper with a rating of 100% International Annealed Copper Standard (IACS). All other materials are compared on a conductivity basis to the IACS standard<sup>21</sup>.

Several alloying elements have pronounced effects on the weldability of copper and copper alloys. Small amounts of volatile, toxic alloying elements are often present in copper and its alloys. As a result, the requirement of an effective ventilation system should be available when welding. Grease, paint, shop dirt and similar contaminants on copper alloys may all cause brittleness and should be removed before welding<sup>21</sup>.

### 2.7.3 Metallurgy of Aluminium-Copper system

The high metallurgical reactivity and affinity between Al and Cu leads to the formation of hard and brittle intermetallic compounds at the joint interface<sup>113-114</sup>. The equilibrium solid phases of the Al-Cu system are (i) (Cu) and (Al), the terminal face centred cubic (fcc) solid solutions; (Cu) is often designated  $\alpha$ ; hence, the low-temperature ordered phase based on the fcc structure is designated  $\alpha_2$ ; (ii)  $\beta$ , the disordered body centred cubic (bcc) solid solution;  $\beta_1$ , the ordered bcc phase, which occurs metastably; and  $\beta_0$ , a high-temperature phase; (iii)  $\epsilon_1$  and  $\epsilon_2$  phases of unknown structure; (iv) phases with structures based on  $\gamma$

brass,  $\gamma_0$ ,  $\gamma_1$  and  $\delta$ ; and (v) the equiatomic phases,  $\eta_1$  and  $\eta_2$ , and near-equi-atomic phases,  $\zeta_1$  and  $\zeta_2$ , with structures related to the  $\eta$  structures; and (vi)  $\theta$ , and metastable transition phases  $\theta'$  and  $\theta''$ , formed from supersaturated (Al) before the  $[\theta + (\text{Al})]$  equilibrium is reached. The solubility of Al in Cu is 19.7 atomic %Al, and solubility decreases below the peritectoid temperature<sup>114</sup>. The Al-Cu phase diagram is shown in Figure 2.6.

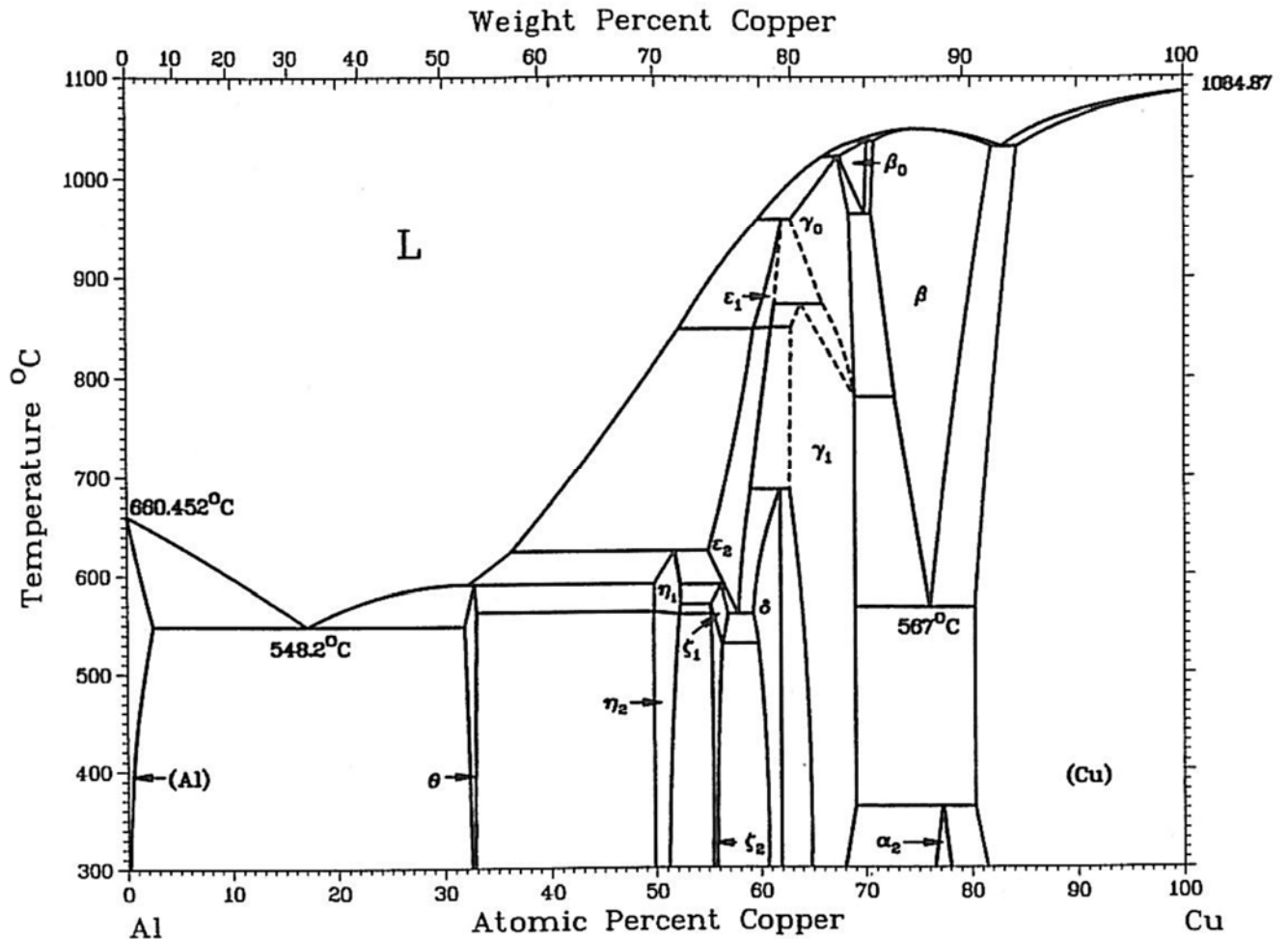


Figure 2.6: The Aluminium-Copper (Al-Cu) Binary phase diagram<sup>114</sup>

Table 2.3 presents a list of the most common intermetallic phases and their percentage atomic and weight composition. The weight percentage compositions stated in the Table were calculated, based on the chemical formulas of the intermetallic compounds, as presented in Appendix A.

Table 2.3: Al-Cu Intermetallic Phases and their Properties<sup>114-119</sup>

Phase	Composition, atomic %Cu	Composition weight %Cu	Chemical formula	Temperature at which they are formed (°C)
(Al)	0 to 2.48	0	Al	0
$\theta$	31.9 to 33.0	54	$Al_2Cu$	550
$\eta_1$	49.8 to 52.4	70	$AlCu$	591
$\eta_2$	49.8 to 52.3	70	$AlCu$	591
$\zeta_1$	55.2 to 59.8	76	$Al_3Cu_4$	624
$\zeta_2$	55.2 to 56.3	76	$Al_3Cu_4$	624
$\delta$	59.3 to 61.9	78	$Al_2Cu_3$	700
$\gamma_0$	59.8 to 69	84	$Al_4Cu_9$	950
$\gamma_1$	62.5 to 69	84	$Al_4Cu_9$	950
$\beta_0$	67.6 to 70.2	88	$AlCu_3$	1048
$\beta$	70.6 to 82.0	88	$AlCu_3$	1048
Cu	80.3 to 100	89 to 100	Cu	1083

## 2.8 Dissimilar metal joining

FSW is one of the most popular welding techniques for joining dissimilar materials. Currently, there is great interest in joining magnesium, steel, titanium and copper to aluminium alloys. The joining of aluminium superstructures to steel-hulled ships, automotive components, for instance steel to aluminium tailor-welded blanks, tank container industries, as well as many aerospace applications all require improved solutions to dissimilar metal joints<sup>12,120-122</sup>. The joining of dissimilar metals is commonly used in the power generation, the chemical, petrochemical, nuclear and electrical / electronic industries for the purpose of desirable combined properties and/or for the advantage of weight reduction<sup>16</sup>.

The weldability of dissimilar metals is determined by their atomic diameter, crystal structure and compositional solubility in their liquid and solid states. Diffusion in the weld pool often results in the formation of intermetallic phases, the majority of which are hard and brittle, and are thus detrimental to the mechanical strength and ductility of the joint<sup>21</sup>.

Because various portions of a process system operate under different service conditions, different structural alloys are used in their design; and hence, dissimilar-metal welded joints may be required. Many factors should be considered when welding dissimilar metals; and the development and qualification of adequate procedures for the various metals and sizes for the specific applications must be undertaken.

Most combinations of dissimilar materials can be joined by solid-state welding (diffusion welding, explosive welding, friction welding, ultrasonic welding and friction stir welding), brazing, or soldering where alloying between the metals is normally insignificant. In these cases, only the differences in the physical and mechanical properties of the base metals and their influence on the serviceability of the joint may be considered. When dissimilar materials are joined by fusion welding processes, alloying between the base metals and a filler metal, when used, becomes a major consideration. The resulting weld material can behave far differently from one or both base materials during subsequent processing or in service<sup>21</sup>. The principal factors that are responsible for failure (cracking), and which greatly influence joint integrity of dissimilar material joining are composition and the properties of the base metal, melting temperatures, thermal conductivity and the coefficient of thermal expansion<sup>21</sup>.

### **2.8.1 Friction Stir Welding of dissimilar materials**

Sound joints between dissimilar materials enable multi-material design methodologies and low cost fabrication processes to be employed. As no filler materials are used, the formation of intermetallic compounds is dependent on the interaction of the joining materials and the welding parameters<sup>16, 120-122</sup>. Many emerging applications in power generation and the chemical, nuclear, aerospace, transportation and electronics industries have led to the joining of dissimilar materials by different joining methods - especially friction welding and friction stir welding<sup>123</sup>. Due to the different chemical, mechanical, and thermal properties of materials, dissimilar metal joining presents more challenging problems than the joining of similar materials.

One of the questions that needs further investigation in FSW of dissimilar materials is which material should be at the advancing or the retreating side during the welding procedure, and where should the tool pin be displaced in order to produce a defect-free weld? Some reports on FSW of dissimilar materials have always placed the material with the higher melting point on the advancing side, with the entire tool pin being placed in the material with the lower melting point<sup>13,124</sup>.

### **2.8.2 Friction Stir Welding of Aluminium Alloys and Copper**

From a joining point of view, aluminium and copper are incompatible metals, because they have a high affinity for each other at temperatures higher than 120°C, and they produce hard, brittle, low strength and high electrical resistance intermetallics on their interface<sup>125</sup>.

Attempts have been made to join aluminium to copper using solid-state welding processes other than FSW. These include: ultrasonic energy welds<sup>126</sup>, magnetic pulse welding<sup>127</sup>, laser welding<sup>128-129</sup> and soldering<sup>130</sup>. Successful welds were made, but all were characterised by the presence of intermetallic compounds, which were observed to increase the electrical resistance at the joints.

A comparative study conducted by Murr *et al.*<sup>131</sup> on the FSW of two dissimilar metal welds i.e. AA1100/6061 and AA6061/Cu 6 mm thick, reported that in the dissimilar joints of aluminium alloys, the weld zones' microstructures represent some degree of dynamic recrystallization, while the dissimilar aluminium/copper system had a more complex microstructure. The feature observed is indicative of a specific stirring sequence, which influences the actual weld contiguity. However, the details of these phenomena were unknown, and the Vickers microhardness profiles observed were low at the weld zones. From all of the above, they concluded that additional work is required for further investigation and observation.

Further work by Murr *et al.*<sup>132</sup> on intercalation vortices and related microstructural features in the friction stir welding of dissimilar metals of AA2024/6061 and AA6061/Cu 6 mm thick, were FS welded at various rotational and transverse speeds. They observed that the mixing or vortex-like intercalation at the aluminium / copper weld zone is a manifestation of the solid-state flow, which is facilitated by dynamic recrystallization noticed in the welds. However, these are preliminary studies of FSW of aluminium/copper systems, as only microstructural evaluation and tensile testing was conducted.

Research work on microstructural evolution in the friction stir welded 6061 aluminium alloy to copper, 12.7 mm thick was conducted by Ouyang *et al.*<sup>123</sup>. They found that it is difficult to weld 6061 aluminium to copper due to the brittle nature of the intermetallic compounds formed in the weld nugget. It was observed that the majority of the welds exhibited a considerable discontinuity and crack propagation, and could thus not be considered as good welds. There was a fluctuating hardness in the weld nugget, and this is related to the different microstructures of intermetallic compounds and material flow patterns. They concluded that the mechanically mixed region in the dissimilar weld consists mainly of several intermetallic compounds. As this was a feasibility study of joining aluminium alloy to copper, only microstructural analysis and microhardness measurements were conducted and no process window was established.

Savolainen *et al.*<sup>112</sup> conducted a preliminary study on FSW of dissimilar joints of copper and aluminium. Oxygen-free electrolytically refined copper (Cu-OF) and aluminium alloy EN-AW 6060 10mm thick, were used in the research work. The varied parameters were rotation and transverse speeds and welds were made by changing the positions of the material. It was reported that better welds were produced with copper on the advancing side and the tool was displaced to the copper side. No report was made on the position of the tool at the centreline or in the aluminium. According to SEM studies, they noticed that the welds cracked through layers of intermetallic compounds. Other characterisations conducted were microhardness profiling, tensile testing and electrical resistivity measurement.

The hardness measurements showed a high variation in the weld nugget. The tensile test results showed that the Ultimate Tensile Strength (UTS) of the welds were between 110-150 MPa and the electrical resistivity measurement of the weld considered was 2.5% higher than the average resistivity of both materials. However, Savolainen *et al.* gave some insights into the FSW of aluminium/copper system, and suggested further work on how the formation of the banded intermetallic compounds formed could be minimised. However, further work is required to find the optimal welding parameter window. A wide range of process parameters is required to produce welds - in order to achieve welds with limited or no formed intermetallic compounds.

Microstructure and XRD analysis of FSW joints for copper T2/aluminium 5A06 3mm thick dissimilar materials was conducted by Liu *et al.*<sup>83</sup>. Some of the welds were made by varying the rotational and transverse speeds. Microstructural analysis indicated that the copper and aluminium close to the copper side in the weld nugget zone showed a lamellar alternating structure; the XRD analysis indicated the presence of Al-Cu intermetallics in the weld nugget zone. As a result, the structure of the weld nugget zone was mainly a plastic diffusion combination of aluminium and copper; the tensile strength of the FSW joints was also measured, and it was observed that they all fractured on the copper side of the weld nugget zone. This research also focused only on microstructural evaluation and tensile tests of the welded samples. According to Braunovic and Alexandrov<sup>113</sup> in their research study on the effect of intermetallic compounds of aluminium and copper on electric current, they reported that joints maintain their electrical and mechanical properties when the thickness of the intermetallic compound layer is less than 2  $\mu\text{m}$ .

However, it is quite difficult to achieve defect-free friction stir welds for a dissimilar aluminium / copper joint, in that there is usually a large void formation, cracks and other distinct defects throughout the weld<sup>131</sup>.

## 2.9 Summary

The literature review featured the basic background of the FSW process, with key interest in welding dissimilar materials. Recently, dissimilar joining by FSW has received attention-as a result of various promising applications. These have stirred up the interest of researchers into FSW of copper, steel and titanium to aluminium alloys.

The 5754 aluminium alloy, belonging to the 5000 series was chosen in this research work, because this alloy has good workability, very good corrosion resistance, weldability, moderate strength and good electrical conductivity. It is readily available in the market and is used in aircraft fuel/oil lines, fuel tanks, other transportation areas, sheet metal work, appliances and lighting, wire, and in rivets. The commercially available pure copper C11000 was also chosen, because it has a high thermal and electrical conductivity and is readily used in electrical applications.

In the optimisation of the FS butt weld processing of Al and Cu for the particular tool geometry used in this research work, alloy and plate thickness lies in the optimisation of the rotational speed and feed rate. Other parameters, such as the plunge depth, pin displacement, tool tilt and the dwell time will be kept constant for the final test matrix. These parameters will be carefully chosen through observation and analysis of the weld quality of the preliminary welds.

In an attempt to achieve the best result and to validate the mechanical and electrical properties of the welded samples compared with the base materials, microstructural evaluation and hardness values will be used at the preliminary stage to evaluate the welds, and these will be repeated on the samples of the final matrix. The positions of the workpieces and the tool displacement during the welding procedure will be further investigated and optimised at the preliminary stage of the work. Microstructural evaluation of the welded samples will be studied to identify the different FSW zones, determine and compare precipitate formation; and the intermetallic compounds formed at the joint interface. Tensile tests will be conducted to evaluate the weld joint efficiencies of the welds.

The electrical resistance of each parameter setting will be measured and compared with the average joint resistance of the base materials to ascertain the joint integrity. The results will be related to the heat input and the formed intermetallic compounds at the joint interface, as they are known to be thermally activated. The XRD analysis of the joint interface will be conducted and the diffractograms of the welds will be compared to that of the parent materials to identify the formed intermetallic compounds and ascertain the joint integrity of the welds.

The reviewed literature indicates that aluminium and copper are difficult to weld with conventional welding processes due to their high affinity and thermal conductivity. Brittle intermetallic phases develop in the joint zone, since copper and aluminium are not very soluble in one another in the solid state. These intermetallic phases lower the toughness of the weld and lead to cracks during and after welding. In this research work, excessive formation of brittle intermetallic phases will be significantly reduced, due to the high cooling rates and lower fusion temperature of the FSW process.

It should be noted that little literature is available on the FSW of aluminium and copper. Recent papers are based on preliminary studies, most of which focused on microstructural evaluation, only a few on mechanical testing. The measurement of electrical properties, which is of high importance to the electrical / electronic industries in terms of applications of aluminium and copper, is inadequately researched and reported, and there is no existing report on the detailed characterisation of FSW between Al / Cu. In this research study, a process window to join both metals will be established, using a matrix of nine combinations of the process parameters, using three shoulder diameter tools. It is also expected that welds with limited or no intermetallics will be produced, considering the wide range of process parameters employed.

A review of the literature related to this research project has been fully discussed in this chapter. The next chapter will focus on the experimental set-up procedures employed in the course of this research study.

## CHAPTER 3 EXPERIMENTAL TECHNIQUES AND TEST MATRIX DETERMINATION

### 3.1 Introduction

This chapter reports the experimental techniques and the results of the preliminary tests conducted in order to determine the operational range of the Friction Stir Welding platform. All detailed experimental procedures and methods of analysis employed in this research work will be discussed. It also presents the laboratory evaluation conducted on the parent materials, the tool designs, and the positions of the work pieces during the welding process, weld defects observed and the final weld matrix design.

### 3.2 The FSW Platform

The FSW machine used to produce the welds is an Intelligent Stir Welding for Industry and Research (I-STIR) Process Development System (PDS) at the Friction Processing Research Institute of Nelson Mandela Metropolitan University, Port Elizabeth. The I-STIR PDS is a robust self-contained system that is capable of welding ferrous and non-ferrous materials. This platform is shown in Figure 3.1. The key sub-systems and the system specifications of the I-STIR PDS FSW platform<sup>133</sup> are both described in Appendices B1 and B2 respectively.

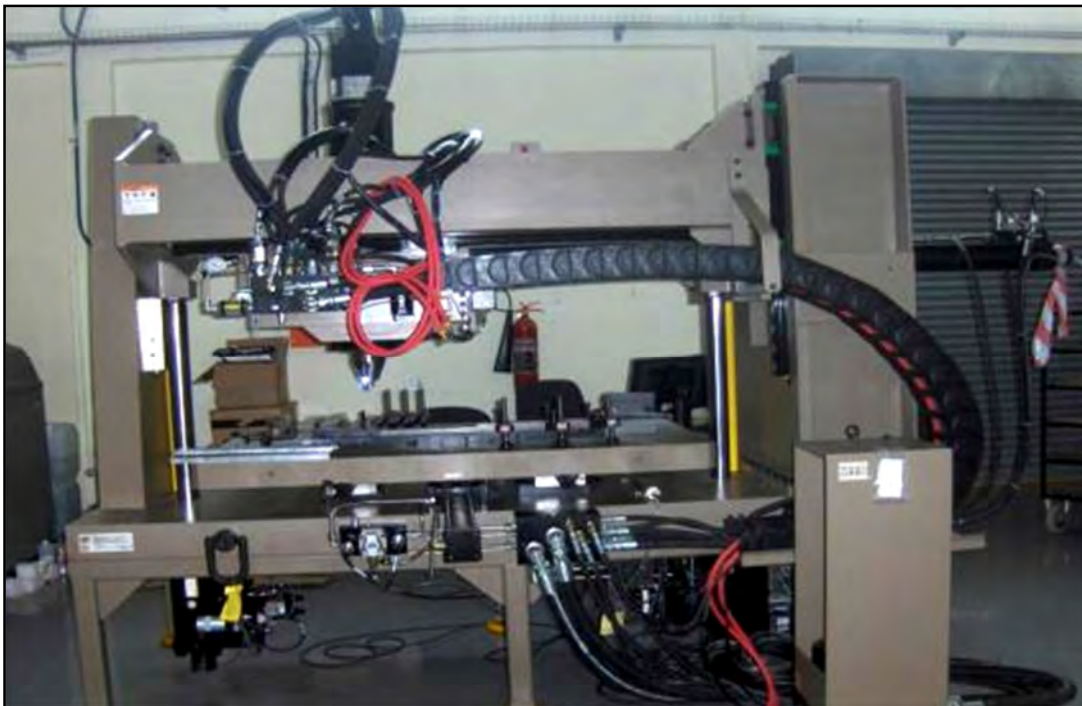


Figure 3.1: The I-Stir PDS FSW Platform

### 3.3 Backing plate and clamping system

Fixtures in FSW is usually the most complicated and critical aspect of the welding process. The work pieces must be clamped to a rigid smooth backing plate and secured to resist the perpendicular and side forces that develop during the welding process. These forces tend to lift and push the work pieces apart. Fixtures are designed to restrain the work pieces and keep them from moving apart. A root opening (gap) of less than 10% of the material thickness can be tolerated for thicknesses up to 13 mm<sup>134</sup>. The fixtures that hold the materials to the backing plate should be placed as close to the joint as possible to ensure that the work pieces are held in place during the welding procedure.

In order to effectively clamp the plates in position during welding, the clamping system of the I-STIR PDS FSW platform was used, and it was supported with flat bars machined with steps to accommodate the tool holder during welding, as shown in Appendix B3.

Common backing plates used in the literature include medium carbon steel and mild steel<sup>56</sup>. Figure 3.2 shows the backing plate and the clamping system prior to the welding process. The backing plate used in this research work is a mild steel plate of 25 x 650 x 265 mm bolted to the welding bed. The detailed drawing for the backing plate is presented in Appendix B4.

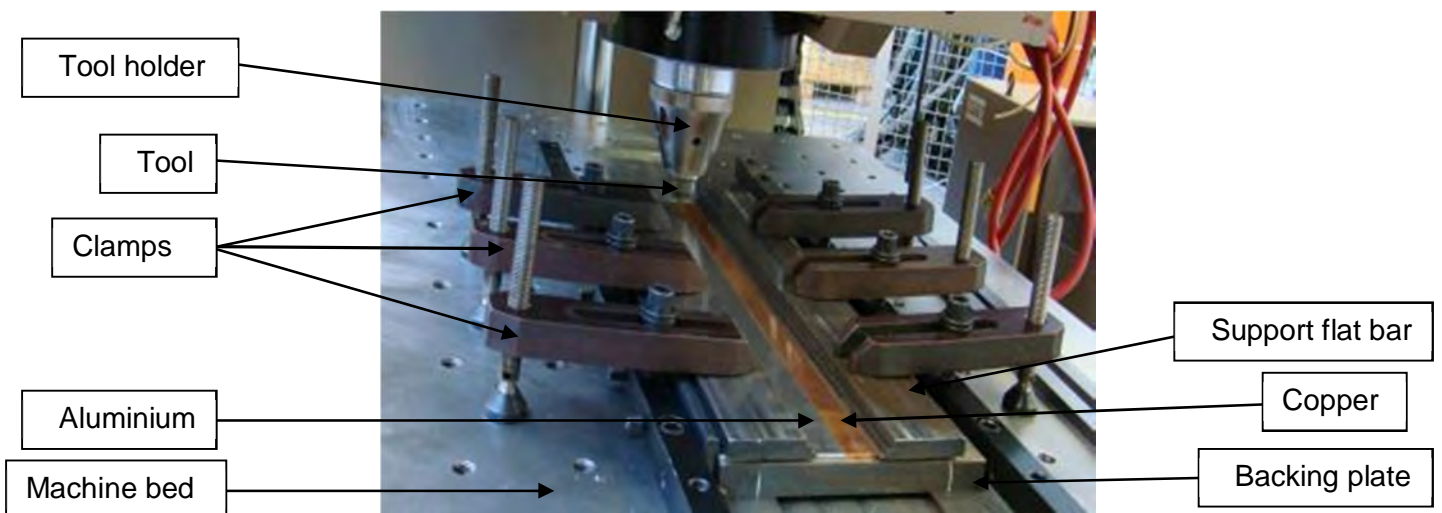


Figure 3.2: The backing plate and clamping system

### 3.4 The Welding Process

Before the actual welding process is conducted, a welding programme must be compiled. The welding programme panel provides the interface for creating and executing welding programmes. This programme defines the motion of the machine and the input process parameters when undertaking a welding process. These include the X, Y, and Z positions of the gantry, as well as the pitch orientation of the weld head assembly, pin and forge position, spindle speed, tool travel, plunge force, traversal force and X control mode. There are two types of modes on the FSW platform, viz the force control and the position control modes. In force control mode, a measured force from initial welds done in position control mode is programmed into the machine to produce the welds. In position control mode, input process parameters (rotational speed, traverse speed, plunge depth, dwell time and the tool tilt angle) are programmed into the system which predetermines the downward vertical force ( $F_z$ )<sup>135</sup>. The position control mode was chosen because the quality of preliminary welds under this mode resulted in vast variations in the downward force ( $F_z$ ) between the various preliminary welds and therefore an ( $F_z$ ) force could not be established as an input parameter for force control welding conditions. Plunge depth is determined by measuring the actual to tool pin length and considering the tilt angle the resultant value is entered into the operating program.

The welding programme is presented as a set of welding commands. When a welding programme is executed, it starts by moving the machine to the first command, and then executes the commands sequentially. The welding is completed when the last command has been executed. Appendix B5 presents a sample copy of the welding programme adapted for this research work.

The welding procedure utilised to produce the FS welds in this research work include:

- i. The weld head assembly is moved to the weld start position.
- ii. The spindle is rotated at the specified speed.
- iii. The tool is plunged into the work pieces at the joint line and allowed to rotate at this point for 2 seconds to obtain a sufficiently plasticized state. This is referred to as the dwell time.
- iv. The tool is then moved along the joint line in a horizontal position at a specified feed rate, and the weld seam is made.
- v. The pin is extracted from the work pieces.

- vi. The weld head assembly is then moved to the initial starting position.

The welding procedure stated above is conducted using the remote station control pendant. Several measures were taken to ensure consistency in the welds. Firstly, the plates were cleaned with Silicon Carbide paper to remove the oxide layer; and then they were cleaned with acetone; and secondly, the acceleration was kept constant for all the welds. To ensure the reproducibility of the welds, the following was done: the tool holder and the tool were cooled to room temperature using compressed air after every weld. This cooling was done to prevent the tool from preheating the next weld. The deposited material on the tool pin and shoulder was cleaned - either by soaking in a solution of 20g of Sodium Hydroxide (NaOH) and 100 ml of water for about four hours or by remachining.

### 3.5 Tool designs for the FSW of Al / Cu

As mentioned in the literature review, tool design in FSW is an important parameter which influences the heat generation, plastic flow, joint integrity and the resulting microstructure and mechanical properties of the welds<sup>6,23,56</sup>. An extensive review of the related literature indicates a scarcity of detailed information relative to tool design for the FSW of Al/Cu 3 mm sheet. The approach taken during the design stage of this research used a shoulder-to-pin ratio of between 2.5 to 1 and 3.0 to 1. This was based on the work of Dawes *et al.*<sup>136</sup> and Hua<sup>137</sup>.

Tool designs A to C given in Table 3.1 were designed in a sequential manner, as the research work progressed. The dimensions and features of these tools are also presented in Table 3.1; and Appendix B6 illustrates the detailed tool drawings. The tools were machined from H13 tool steel (W302) and then heat-treated to 52 HRC, according to the stipulated procedures<sup>56</sup>.

**Table 3.1: FSW Tool designs, dimensions and features**

Dimension	Tool designs		
	A	B	C
Pin $\phi$ (mm)	4,8	4,8	5,0
Pin Length (mm)	2,8	2,8	2,8
Shoulder $\phi$ (mm)	12	12	18
Features	Threaded pin and concave shoulder	Unthreaded pin and concave shoulder	Threaded pin and concave shoulder

It is a common practice to use the cooling head when welding high melting point metals<sup>138</sup>. Tool design 'A' was used with the cooling head tool holder to produce the initial welds in order to achieve cooling during the welding process based on the high melting temperature of Copper (1085°C). Due to the resultant excessive vibration of the machine during the welding process probably resulting from the higher forging pressure required to join dissimilar materials, the head had to be changed to the one without the coolant, in order to avoid machine breakdown. Therefore, all further welds produced in this research work were made without the cooling head (see section 4.2).

### 3.5.1 Initial weld

Tool design 'A' was used to make bead-on-plate welds on the AA and Cu sheets respectively, using varying process parameters. The AA gave a good top surface appearance, with less flash at 500 rpm and 100 mm/min, and on the Cu sheets at 800 rpm and 100 mm/min, as shown in Figure 3.3 (a) and (b). These process parameters were based on successful Aluminium welds produced by Adamowski and Szkodo<sup>139</sup> and the FSW of Cu by Barlas and Uzun<sup>140</sup>.

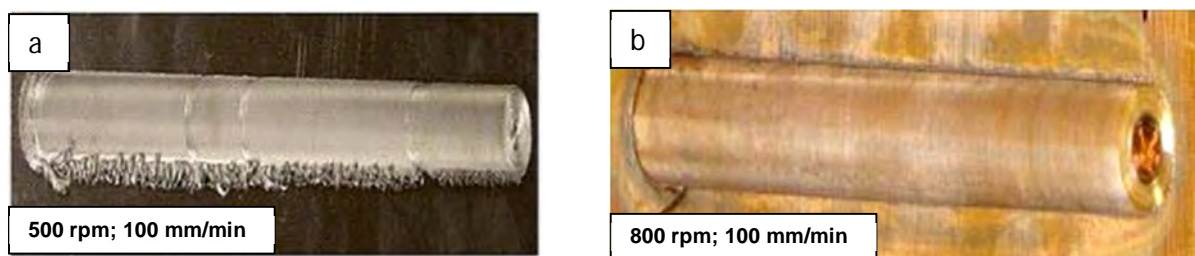


Figure 3.3: Bead-on-Plate (a) AA (b) Cu

The first trial weld of Al/Cu (Figure 3.4) was then made considering the process parameters used for bead-on-plate of Cu with the tool pin plunged at the weld centre line. This resulted in wormhole defects, which are visibly seen as elongated pores on the weld surface. Other welds produced using tool design 'A' at 950 rpm and 100 mm/min, and 1200 rpm and 100 mm/min also had wormhole defects, as shown in Figure 3.5 (a) and (b).

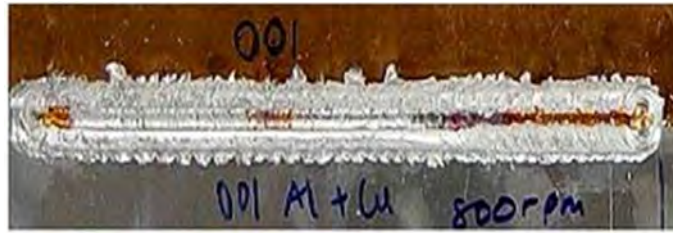


Figure 3.4: First trial FSW of Al / Cu produced at 800 rpm and 100 mm/min

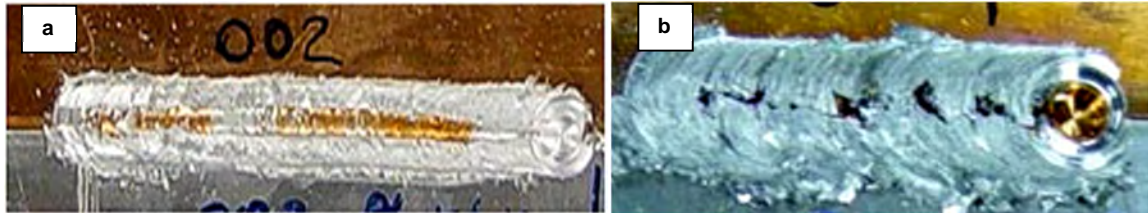


Figure 3.5: FSW Al / Cu with tool design 'A' at (a) 950 rpm and 100 mm/min (b) 1200 rpm and 100 mm/min

Reports have shown that unthreaded tools have been used to produce good welds in the joining of aluminium alloys<sup>64</sup>. Tool design 'B' with an unthreaded pin feature but the same outer dimensions as tool design 'A', was then machined and used, but the wormhole defect was still evident, as shown in Figure 3.6 (a) and (b).

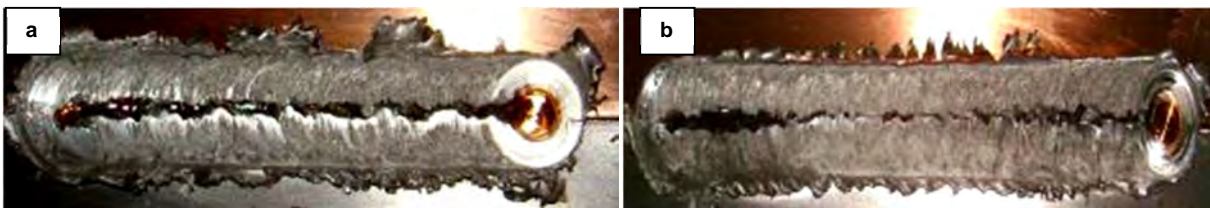


Figure 3.6: FSW Al/Cu with tool design B at (a) 800 rpm and 100 mm/min (b) 1200 rpm and 100 mm/min

It was apparent from the reviewed literature that these tools' effective shoulder diameters were too narrow to adequately heat and confine the plasticised material<sup>56,63-64</sup>. Therefore, the shoulder diameter was increased from 12 to 18 mm and tool design 'C' was produced, in an attempt to eliminate the wormhole defect. Welds produced with this tool resulted in defect-free welds, i.e. the wormhole defect was eliminated (Figure 3.7 (a) to (d)). The tool pin in the Cu configuration was employed to produce all these welds.

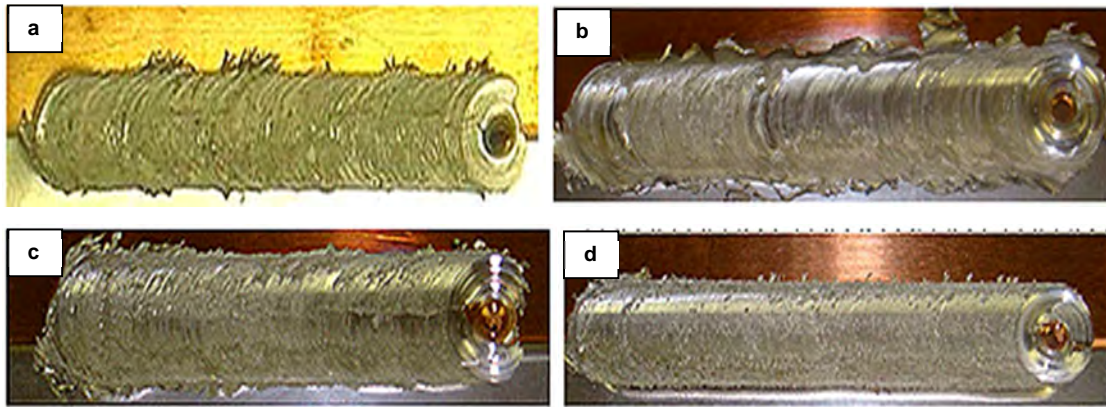


Figure 3.7: FSW Al/Cu with tool design 'C' at (a) 800 rpm and 100 mm/min (b) 1200 rpm and 100 mm/min (c) 950 rpm and 100 mm/in (d) 950 rpm and 300 mm/min

Tool designs 'A' to 'C' presented in Table 3.1, were used to make all the preliminary welds, and designs 'D' to 'F' presented in Table 3.2, were used to produce the final weld matrix. The three shoulder diameter tools were chosen to have varied welding conditions viz: cool, medium and hot. These varied welding conditions were expected to influence the formation of intermetallics, as they are known to be thermally activated. Appendix B7 indicates the detailed tool drawings.

Table 3.2: FSW tool designs, dimensions and features

Dimension	Tool designs		
	D	E	F
Pin $\phi$ (mm)	5,0	5,0	5,0
Pin Length (mm)	2,6	2,6	2,6
Shoulder $\phi$ (mm)	<b>15</b>	<b>18</b>	<b>25</b>
Features	Threaded pin and concave shoulder	Threaded pin and concave shoulder	Threaded pin and concave shoulder

### 3.5.2 The use of Magnesium Oxide (MgO) as a refractory layer

Observations during the preliminary work revealed frequent shearing of the pin during the welding process, as well as constant adherence of the welded plates to the backing plate. It was observed that during the welding process, the joint interface becomes hot and these results in heavy flash; the pin penetrates into the backing plate and is broken. This situation necessitated the introduction of the rubbing of Magnesium Oxide (MgO), (which forms a ceramic coating when dry) on the backing plate. However, EDS analysis indicated that the MgO was drawn into the weldment, as a result of the heat generated, and this resulted in a weak weldment<sup>141</sup>. Mashinini<sup>141</sup> found that welds produced with the MgO used as a

refractory layer have lower UTS compared to welds produced without the MgO. Therefore, the MgO was not used for the final weld matrix. Figure 3.8 shows the joint interface and the result of the EDS analysis. This was conducted using the Scanning Electron Microscope (SEM) on a weld produced with the 18 mm shoulder diameter tool at 1200 rpm and 150 mm/min. The EDS shows a high peak for Magnesium (Mg).

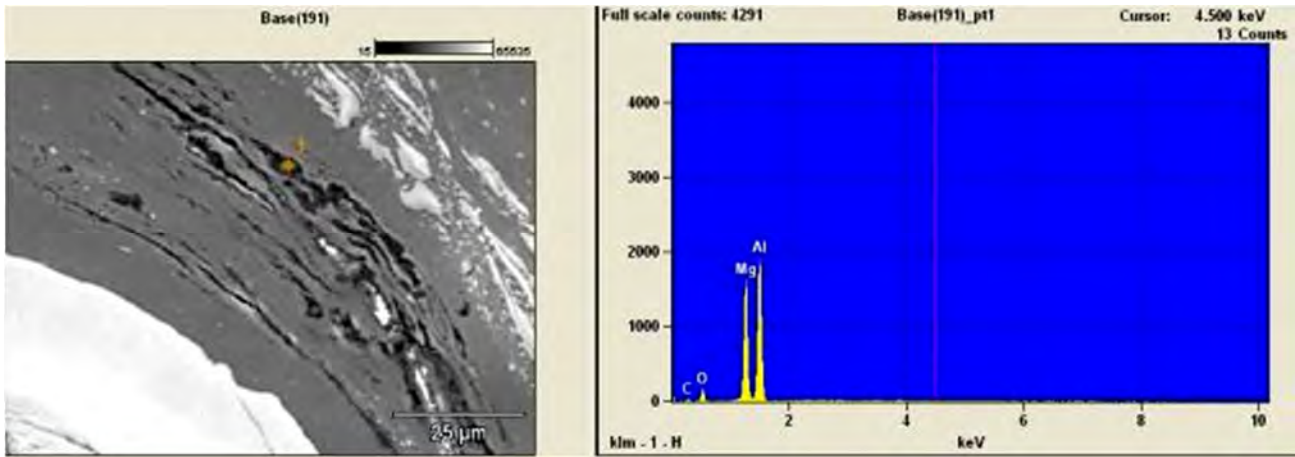


**Figure 3.8: Joint interface of FSW Al / Cu produced at 1200 rpm and 150 mm/min and EDS analysis result**

To avoid the shearing of the pin during the welding process, the pin length of the tools for the final weld matrix were reduced from 2.8 mm to 2.6 mm. The three different shoulder diameters viz: 15, 18 and 25 mm of designs 'D' through 'F' were chosen not only to optimise the process but also to be able to compare the heat inputs into the welds. This is based on the premise that the primary heating during the FSW process occurs from the shoulder periphery<sup>142</sup>.

In this research work, welds produced by varying the input process parameters using the different shoulder diameter tools will be characterised with respect to the heat input. They will then be related to the formed intermetallic compounds at the joint interface, because they are known to be thermally activated<sup>143</sup>.

### 3.6 The position of the work pieces during the FSW process

In FSW of dissimilar materials, the rotation direction (indicating which material should be on the advancing or retreating side) is significant due to the directional flow of the material during the process<sup>62-63</sup>. Limited published literature addresses the positions of the work pieces in the FSW of dissimilar materials. Uzun *et al.*<sup>13</sup> reported that the material with the

higher melting point should be placed on the advancing side during the welding process. This was further investigated in this research work by interchanging the positions of the work pieces. Welds were produced at the same input process parameters of 600 rpm and 150 mm/min. It was observed that better surface appearances were obtained in the welds produced with Cu on the advancing side, thereby substantiating the findings of Uzun *et al.* Welds produced with Cu on the retreating side showed wormholes throughout the weld length and heavy flash, as indicated in Figure 3.9.

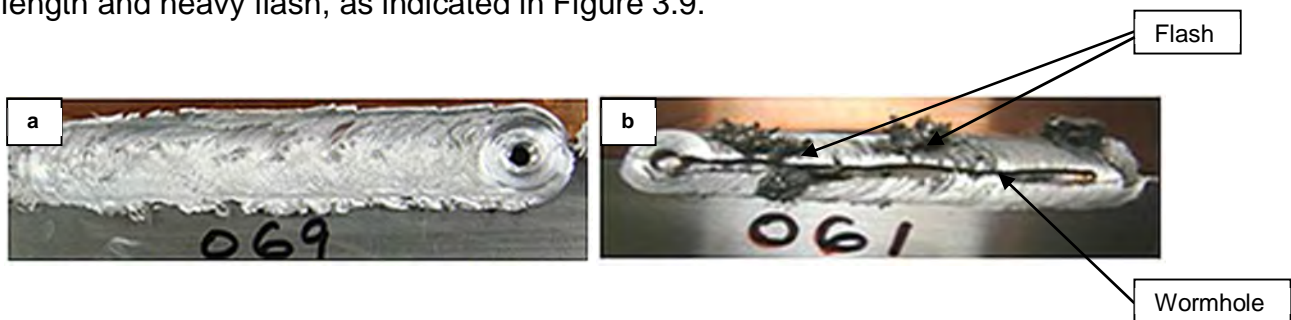


Figure 3.9: FSW Al/Cu at 600 rpm and 150 mm/min (a) Cu on the advancing side (b) Cu on the retreating Side

### 3.7 Optimisation of the FSW process parameters

In order to achieve quality welds in FSW, the process parameters have to be optimised<sup>19, 70</sup>. Based on the existence of limited information relative to FSW Al / Cu, 91 preliminary welds were made to optimise the process parameters in this research work. The table of the preliminary weld matrix is attached in Appendix B8. The welds were sectioned and investigated through microstructural evaluation. Each parameter was studied separately employing the following approach:

#### 3.7.1 Spindle speed

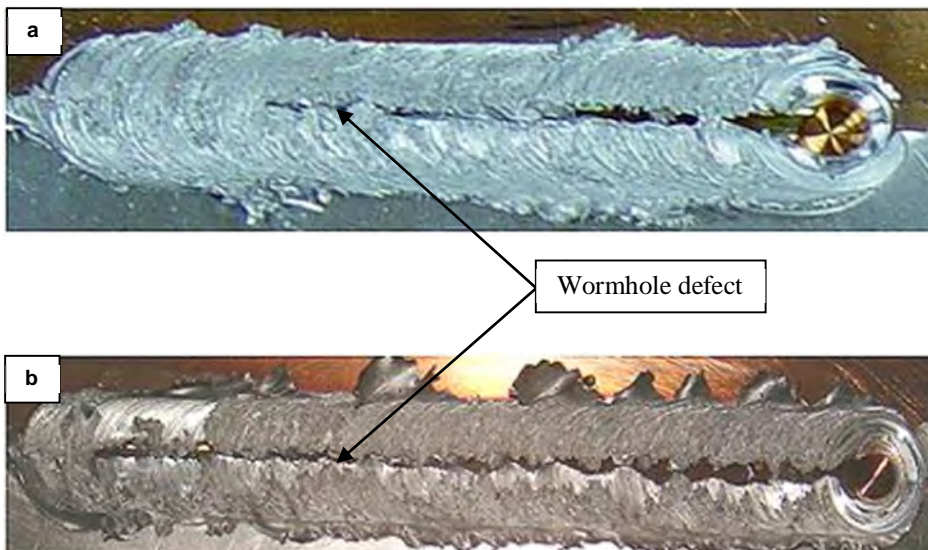
Spindle speeds of 600, 700, 800, 900, 950, 1200 and 1500 rpm were investigated. It was observed that the FSW platform vibrated excessively at spindle speeds lower than 600 rpm, and all the welds produced at 1500 rpm had wormhole defects. Therefore, the lowest and the highest spindle speed values were chosen as 600 and 1200 rpm, respectively. The rotational speed between the low and high setting was chosen as 950 rpm. Consequently, the three rotational speeds representing the low, medium and high settings in the final weld matrix were 600, 950 and 1200 rpm respectively.

### 3.7.2 Traverse speed

The traverse speeds used in the preliminary welds were 50, 100, 150, 200, 250, 300 and 350 mm/min. The minimum traverse speed that caused minimal machine vibration was 50 mm/min, while the maximum speed where no weld defect was observed was 300 mm/min. The three speeds chosen to represent low, medium and high speeds were 50, 150 and 300 mm/min respectively.

### 3.7.3 Tool displacement

Tool displacement (linear) has a significant effect in the FSW of dissimilar materials<sup>124</sup>. This was further investigated in this research work. Welds were made by varying the traverse speed and the rotational speeds, while other parameters, viz: the tool tilt angle, the dwell time and the effective plunge depth, were kept constant. Copper was placed at the advancing side during the welding process. Welds produced with the tool pin plunged in (1) Cu, (2) at the weld centre line, and (3) in the AA are presented in Figure 3.10 (a) – (c). Welds produced with the tool pin plunged in Cu, and at weld centre line, resulted in wormhole formation. An acceptable appearance without any defects was achieved with the tool pin plunged in the AA, as shown in Figure 3.10 (c).



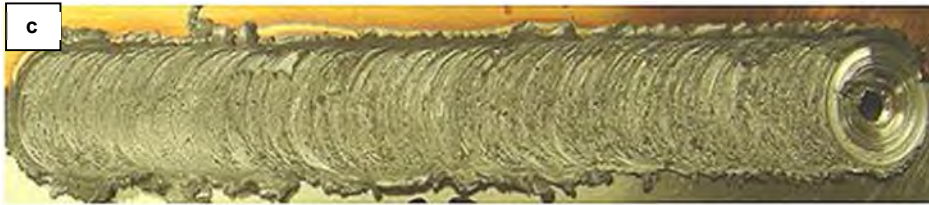


**Figure 3.10: Welds produced at 1200 rpm and 150 mm/min with the tool pin plunged in (a) Cu (b) at centreline (c) in AA**

Further examination of the metallographic cross-sections of the welds produced at the same input process parameters showed that metallurgical bonding and the mixing of both materials were achieved more effectively at the joint interface with the tool pin plunged in the AA, as presented in Figure 3.11 (a) to (c). Therefore, the final weld matrix used in this research work was produced with the tool pin plunged in the AA.

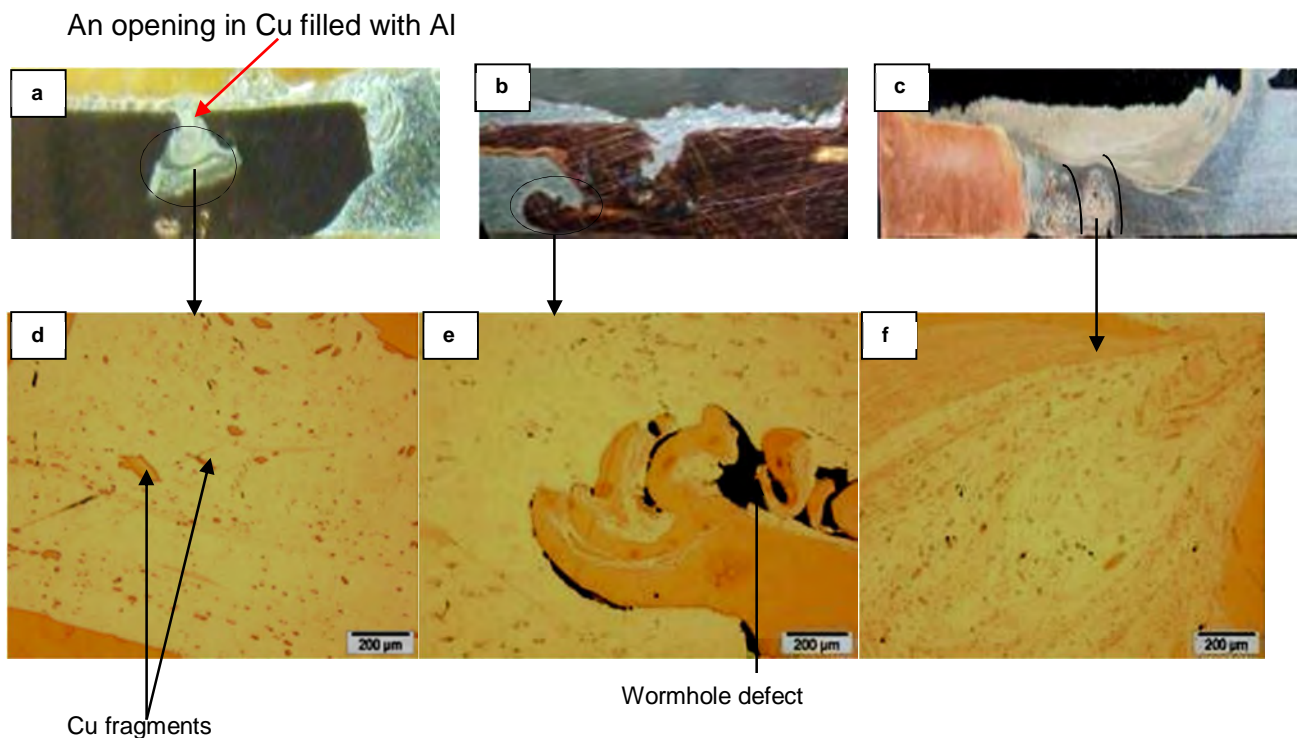


**Figure 3.11: Macro and micro-graphs of welds produced at 1200 rpm and 150 mm/min with the tool pin plunged in (a) and (d) Cu, (b) and (e) at centreline (c) and (f) in AA**

The resulting macrographs of the welds are discussed as follows:

- It was observed that in the welds produced with the tool pin plunged in Cu, (Figure 3.11 (a)), the Cu deforms at a slower rate compared with the AA due to its higher melting point; and it then moves towards the AA at the joint interface. The macrograph showed that during welding, there was an opening in the Cu (indicated

by the red arrow) filled with AA, with some copper fragments at the centre of the weld, as shown in the micrograph in Figure 3.11(d).

- When the tool pin was plunged at the weld centreline (Figure 3.11(b)), both materials deformed at different rates, due to the large difference in the melting temperatures of AA and Cu. Therefore, the stirring at the centre was not sufficient to achieve the required mixing, subsequent to the bonding of the materials; this then resulted in wormhole formation, as shown in the micrograph in Figure 3.11 (e).
- The resulting good top surface and better mixing achieved in welds produced with the pin plunged in the AA, (Figure 3.11 (c)), can be linked to the fact that AA with its lower melting point will deform plastically faster than copper. Hence, it deforms and mixes with Cu, and then fills the gap behind the stirring pin. Also, it was observed that no other critical weld defects were found in the weld.

#### 3.7.4 Dwell time

The dwell times used at the preliminary stage were 2, 5, and 10 seconds. It was observed that the 10 seconds dwell time was too long, because it resulted in heavy flash at the start of the welds. Five seconds dwell time resulted in welds with no visible defects when the pin was plunged in Cu. However, when the tool displacement was optimised and the pin was plunged in aluminium, significant flash was found at the beginning of the weld using 5 seconds dwell time, hence, the dwell time needed to be optimized in order to eliminate the heavy flash. Therefore, the dwell time was reduced to 2 seconds, which gave less flash; and this dwell time was used for the final weld matrix.

#### 3.7.5 Tool tilt

Tilting the tool so that the rear of the tool is lower than the front, has been found to assist the forging process and the material flow during FSW<sup>4, 73</sup>. Welds were made by varying the tool tilt angles between 1 and 3<sup>o</sup>. The resulting weld top surface appearances are shown in Figure 3.12 (a) to (c). It was observed that at 1<sup>o</sup> tilt, the front end of the shoulder did not touch the material at the exit hole. As shown in Figure 3.12 (a) and at 3<sup>o</sup> tilt, there was significant flash. Therefore a 2<sup>o</sup> tilt, which gave a good weld without visible defect and less flash, was chosen for the final weld matrix.



Figure 3.12: Welds produced at 950 rpm and 100 mm/min with (a) 1° tool tilt (b) 2° tool tilt (c) 3° tool tilt

### 3.7.6 Plunge depth

At the preliminary stage of using designs 'A' to 'C', the plunge depths used were 2.6, 2.7, 2.8, 2.85, 2.9 and 2.95 mm. The plunge depths varied from one shoulder diameter to the other, because of the different sizes of the shoulder diameters used. From literature<sup>23, 142</sup>, it was reported that when the tool is tilted, it gives rise to a shoulder plunge,  $P$  as shown in Figure 3.13.

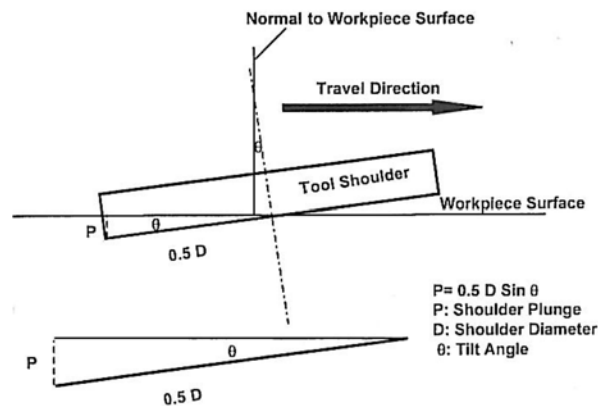


Figure 3.13: Shoulder plunge in FSW<sup>23</sup>

Shoulder plunge,  $p$  can be calculated as:

$$P = 0.5 D \sin \theta \quad 3.1$$

Where,

$P$  = Shoulder plunge

$D$  = Shoulder Diameter

$\theta$  = Tilt angle

The effective plunge depth is the sum of the nominal plunge depth and the shoulder plunge depth. The effective plunge depth used for the final weld matrix was 2.96 mm, as calculated below. The plunge rate is 5 mm/min and the position control setting was used to make all the welds.

For the 15 mm shoulder diameter tool, the shoulder plunge is:

$$P = 0.5 \times 15 \sin 2^\circ = 0.26 \text{ mm}$$

The nominal plunge depth used for welding was 2.70 mm,

The effective plunge depth = 2.70 mm + 0.26 mm = **2.96 mm.**

For the 18 mm shoulder diameter tool, the shoulder plunge is:

$$P = 0.5 \times 18 \sin 2^\circ = 0.31 \text{ mm}$$

The nominal plunge depth used for welding was 2.65 mm,

The effective plunge depth = 2.65 mm + 0.31 = **2.96 mm.**

And for 25 mm shoulder diameter tool, the shoulder plunge is:

$$P = 0.5 \times 25 \sin 2^\circ = 0.43 \text{ mm}$$

The nominal plunge depth used for welding was 2.53 mm,

The effective plunge depth = 2.53 + 0.43 = **2.96 mm.**

### 3.8 Final Weld Matrix

Based on the preliminary welds produced, the final weld matrix (3 x 3 x 3) comprised 27 welds (nine welds with each shoulder diameter). It should be noted that the weld settings were selected to represent the widest range of possible combinations within the FSW platform's limits, thereby avoiding excessive machine vibration. The rotational speeds of 600, 950 and 1200 rpm were chosen to represent low, medium and high (L, M and H) settings respectively, while 50, 150 and 300 mm/min were the feed rates considered representing low, medium and high (l, m and h) settings. A listing of the parameter combinations and their corresponding weld numbers are presented in Table 3.3.

Table 3.3: Final weld matrix using the 15, 18 and 25 mm shoulder diameter tools

Rotational Speed (rpm)	Feed rate (mm/min)	Alphabetical code
600	50	LI
600	150	Lm
600	300	Lh
950	50	MI
950	150	Mm
950	300	Mh
1200	50	HI
1200	150	Hm
1200	300	Hh

Where,

L = low rotational speed, l = low feed rate

M = medium rotational speed, m = medium feed rate

H = high rotational speed, h = high feed rate

### 3.9 Parent Materials

The parent materials used in the research work were 5754 Aluminium Alloy (AA) and C11000 copper. The dimensions of the test coupon for each plate were 600 x 120x 3.175 mm, as shown in Figure 3.14. The length of the welds produced was 160 mm.



Figure 3.14: Research test coupon

Evaluations conducted on each of the parent materials include:

### 3.9.1 Chemical analysis

The chemical compositions of the parent materials were confirmed, using a spectrometer; and these were found to be the same, according to the manufacturers' specifications. The copper was found to be commercially pure, and the aluminium is Al-Mg 5000 series. The spectrometric chemical analyses results are given in Appendix B9, while the material test reports are presented in Appendix B10.

### 3.9.2 Microstructure

In order to be familiar with the microstructure of the parent material, samples were prepared and etched; the micrographs are presented in Figure 3.15 (a) and (b). It was found that the grains in the aluminium are elongated, while those of copper were equi-axed, i.e. the aluminium was in the cold-rolled condition whereas the copper was in the normalized/annealed state.

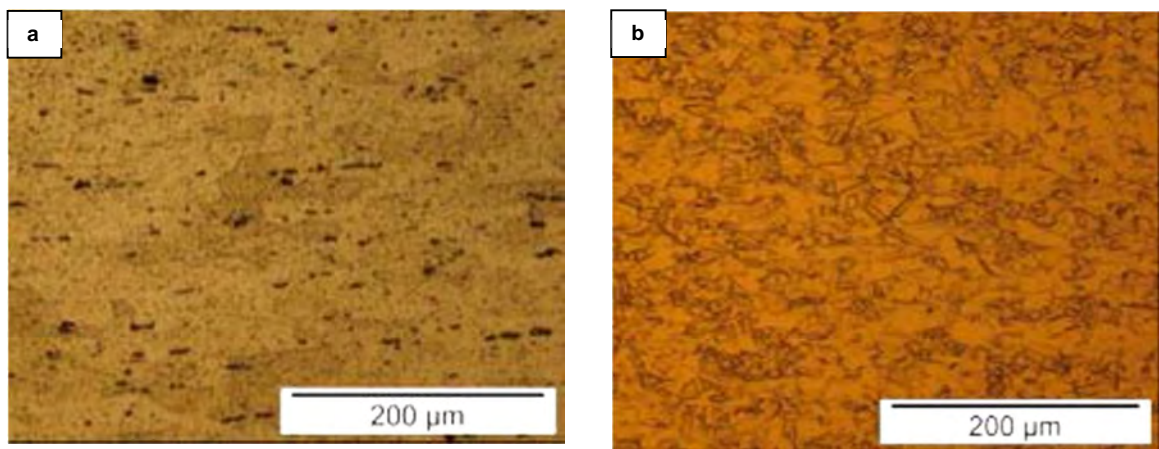


Figure 3.15: Microstructure of the parent materials (a) 5754 AA and (b) C11000 Cu

### 3.10 Specimen Layout

All the specimens for analyses were taken from prescribed locations along the weld, as shown in the layout in Figure 3.16. In order to eliminate the unstable effects during the starting and ending stages of the FSW process, specimens were taken from 22,5 mm, from the starting position up to 137,5 mm of weld length.

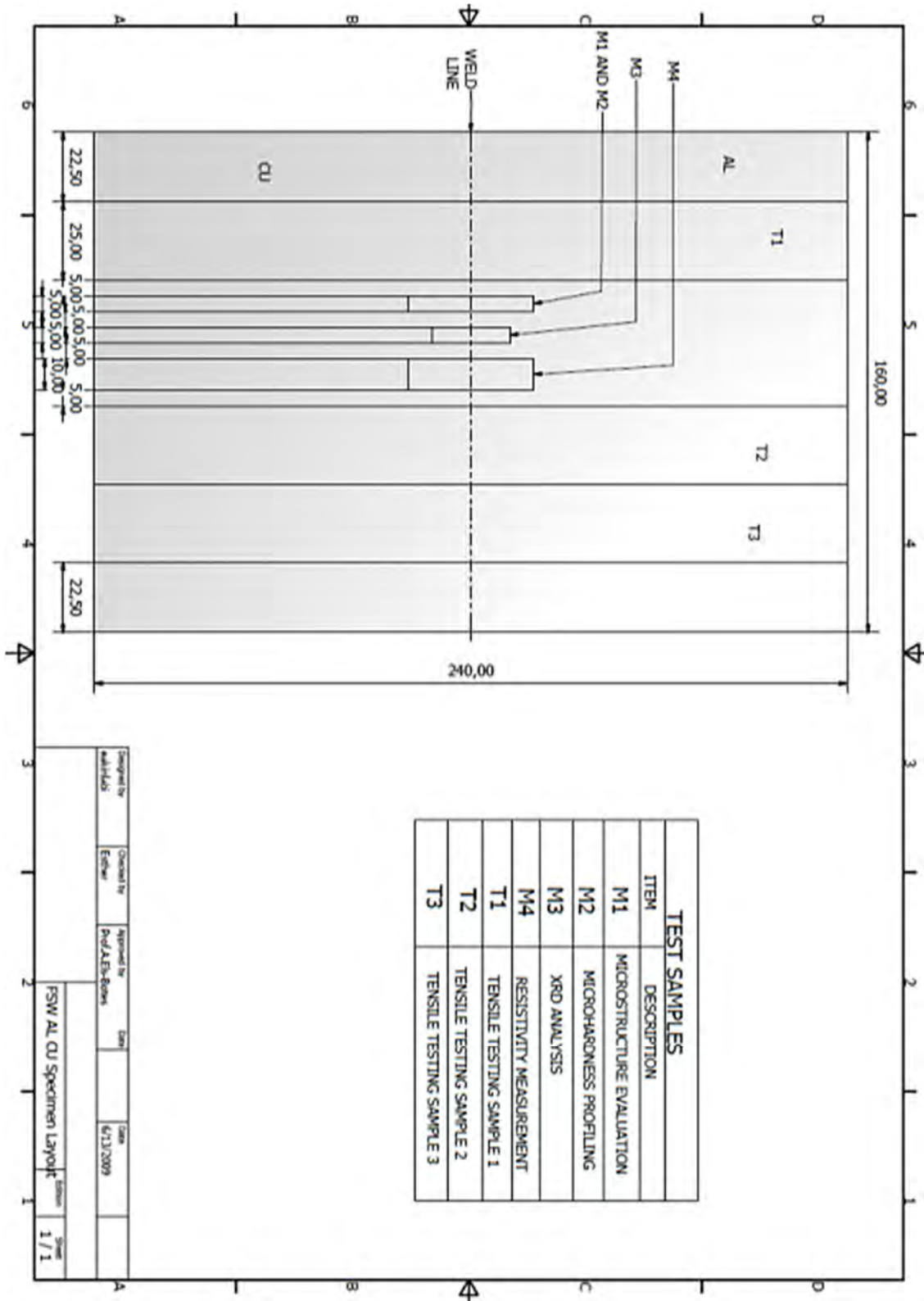


Figure 3.16: Layout of specimens

### 3.11 Material Characterisation

The welded samples were characterised by microstructural evaluation, mechanical testing, electrical resistivity and XRD analysis - in order to determine the weld joint integrity.

#### 3.11.1 Optical Microscopy

Samples of size 40 x 5 x 3.175 mm at the joint interface were sectioned and mounted in polyfast thermoplastic hot mounting resin. The samples were mounted such that the advancing side of the weld was always to the right. The mounted samples were prepared using standard metallographic procedures<sup>144-145</sup>, as presented in Appendix B11. At the initial stage of the work, the Al was etched with Flick's reagent and the Cu was etched with a solution of 100ml water and 10g ammonium peroxydisulphate but the grains were not visible, hence modified Poulton's reagent was used, its constituents are outlined in Appendix B11. Observations on the microstructures were performed using an Olympus PMG3 optical microscope.

The grain sizes of the FS welded microstructure zones were carried out, according to the standard test method for determining average grain size: ASTM E112 – 96<sup>ε1(146)</sup>. The Scanning Electron Microscope (SEM) was used to analyse the chemical composition of the phases at the joint interface, and also to quantify the chemical composition of the intermetallic compounds.

#### 3.11.2 X-Ray Diffraction Analysis

Samples of size 20 x 10 x 3.175 mm were sectioned, grinded and polished for the XRD analysis. The XRD was used to determine the presence of intermetallics and their possible compositions. The XRD analysis was carried out, using an X-ray diffractometer (Bruker D8 Advance), as shown in Appendix B12. It is equipped with standard Bragg-Brentano geometry, with Cu ( $K\alpha$ ) radiation and a Ni filter at the detector. The  $2\theta$  scan range was from 20 to 70° at 0.02 degree per step. The source and detector slit width were 1 mm and 0.2 mm respectively. The instrument was calibrated using a National Institute of Standard and Technology (NIST) alumina standard. The diffraction pattern results were compared with the standard Powder Diffraction Files (PDF), obtained from International Centre for Diffraction Data (ICDD)<sup>147</sup>.

### 3.11.3 Mechanical Characterisation

The mechanical property evaluations carried out on the welded samples are microhardness measurements and tensile testing. The Vickers microhardness profiles were measured using an FM-ARS 9000 automatic indenter, according to ASTM 384<sup>148</sup>. The measurements were made along the cross-sections of the welds at 1.5 mm below the surface, with a load of 200g and a dwell time of 15 seconds. The standard test method for Vickers microhardness of metallic materials recommends the use of 1 to 120 kgf load, the 200g used in this research study was based on literature<sup>143</sup>. The indentations were taken at 0.7 mm intervals in aluminium and 0.3 mm in copper. All the indentations were manually focused and read, to ensure that measurements were not made on weld defects. Measurements were taken in the as-polished condition. The tensile samples were tested, in accordance with ASTM E-8<sup>149</sup>. A servo-hydraulic Instron 8801 tensile testing machine was used to conduct the tests. An extension rate of 5 mm/min and a gauge length of 50 mm were used.

The Vickers microhardness of the parent materials was measured. It was found that the average Vickers microhardness values of 5754AA and C11000 Cu were 48 and 90 HV respectively. The tensile test results of the parent materials are presented in Table 3.4. The average Ultimate Tensile Strength (UTS) and the Standard Deviation (s) of the three samples tested are also presented.

**Table 3.4: Tensile test results of the parent materials**

Parent material	Ultimate Tensile Strength (MPa)			Mean UTS (MPa)	s (MPa)
	T1	T2	T3		
Al	266.0	266.0	266.4	266.1	0.23
Cu	243.0	246.0	243.0	244.0	1.73

Al – Aluminium.

Cu – Copper.

The data labelled T1, T2 and T3 represent the first, second and the third tensile samples taken from the parent plate. Based on the Standard Deviation, s, there was minor variation in the data. The dimensions of the test specimens for the parent materials and welded

samples are presented in Appendix B13. The tensile curves of the aluminium and copper parent materials are presented in Appendix B14.

### 3.11.4 Electrical Resistivity Determination

The resistivity of the joint was determined by means of a calculation derived from the measurement of electrical resistances across the welds (refer to Section 2.6.4 page 24). The sample size for the electrical resistance measurement was 40 x 10 x 3.175 mm. A Signatone (s-302-4) Four-Point probe meter with 1.6 mm probe spacing was used to measure the electrical resistance. The experimental set-up is presented in Appendix B15, and the circuit diagram is presented in Figure 3.17.

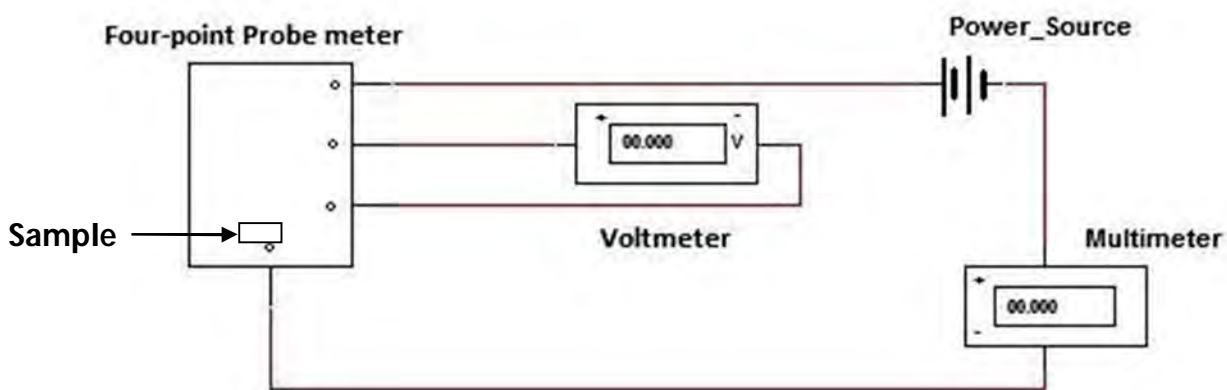


Figure 3.17: Circuit diagram of the electrical resistance measurement

The electrical resistance of the samples was measured, in accordance with the ASTM standard<sup>150</sup>. The Four-Point probe meter consists of two probes carrying the current, with the other two probes sensing the voltage. The probes are generally collinear, that is, they are arranged in-line with equal probe spacing.

## 3.12 Summary

Based on the preliminary investigations, other FSW input process parameters being kept constant in producing the final weld matrix, were the tool tilt angle at 2°, the dwell time at 2 seconds and the effective plunge depth of 2.96 mm. Copper was placed on the advancing side, and the tool pin was plunged in the Aluminium Alloy during the welding process. The position control mode was employed in producing the welds. The experimental set-up, the preliminary investigations conducted in this research project, and the decisions taken prior

to producing the final weld matrix have been presented and discussed. The next chapter reports the results and discussion of the twenty seven welds produced using the weld matrix.

## **CHAPTER 4 RESULTS AND DISCUSSION**

### **4.1 Introduction**

This chapter reports the results and provides a discussion on the welds produced using the final weld matrix, as presented in Chapter 3. The welds were produced using the position control mode and analysed through microstructural evaluation, tensile testing, microhardness profiling through the cross-section of the weld region, X-Ray Diffraction analysis and electrical resistance measurements. The results obtained are correlated to the process parameters used in producing the welds and will be used to formulate conclusions.

### **4.2 Inter-relationship between input and output FSW process parameters**

As discussed in section 2.3.2 (p.19), the spindle speed and the feed rate are known to have the most significant influence on the weld quality in FSW<sup>23</sup>; hence, they were the only input process parameters varied in this research study. Table 4.1 lists the weld numbers, the input parameters and the pitch for all the weld settings. The pitch is a ratio of the feed rate to the spindle speed of a weld. The pitch of the welds produced in this research work ranges between 0.042 and 0.5.

Table 4.1: Input process parameters of the welds

Weld No	Spindle speed (rpm)	Feed rate (mm/min)	Pitch (mm/rpm)
S15_01	600	50	0.083
S15_02	600	150	0.250
S15_03	600	300	0.500
S15_04	950	50	0.053
S15_05	950	150	0.158
S15_06	950	300	0.316
S15_07	1200	50	0.042
S15_08	1200	150	0.125
S15_09	1200	300	0.250
S18_01	600	50	0.083
S18_02	600	150	0.250
S18_03	600	300	0.500
S18_04	950	50	0.053
S18_05	950	150	0.158
S18_06	950	300	0.316
S18_07	1200	50	0.042
S18_08	1200	150	0.125
S18_09	1200	300	0.250
S25_01	600	50	0.083
S25_02	600	150	0.250
S25_03	600	300	0.500
S25_04	950	50	0.053
S25_05	950	150	0.158
S25_06	950	300	0.316
S25_07	1200	50	0.042
S25_08	1200	150	0.125
S25_09	1200	300	0.250

The output parameters i.e. Force, Torque and calculated heat input taken from an average of the recorded values of the data obtained during the welding procedure from 25 to 135 mm (stable region) of the weld length are presented in Table 4.2. The torque values reported are measured response values and the heat input was calculated using the formula 2.1, as given in section 2.3.5 (p.20).

Table 4.2: FSW output data obtained

Weld No	F <sub>x</sub> (kN)	F <sub>y</sub> (kN)	F <sub>z</sub> (kN)	Torque (kNm)	Q <sub>input</sub> (J/mm)
S15_01	2.11	-1.17	10.14	16.50	<b>1119.92</b>
S15_02	2.60	-0.04	13.87	19.97	451.69
S15_03	3.02	-0.90	17.94	23.63	289.86
S15_04	1.63	-1.04	6.97	8.59	<b>923.18</b>
S15_05	2.02	-0.27	10.67	12.09	432.83
S15_06	2.63	-0.67	12.25	13.12	219.31
S15_07	1.52	-0.76	7.45	8.01	<b>1087.67</b>
S15_08	3.14	-0.65	11.59	12.67	524.30
S15_09	3.54	-0.77	13.07	15.24	299.59
S18_01	2.87	-0.93	10.47	17.47	<b>1185.71</b>
S18_02	3.42	-0.60	14.27	20.96	474.02
S18_03	4.06	-0.09	18.53	26.20	296.37
S18_04	2.85	-0.72	11.56	12.80	<b>1374.86</b>
S18_05	3.12	-0.75	14.47	15.15	542.63
S18_06	3.47	-0.12	16.69	17.37	293.06
S18_07	2.26	-0.18	10.60	12.95	<b>1765</b>
S18_08	2.68	-0.23	12.51	15.12	683
S18_09	3.16	-0.01	14.91	17.44	405
S25_01	3.26	-0.08	20.94	25.51	<b>1731.02</b>
S25_02	3.90	-0.64	22.49	26.12	590.92
S25_03	3.99	-0.75	24.28	28.91	326.91
S25_04	2.33	-0.09	12.14	14.74	<b>1583.49</b>
S25_05	4.43	0.12	26.08	29.26	934.11
S25_06	5.20	0.26	32.24	36.74	577.29
S25_07	3.34	0.17	15.23	20.51	<b>2067.58</b>
S25_08	4.54	0.48	21.00	33.02	950.15
S25_09	5.91	-0.07	24.64	35.81	557.24

It was observed from the data obtained for all the weld settings that the advancing force (F<sub>x</sub>) and the torque (T) increase as the vertical downward force (F<sub>z</sub>) increases, while the heat input to the welds, (Q), decreases. Analysis of forces acting during the FSW process was conducted by Vilaça *et al.*<sup>151</sup>; in which the downward vertical force was related to the mechanical power delivered by the tool into the plates. They reported that both the advancing force and torque, and consequently, the total mechanical power delivered by the tool into the parts being welded, increased with an increase in the vertical downward force.

It should be noted that all the welds produced at the lowest travel speed of 50 mm/min (highlighted) have high heat input compared with the welds produced at 150 and 300 mm/min; this is because at low traverse speeds; the heat generated is high and is contained within the weld. With respect to the shoulder diameter of the tools employed, it was observed that the heat input using the 25 mm shoulder diameter tool is higher than that obtained when using the 15 and 18 mm shoulder diameter tools. This observation agrees with the report of Zhang *et al.*<sup>152</sup>. They reported that using the same pin diameter and varying the shoulder diameters, the numerical results indicated that the maximum temperature during the welding process may be increased with an increase in the shoulder diameter. It should be noted that the research study by Zhang *et al.* was conducted on similar metal welds. This trend was suspected, but needed to be confirmed for dissimilar metal welds taking into account the difference in the thermal conductivities of the two metals, i.e. 228 W/mK for Al and 369 W/mK for Cu at 300°C<sup>153</sup>. Further discussion on the inter-relationship of FSW process parameters and the joint properties using statistical analysis will be reported later in this chapter.

### 4.3 Macro appearances of the welds

#### 4.3.1 The effect of input process parameters on resulting macrostructures

The resulting macrostructures of welds are known to be greatly influenced by the heat input into the welds<sup>154</sup>. The estimated heat inputs into the welds were presented in Table 4.2. The macrographs of the representative samples with respect to the shoulder diameter tools and their corresponding input process parameters are presented in Figures 4.2 (a) to (c). The macrographs of all the 27 welds produced are presented in Appendix C1. The macrographs are characterised by mixture layers of Al and Cu.



Figure 4.2 (a): Macro appearance of weld produced with the 15 mm shoulder diameter tool at 950 rpm and 50 mm/min



**Figure 4.2 (b): Macro appearance of weld produced with the 18mm shoulder diameter tool at 950 rpm and 50 mm/min**



**Figure 4.2 (c): Macro appearance of weld produced with the 25mm shoulder diameter tool at 950 rpm and 50 mm/min**

Typical flow lines at joint interfaces, which are usually found in areas of layered material, indicates flow patterns during the welding process. These can be visibly seen in the macrographs of most of the welds produced (Figure 4.2 (a) and (b)). Flow lines are mixture layers of the two types of metals joined, showing the pattern of material flow during the FSW process. Good material flow during the welding process is synonymous with a good weld<sup>61-63</sup>.

It was observed that in welds S15\_05 (950 rpm and 150 mm/min), S15\_06 (950 rpm and 300 mm/min), S15\_09 (1200 rpm and 300 mm/min), S18\_06 (950 rpm and 300 mm/min), S18\_09 (1200 rpm and 300 mm/min), S25\_03 (600 rpm and 300 mm/min) and S25\_06 (950 rpm and 300 mm/min) that were produced at higher travel speeds of 150 mm/min and 300 mm/min, there were openings in the Copper, which were filled with the Aluminium Alloy during the welding process, as indicated by the red arrows, as shown in the Appendix C1. A representative sample is shown in Figure 4.3. This can be attributed to the fast movement of the tool at these speeds; and as a result, the frictional heat generated was not enough to achieve coalescence and proper mixing of both materials.



**Figure 4.3: Macro appearance of weld produced with the 18mm shoulder diameter tool at 950 rpm and 300 mm/min**

Although the resulting macrographs did not look like a typical FSW macrograph, the morphological feature viewed under the optical microscope consisted of all the FSW microstructural zones viz: the Stir Zone (SZ) or the Nugget Zone (NZ), the Thermo-mechanically Affected Zone (TMAZ), the Heat Affected Zone (HAZ) and the Parent material, as characterised by Threadgill<sup>79-81</sup>. A macrograph, showing the various FSW microstructural zones, viz the Stir Zone - SZ, Thermo-mechanically Affected Zone – TMAZ and Heat Affected Zone – HAZ in a typical weld produced at 950 rpm and 50 mm/min is shown in Figure 4.4.



**Figure 4.4: Macro appearance of weld produced with the 18 mm shoulder diameter tool at 950 rpm and 50 mm/min**

A Typical oval-shaped Stir Zone reported by Gould and Feng<sup>155</sup> that is often found in many FS welds, where extensive plasticisation of the materials has occurred, was seen in welds S15\_01 (600 rpm and 50 mm/min), S15\_04 (950 rpm and 50) and S18\_01 (600 rpm and 50 mm/min). A representative sample is shown in Figure 4.5.



**Figure 4.5: Macro appearance of weld produced with the 18mm shoulder diameter tool at 600 rpm and 50 mm/min**

Notably, these welds were all produced at a low traverse speed of 50 mm/min (high heat input), which supports the fact that better mixing is achieved at low travel speeds, as the material is then more plasticised, and therefore flows more easily.

Measurements of the SZ and TMAZ revealed that the size of the shoulder diameters influenced the widths of these zones in the welds. It was observed that the bigger the shoulder diameter, the wider the SZ and TMAZ. Typical macrographs of welds produced with the same input process parameters (600 rpm and 50 mm/min), but with different shoulder diameters indicating the widths of the SZ and TMAZ, are presented in Appendix C2. The data obtained are presented in Table 4.3.

**Table 4.3: Data obtained for microstructure zones for welds produced at 600 rpm and 50 mm/min.**

Sample	SZ+TMAZ (mm)	Compared to the pin $\phi$	% of the width compared to the shoulder $\phi$
S15_01	10.81	2.16 x pin $\phi$	72
S18_01	13.11	2.62 x pin $\phi$	73
S25_01	14.11	2.82 x pin $\phi$	56

As presented in Table 4.3, it was observed that the increase in the widths of the microstructural zones of the welds increases as the shoulder diameter increases; this can be attributed to the increase in the heat input into the welds which increases as the shoulder diameter increases. This further confirms the claim of Zhang *et al* which reports that the stirring zone of FS welds can be enlarged by an increase in the shoulder size using the same pin diameter. When the widths of the stir zones were compared to the pin diameter, it was also observed that the multiplying effect also increases as the shoulder diameter increases. It can be said that increasing the size of the stir zone is a function of the of the shoulder diameter.

#### 4.3.2 Weld defects

The defects identified in the welds using an optical microscope are classified according to Figure 2.5, p. 23. Typical samples showing the wormhole and root defect are presented in Figure 4.6 (a) and (b), respectively.

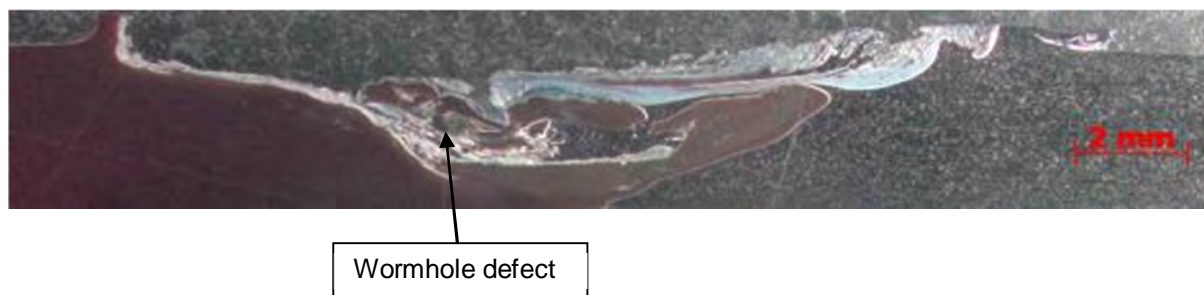


**Figure 4.6 (a): Macro appearance of weld produced with the 15mm shoulder diameter tool at 600 rpm and 50 mm/min with a wormhole defect**

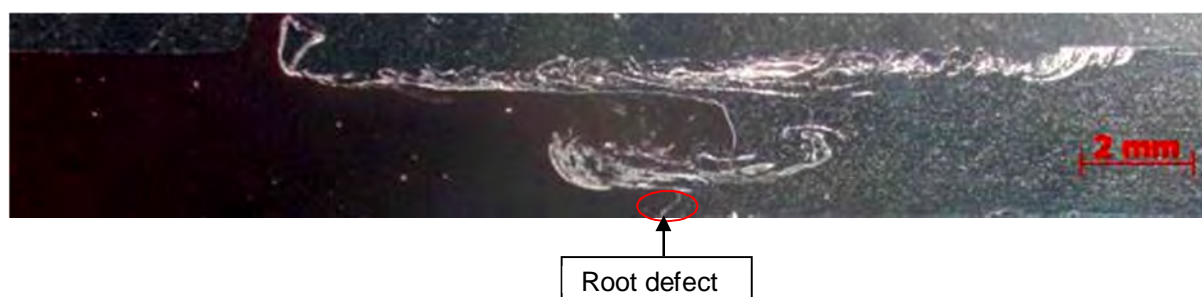


**Figure 4.6 (b): Macro appearance of weld produced with the 15mm shoulder diameter tool at 950 rpm and 300 mm/min showing root defect**

The weld defects characterisation of the joints produced are presented in Table 4.4.

**Table 4.4: Weld defects characterisation of welds produced with the 15, 18 and 25 mm shoulder diameter tool**

<b>Weld No.</b>	<b>Defect</b>
S15_01	Wormhole defect
S15_02	None
S15_03	Root defect
S15_04	None
S15_05	None
S15_06	Root defect
S15_07	Root defect
S15_08	Root defect
S15_09	None
S18_01	None
S18_02	Root defect
S18_03	None
S18_04	None
S18_05	None
S18_06	None
S18_07	None
S18_08	None
S18_09	None
S25_01	None
S25_02	Root defect
S25_03	Root defect
S25_04	None
S25_05	Joint mismatch
S25_06	None
S25_07	None
S25_08	Root defect
S25_09	None

Trends apparent from the weld defect data are hereby discussed. It is evident that only one setting (S15\_01) produced at 600 rpm and 50 mm/min resulted in a wormhole defect. At the preliminary stage of this work (Chapter 3), it was found that too small a shoulder diameter can result in the formation of wormhole defects in welds. It can be said that the 15 mm shoulder diameter tool used to produce this weld is too narrow to adequately confine the plastically deformed material; and hence, this resulted in wormhole formation. The joint mismatch defect that is observed only in S25\_05 (produced at 950 rpm and 150 mm/min), is due to the low clamping force on the work pieces, although all efforts were made to ensure that the plates were properly clamped before the welding process commenced.

The most common defect detected in the welds produced in this research work is root defects, which are found in an area at the bottom of the joint that is not joined (section 2.6.1, p. 23). This may be expected to occur, because the welds were produced with the tool pin raised 0.21 mm from the backing plate, to prevent the plates (after welding) from being stuck to the backing plate, a situation that was observed while making preliminary welds. The effective plunge depth used to produce the welds is 2.96 mm, while the plate thickness is 3.17 mm; hence, there was a difference of 0.21 mm at the bottom of the plates. The extent of the incomplete fusion regions was measured and found to be an average of 0.2 mm, which is 6% of the workpiece thickness. From the discussion above on defects observed in the welds produced using the three different shoulder diameter tools employed in this research work, it can be concluded that the most appropriate tool is the 18 mm shoulder diameter tool. This tool produced welds with the least amount of defects.

#### **4.3.3 FSW force feed back**

The FSW force feedback plots were evaluated and correlated to the resulting weld defects. Figure 4.7 (a) presents the force feedback plots for the weld with the highest UTS produced at 950 rpm and 50 mm/min with the 18 mm shoulder diameter tool; and Figure 4.7 (b) presents the force feedback of a weld with a low UTS produced at 950 rpm and 300 mm/min.

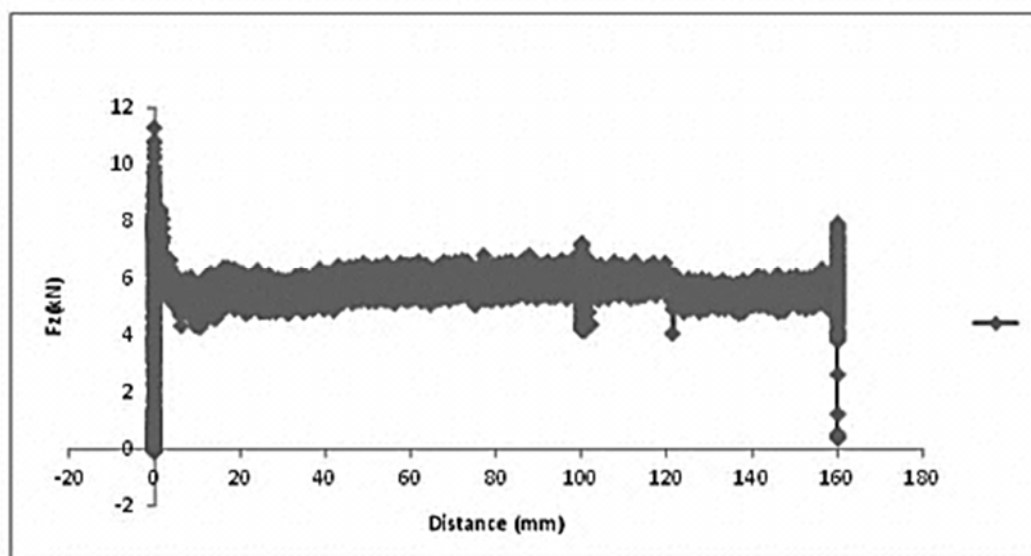


Figure 4.7 (a): Force feedback plot for weld produced at 950 rpm and 50 mm/min with 18mm shoulder diameter tool (Figure 4.4 shows the macro appearance through the cross section of the weld)

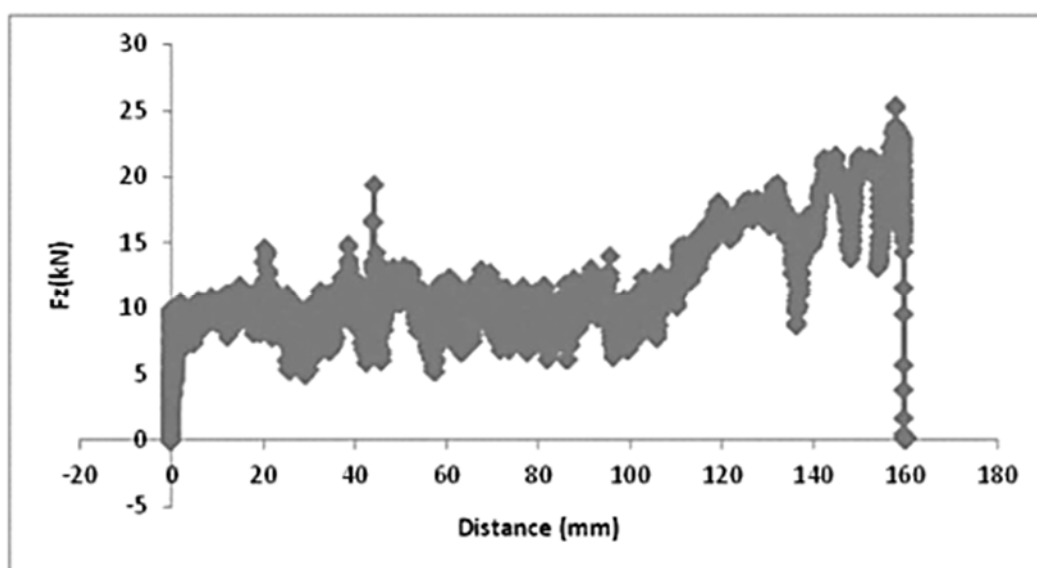


Figure 4.7 (b): Force feedback plot for weld produced at 1200 rpm and 150 mm/min with 25 mm shoulder diameter tool (Macro appearance is shown in Appendix C1, Figure h (S25\_08, p.167))

During the welding process, a high degree of variation in the downward vertical force ( $F_z$ ) was observed in the weld produced with the 25 mm shoulder diameter tool (1200 rpm; 150 mm/min) compared to the weld produced with the 18 mm shoulder diameter tool (950 rpm; 50 mm/min). Considering Figure 4.7 (b), the initial weld

length (first 100 mm) is considered to be fairly constant average Fz thereafter, the Fz shows a continuously increasing average trend up to 160 mm weld length which is considered by the author to be a poor quality weld as previously indicated. This is further substantiated by the observed weld defect (Table 4.4, p.62) and tensile results (Table 4.5, p.67).

## 4.4 Tensile Results

### 4.4.1 Tensile data of the welds

The tensile data of the welds produced using the 15, 18, and 25 mm shoulder diameter tools are presented in Tables 4.5 (a) to (c), respectively. The tensile samples were taken from different positions on the weld, and are designated as T1, T2 and T3 corresponding with the first, second and third samples respectively, as indicated on the specimen layout in Figure 3.10 (p. 51). The dimensions of all the samples tested are given in Appendix B13. The standard deviation of each weld setting was also calculated. The standard deviation is an estimate of the variability in the observed values. In industry, the 95% errors (3s) are commonly used to specify precisions required. The so-called three-sigma ( $3\sigma$ ) or (3s) error is often used as a criterion for rejecting individual observations. In a group of data, any value whose residual exceeds  $\pm 3s$  is considered out of range<sup>156-157</sup>. The average Ultimate Tensile Strength and the Standard Deviations of the weld settings were compared using equation 4.1 to determine which values were outside the three standard deviation range. It was observed that all the values are within acceptable range.

$$\bar{\sigma}_{UTS} \pm 3s$$

4.1

Table 4.5 (a): Tensile test results of the welds produced with 15 mm shoulder diameter tool

Weld No	Rotational Speed (rpm)	Feed rate (mm/min)	Ultimate Tensile Strength (MPa)			Mean UTS (MPa)	s (MPa)
			T1	T2	T3		
S15_01	600	50	156	100	146	134	29.8
S15_02	600	150	194	168	170	177	14.5
S15_03	600	300	195	215	166	192	24.6
S15_04	950	50	186	103	192	160	49.7
S15_05	950	150	153	219	201	191	34.1
S15_06	950	300	168	112	118	133	30.7
S15_07	1200	50	155	86	192	144	53.7
S15_08	1200	150	160	170	217	182	30.4
S15_09	1200	300	135	115	165	138	25.2

Table 4.5 (b): Tensile test results of the welds produced with the 18 mm shoulder diameter tool

Weld No	Rotational Speed (rpm)	Feed rate (mm/min)	Ultimate Tensile Strength (MPa)			Mean UTS (MPa)	s (MPa)
			T1	T2	T3		
S18_01	600	50	155	174	195	175	20
S18_02	600	150	168	152	132	151	18
S18_03	600	300	131	160	151	147	14.8
S18_04	950	50	229	187	209	208	21
S18_05	950	150	195	190	210	198	10.4
S18_06	950	300	141	182	105	143	38.5
S18_07	1200	50	214	202	197	204	8.7
S18_08	1200	150	131	190	198	173	36.6
S18_09	1200	300	134	166	198	166	32.0

Table 4.5 (c): Tensile test results of the welds produced with the 25 mm shoulder diameter tool

Weld No	Rotational Speed (rpm)	Feed rate (mm/min)	Ultimate Tensile Strength (MPa)			Mean UTS (MPa)	s (MPa)
			T1	T2	T3		
S25_01	600	50	156	170	158	161	7.6
S25_02	600	150	127	126	105	119	12.4
S25_03	600	300	126	154	123	134	17.1
S25_04	950	50	132	174	183	163	27.2
S25_05	950	150	159	195	180	178	18.1
S25_06	950	300	92	135	150	126	30.1
S25_07	1200	50	165	141	95	134	35.6
S25_08	1200	150	101	120	146	122	22.6
S25_09	1200	300	92	132	182	135	45

Although, all the tensile results are within the  $\pm 3s$  range, it was observed that some samples have low UTS which can be attributed to the presence of weld defects. These samples were further investigated by evaluating the fracture locations. They will be discussed later in this chapter.

A typical force / extension graph of a weld produced at 950 rpm and 50 mm/min using the 18 mm shoulder diameter tool showing ductile behaviour, is shown in Figure 4.8. The comprehensive graphical results (force-extension) of the individual weld are given in Appendix C3.

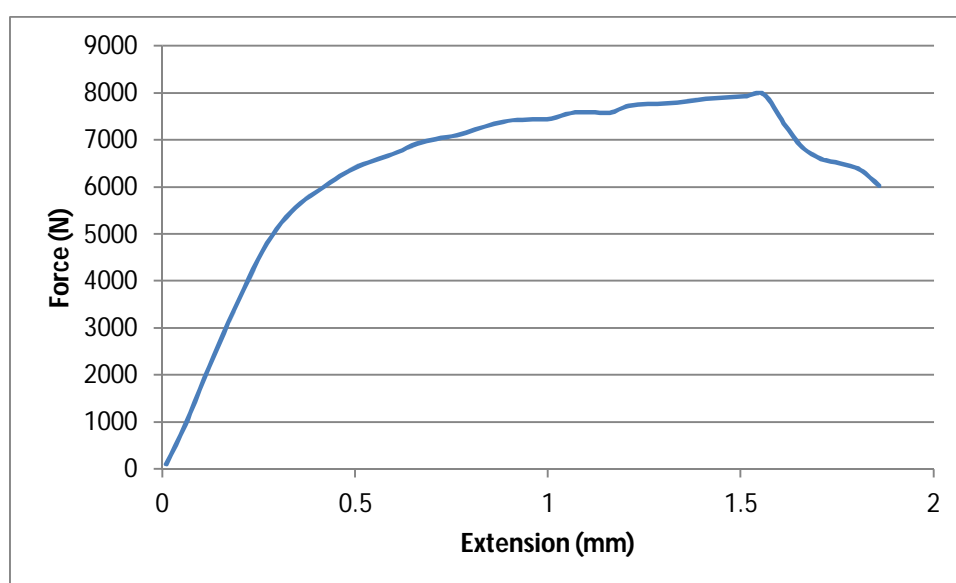


Figure 4.8: Tensile behaviour of FSW Al / Cu produced at 950 rpm and 50 mm/min

Amongst the three shoulder diameters evaluated in this research work, the tool with the 18 mm shoulder diameter (Table 4.5 (b)) produced welds with the highest average UTS of 208 MPa produced at 950 rpm and 50 mm/min.

From the data analyses of the tensile results, it was observed that at a spindle speed of 600 rpm using the 15 mm shoulder diameter tool, as shown in Figure 4.9 (a), the average UTS increases as the weld pitch increases.

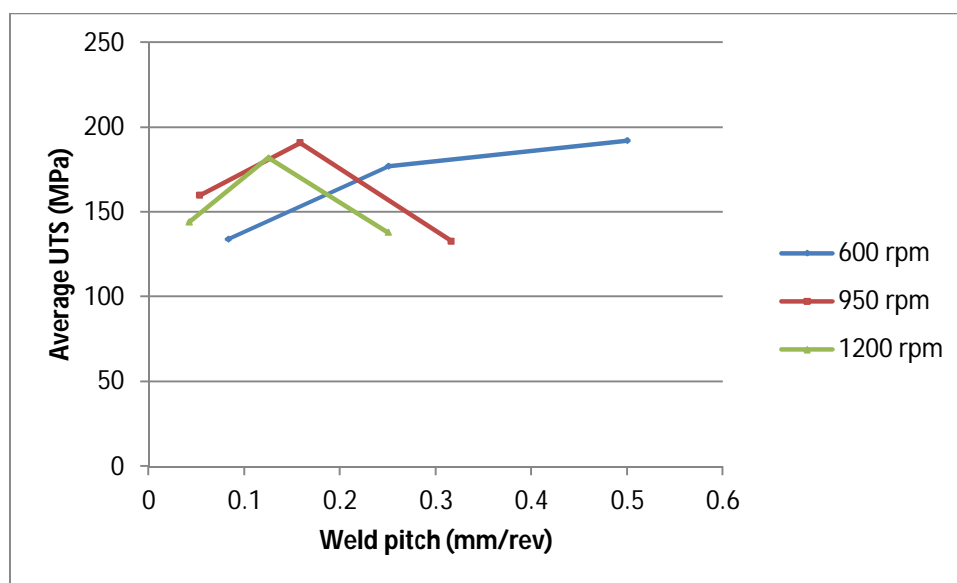
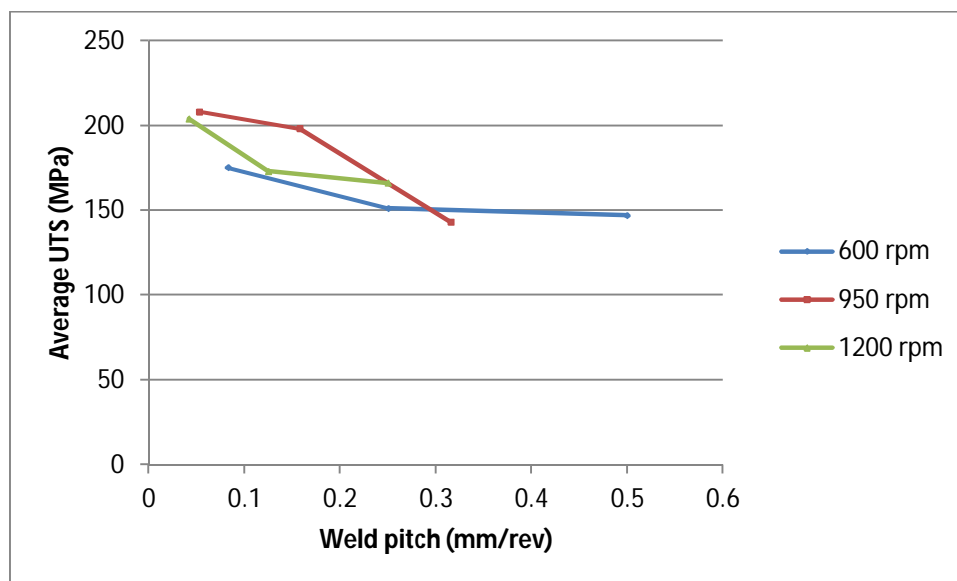


Figure 4.9 (a): Average UTS versus Weld Pitch of all the welds produced with the 15 mm shoulder diameter tool

At 950 rpm and 1200 rpm, the UTS increases from low-to-medium weld pitch, but decreases at high weld pitch. A high weld pitch corresponds with a high travel speed and low heat input (See Tables 4.1 and 4.2 p. 56 and 57).

The average UTS versus weld pitch of all the welds produced with the 18 mm shoulder diameter tool are presented in Figure 4.9 (b). The trend evident from the graph is that at spindle speeds of 600, 950 and 1200 rpm, the average UTS decreases as the weld pitch increases.



**Figure 4.9 (b): Average UTS versus Weld Pitch of all the welds produced with the 18 mm shoulder diameter tool**

This observation can be related to the heat input, which is lower at a higher traverse speed (high weld pitch), and thus causes less vertical transport and mixing of materials during welding. This observation agrees with that of Saeid *et al.*<sup>159</sup> in their report on weldability and the mechanical properties of dissimilar aluminium-copper lap joints made by FSW.

Figure 4.9 (c) present the average UTS versus weld pitch for welds produced with the 25 mm shoulder diameter tool. Welds produced at 600 rpm and 1200 rpm shows a similar trend, but those produced at 950 rpm shows the inverse. This can be attributed to the higher amount of weld defects present in welds produced with the 15 and 25 mm shoulder diameter tools.

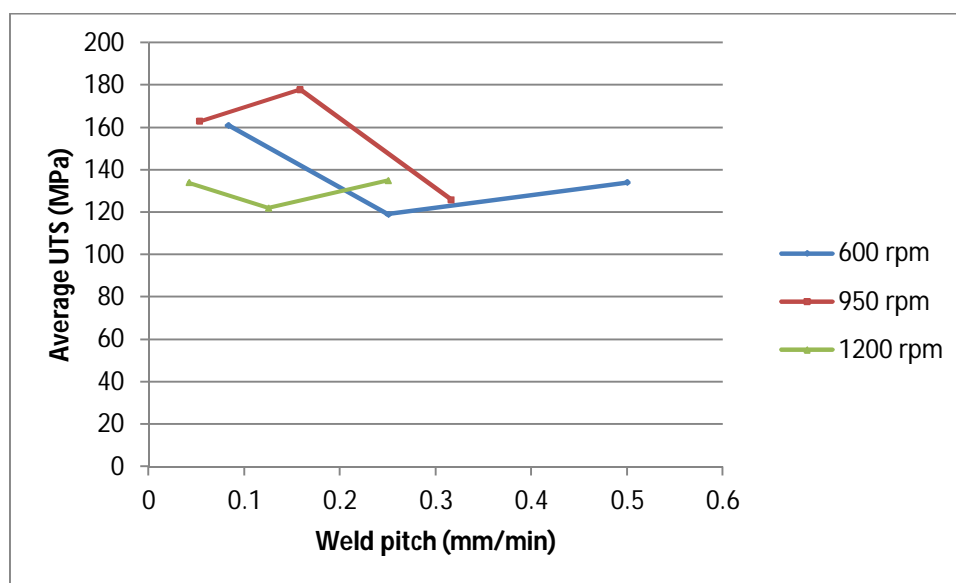


Figure 4.9 (c): Average UTS versus Weld Pitch of all the welds produced with the 25 mm shoulder diameter tool

The trend observed for all the welds produced at 950 rpm is the same for all the shoulder diameters. This is an indication that a medium rotational speed is appropriate for joining Al and Cu.

#### 4.4.2 Percentage elongation data

The percentage elongation of a material is an indication of its ductility. The ductility of a material is an important mechanical property, and is a measure of the degree of plastic deformation sustained at fracture. The percentage elongation data of the parent materials and the welds are presented in Tables 4.6 (a) to (d).

Table 4.6 (a): Percentage Elongation data of the parent materials

Weld No	% Elongation			Mean % Elongation	Mean UTS (MPa)
	T1	T2	T3		
PM Al	12.0	11.9	11.7	11.8	266.1
PM Cu	44.1	44.7	46.6	45.1	244

Table 4.6 (b): Percentage Elongation data of the welds produced with the 15 mm shoulder diameter tool

Weld No	Rotational Speed (rpm)	Feed rate (mm/min)	% Elongation			Mean % Elongation	Mean UTS (MPa)
			T1	T2	T3		
S15_01	600	50	2.0	1.0	3.0	2.0	134
S15_02	600	150	4.5	3.0	3.6	3.7	177
S15_03	600	300	7.6	5.5	3.7	5.6	192
S15_04	950	50	7.0	1.2	1.5	3.2	160
S15_05	950	150	1.9	5.7	7.3	5.0	191
S15_06	950	300	5.7	3.5	2.2	3.8	133
S15_07	1200	50	3.4	1.8	4.1	3.1	144
S15_08	1200	150	2.6	2.1	7.3	4.0	182
S15_09	1200	300	2.0	2.1	5.0	3.1	138

Table 4.6 (c): Percentage Elongation data of the welds produced with the 18 mm shoulder diameter tool

Weld No	Rotational Speed (rpm)	Feed rate (mm/min)	% Elongation			Mean % Elongation	Mean UTS (MPa)
			T1	T2	T3		
S18_01	600	50	3.0	2.5	6.6	4.0	175
S18_02	600	150	3.6	1.4	1.3	2.6	151
S18_03	600	300	3.0	2.8	1.9	2.1	147
S18_04	950	50	7.9	1.2	5.8	6.1	208
S18_05	950	150	4.2	6.1	7.9	5.0	198
S18_06	950	300	4.0	5.3	1.9	3.7	143
S18_07	1200	50	3.7	3.7	3.0	4.7	204
S18_08	1200	150	3.6	4.9	5.7	3.5	173
S18_09	1200	300	3.3	2.0	1.9	2.4	166

**Table 4.6 (d): Percentage Elongation data of the welds produced with the 25 mm shoulder diameter tool**

Weld No	Rotational Speed (rpm)	Feed rate (mm/min)	% Elongation			Mean % Elongation	Mean UTS (MPa)
			T1	T2	T3		
S25_01	600	50	6.9	2.6	2.2	3.9	161
S25_02	600	150	1.2	2.0	2.7	2.0	119
S25_03	600	300	3.7	2.5	3.5	3.2	134
S25_04	950	50	2.2	2.5	2.8	2.5	163
S25_05	950	150	6.1	3.3	6.3	5.2	178
S25_06	950	300	1.5	4.1	2.7	2.8	126
S25_07	1200	50	5.0	2.8	3.8	3.9	134
S25_08	1200	150	1.1	1.3	5.6	2.7	122
S25_09	1200	300	1.9	1.7	4.0	2.5	135

It was observed that the percentage elongation of the welds is relatively low compared with that of the parent materials. Blight<sup>159</sup> reported that, usually the relationship that exists between UTS and ductility, i.e percentage elongation, is that an increase in ductility corresponds with a slight decrease in the strength of the material; it was observed that aluminium with a percentage elongation of 11.8% has an average UTS of 266.1 MPa while copper with a high percentage elongation of 45.1%, has an average UTS of 244 MPa. In contrast to this fact, a common trend observed in the welds is that there is a slight increase in the percentage elongation with an increase in the UTS of the welds. This behaviour can be attributed to the inhomogeneity in the microstructure of the joint interfaces of the welds produced due to the presence of intermetallic compounds.

The graphical representations of the average percentage elongation data versus the weld pitch of all the welds produced with the three shoulder diameters 15, 18 and 25 mm are shown in Figures 4.10 (a) to (c). It was observed that for the welds produced with the 15 mm shoulder diameter tool, at a constant rotational speed of 600 rpm, the average percentage elongation of the welds increases as the weld pitch increases, as shown in Figure 4.10 (a). At 950 rpm and 1200 rpm, the values increased from low to medium weld pitch, but decreased at high weld pitch. This

trend is similar to the average UTS of the welds using the same shoulder diameter tool.

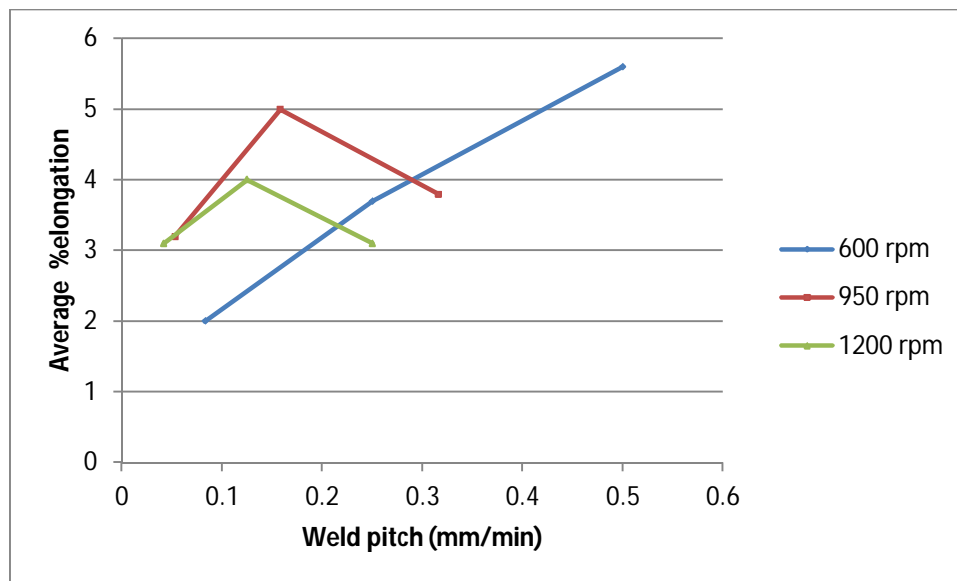


Figure 4.10 (a): Average % Elongation versus Weld Pitch of all the welds produced with the 15 mm shoulder diameter tool

A common trend observed in the average percentage elongation of welds produced with the 18 mm shoulder diameter tool was that at constant spindle speeds of 600, 950 and 1200 rpm, the average percentage elongation decreases as the weld pitch increases, as shown in Figure 4.10 (b).

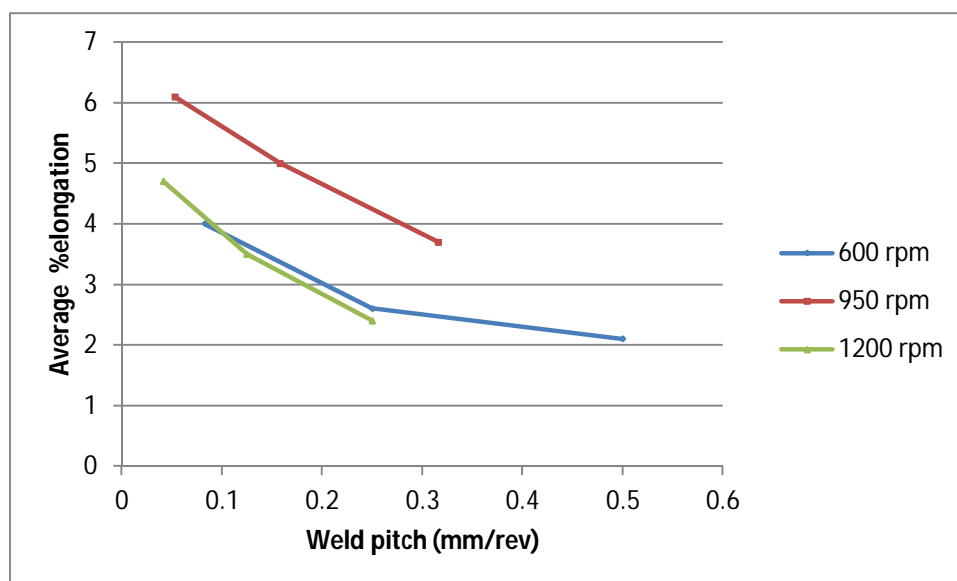


Figure 4.10 (b): Average % Elongation versus Weld Pitch of all the welds produced with the 18 mm shoulder diameter tool

For welds produced with the 25 mm shoulder diameter tool, it was observed that at spindle speeds of 600 rpm and 1200 rpm, the trend was similar, but at 950 rpm, the inverse was observed, as compared with values for 600 rpm and 1200 rpm. This can also be attributed to weld defects in the welds produced at 600 rpm and 1200 rpm.

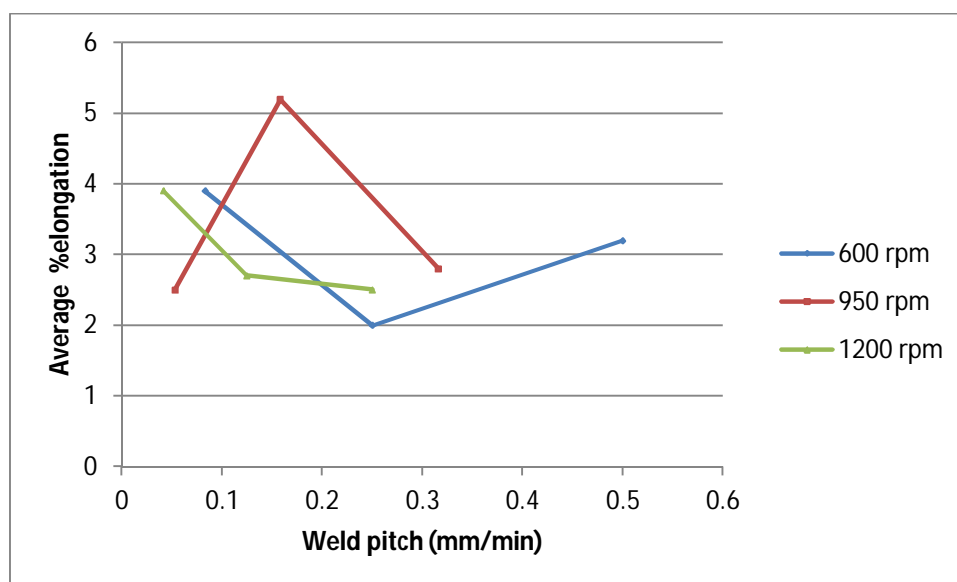


Figure 4.10 (c): Average % Elongation versus Weld Pitch of all the welds produced with the 25 mm shoulder diameter tool

#### 4.4.3 Joint efficiency of the welds

It is reported that welded joints are not usually as strong as the parent materials<sup>160</sup>. This strength reduction is characterised by weld joint efficiency. The Weld Joint Efficiency ( $\eta$ ) is the ratio of the joint strength compared with the strength of the parent material usually expressed as a percentage. Welded Joint Efficiency varies from 100 % for a perfect weld down to 75% for an acceptable weld. Tables 4.7 (a) to (c) show the Weld Joint Efficiency of the welds produced in this research work compared with the Cu parent material. The Cu parent material was chosen for this comparison because of its lower UTS compared with the Al parent material. It is expected that the joint cannot achieve a UTS higher than that of the weaker material (Cu). Hence, the UTS of Cu will be considered for design purposes. The Weld Joint Efficiencies of welds that are above the minimum specified limit are printed in blue.

Table 4.7 (a): Weld Joint Efficiency ( $\eta$ ) of welds produced with the 15 mm shoulder diameter tool

Weld No	Rotational Speed (rpm)	Feed rate (mm/min)	Mean UTS (MPa)	$\eta$ compared to Cu parent material
S15_01	600	50	134	55
S15_02	600	150	177	73
S15_03	600	300	192	<b>79</b>
S15_04	950	50	160	66
S15_05	950	150	191	<b>78</b>
S15_06	950	300	133	55
S15_07	1200	50	144	59
S15_08	1200	150	182	<b>75</b>
S15_09	1200	300	138	57

Table 4.7 (b): Welded Joint Efficiency ( $\eta$ ) of welds produced with the 18 mm shoulder diameter tool

Weld No	Rotational Speed (rpm)	Feed rate (mm/min)	Mean UTS (MPa)	$\eta$ compared to Cu parent material
S18_01	600	50	175	72
S18_02	600	150	151	62
S18_03	600	300	147	60
S18_04	950	50	208	<b>86</b>
S18_05	950	150	198	<b>81</b>
S18_06	950	300	143	59
S18_07	1200	50	204	<b>84</b>
S18_08	1200	150	173	71
S18_09	1200	300	166	68

**Table 4.7 (c): Weld Joint Efficiency ( $\eta$ ) of welds produced with the 25 mm shoulder diameter tool**

Weld No	Rotational Speed (rpm)	Feed rate (mm/min)	Mean UTS (MPa)	$\eta$ compared to Cu parent material
S25_01	600	50	161	66.0
S25_02	600	150	119	48.8
S25_03	600	300	134	54.9
S25_04	950	50	163	66.8
S25_05	950	150	178	73.0
S25_06	950	300	126	51.6
S25_07	1200	50	134	54.9
S25_08	1200	150	122	50.0
S25_09	1200	300	135	55.3

It was observed that 33% of the welds produced with the 15 and 18 mm shoulder diameter tools have Weld Joint Efficiencies within the acceptable range, but none of the welds produced with the 25 mm shoulder diameter tool are within that range. The closest weld setting among this group was a weld produced at 950 rpm and 150 mm/min with a Weld Joint Efficiency of 73%. The majority of the welds that have acceptable Weld Joint Efficiency were produced at 50 and 150 mm/min.

#### 4.4.4 Tensile fracture location characterisations

The fracture locations of all the tensile samples of the final weld matrix with respect to the shoulder diameter tools are presented in Appendix C4. The locations were identified using the Zeiss microscope. Table 4.8 present the fracture locations and the percentage compared with the overall number of samples.

**Table 4.8: Fracture location characterization of the tensile samples**

Shoulder $\phi$	TMAZ Al	% compared to total number of samples	TMAZ Cu	% compared to total number of samples
15	8	30	19	70
18	8	30	19	70
25	10	37	17	63

From Table 4.8, it was observed that 70, 70 and 63% of the tensile samples fractured in the region of the TMAZ of copper in welds produced with 15, 18 and 25 mm respectively. In FSW, it is known that the advancing sides in welds are usually weaker than the retreating side because defects such as voids and wormholes are

usually formed on the advancing side<sup>6</sup>. The higher percentage of the fractured samples on the TMAZ of copper placed at the advancing side during the welding process can be attributed to this fact.

The fracture locations of the welds that had low UTS were further evaluated for the presence of weld defects. A representative sample due to a lack of fusion is shown in Figure 4.11. The photo montages of the remaining samples investigated are presented in Appendix C5.



**Figure 4.11: Photo montage of fracture location of weld produced at 950 rpm and 300 mm/min with the 18 mm shoulder  $\phi$  due to weld defect**

It was observed that the fracture locations of these welds all occurred in the TMAZ of Al on the retreating side of the welds. Considering the morphological feature of the joint interface, with very little mixing of the two metals achieved; it can be said that the low UTS values obtained in these samples are due to lack of fusion and low metallurgical bonding at the joint interface. It should further be noted that most of these welds were produced at high travel speed. This resulted in limited coalescence and bonding at the joint interface.

The fracture locations of samples that failed due to the presence of intermetallic compounds at the joint interface are presented in Appendix C6. A representative sample is presented in Figure 4.12. The microstructure of the region indicated is shown at higher magnifications.

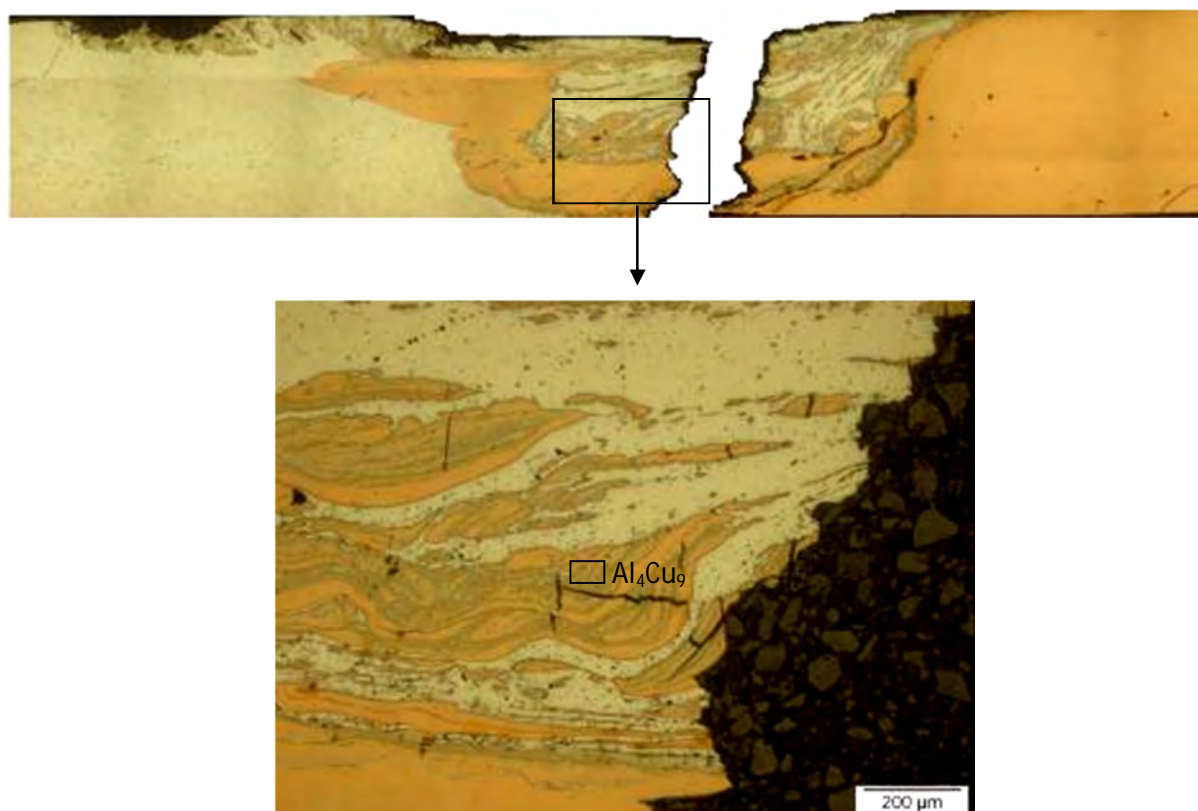


**Figure 4.12: Photo montage of fractured surface and microstructure of weld produced at 1200 rpm and 50 mm/min with the 15 mm shoulder diameter tool (S15\_07 T2) due to the presence of intermetallic compound at the joint interface**

It was observed that most of the samples failed in the region of the TMAZ / SZ of Cu on the advancing side. An Energy Dispersive Spectroscopy (EDS) of the various phases in the samples showed that the regions had a chemical composition similar to that of a known intermetallic compound ( $\text{Al}_4\text{Cu}_9$ ), and it is therefore assumed that the region analysed contains intermetallics of this composition. These will be confirmed later by microhardness measurements. Intermetallic phases are hard and brittle in nature; the Vickers microhardness values in regions where they exist are expected to be high. Due to the nature of intermetallics, they would therefore rather fracture than be plastically deformed, hence, the presence of secondary cracks running parallel to the main fracture surface.

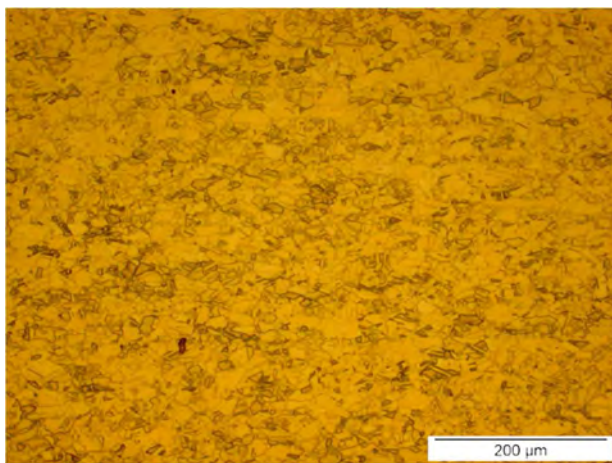
In summary, the evaluation of the tensile fracture locations revealed that the fracture locations of the welds are dependent on the internal structures of the weld regions,

either due to the presence of weld defects or the presence of intermetallic compounds in the joints.

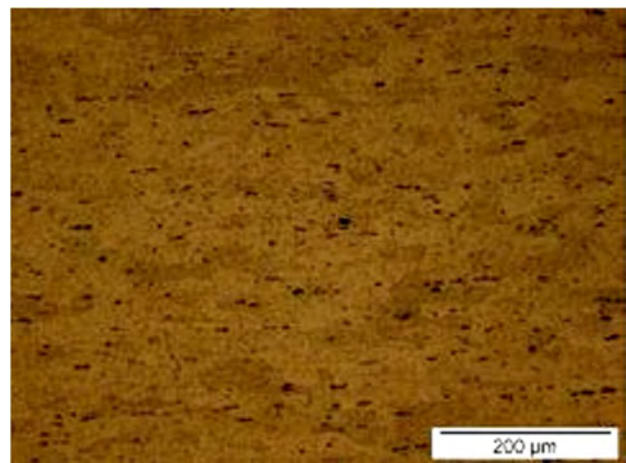
## 4.5 MICROSTRUCTURAL EVALUATION

### 4.5.1 Weld microstructure zones

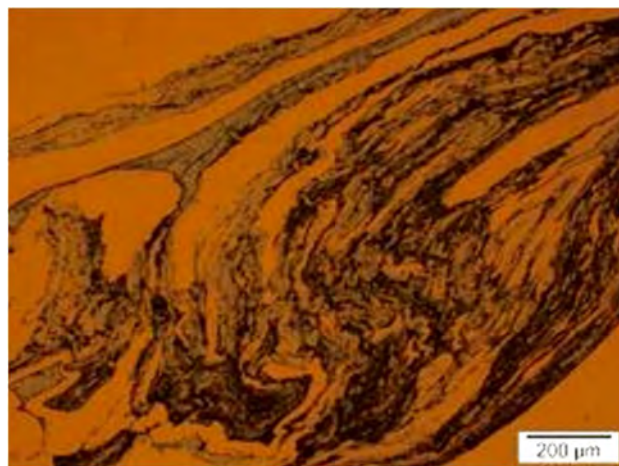
Typical FSW microstructure zones as discussed in section 2.4 (p.21-22) were identified in all the welds produced using an optical microscope. Typical microstructures of the various zones are presented in Figure 4.13 (a) to (e).



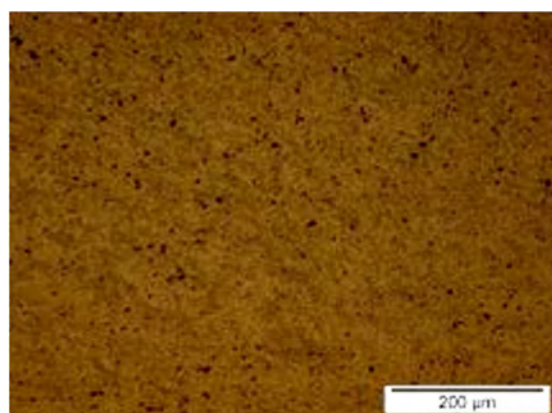
(a) HAZ Cu



(b) HAZ Al



(c) SZ Al/Cu



(d) TMAZ Al



(e) Cu TMAZ

**Figure 4.13 (a) to (e): Typical Microstructures of the various weld zones.**

All the welds produced by varying the tool diameters and weld parameter settings were analysed for microstructural appearance. The micrographs of all the etched microstructural zones of the welds grouped with respect to the shoulder diameter tools employed are presented in Appendix C7.

It was observed that the Stir Zones of all the welds are characterised by a mixture of layers containing aluminium and copper, as a result of the stirring action of the tools. These observations agree with many reports<sup>27,78</sup> on the microstructural characterisation of the FS welds.

The typical onion ring structure<sup>62,97</sup> which is a special case of flow lines that arises when the flow lines form complete, concentric circles usually formed in similar plate butt welding. This is known to result from good material flow during the FSW process. However, this was not observed in the SZ of the welds produced in this research work. Nevertheless, a similar pattern of flow lines (similar to the onion ring structure) was observed as semi-circular flow lines in some of the welds.

It was observed that the TMAZ of Al and Cu in all the weld settings experienced grain deformation and hence appears similar irrespective of the shoulder diameters

used. Typical micrographs with respect to the shoulder diameters are shown in Appendix C8. The HAZ of all the welds also appear to be similar to one another. Typical HAZ grouped according to the shoulder diameters used, are also presented in Appendix C9.

#### 4.5.2 Grain size determination of microstructure zones

Following the observation of grain deformation experienced in the microstructure zones of the welds, as discussed earlier, the grain sizes of these zones were determined. The measurement tools on the optical microscope were used to measure the size of the individual grains in the microstructure zones. The data obtained and the average individual grain size of five measurements for aluminium and copper are presented in Table 4.9 and 4.10, respectively. The micrographs showing the measurements are presented in Appendix C10. A representative sample, S18\_04, produced at 950 rpm and 50 mm/min with the 18 mm shoulder diameter tool was used for the grain size determination. The five readings are the measurements of five individual grains.

**Table 4.9: Average grain size determination for Al microstructure zones**

Grain	Band of Al in SZ( $\mu\text{m}$ )	TMAZ( $\mu\text{m}$ )	HAZ( $\mu\text{m}$ )	PM ( $\mu\text{m}$ )	
				Width	Length
1	5.677	3.384	52.647	18.771	58.018
2	4.803	2.426	37.968	15.699	51.192
3	3.461	5.171	43.666	18.429	37.200
4	4.459	4.706	29.973	24.726	59.600
5	4.318	3.229	55.495	15.358	39.93
<b>Average</b>	<b>4.544</b>	<b>3.783</b>	<b>43.949</b>	<b>18.597</b>	<b>49.188</b>

It should be noted that the aluminium parent material shows elongated grains, hence the average of the width and length was calculated and used for comparison purposes.

Average grain size of Aluminium parent material =  $(18.597 + 49.188)/2 = 33.893\mu\text{m}$

**Table 4.10: Average grain size determination for Cu microstructure zones**

<b>Grain</b>	<b>Band of Cu in SZ(<math>\mu\text{m}</math>)</b>	<b>TMAZ(<math>\mu\text{m}</math>)</b>	<b>HAZ(<math>\mu\text{m}</math>)</b>	<b>PM(<math>\mu\text{m}</math>)</b>
1	4.070	12.365	22.600	65.911
2	2.970	14.357	25.146	29.635
3	5.746	15.119	13.821	18.379
4	4.556	6.596	23.61	19.127
5	1.670	22.523	11.117	29.637
<b>Average</b>	<b>3.802</b>	<b>14.192</b>	<b>19.259</b>	<b>32.538</b>

Although the microstructure zones of all the welds appear similar, as earlier mentioned, the percentage decreases in the grain sizes were quantified; and are reported in Table 4.11. The percentage decrease in grain size was compared with the parent material.

**Table 4.11: Percentage decrease in grain size of microstructure zones**

<b>Microstructure zone (Al)</b>	<b>Grain size (<math>\mu\text{m}</math>)</b>	<b>% Decrease/increase in grain size compared to PM</b>	<b>Microstructure zone (Cu)</b>	<b>Grain size (<math>\mu\text{m}</math>)</b>	<b>% Decrease in grain size compared to PM</b>
PM	33.893	-	PM	32.538	
HAZ	43.949	10	HAZ	19.259	41
TMAZ	3.783	89	TMAZ	14.192	56
SZ	4.544	87	SZ	3.802	88

It was observed that higher percentage decrease was observed in the SZ and TMAZ of aluminium compared to copper, this can be attributed to its original elongated grains which are expected to deform at a faster rate compared to copper with equiaxed grains. A graphical representation of the degree of grain deformation experienced in each microstructural zone is presented in Figure 4.14.

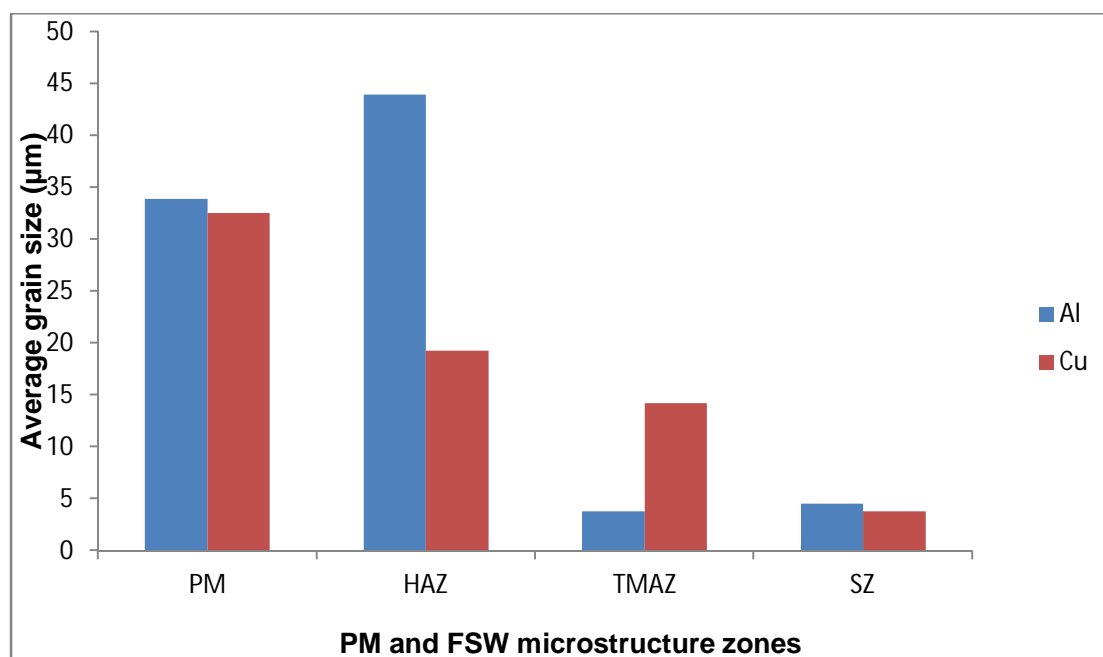


Figure 4.14: Average grain sizes of the PM and microstructure zones

It was observed that the grain sizes of the microstructure zones decreases from the parent material to the SZ except for the HAZ of aluminium which experienced a grain growth. The frictional heat generated and the mechanical effect of the rotating tool during the welding process caused plastic deformation at the joint interface. This resulted in the formation of recrystallized grains in these regions. It should be noted that there are some regions where grains could not be measured due to plastic deformation; hence these grains were measured where they were visible.

### 4.5.3 Scanning Electron Microscopy

A Scanning Electron Microscope (SEM) was used to carry out Energy Dispersive Spectroscopy (EDS) on various regions of the welded samples. The EDS was conducted to analyse the chemical composition of the joint interface regions, and to investigate the presence of intermetallic compounds formed in the welds. A representative sample was chosen from each shoulder diameter group. Figure 4.15 (a) presents the micrograph of the joint interface of weld S15\_02 produced at 600 rpm and 150 mm/min with 15 mm  $\phi$  tool. The positions of the analysis are indicated by numbers.

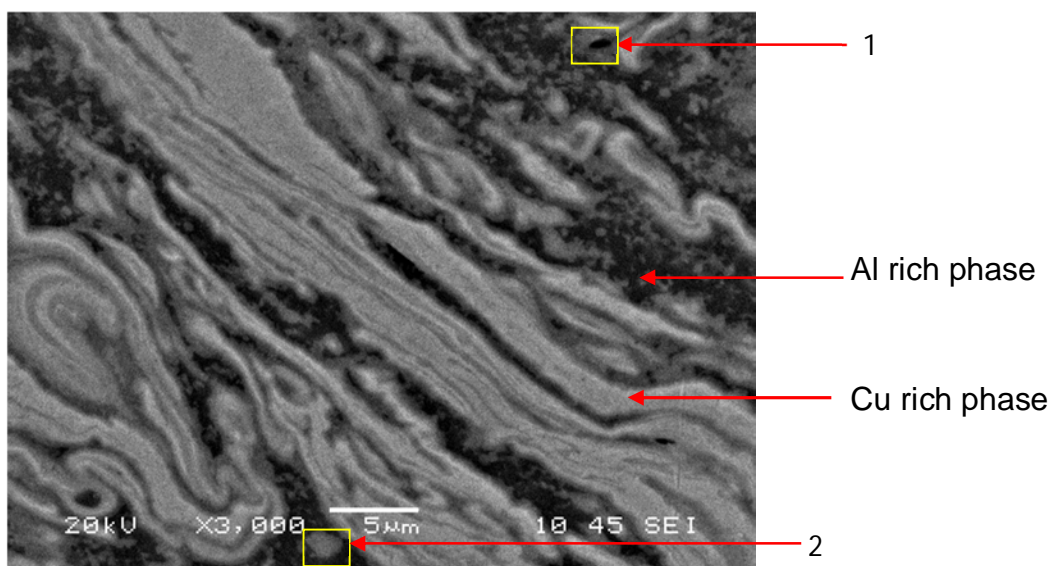


Figure 4.15 (a): Joint interface of S15\_02 (produced at 600 rpm and 150 mm/min with 15 mm shoulder diameter tool)

The EDS analysis on weld sample S15\_02 is presented in Table 4.12.

The micrograph of the joint interface of weld S18\_04 produced at 950 rpm and 50 mm/min with 18 mm  $\Phi$  tool indicating the positions of the EDS analysis is shown in Figure 4.15 (b).

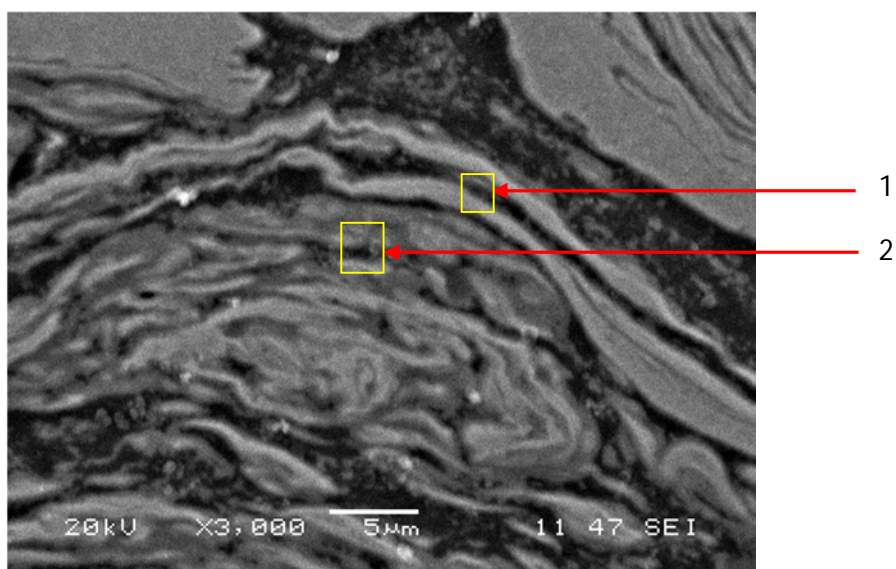


Figure 4.15 (b): Joint interface of S18\_04 (produced at 950 rpm and 50 mm/min with 18 mm shoulder diameter tool)

Figure 4.15 (c) presents the micrograph of the joint interface of weld S25\_01 produced at 600 rpm and 50 mm/min with 25 mm  $\phi$  tool, and the regions analysed with EDS.

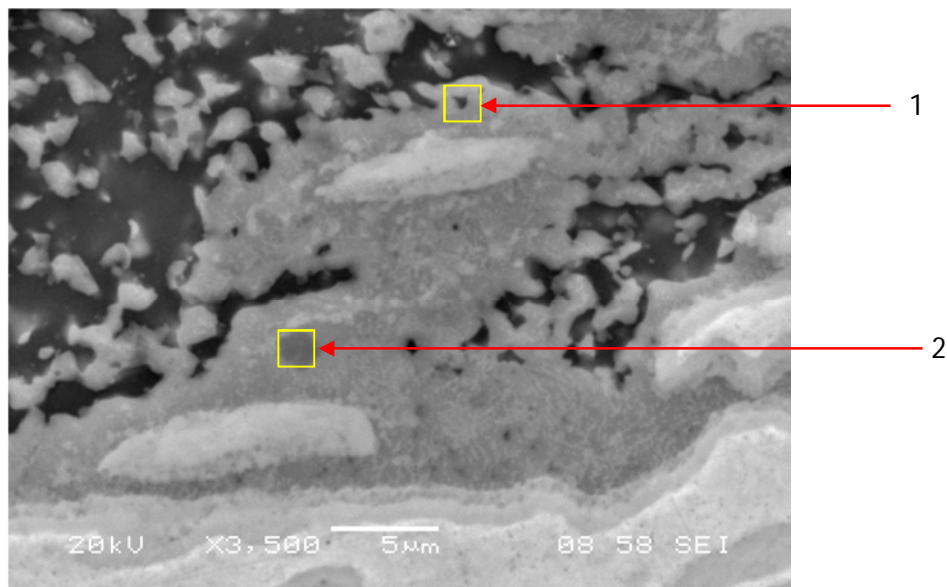


Figure 4.15 (c): Joint interface of S25\_01 produced at 600 rpm and 50 mm/min shoulder diameter tool

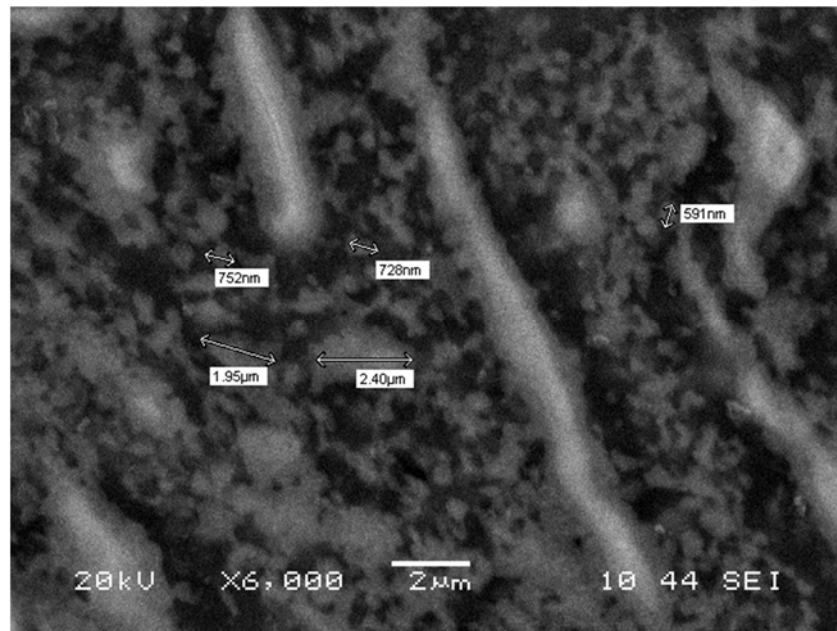
The results of the EDS analysis of the three welded samples are presented in Table 4.12.

Table 4.12: EDS analysis of representative weld samples

Sample	Position	Main alloying elements		Intermetallic
		Al, weight %	Cu weight %	
S15_02	1	22,5	66,84	AlCu
	2	43,01	55,94	Al <sub>2</sub> Cu
S18_04	1	25,65	68,79	AlCu
	2	13,12	86,71	Al <sub>4</sub> Cu <sub>9</sub>
S25_01	1	10,65	88,30	AlCu <sub>3</sub>
	2	33,24	58,49	Al <sub>2</sub> Cu

#### 4.5.4 Measurement of the size of intermetallics

Following the report of Braunovic and Alexandrov<sup>113</sup> on their study on Al to Cu electrical interfaces, that the electrical resistivity of the soldered joint of Al/Cu is not affected negatively when the thickness of the intermetallic layer is not greater than 2 $\mu$ m; the measurement tools on the SEM were used to measure the size of the intermetallics found at the joint interfaces, as presented in Figure 4.16. The results of the electrical resistivities of the welded joints will be discussed later.



**Figure 4.16: Measurements of the thicknesses of intermetallics**

It was found that majority of the intermetallic particles were in the nanoscale range, and were subsequently difficult to measure accurately. This is an indication that the concentrations of the intermetallics formed were low and non-continuous, and should not negatively affect the resistivities of the joints.

#### **4.6 Microhardness Profiling results of the welds**

The microhardness profiling of all the welds produced was carried out at a depth of 1.5 mm below the weld top surface. The average Vickers microhardness values of the parent materials – Aluminium Alloy (AA) and Copper (Cu) are HV 60 and HV 95, respectively.

A typical microhardness profile for a FS weld in aluminium is presented in Figure 4.17.

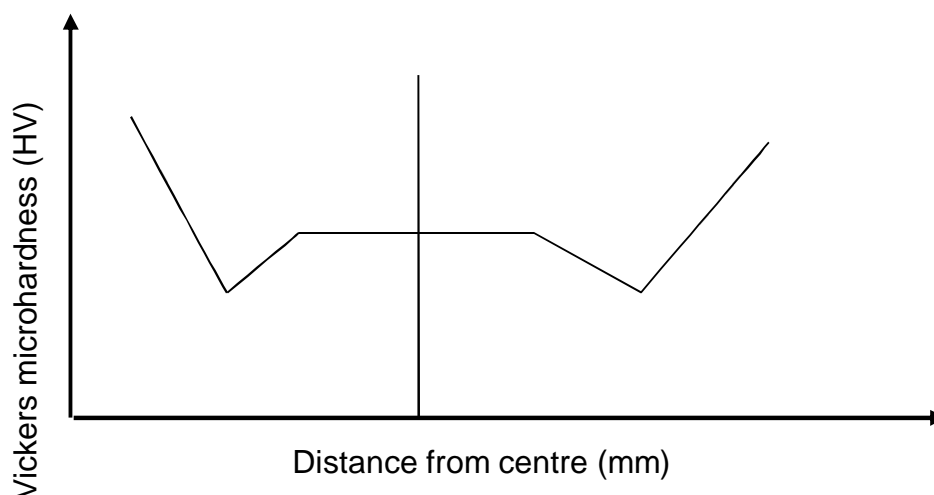


**Figure 4.17: Typical microhardness profile of FS weld of aluminium**

From the typical microhardness profile of FS weld of aluminium shown in Figure 4.17, a softening trend over the weld region can be observed.

The microhardness profiles of the welds grouped with respect to the shoulder diameters (15, 18 and 25 mm) at constant rotational speed of 950 rpm are presented in Figures 4.18 (a) to (c), respectively. The remaining microhardness profiles are presented in Appendix C11. It was observed that the microhardness profiles in the welds produced are inverse to what is usually obtained for similar FS welds of similar materials. That is, the joint interface of the welds are characterised by high peaks resulting from the presence of intermetallics compared to the softening trend observed in typical FS weld of aluminium.

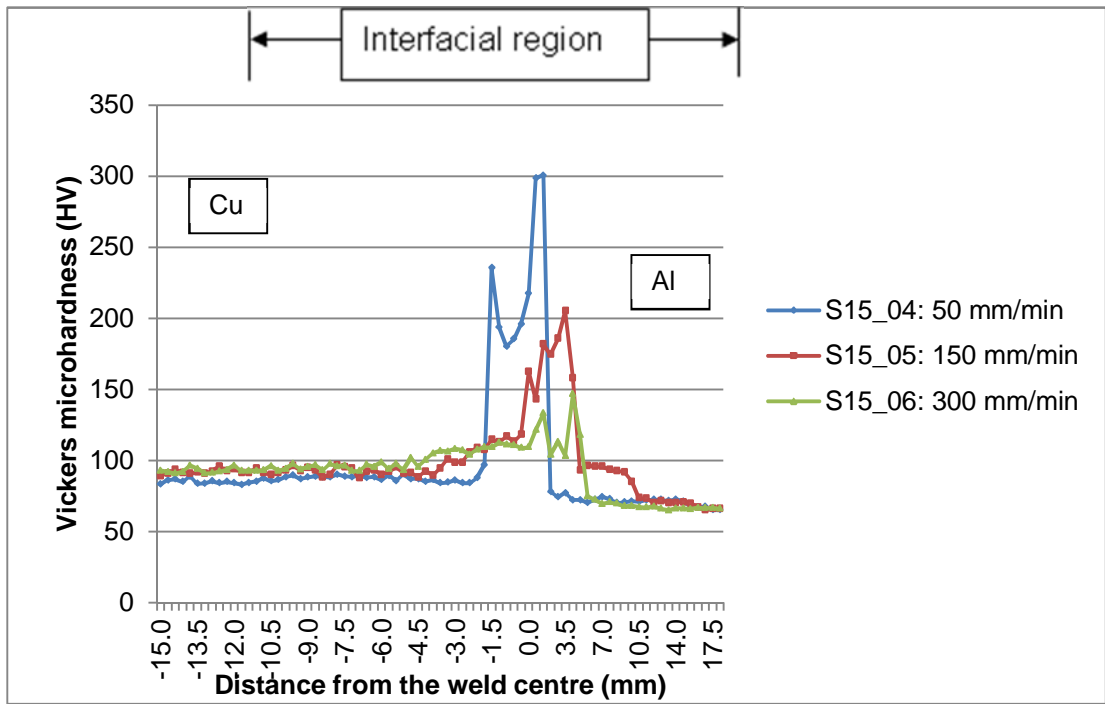


Figure 4.18 (a): Microhardness profiles of welds produced at a constant spindle speed of 950 rpm with the 15 mm  $\phi$

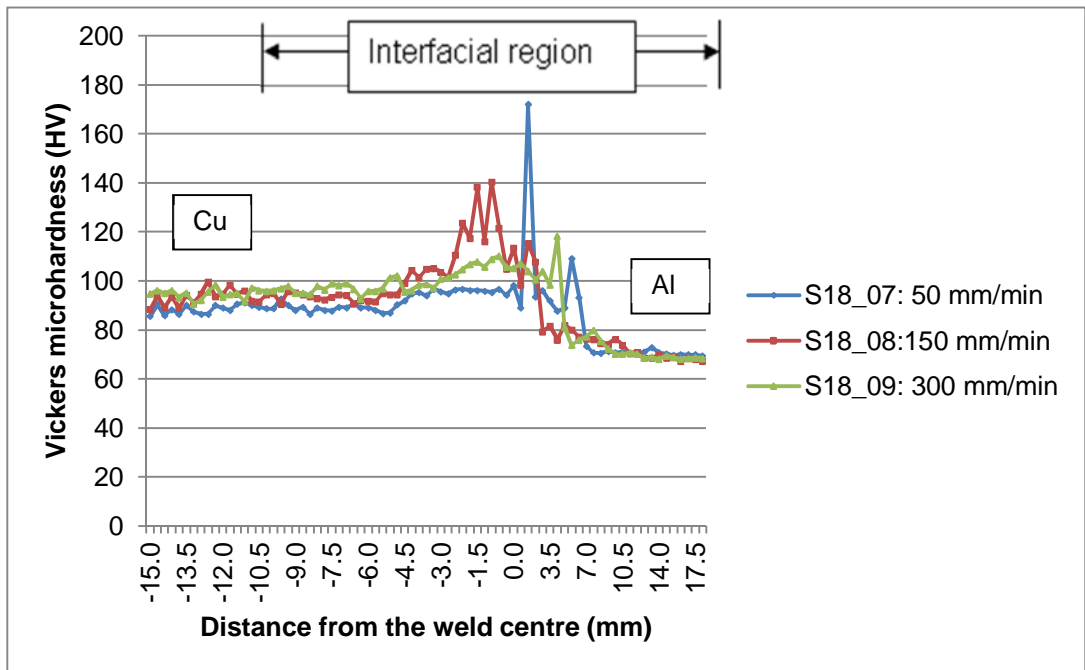
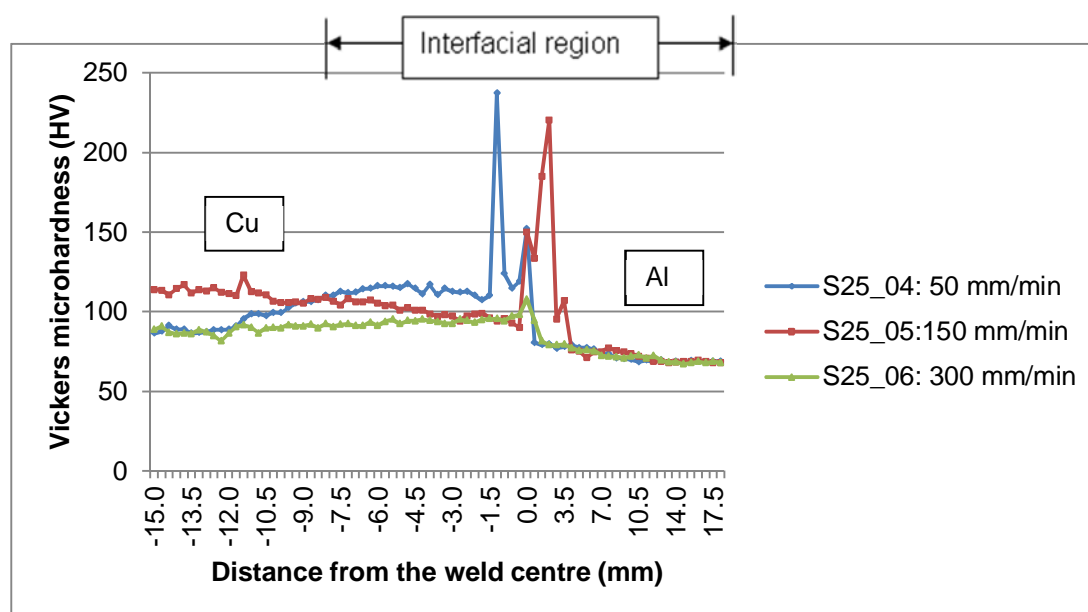


Figure 4.18 (b): Microhardness profiles of welds produced at a constant spindle speed of 950 rpm with the 18 mm  $\phi$



**Figure 4.18 (c): Microhardness profiles of welds produced at a constant spindle speed of 950 rpm with the 25 mm  $\phi$**

The microhardness variation was low in the Heat Affected Zone (HAZ) regions of both metals. This is in the range between 90 HV and 110 HV for Cu, and between 60 HV and 80 HV ( $HV_{min}$  and  $HV_{max}$ ) for Al. It was observed that in all the welds that higher Vickers microhardness values in a range of between 130 HV and 350 HV were measured in the Thermomechanically Affected Zones (TMAZ) and the Stir Zones (SZ) of both Al and Cu. These are regions previously occupied by the tool pin and the shoulder during the welding process. These regions are referred to in the Figures as interfacial regions. The increase in the microhardness values at the interfacial regions can be attributed to plastic deformation that has occurred in the regions during the welding process, and also to the presence of intermetallic compounds. Energy Dispersive Spectroscopy (EDS) and further microscopic examinations of the joint interfaces of all the weld samples confirmed that the high microhardness values at the SZ and the TMAZ are due to the presence of intermetallic compounds in these regions. The difference in the positions of the hardness peaks is due to variation in distribution of material layers within the SZ and TMAZ and also due to the uneven distribution of intermetallic particles at the interface regions between the various alloy layers.

Figure 4.19 presents the interfacial region of a typical sample S18\_04 (produced at 950 rpm and 50 mm/min) showing Vickers microhardness indentations. The line showing across the sample is a pencil mark drawn to indicate the intended positions of indentations before the profiling. The EDS analysis revealed the presence of AlCu and Al<sub>4</sub>Cu<sub>9</sub> intermetallic compounds. These intermetallics are hard and brittle; therefore, high Vickers microhardness values were measured at those points where they are situated.



**Figure 4.19: Microhardness indentations at the interfacial region of S18\_04 produced at 950 rpm and 50 mm/min**

It is difficult to determine the effect of the FSW process parameters on the microhardness profiles of all the samples, but some trends are apparent. It was observed that all the welds produced at the highest travel speed of 300 mm/min have a fairly flat profile (indicated as green lines on the microhardness profiles); these flat profiles are due to the fact that these welds were produced at low heat inputs that do not favour the formation of intermetallic compounds.

#### **4.7 X-Ray Diffraction Analysis**

The identified intermetallic compounds found in the weld samples using Energy Dispersive Spectroscopy (EDS) were further investigated by X-Ray Diffraction (XRD) analysis. Figure 4.20 shows the PDF diffractograms for Aluminium (Al) and Copper (Cu) parent materials used in this study. Their respective PDF numbers are shown and all the subsequent diffraction patterns were compared respectively. Cu indicated with the red lines diffracts at 43.8° and 50.6° while Al indicated with the blue lines diffracts at 38.5° and 44.7°.

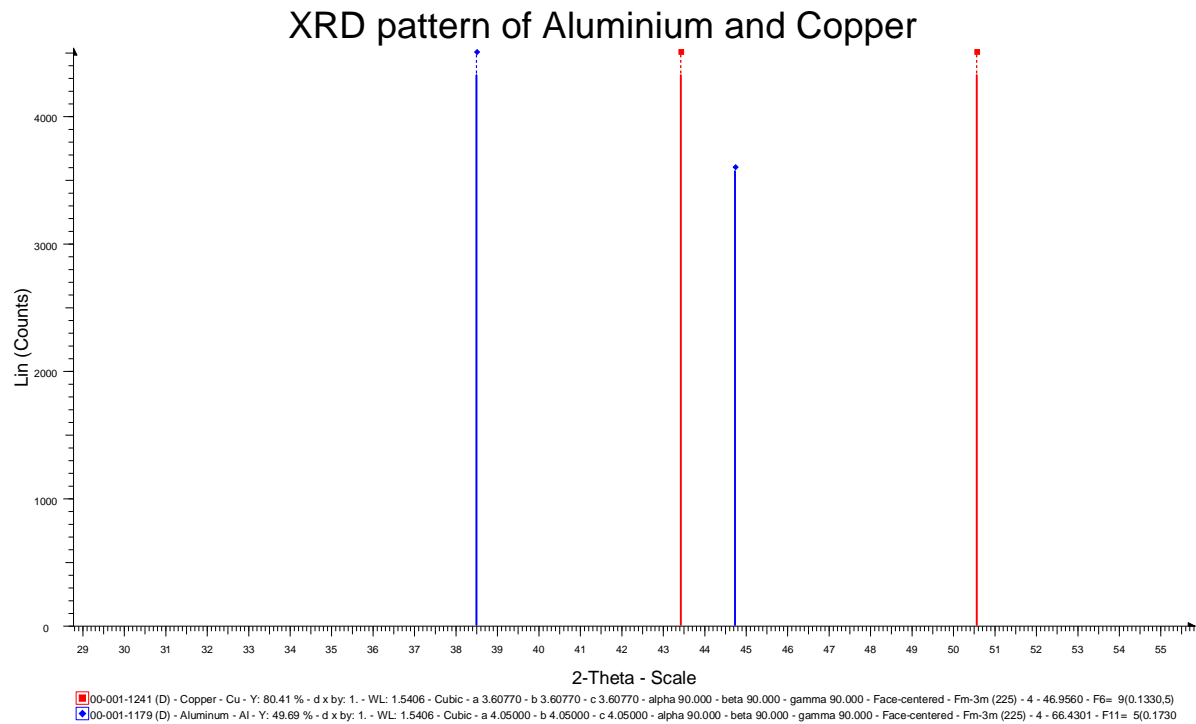


**Figure 4.20: PDF Diffractogram of Al and Cu up to 55 2θ**

The summary of the peaks of all the welds produced with the three shoulder diameter tools (15, 18 and 25 mm), the corresponding intermetallic compounds and the estimated heat input are presented in Table 4.13. Due to the fact that their concentrations in the samples were very low, only one or two of the main diffraction peaks could be identified.

**Table 4.13: Peaks, intermetallic compounds and the estimated heat input into the welds**

<b>Weld No</b>	<b>Peak(2<math>\theta</math>)</b>	<b>Intermetallic compounds</b>	<b>Qinput (J/mm)</b>
S15 01	34.6, 39.0	Al <sub>4</sub> Cu <sub>9</sub> , Al <sub>2</sub> Cu	1119.92
S15 02	34.6, 39.0	Al <sub>4</sub> Cu <sub>9</sub> , Al <sub>2</sub> Cu	451.69
S15 03	34.6, 39.0	Al <sub>4</sub> Cu <sub>9</sub> , Al <sub>2</sub> Cu	289.86
S15 04	34.6	Al <sub>4</sub> Cu <sub>9</sub>	923.18
S15 05	34.6, 39.0	Al <sub>4</sub> Cu <sub>9</sub> , Al <sub>2</sub> Cu	432.83
S15 06	34.6, 39.0	Al <sub>4</sub> Cu <sub>9</sub> , Al <sub>2</sub> Cu	219.31
S15 07	44.2	Al <sub>4</sub> Cu <sub>9</sub>	1087.67
S15 08	34.6	Al <sub>4</sub> Cu <sub>9</sub>	524.3
S15 09	None		299.59
S18 01	44.2	Al <sub>4</sub> Cu <sub>9</sub>	1185.71
S18 02	44.2	Al <sub>4</sub> Cu <sub>9</sub>	474.02
S18 03	39.0	Al <sub>2</sub> Cu	296.37
S18 04	34.6, 39.0	Al <sub>4</sub> Cu <sub>9</sub> , Al <sub>2</sub> Cu	1374.86
S18 05	34.6, 39.0	Al <sub>4</sub> Cu <sub>9</sub> , Al <sub>2</sub> Cu	542.63
S18 06	39.0	Al <sub>2</sub> Cu	293.06
S18 07	34.6, 39.0	Al <sub>4</sub> Cu <sub>9</sub> , Al <sub>2</sub> Cu	1439.14
S18 08	39.0	Al <sub>2</sub> Cu	565.9
S18 09	None		337.29
S25 01	39.0	Al <sub>2</sub> Cu	1731.02
S25 02	39.0	Al <sub>2</sub> Cu	590.92
S25 03	39.0	Al <sub>2</sub> Cu	326.91
S25 04	39.0	Al <sub>2</sub> Cu	1583.49
S25 05	39.0	Al <sub>2</sub> Cu	934.11
S25 06	34.6, 39.0	Al <sub>4</sub> Cu <sub>9</sub> , Al <sub>2</sub> Cu	577.29
S25 07	34.6, 39.0	Al <sub>4</sub> Cu <sub>9</sub> , Al <sub>2</sub> Cu	2067.58
S25 08	34.6, 39.0	Al <sub>4</sub> Cu <sub>9</sub> , Al <sub>2</sub> Cu	950.15
S25 09	39.0	Al <sub>2</sub> Cu	557.24

The full PDF for the Aluminium-Copper intermetallic phases<sup>147</sup> can be found in Appendix C12. Table 4.14 presents the list of the main peaks and the corresponding intermetallic compounds of Al and Cu.

**Table 4.14: Peaks and the corresponding intermetallic compounds of aluminium and copper**

Peak ( $2\theta$ )	Intermetallic compound
34.6°	Al <sub>4</sub> Cu <sub>9</sub>
39.0°	Al <sub>2</sub> Cu
44.2°	Al <sub>4</sub> Cu <sub>9</sub>

From Tables 4.13 and 4.14, it was observed that the most common intermetallic compounds formed at the joint interfaces of the welds are Al<sub>4</sub>Cu<sub>9</sub> and Al<sub>2</sub>Cu. The software available could not identify the intermetallic compound at 34.6 (2 $\theta$ ), but Moreno *et al.*<sup>161</sup> in a research study on a technique for rapid characterisation of intermetallics and interfaces indicated that Al<sub>4</sub>Cu<sub>9</sub> also diffracts at approximately 34° (2 $\theta$ ).

In FSW, the welding temperature is known to be between 60 and 80% of the melting temperature of the materials being joined<sup>6</sup>. The melting temperatures of Al and Cu are 660°C and 1085°C, respectively. The most common identified Al<sub>2</sub>Cu intermetallic compound formed at the joint interfaces of the welds is expected because Al<sub>2</sub>Cu is formed at about 550°C (Table 2.3, p. 29). This is below 651°C (60% of the melting temperature of Cu).

A typical diffraction pattern of the interface region of a weld produced with the 15 mm shoulder diameter tool at 950 rpm and 150 mm/min is shown in Figure 4.21. Any additional diffraction peaks shown in the Figure are due to the presence of intermetallic compounds such as Al<sub>2</sub>Cu or Al<sub>4</sub>Cu<sub>9</sub>. These compounds were identified as far as possible by matching the PDF data files<sup>147</sup>. The slight shift in the main Al and Cu peak positions observed in the entire diffraction patterns is possibly due to sample displacement and preparation on the diffractometer and also due to the presence of residual stresses induced by the thermo-mechanical process and formation of intermetallic phases in the matrix. The diffractograms of all the remaining welds can be seen in Appendix C13.

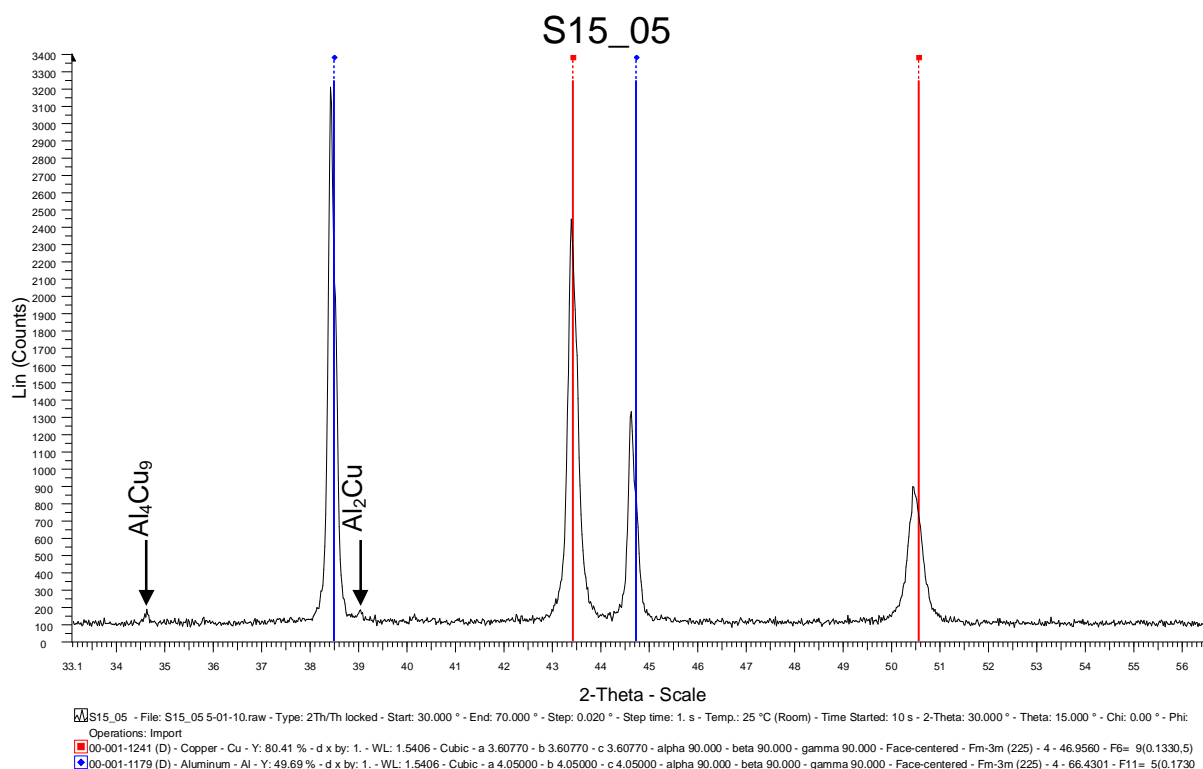


**Figure 4.21: PDF Diffractogram of a weld produced with the 15 mm shoulder diameter tool at 950 rpm and 150 mm/min**

It should be noted that all the peaks were weak in all the welds, due to low concentrations of the intermetallic compound formed, and no intermetallics were identified in welds S15\_09 and S18\_09 (A typical result is shown in Figure 4.22). These welds were produced at high rotational speeds and high feed rates; hence, a low heat input was generated compared with the other welds. The heat inputs into these welds were not high enough to favour the formation of intermetallic compounds, as they are known to be thermally activated<sup>143</sup>.

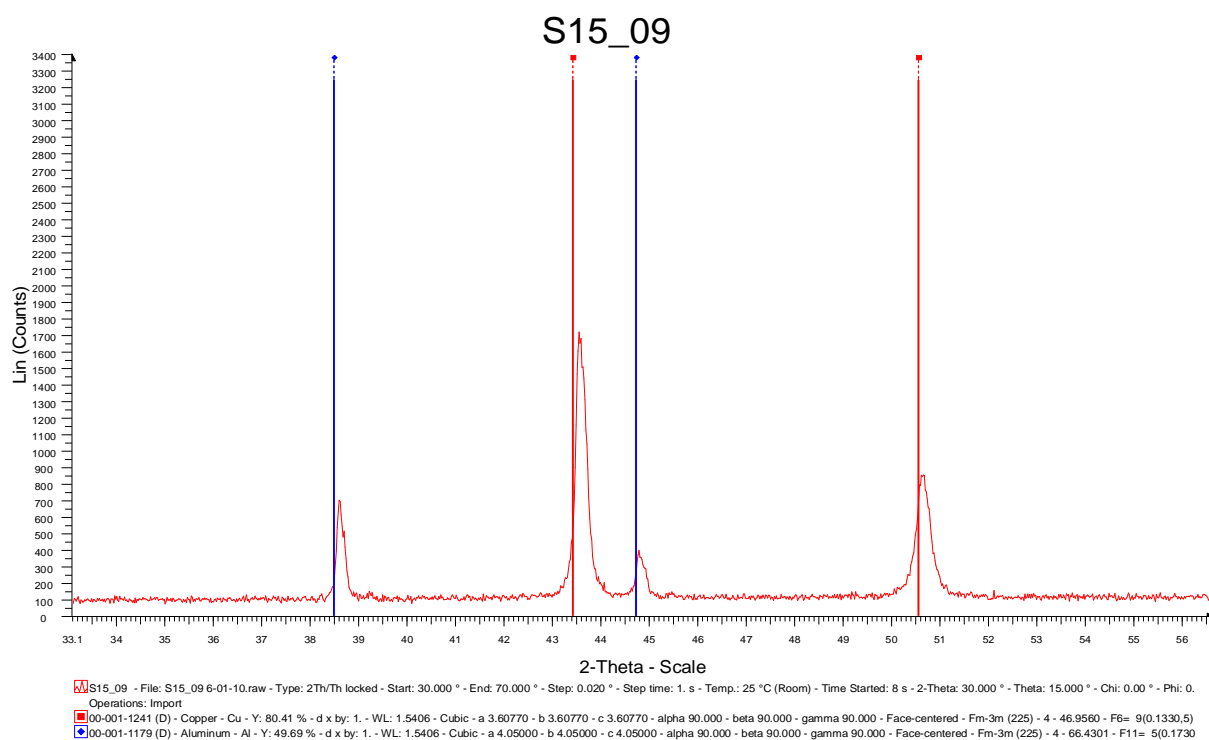


**Figure 4.22: PDF Diffraction of S15\_09 produced at 1200 rpm and 300 mm/min.**

The trend observed is that low heat input welds show a lower likelihood of intermetallic formation. These results confirm the EDS results in that only  $\text{Al}_4\text{Cu}_9$  and  $\text{Al}_2\text{Cu}$  were observed in the SEM.

## 4.8 Electrical Resistivity measurement

Intermetallic compounds at the joint interface of aluminium and copper are known to exhibit high electrical resistivity<sup>118</sup>. The X-Ray Diffraction and Energy Dispersive Spectroscopy (EDS) analyses revealed that the volume fractions of the intermetallic compounds at the joint interfaces of the weld samples are very low. The joint electrical resistances of the welds were measured in order to confirm the results of the XRD and EDS earlier discussed. Table 4.15 presents the joint electrical resistivities and heat input of all the welds produced with the final weld matrix.

Table 4.15: Summary of joint electrical resistivity and heat input into the welds

Weld No	Resistivity $\rho$ , ( $\mu\Omega$ )	Percentage change in resistivities compared to average $\rho$ the parent material	Heat Input (J/mm)
PM AL	0.088		
PM CU	0.096		
Average $\rho$	0.092		
S15 01	0.101	9.8 ↑	1119
S15 02	0.097	5.4 ↑	451
S15 03	0.090	2.1 ↓	289
S15 04	0.101	9.8 ↑	923
S15 05	0.098	6.5 ↑	432
S15 06	0.095	3.3 ↑	219
S15 07	0.101	9.8 ↑	1087
S15 08	0.098	6.5 ↑	524
S15 09	0.088	4.3 ↓	299
S18 01	0.101	9.8 ↑	1185
S18 02	0.097	5.4 ↑	474
S18 03	0.095	3.3 ↑	296
S18 04	0.101	9.8 ↑	1374
S18 05	0.090	2.1 ↓	542
S18 06	0.089	3.3 ↓	293
S18 07	0.101	9.8 ↑	1439
S18 08	0.095	3.3 ↑	565
S18 09	0.087	5.4 ↓	337
S25 01	0.101	9.8 ↑	1731
S25 02	0.096	4.3 ↑	590
S25 03	0.092	0	326
S25 04	0.101	9.8 ↑	1583
S25 05	0.097	5.4 ↑	934
S25 06	0.095	3.3 ↑	577
S25 07	0.101	9.8 ↑	2067
S25 08	0.098	6.5 ↑	950
S25 09	0.090	2.1 ↓	557

The electrical resistivities were calculated from the electrical resistances measured, as explained in Section 2.6.4 (p. 25). The electrical resistivities of the welds ranged between 0.087 and 0.1  $\mu\Omega$ . The percentage increase or decreases in the resistivity of each weld compared with the average joint resistance areas indicated. It was

observed that welds with the highest percentage increase of 9.8% were measured in those welds produced with high heat inputs.

The electrical resistivities of the joints at constant spindle speeds with respect to the shoulder diameter tools employed are presented in Figures 4.23 (a) to (c).

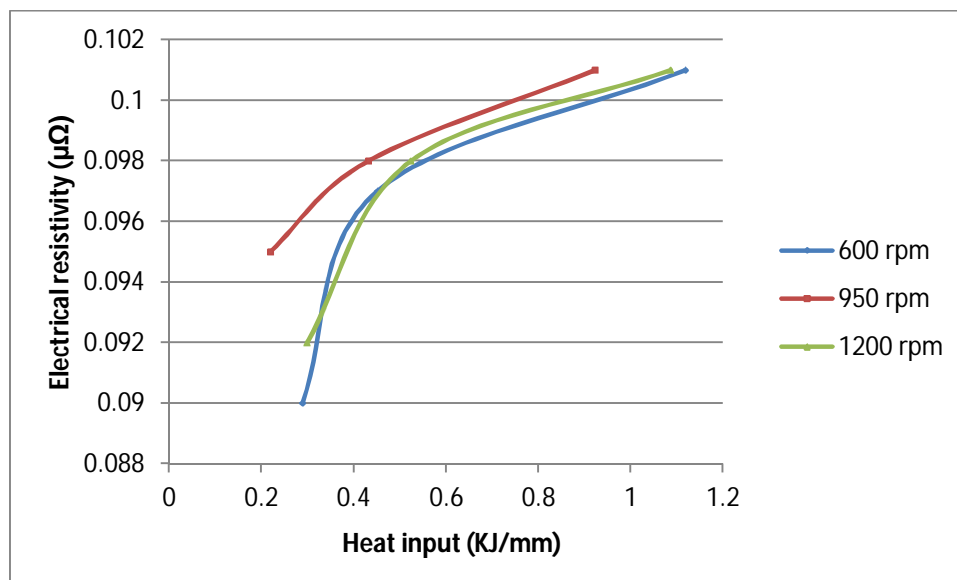


Figure 4.23 (a): Electrical Resistivity versus Heat input of welds produced at constant rotational speed with the 15 mm shoulder diameter tool

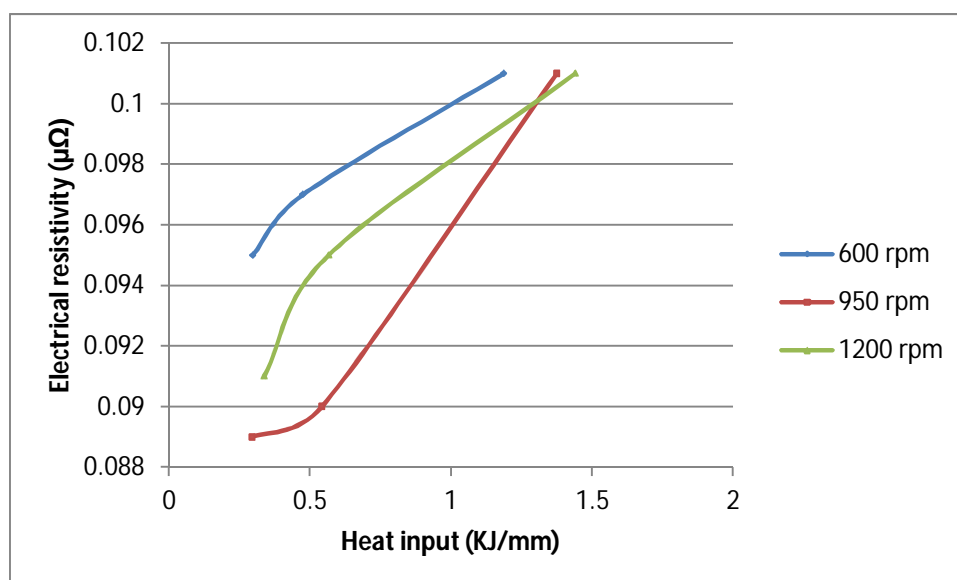
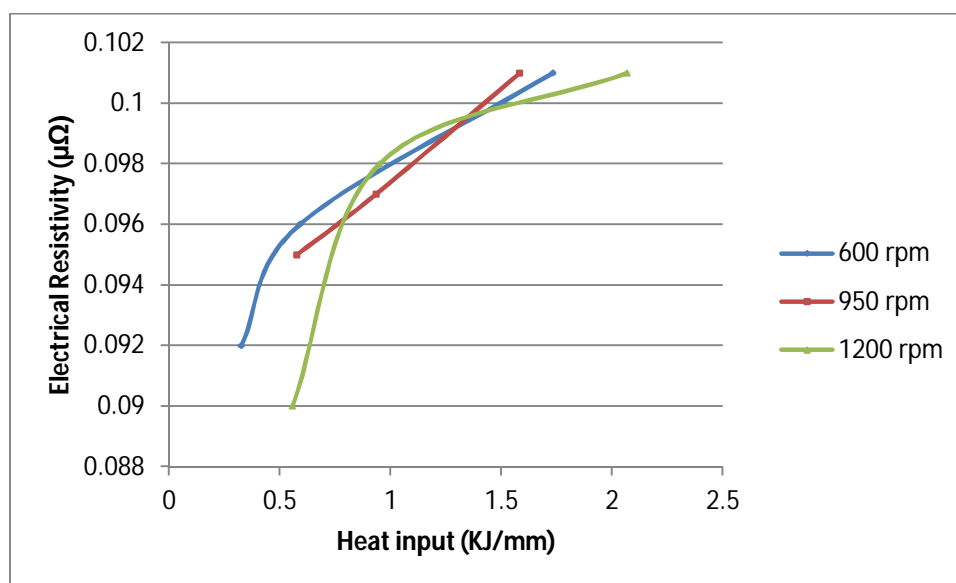


Figure 4.23 (b): Electrical Resistivity versus Heat input of welds produced at constant rotational speed with the 18 mm shoulder diameter tool



**Figure 4.23 (c): Electrical Resistivity versus Heat input of welds produced at constant rotational speed with the 25 mm shoulder diameter tool**

It was observed that for all the weld settings, as presented in Figures 4.23 (a) to (c), the joint electrical resistivities increases as the heat input increases at constant spindle speeds, although, there is not any significant difference in the electrical resistivities from one weld to the other.

Sample S15\_09 (produced at 1200 rpm and 300 mm/min with 15 mm  $\phi$ ) and S18\_09 (produced at 1200 rpm and 300 mm/min with 18 mm  $\phi$ ) have very low resistivity values of 0.087  $\mu\Omega$  and 0.088  $\mu\Omega$  respectively compared with other welds. This further confirms the XRD results that no intermetallics were found in these welds. This is further supported by intermetallic particle measurements found to be in the nanoscale range.

## 4.9 Statistical Analysis

This section reports the statistical analysis conducted on some of the results from this research work. This was done to evaluate the effects of a parameter on other results, and to establish if relationships exist amongst the parameters. The Statistica (version 9.0) statistical analysis software package was used by the NMMU Unit for statistical support to generate the scatter and surface plots relative to the experimental results obtained from the tensile testing and the FSW data. Regression analysis was also done on the weld data.

Scatter plots are utilised to conduct a correlation analysis on the weld data. This method describes the direction and strength of a relationship between two variables. The correlation could be positive or negative<sup>162</sup>.

**Positive correlation:** when an increase in values for one variable is associated with an increase in values of the other.

**Negative correlation:** when an increase in values for one variable is associated with a decrease in values of another variable.

The relationships that exist between the FSW process variables are explained using the strength of correlation,  $r$  value or the Pearson product-moment correlation coefficient, the  $p$  value, which indicates the statistical significance of the correlation. As a general guideline, a value of  $r$  ranging from 0.1 to 0.4 would be classed as a weak correlation, while a value above 0.5 would be regarded as a strong correlation. Correlations close to 1.0 show a strong linear correlation and values close to zero indicate the absence of a linear relationship between the two variables. If the  $p$  value is less than 0.05 the corresponding correlation is statistically significant at the 5% level. The statistical analysis carried out on the weld data is presented in the following subsections.

#### 4.9.1 Regression analysis

Multiple regression analysis was carried out on the data obtained from the FSW process and the results from the characterisation of the weld samples; in order to derive linear equations relating the dependent to the independent variables.

In regression analysis, the regression line expresses the best prediction of the dependent variable on the independent variables. However, there is usually substantial variation of the observed points around the fitted regression line. The deviation of a particular point from the regression line (its predicted value) is called the residual value.

*R-square*, also known as the coefficient of determination, is commonly used in statistics to evaluate model fit. *R-square* is 1 minus the ratio of residual variability. When the variability of the residual values around the regression line relative to the overall variability is small, the predictions from the regression equation are good. In most cases, the ratio and *R-square* will fall somewhere between 0.0 and 1.0. The *R-square* value is an indicator of how well the model fits the data<sup>163</sup>.

The adjusted *R-square* value is calculated by adjusting the *R-square* value for the number of independent variables. By reducing the number of independent variables, the adjusted *R-square* value will move closer to the unadjusted *R-square*. Usually, the degree to which two or more predictors (independent variables) explain the variation in the dependent variable is expressed in the correlation coefficient *R*, which is the square root of *R-squared*.

The beta values are used to create the linear equation to predict the dependent variable (*Y*), when the independent variables (*X<sub>i</sub>*) are specified. The generalized equation is given as<sup>163-164</sup>:

$$Y_i = \beta_0 + \beta_1 X_{1i} + \beta_2 X_{2i} + \beta_3 X_{3i} + \dots + \beta_k X_{ki} + \epsilon_i \quad 4.1$$

The beta values that appear in red print in the Tables are statistically significant at the 5% level, i.e. the *p*-value is less than 0.05, and the corresponding predictor can be viewed as having a significant effect on the system. However, because the number of tests (sample size) is relatively small, variables whose *P*-values are bigger than 0.05, but still in the region of 0.05, could also be seen as having a noticeable effect.

It is important not to overlook any variable that may have an important influence when a larger matrix is considered. The results of the multiple regression analysis of the entire weld data with respect to the shoulder diameters employed are presented in Appendix C14.

The equations derived from the multiple regression analysis are stated in equations 4.2 to 4.6. The parameters are represented as follows: Torque – T, Feed rate – F, Spindle speed – S, and Interaction – I.

$$\text{Torque (Nm)} = 25.63624 - 0.01334 * S + 0.03330 * F - 0.00001 * I \quad 4.2$$

$$\begin{aligned} \text{Heat input (KJ/mm)} \\ = 1.13653501 - 0.00346301 * F + 0.00033264 * S - 0.00000053 * I \end{aligned} \quad 4.3$$

$$\text{UTS (MPa)} = 146.9909 + 0.275 * S + 0.0511 * F - 0.0001 * I \quad 4.4$$

$$\begin{aligned} \text{Electrical resistivity } (\mu\Omega) \\ = 0.10151956 - 0.00002725 * F + 0.00000081 * S - 0.0000001 * I \end{aligned} \quad 4.5$$

$$\text{UTS (MPa)} = 194.6103 + 10.8737 * F_x + 24.9234 * F_y - 3.0675 * F_z - 0.4985 * T \quad 4.6$$

The linear equations outlined above can be used to predict independent variables (weld properties) when the dependent variables are known. It was observed that statistically, (F<sub>y</sub>) and (F<sub>z</sub>) could contribute significantly to changes in the UTS of welds. This can be explained further because the forces acting on the tool during the welding process dictate the forging force, the amount of heat input into the welds and the resulting weld defect, which can be related to the UTS of the welds. The Analysis of Variants (ANOVA) of the weld data is presented in Appendix C15.

#### 4.9.2 Analysis of scatter plots

The 2-dimensional scatter plot is a statistical technique used to visualize a relationship (correlation) between a dependent and an independent variable. Individual data points are represented in two-dimensional space, where the axes represent the variables<sup>164</sup>. The scatter plots of percentage elongation versus heat input and electrical resistivity versus heat input are presented in Figures 4.24 (a) and (b) respectively.

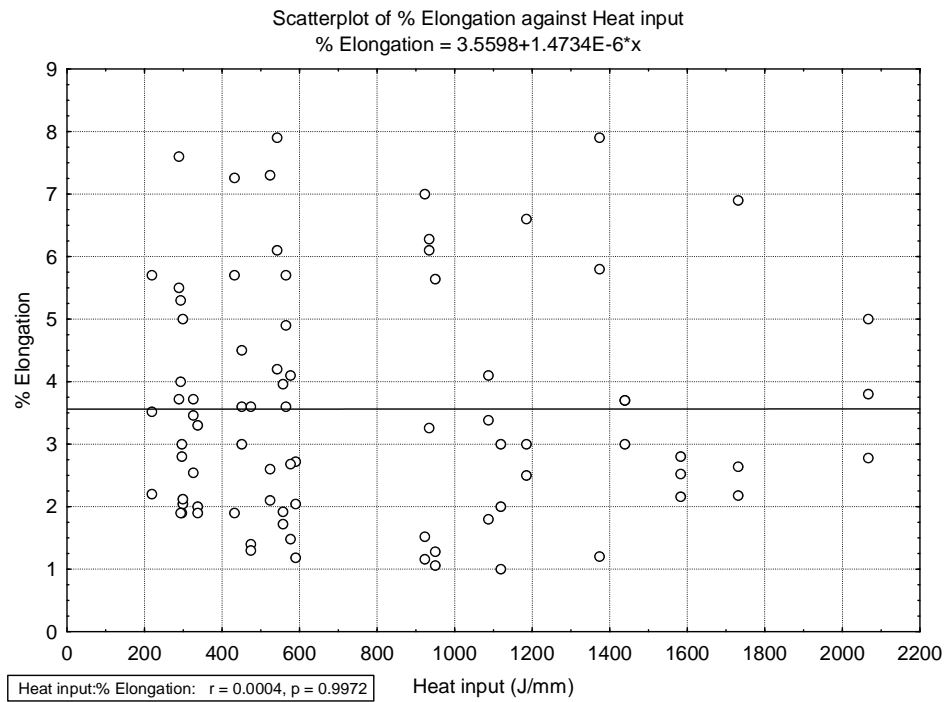


**Figure 4.24 (a): Scatter plot of percentage elongation versus heat input for all the welds**

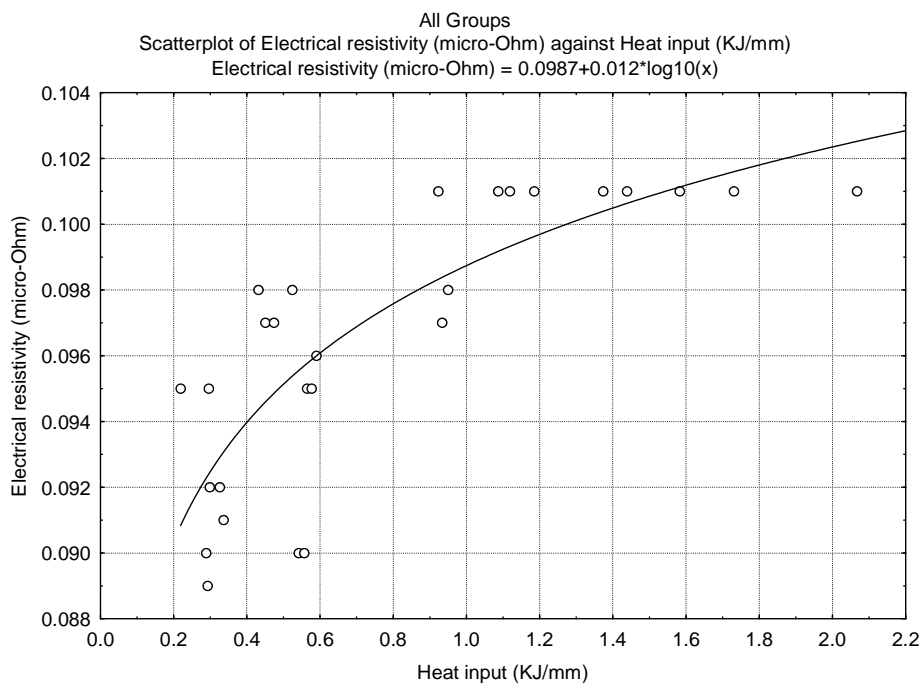


**Figure 4.24 (b): Scatter plot of Electrical resistivity versus heat input for all the welds**

Considering the scatter plot of heat input versus percentage elongation of all the weld data, it can be said that statistically, there is no strong relationship that exists

between them, but a fairly strong relationship exists between the electrical resistivity and the heat input. The scatter plot of electrical resistivity versus heat input revealed that the electrical resistivity increases as the heat input increases, but is limited at a certain point when the electrical resistivity become constant. This further confirms the relationship between electrical resistivity and heat input presented in section 4.8. The scatter plots of electrical resistivity against heat input with respect to the shoulder diameter tools employed are presented in Appendix C16. Similar patterns of relationship, as discussed above, were also observed in the welds with respect to the shoulder diameters.

### **4.9.3 Analysis of surface plots**

Surface plots were created from the weld data to aid visualization of the interrelationship that could exist between a dependent variable and two independent variables. In 3D- surface plots, the surface is defined by a smoothing technique or a defined mathematical expression fitted to the data (variables corresponding to sets of XYZ co-ordinates for subsets of data)<sup>164</sup>. The data used for surface plot analysis include: the FSW force feedbacks, Ultimate Tensile Strength and the percentage elongation. The plots are presented in Figures 4.25 (a) to (g).

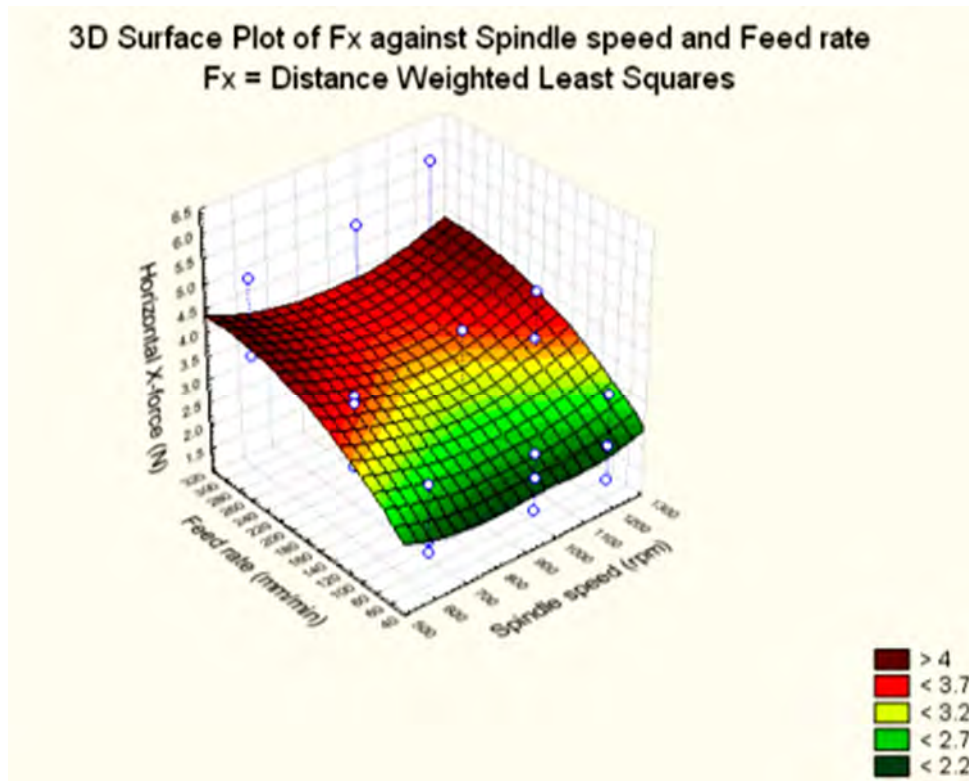


Figure 4.25 (a): Surface plot relating horizontal force ( $F_x$ ), spindle speed and feed rate for all the welds

It was observed from Figure 4.25 (a) that the horizontal force ( $F_x$ ) increases as the feed rate increases, while the spindle speed does not seem to have any significant effect on the horizontal force acting during the welding process. This is important information for design purposes when considering the forces acting on the tool during the welding process.

3D Surface Plot of  $F_y$  against Spindle speed and Feed rate  
 $F_y = \text{Distance Weighted Least Squares}$

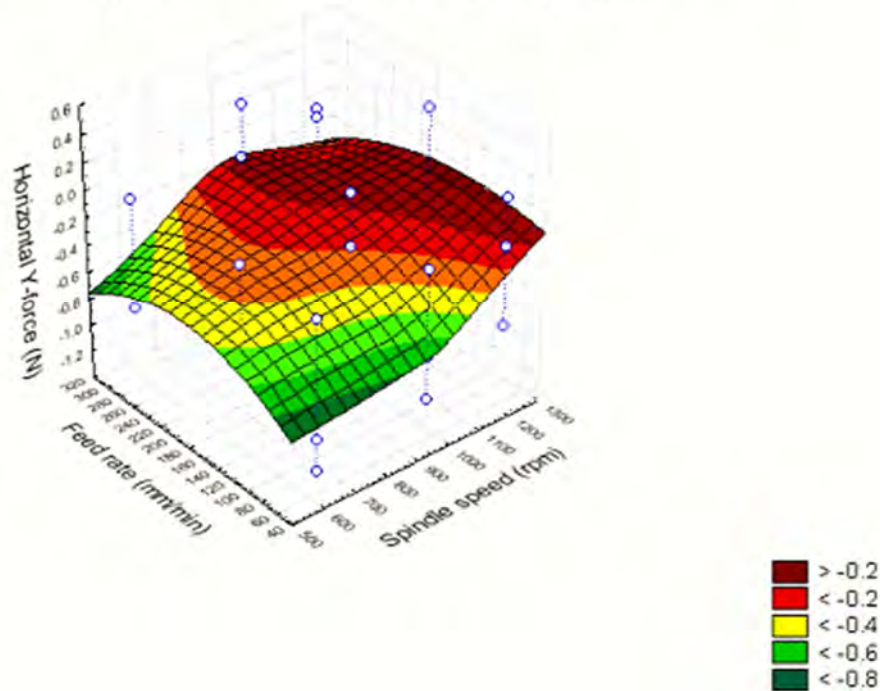


Figure 4.25 (b): Surface plot relating horizontal force  $F_y$ , spindle speed and feed rate for all the welds

The surface plot of the horizontal force ( $F_y$ ) acting perpendicular to the ( $F_x$ ) compared with the spindle speed and the feed rate considered, revealed that the ( $F_y$ ) increases as the spindle speed increases, while the feed rate does not seem to have much effect on the ( $F_y$ ) acting on the tool. It stands to reason that side force ( $F_y$ ) would increase slightly, because the material is pushed faster in the X and Y directions, as a result of increasing the spindle speed.

3D Surface Plot of  $F_z$  against Spindle speed and Feed rate  
 $F_z$  = Distance Weighted Least Squares

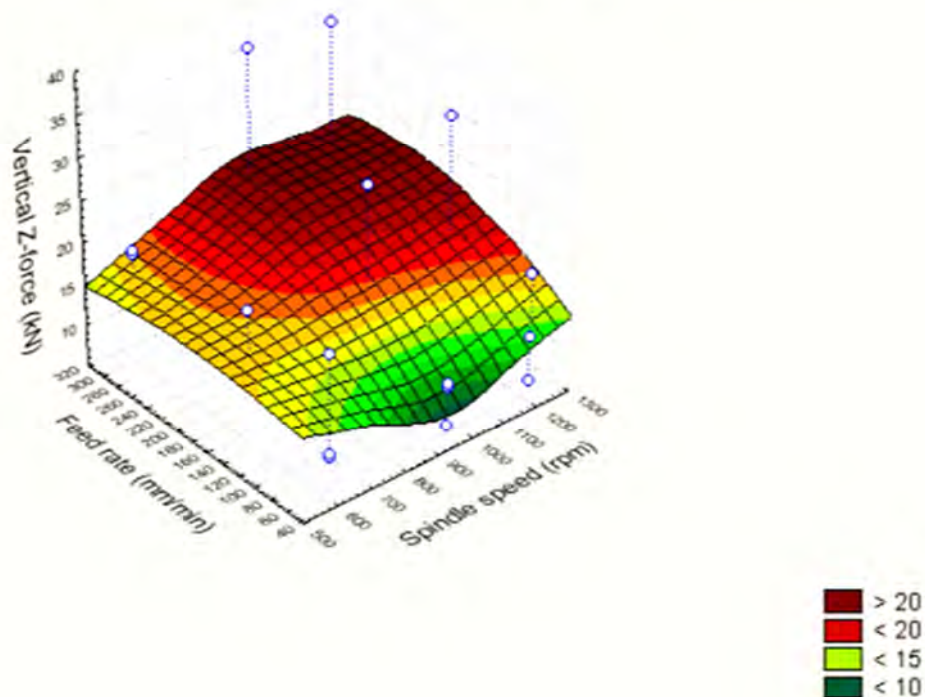


Figure 4.25 (c): Surface plot relating vertical force ( $F_z$ ), spindle speed and feed rate for all the welds

In the case of ( $F_z$ ) (Figure 4.25 (c)), which is the downward vertical force acting on the rotating tool during the welding process, it was observed that the vertical force increases as the feed rate and spindle speed increase. This is expected because at high feed rates and high spindle speeds, the tool moves relatively fast; hence, less heat input is generated. As such, a high vertical force is practically required to ensure forging during the welding process.

3D Surface Plot of Torque against Spindle speed and Feed rate  
Torque = Distance Weighted Least Squares

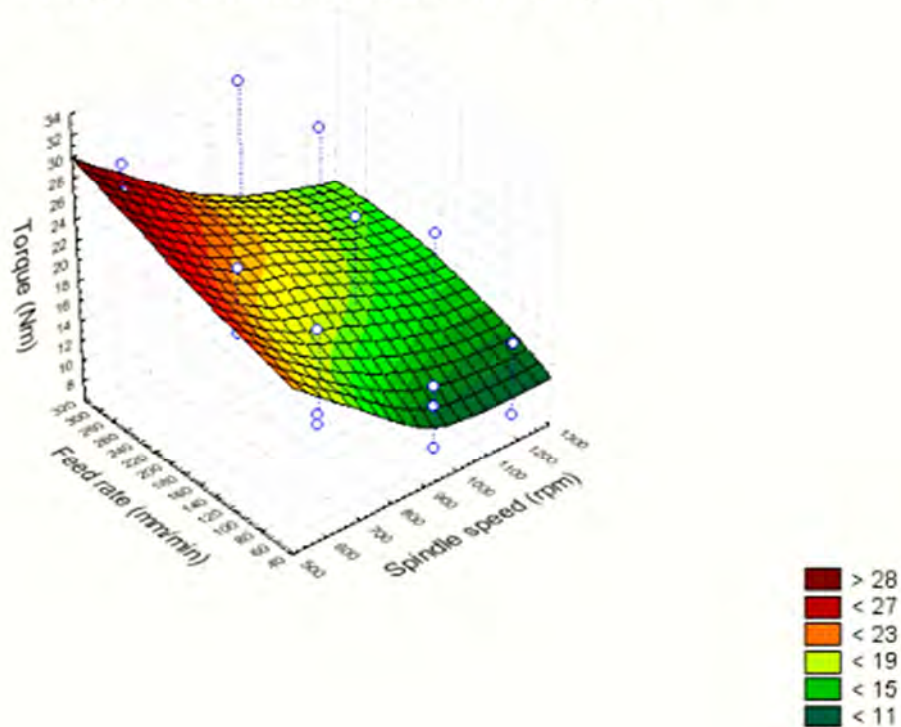


Figure 4.25 (d): Surface plot relating torque (T), spindle speed and feed rate for all the welds

The trend observed in the torque values shown in the surface plot (Figure 4.25 (d)) was that the torque increases as the feed rate increases, but it decreases as the spindle speed increases. The explanation given earlier on the relationship between vertical force, spindle speed and feed rate is also related to this case, since a linear relationship exists between vertical force and torque; that is to say, an increase in the downward vertical force gives an increase in torque values. Hence, it is revealed in this plot, that the feed rate plays a significant role in the resulting torque values compared with the spindle speed.

3D Surface Plot of  $Q_{input}$  against Spindle speed and Feed rate  
 $Q_{input}$  = Distance Weighted Least Squares

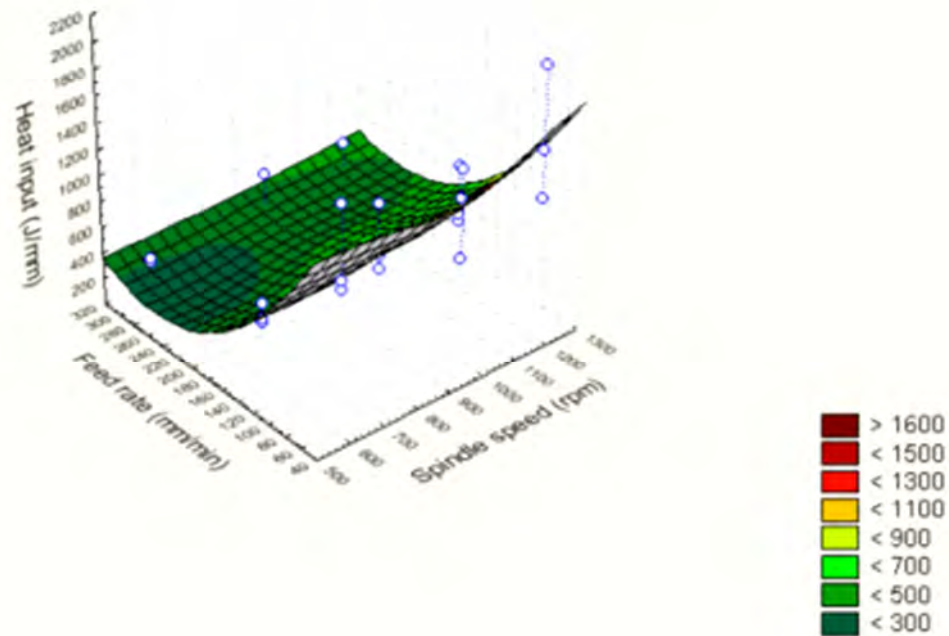


Figure 4.25 (e): Surface plot relating heat input, spindle speed and feed rate for all the welds

From the surface plot relating heat input to the process parameters (Figure 4.25 (e)), it was observed that the heat input into the welds increases as the feed rate decreases, but not linearly. The spindle speed does not have a significant effect on the heat input. The explanation for this is based on the fact that the tool moves slowly at low feed rates; hence most of the heat generated is contained in the welds.

3D Surface Plot of UTS against Spindle speed and Feed rate  
UTS = Distance Weighted Least Squares

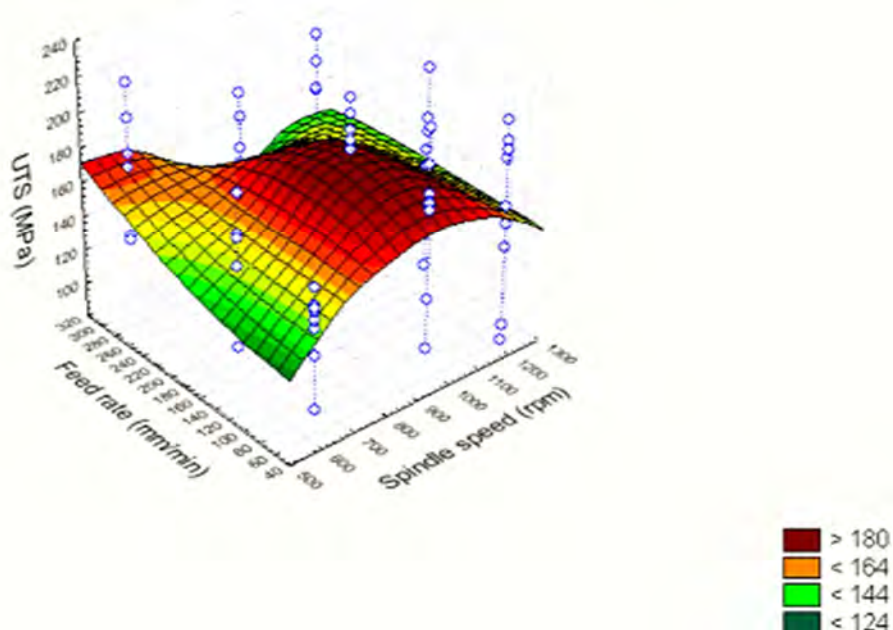


Figure 4.25 (f): Surface plot relating UTS, spindle speed and feed rate for all the welds

The surface plot relating the UTS, spindle speed and feed rate of the entire weld data (Figure 4.25 (f)) revealed that the UTS increases as the feed rate decreases, but decreases slightly at high spindle speeds. With respect to the entire weld matrix considered in this research, it can be said that the optimum weld setting with respect to the UTS, is 950 rpm and 150 mm/min based on the statistical analysis.

3D Surface Plot of % Elongation against Spindle speed and Feed rate  
 % Elongation = Distance Weighted Least Squares

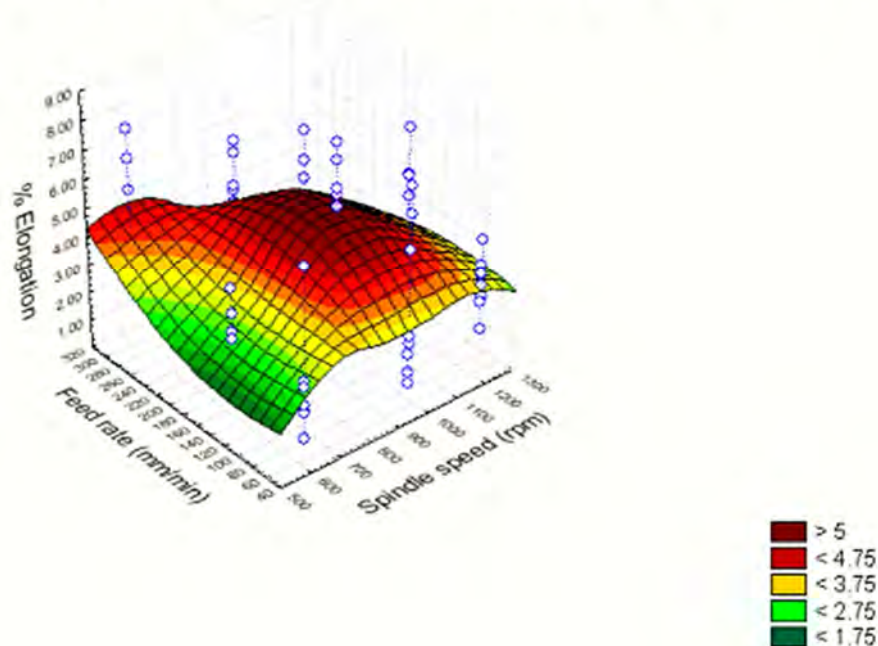


Figure 4.25 (g): Surface plot relating percentage elongation, spindle speed and feed rate for all the welds

The red region of the surface plot relating the percentage elongation and the process parameters (Figure 4.25 (g)), considered statistically significant; looked similar to that of the UTS earlier discussed. Hence, the trends observed in both properties are similar.

The surface plots with respect to the shoulder diameters employed are presented in Appendix C17.

#### 4.10 Summary

The results obtained from the various characterisation techniques employed have been presented and discussed in this chapter. Microstructural evaluation revealed that the interfacial regions of all the welds produced are characterised by mixture layers of both metals joined though the degree of mixing is improved in welds produced at the lowest travel speed of 50 mm/min. Evaluation of the tensile test results showed that the welds produced at 950 rpm and 50 mm/min with the 18 mm shoulder diameter tool had the highest average Ultimate Tensile Strength, it can be

said that this weld setting is the optimum with respect to the UTS, when compared with other welds produced.

The microhardness distribution shows that high Vickers microhardness values measured at the joint interface correspond with the presence of intermetallic compounds revealed through the EDS analysis and XRD. Joints containing no intermetallic compounds showed little variation in their microhardness values. The thicknesses of the intermetallic layers measured were in nanoscale. The electrical resistivities of the welds are very low which is an indication that these welds are successful welds with limited intermetallic compounds formed at the joint interfaces. The process window evaluated in this research work can be recommended. Statistical analysis of the weld data obtained revealed that the downward vertical force, ( $F_z$ ) has a significant effect on the UTS of the welds. There is also an indication of a strong relationship between the electrical resistivity and the heat input into the welds. The next chapter will highlight the general conclusions and suggestions for future work.

## CHAPTER 5 CONCLUSIONS AND FUTURE WORK

### 5.1 Introduction

The objective of this research work was to join 5754 Aluminium Alloy (AA) and C11000 Copper (Cu), using the FSW process and quantifying the welds produced through metallurgical evaluation, mechanical testing, X-Ray Diffraction analysis and electrical resistance measurements to achieve the best welds with limited or no intermetallic compounds at the joint interface.

An extensive literature review, as presented in Chapter 2, has discussed in detail the FSW process and the significance of its essential parameters. Dissimilar metal joining and a critical look at the available literature sources on FSW of aluminium and copper alloys have also been discussed.

The reviewed literature revealed the difficulty in joining aluminium and copper by means of conventional welding processes due to the high affinity between both metals; and attempts to join these metals, using solid state processes have resulted in the formation of hard and brittle intermetallic compounds at the joint interfaces. These intermetallics are known to lower the toughness of the weld and increase the joint electrical resistivity.

The knowledge gap identified in the literature is that there is no existing report on any established process window for the FSW of Al and Cu. Also, detailed characterisation (mechanical and electrical) of FSwelds between Al and Cu, as dealt with in this thesis, do not exist. In addition, there is no published work on joints between Al and Cu without the formation of intermetallic compounds at the joint interface.

The detailed experimental procedures employed in this research work were presented in Chapter 3. These include the various methods of analysis conducted on the welded samples, viz: metallurgical characterisation, mechanical testing, electrical resistance measurements and X-Ray Diffraction. The decisions on the final weld matrix employed in this research work were based on the analysis of the joint quality

of welds produced during the preliminary investigation phase. Different tool dimensions were considered; and it was decided to use three different shoulder diameter tools, viz: 15, 18 and 25 mm (all the other dimensions remain constant) for the final weld matrix in order to vary the heat input into the welds. This was done to compare the formed intermetallics at the joint interfaces of the welds, as they are known to be thermally activated. Also, the range of process parameters and the different shoulder diameter tools considered were employed to achieve welds with limited or no intermetallics.

Other conclusions based on the preliminary investigation were to place Copper at the advancing side during the welding process, and to offset the tool pin to 2.5 mm in to the aluminium alloy sheet (tool pin in aluminium) from the joint interface<sup>165</sup> for all the welds produced with the final weld matrix to achieve the best results.

### 5.1.1 Conclusions

The results and discussions of the welds produced with the final weld matrix comprising 27 weld samples were presented in Chapter 4. This section reports the summary of the analyses conducted on the weld samples, as well as the trends observed.

The common trend observed in the inter-relationship between the input and output process parameters, is that the advancing force ( $F_x$ ) and the torque ( $T$ ) increases as the vertical downward force ( $F_z$ ) increased but the heat input into the welds, ( $Q$ ), decreases. The welds produced at the lowest travel speeds of 50 mm/min have the highest heat inputs. This is expected, because the tool travels slowly, therefore, majority of the heat generated during the welding process is contained in the weld. The interrelationships observed between the process parameters and weld properties are discussed later.

The macrographs revealed that the joint interfaces of all the welds were characterised by mixture layers containing aluminium and copper. This indicates good material flow during the welding process. An increase in the tool shoulder diameters led to a significant increase in the Stir Zone (SZ) and Thermal-

Mechanically Affected Zone (TMAZ) of the welds due to an increase in the heat input which increases as the shoulder diameter increases.

It should be noted that all microstructural zones viz: HAZ, TMAZ and SZ were observed in the weld cross-sections although it was not representative of a typical FSW of a single phase alloy like aluminium. Optical micrographs of all the welds compared with the process parameters, revealed that better mixing and metallurgical bonding of both metals were achieved at the lowest travel speed considered in this research work. The better mixing achieved at the lowest travel speed is related to the tensile results. It was observed that 100% of the welds produced at the lowest travel speed of 50 mm/min with the 18 mm shoulder diameter tool have higher UTS compared with the welds produced at 150 and 300 mm/min. The TMAZ and the SZ of all the weld settings experienced grain deformation in a similar way regardless of the shoulder diameter tools employed. The grain sizes decreased from the parent material towards the SZ of the welds.

The tensile test data revealed that the Ultimate Tensile Strength (UTS) of welds decreased as the feed rate increases. This was related to the heat input into the welds, which is lower at high feed rates. Hence, the coalescence of both materials joined is not satisfactorily achieved. This has resulted in the low UTS values obtained in welds produced at higher feed rates. The Weld Joint Efficiencies of the welds were considered, and it was found that 33% of the welds produced with the 15 and 18 mm shoulder diameter tools are within the acceptable range. But none of the welds produced with the 25 mm shoulder diameter tool had acceptable Weld Joint Efficiency. It can be concluded that the 25 mm shoulder tool is too wide for this application and should not be considered for further research.

The microhardness profiles of the weld samples were correlated with the microstructures of the joint interfaces; and it was found that the high Vickers microhardness values measured corresponded with the intermetallic compounds in those regions. Energy Dispersive Spectroscopy (EDS) analysis revealed that the hardness values at the interfacial regions varies due to the distribution pattern of the intermetallic phases present, as well as the variation in the amount of deformation

the material had experienced. Fairly homogeneous microhardness profiles were achieved in welds produced at high feed rates of 300 mm/min due to the low heat input. These do not favour the formation of intermetallics in such welds.

In general, the effect of grain size on strength is given by the Hall-Petch equation,

$$\sigma_0 = \sigma_i + kd^{-1/2} \quad 5.1$$

Where,

$\sigma_0$  = the yield stress.

$\sigma_i$  = the "friction stress," representing the overall resistance of the crystal lattice to dislocation movement.

$k$  = a constant, "locking parameter," which measures the relative hardening contribution of the grain boundaries.

$d$  = grain diameter.

From the Hall-Petch equation, it is known that as the average grain size decreases, the metal becomes stronger (more resistant to plastic flow)<sup>166</sup>, hence, the strength increases. In this research work, it was observed that the properties of the joints produced obeyed the Hall-Petch equation in that the strength increases as the grain size decreases. It should be noted that in the welds produced with the 18 mm shoulder diameter tool, the tensile strength decreases as the feed rate increases. This is as a result of higher degree of deformation (decrease in grain size) experienced in welds produced at lower feed rates compared with the higher feed rates.

The XRD analysis revealed the formed intermetallic compounds at the joint interfaces of the FS welds produced in this research work, the most common intermetallics being  $\text{Al}_2\text{Cu}$  and  $\text{Al}_4\text{Cu}_9$ , though their concentrations in the welds were very low. The  $\text{Al}_2\text{Cu}$  intermetallic compound was expected, because it is formed at a temperature lower than the expected welding temperature, and the  $\text{Al}_4\text{Cu}_9$  intermetallic compound were also formed due to high temperature welding conditions. Welds S15\_09 and S18\_09 produced at 1200 rpm and 300 mm/min with the 15 and 18 mm shoulder diameter tools respectively, have very low volume fraction volume of intermetallics.

The joint electrical resistivities increased, as the heat input increased at the constant rotational speeds employed. Very little variation compared with the average joint resistance of the parent materials was observed in the electrical resistivity reading from one weld to the other. The weld settings used in this research work can therefore be recommended to produce welds with low or no electrical resistivity.

The results of the statistical analysis of some of the weld data are as follows:

Analysis of Variants (ANOVA) revealed that there is an indication of interaction between the spindle speed and the feed rate on the weld properties. Regression analysis revealed that downward vertical force, ( $F_z$ ) has a significant effect on the UTS of welds. Scatter plots of electrical resistivities of the joints compared with the heat input, showed that the electrical resistivity of the joints increases as the heat input increases, but it is limited at a certain point when the electrical resistivity becomes constant. Surface plots relating the downward vertical force, ( $F_z$ ) to the most important FSW input process parameters (spindle speed and feed rate) revealed that ( $F_z$ ) increases as the feed rate and spindle speed increases.

### **6.1.1 Final Conclusions**

The proposed objective and the sub-objectives of this research work were successfully achieved. Dissimilar metal Friction Stir welds between 5754 Aluminium Alloy and C11000 Copper were produced, and detailed characterisation and statistical valid analyses were conducted.

Based on the range of parameter settings considered, the research work has been able to establish a process window at a medium spindle speed of 950 rpm; and feed rate between 50 and 150 mm/min, as the most appropriate to join aluminium and copper. Furthermore, successful FS welds between Al/Cu with limited and without identified intermetallic compounds were produced. This is a success story in the joining of Aluminium and Copper, because the presence of intermetallic compounds is known to increase the electrical resistivities of the joints, which negatively affects the performance of the joints. All the welds produced were characterised by low joint electrical resistivities; and the results showed that the process window evaluated in this research work can be recommended.

This research work has also provided a platform for the availability of literatures relative to detailed characterisation of FS welded joints between Aluminium and Copper. This should be a handy tool for industry for commercialisation and the research community.

## 5.2 Future work

While significant work has already been achieved in this study, there are still some aspects that require further investigation. These include:

1. Statistical analysis has revealed that the vertical downward force, ( $F_z$ ), could have a significant effect on the weld qualities; and it was observed that the FSW force feedback plots had unstable patterns. Further investigation is required to achieve a more stable welding condition. All the welds produced in this research work were produced using position control; employing force control mode during the welding process might, in any case, be on the way out.
2. Study the effect of different tool geometries on the joint integrity of the FSW of Al/Cu.
3. Detailed characterisation of welds produced over a range of parameter settings should be conducted on lap joints of aluminium and copper.
4. The joining of aluminium to copper is a metal-to-metal contact; further work should be done by conducting corrosion tests on the welded samples and relating this to the electrical resistivities of the joints.
5. Temperature measurements during the welding process should be conducted to ascertain that the Aluminium alloy with a lower melting point to Copper is not melted during the process.

The above listed tests coupled with the work completed in this study would provide a comprehensive study on the Friction Stir Welding of Aluminium and Copper.

---

## REFERENCES

1. Thomas W M, Nicholas ED, Needham JC, Murch MG, Templesmith P, Dawes CJ. *Improvements relating to Friction Welding. International Patent Application*, PCT/GB92/02203 (Patent) December 1991.
2. Shinoda T, Tokisue H, Enomoto M. *Recent Trends of research and development of FSW Technology in Japan*. 3<sup>rd</sup> International FSW Symposium, Kobe, Japan, 27-28 September 2001. TWI (UK). Retrieved: CD-ROM.
3. Reynolds AP. Friction stir welding of aluminium alloys. In: Totten GE, MacKenzie DS (eds.) *Handbook of Aluminium, Volume 2 Alloy Production and Materials Manufacturing*. New York, Marcel Dekker; 2003. p. 579-700.
4. Friction stir welding. Available from:  
[http://en.wikipedia.org/wiki/Friction\\_stir\\_welding](http://en.wikipedia.org/wiki/Friction_stir_welding) [Accessed April 2008].
5. Friction stir welding. Available from:  
[http://www.fpe.co.uk/frictionstir\\_welding.htm](http://www.fpe.co.uk/frictionstir_welding.htm) [Accessed July 2008].
6. Nandan R, DebRoy T, Bhadeshia HKDH. Recent advances in friction stir welding- Process, weldment structure and properties. *Progress in Material Science* 2008; 53: p. 980-1023.
7. Bhadeshia HKDH. Friction stir welding. Available from:  
<http://www.msm.cam.ac.uk/phase-trans/2003/FSW/aaa.html> [Accessed August 2009].
8. Thomas WM, Norris I, Staines D, Clarke P, Horrex N. *Friction stir welding- variants and process techniques*. 1<sup>st</sup> International Conference 'Joining of Aluminium structures'. Moscow, Russia. 3-5 December 2007.

9. Moriera PMGP, Santos T, Tavares SMO, Richter-Trummer V, Vilaca P, De Castro PMST. Mechanical and metallurgical characterisation of friction stir welding joints of AA6061–T6 with AA6082-T6. *Materials and Design* 2009; 30: p. 180-187.
10. Larsson H, Karlsson L, Svensson L. Friction stir welding of AA 5083 and AA 6082 aluminium. *A welding review published by ESAB AB, Svetsaren, Sweden*. 2000 Vol 54 No 2.
11. Yoshikawa K. *A joining criterion for lap welding of dissimilar metal materials of aluminium and stainless steel*. 4<sup>th</sup> International FSW symposium, Park City, Utah. 14-16 May 2003. TWI (UK). Retrieved: CD-ROM.
12. Fukumoto M, Yasui T, Shinoda Y, Tshubaki M, Shinoda T. *Butt welding between dissimilar metals by friction stirring*. 5<sup>th</sup> International FSW symposium, Metz, France. 14-16 September 2004. TWI (UK). Retrieved: CD-ROM.
13. Uzun H, Dalle CD, Argagnotto A, Ghidini T, Gambaro C. Friction stir welding of dissimilar Al 6013-T4 to X5CrNi 18-10 stainless steel. *Materials and Design* 2005; 26: p. 41-46.
14. Zettler R, Dos Santos JF, Blanco A, Silver A. *A study of dissimilar friction stir welds between Al and Mg alloys*. 7<sup>th</sup> International conference on trends in welding research. Georgia, USA. ASM International. 16-20 May 2005.
15. Watanabe T, Hirofumi T, Yanagisawa A. Joining of aluminium alloy to steel by friction stir welding. *Materials Processing Technology* 2006; 178: p. 342-349.
16. Mai TA, Spowage AC. Characterisation of dissimilar joints in laser welding of steel – kovar, copper – steel and copper- aluminium. *Materials Science and Engineering A* 2004; 374; p. 224-233.

- 
17. Bus-bar. Available from: <http://en.wikipedia.org/wiki/Bus-bar> [Accessed June 2009].
  18. Design Considerations. Available from: <http://www.copperinfo.co.uk/bus-bars/pub22-copper-for-bus-bars/sec1.htm> [Accessed June 2009].
  19. Record JH, Covington JL, Nelson TW, Sorensen CD, Webb BW. *Fundamental characterisation of friction stir welding*. 5<sup>th</sup> International FSW symposium Metz, France. 14-16 September 2004. TWI (UK). Retrieved: CD-ROM.
  20. Blignault C. *Design, development and analysis of the friction stir welding process*. M.Tech dissertation. Faculty of Engineering, Port Elizabeth Technikon, South Africa; 2002.
  21. Zorc TB, Reidenbach F, Sobie NM, Harrison LA (eds.) *ASM Handbook Welding, brazing and soldering*. Vol 6. ASM International, USA; 1993.
  22. O'Brien A, Guzman C (eds.) *American Welding Society, Welding Handbook Welding Processes*, part 2 volume 3 Ninth Edition Miami: American Welding Society; 2007.
  23. Khaled T. *An outsider looks at Friction stir welding*. Federal Aviation Administration. Report number: ANM-112N-05-06, 2005.
  24. Mishra RS, Mahoney MW. *Introduction*. In: *Friction stir welding and processing*. Mishra RS, Mahoney MW (ed.) Materials Park Ohio: ASM International; 2007.
  25. Mishra RS, Ma ZY. Friction stir welding and processing. *Materials Science and Engineering R*. 2005; 50: p1-78.
  26. London B, Mahoney M, Bringel WB, Calabrese M, Bossi RH, Waldron D. Material flow in friction stir welding monitored with Al-SiC and Al-W composite

- markers. *Friction Stir Welding and Processing II*. Jata KV, Mahoney MW, Lienert TJ, Mishra RS (eds.) The Minerals, Metals and Materials Society (TMS). 2003; p. 3-12.
27. Rhodes CG, Mahoney MW, Bingel WH, Spurling RA, Bampton CC. Effects of friction stir welding on microstructure of 7075 aluminium. *Scripta Materialia*. 1997; 36(1): p. 69-75.
28. Liu G, Murr LE, Niou CS, McClure JC, Vega FR. Microstructural aspects of the friction stir welding of 6061-T6 aluminium. *Scripta Materialia*. 1997; 37(3): p. 355-361.
29. Jata KV, Semiatin SL. Continuous dynamic recrystallization during friction stir welding of high strength aluminium alloys. *Scripta Materialia* 2000; 43(8): p. 743-749.
30. Dawes CJ, Thomas WM. *Development of improved tool designs for friction stir welding of aluminium*. 1<sup>st</sup> International FSW symposium, Thousand Oaks, CA, USA. 14-16 June 1999. TWI (UK). Retrieved: CD-ROM.
31. Staron P, Kocak M, Williams S, Wescott A. Residual stress in friction stir-welded Al sheets. *Physica B* 2004; 350: p. 491-493.
32. Steuwer A, Peel MJ, Withers PJ. Dissimilar friction stir welds in AA5083-AA6082: The effect of process parameters on residual stress. *Materials Science and Engineering A* 2006; 441: p. 187-196.
33. Prime MB, Gnäupel-Herold T, Baumann JA, Lederich RJ, Bowden DM, Sebring RJ. Residual stress measurements in a thick, dissimilar aluminium alloy friction stir weld. *Acta Materialia* 2006; 54: p. 4013-4021.

- 
34. James MN, Hughes DJ, Chen Z, Lombard H, Hattingh DG, Asquith D, Yates JR, Webster PJ. Residual stresses and fatigue performance. *Engineering failure analysis* 2007; 14: p. 384-395.
35. Lombard H, Hattingh DG, Steuwer A, James MN. Effect of process parameters on the residual stresses in AA5083-H321 friction stir welds. *Materials Science and Engineering A* 2009; 501: p. 119-124.
36. Shukla AK, Baeslack WA. *Process-property relationship and microstructure evolution in friction stir welded thin sheet 2024-T3 aluminium alloy*. 7<sup>th</sup> International conference on trends in welding research. Georgia, USA. ASM International; 16-20 May 2005. p. 173-178.
37. Kurt A, Uygur I, Ates H. *The effect of shoulder diameter to weldability on the friction stir welding*. 6<sup>th</sup> International FSW symposium Montreal, Canada. 10-13 October 2006. TWI (UK). Retrieved: CD-ROM.
38. Buffa G, Campanile G, Fratini L, Prisco A. Friction stir welding of lap joint: Influence of process parameters on the metallurgical and mechanical properties. *Materials Science and Engineering A* 2009; 519:p. 19-26.
39. Dubourg L, Dacheux P. *Design and properties of FSW tools*. 6<sup>th</sup> International FSW symposium Montreal, Canada. 10-13 October 2006. TWI (UK). Retrieved: CD-ROM.
40. St-Georges L, Dasyva-Raymond V, Kiss LI, Perron AL. *Prediction of optimal parameters of friction stir welding*. 6<sup>th</sup> International FSW symposium Montreal, Canada. 10-13 October 2006. TWI (UK). Retrieved: CD-ROM.
41. Commin L, Dumont M, Masse JE, Barrallier L. Friction stir welding of AZ31 magnesium alloy rolled sheets: influence of processing parameters. *Acta Materialia* 2009; 57: p. 326-334.

- 
42. Steuwer A, Peel MJ, Withers PJ. *Influence of welding speed on the properties of AA 5083 – AA 6082 dissimilar friction stir welds*. 6<sup>th</sup> International FSW symposium. 2006. Montreal, Canada. 10-13 October 2006. TWI (UK). Retrieved: CD-ROM.
43. Fuller C, Mahoney M, Bingel W. *A study of friction stir processing tool designs for micro structural modifications as demonstrated by aluminium fusions welds*. 5<sup>th</sup> International FSW symposium, Metz, France. 14-16 September 2004. TWI (UK). Retrieved: CD-ROM.
44. Nelson TW, Hunsaker B, Field DP. *Local texture characterisation of friction stir welds in 1100 Aluminium*. 1<sup>st</sup> International FSW symposium, Thousand Oaks, CA. 14-16 June 1999. TWI (UK). Retrieved: CD-ROM.
45. Nelson TW, Hang HZ, Haynes T. *Friction stir welding of aluminium MMC 6061 Boron Carbide*. 2<sup>nd</sup> International FSW symposium, Gothenburg, Sweden. 26-28 June 2000. TWI (UK). Retrieved: CD-ROM.
46. Colligan K. *Dynamic material deformation during friction stir welding of aluminium*. 1<sup>st</sup> International FSW symposium, Thousand Oaks, CA. 14-16 June 2000. TWI (UK). Retrieved: CD-ROM.
47. Packer S, Nelson T, Sorensen C, Steel R, Matsunaga M. *Tool and equipment requirements for FSW ferrous and other high Melting temperature alloys*. 4<sup>th</sup> International FSW symposium, Park City, UT. 14-16 May 2003. TWI (UK). Retrieved: CD-ROM.
48. Colligan KJ, Xu J, Pickens JR. Welding tool and process parameter effects in friction stir welding of aluminium alloys. *Friction Stir Welding and Processing II*, Jata KV, Mahoney MW, Mishra RS, Semiatin SL, Lienert T (eds.) The Minerals, Metals and Materials Society (TMS). 2003; p. 181-190.

49. Subramanian PR, Nirmalan NV, Young LM, Sudkamp P, Larsen M, Dupree PL, Shukla AK. Effect of microstructural evolution in mechanical and corrosion behaviour of friction stir processed aluminium alloys. *Friction Stir welding and Processing II*. Jata KV, Mahoney MW, Mishra RS, Semiatin SL, Lienert T (eds.) The Minerals, Metals and Materials Society (TMS). 2003; p. 235-242.
50. Lienert TJ, Stellwag WL, Lehman LR. *Heat inputs, peak temperatures, and process Efficiencies for FSW*. 4<sup>th</sup> international FSW symposium, Park City, Utah. 14-16 May 2003. TWI (UK). Retrieved: CD-ROM.
51. Savolainen K, Mononen J, Saukkoren T, Hanninen H, Koivula J. *Friction stir weldability of copper alloys*. 5<sup>th</sup> International FSW symposium, Metz, France. 14-16 September 2004. TWI (UK). Retrieved: CD-ROM.
52. Stahl AL, Sorensen CD. Experimental measurements of load distributions on friction stir welding pin tools. *Friction Stir Welding and Processing III*. Jata KV, Mahoney MW, Mishra RS, Semiatin SL, Lienert T (eds.) Minerals, Metals and Materials Society (TMS). 2005. p. 179-190.
53. Fuller CB. *Friction stir tooling: Tool materials and designs*. In: *Friction stir welding and processing*. Mishra RS, Mahoney MW (eds.) Materials Park Ohio; ASM International; 2007.
54. Brinckmann S, von Strombeck A, Schilling C, dos Santos JF, Lohwasser D and Koçak M. *Mechanical and toughness properties of robotic-FSW repair welds in 6061-T6 aluminium alloys*. 2<sup>nd</sup> International FSW symposium, Gothenburg, Sweden. 26-28 June 2000. TWI (UK). Retrieved: CD-ROM.
55. Guerra M, Schmidt C, McClure JC, Murr LE, Nunes AC. Flow patterns during friction stir welding. 2003. *Materials Characterisation* 2003; 49: p. 95-101.
56. Blignault C. *A friction stir weld tool-force and response surface model characterizing tool performance and weld joint integrity*. D.Tech thesis. Faculty

---

of Engineering, Nelson Mandela Metropolitan University, Port Elizabeth, South Africa; 2006.

57. Thomas WM, Johnson KI, Wiesner CS. Friction stir welding- recent development in tool and process technologies. *Advanced engineering materials*. 2003. 5: 485-490. In: Nandan R, DebRoy T, Bhadeshia HKDH. Recent advances in friction stir welding- process, weldment structure and properties. *Progress in Material science* 2008; 53: p. 980-1023.
58. Thomas WM, Braithwaite ABM, John R. *Skew-Stir™ technology*. 3<sup>rd</sup> International FSW Symposium. Kobe, Japan. 27-28 September 2001. Retrieved: CD-ROM.
59. Thomas WM, Dolby RE. *Friction stir welding developments*. 6<sup>th</sup> International conference on trends in welding research. Georgia, USA. ASM International. 15-19 April 2002.
60. Thomas WM, Staines DG, Norris IM, Frias R. *Friction stir welding- Tools and development. FSW seminar*. IST Porto, Portugal. 03 December 2002.
61. Zhao YH, Lin SB, Qu F, Wu L. Influence of pin geometry on process material flow in friction stir welding process. *Material Science Technology* 2006. 22: p. 45-60.
62. Kumar K, Kailas SV. The role of friction stir welding tool on material flow and weld formation. *Materials Science and Engineering A* 2008; 485: p. 367- 374.
63. Leal RM, Leitão C, Loureiro A, Rodrigues DM, Vilaca P. Material flow in heterogeneous friction stir welding of thin aluminium sheets: Effect of shoulder geometry, *Material Science and Engineering A* 2008; 498: p. 384 – 391.

- 
64. Clark DE, Miller KS, Tolle CR. *Tool designs in friction stir processing dynamic forces and material flow*. 7<sup>th</sup> International conference on trends in welding research. Georgia, USA. ASM International. 16-20 May 2005. p. 173-178.
65. Fujii H, Cui L, Maeda M, Nogi K. Effect of tool shape on mechanical properties and microstructure of friction stir welded aluminium alloys. *Materials Science and Engineering A* 2006; 419: p. 25-31.
66. Rodrigues DM, Loureiro A, Leitão C, Leal RM, Chaparro BM, Vilaca P. Influence of friction stir welding parameters on the microstructural and mechanical properties of AA 6016 – T4 thin welds. *Materials and Design* 2008. *J Mater Design* (2008), doi:10.1016/j.matdes.2008.09.016. Article in press.
67. Cui S, Chen ZW. Effects of rotation speed and welding zone formation during friction stir welding and processing. *Friction Stir Welding and Processing V*. 2009. Mishra RS, Mahoney MW, Lienert TJ (eds.) Minerals, Metals and Materials Society (TMS). p. 125-133.
68. London B, Mahoney M, Bingel WB, Calabrese M, Waldron D. *Experimental methods for determining material flow in friction stir welds*. 3<sup>rd</sup> International FSW Symposium, Kobe, Japan, 27-28 September 2001. TWI (UK). Retrieved: CD-ROM.
69. Hashimoto T, Jyogan S, Nakata K, Kim YG, Ushio M. *FSW joints of high strength aluminium alloy*. 1<sup>st</sup> International FSW symposium, Thousand Oaks, CA, USA. 14-16 June 1999. TWI (UK). Retrieved: CD-ROM.
70. Lombard H. *Optimized fatigue and fracture performance of friction stir welded aluminium plate: A study of the inter-relationship between process parameters, TMAZ, microstructure, defect population and performance*. PhD thesis. University of Plymouth, England; 2007.

71. Cavaliere P, Campanile G, Panella F, Squillace A. Effect of Welding parameters on mechanical and microstructural properties of AA 6056 joints produced by friction stir welding. *Materials Processing Technology*. 2006. 180: p. 263-270.
72. Cavaliere P, De Santis A, Panella F, Squillace A. Effect of Welding parameter on mechanical and microstructural properties of AA 6082 –AA2024 joints produced by friction stir welding. 2009. *Materials and Design* 2009. 30: p. 609 – 616.
73. Shinoda T. *Effect of tool angle on metal flow phenomenon in friction stir welds*. 3<sup>rd</sup> International FSW Symposium, Kobe, Japan, 27-28 September 2001. TWI (UK). Retrieved: CD-ROM.
74. Arici A, Selale S. Effects of tool tilt angle on tensile strength and fracture locations of friction stir welding of polyethylene. *Science and Technology of Welding and Joining*. 2007. 12 (6): p. 536-539.
75. Friction Stir Welding - Joint geometries. Available from <http://www.twi.co.uk/content/FSWjoint.html> [Accessed July 2007].
76. Colligan KJ, Mishra RS. A conceptual model for the process variables related to heat generation in friction stir welding of aluminium. *Scripta Materialia*. 2008. (58): p. 327-331.
77. Tutum CC, Schmidt H, Hattel J, Bendsoe MP. *Estimation of the welding speed and heat input in friction stir welding using thermal models and optimisation*. 7<sup>th</sup> World Congress on Structural and Multidisciplinary Optimisation. Seoul, Korea. 21-25 May 2007.
78. Reynolds AP. Microstructure development in aluminium alloy friction stir welds. In: Mishra RS, Mahoney MW. (ed.) *Friction Stir Welding and Processing*. Materials Park Ohio, ASM International, 2007.

79. Threadgill PL. *Friction stir welds in aluminium alloys – preliminary microstructural assessment*. TWI Bulletin, March/April 1997. Available from: [http://www.twi.co.uk/content/bulletin\\_38\\_2a2.html](http://www.twi.co.uk/content/bulletin_38_2a2.html) [Accessed April 2009].
80. Threadgill PL. Terminology in friction stir welding. *Science and Technology of Welding and Joining*. 2007; 12(4): p. 357- 360.
81. TWI (The Welding Institute) Microstructural classification of friction stir welds. Available from: [http://www.twi.co.uk/j32k/unprotected/band\\_1/FSWqual.html](http://www.twi.co.uk/j32k/unprotected/band_1/FSWqual.html). [Accessed May 2009].
82. Mahoney MW. Mechanical properties of friction stir welded aluminium alloys. In: Mishra RS, Mahoney MW. (ed.) *Friction Stir Welding and Processing*. Materials Park Ohio, ASM International, 2007.
83. Liu P, Shi Q, Wang W, Wang X, Zhang Z. Microstructure and XRD analysis of FSW joints for copper T2/aluminium 5A06 dissimilar materials. *Materials letters* 2008; 62: p. 4106- 4108.
84. Venkateswaran P, Xu Z, Li X, Reynolds AP. Determination of mechanical properties of Al-Mg alloys dissimilar friction stir welded interface by indentation methods. *Journal of Material Science* 2009; 44: p. 4140-4147.
85. Lee WB, Bang KS, Jung SB. Effects of intermetallic compound on the electrical and mechanical properties of friction welded Cu/Al bimetallic joints during annealing. *Journal of Alloys and Compounds* 2005; 390: p. 212-219.
86. Afrin N, Chen DL, Cao X, Jahazi M. Microstructure and tensile properties of friction stir welded AZ31B magnesium alloy. *Materials Science Engineering A* 2008; 472: p. 179-186.

87. Attalah MM, Davis CL, Strangwood M. Microstructure-microhardness relationships in friction stir welded AA5251. *Journal of Material Science* ©Springer Science Business Media, LLC 2007.
88. Blignault C, Kallee SW, Thomas WM, Russell MJ. *Friction stir weld integrity and its importance to the rolling stock industry*. Proceedings of the 60<sup>th</sup> Anniversary of SAIW at Johannesburg, South African Institute of Welding, 28-29 May 2008.
89. Leonard AJ, Lockyer SA. *Flaws in friction stir welds*. 4<sup>th</sup> International FSW symposium, Park City, Utah. 14-16 May 2003. TWI (UK). Retrieved: CD-ROM.
90. Reynolds AP, Khandkar Z, Long T, Tang W and Khan J. Utility of relatively simple models for understanding process parameter effects on FSW. *Materials Science Forum* 2003; 426: p. 2959-2694.
91. Defects/imperfections in welds – porosity. Available from: <http://www.twi.co.uk/content/j42.html> [Assessed July 2009].
92. Arbegast WJ. A flow-partitioned deformation zone model for defect formation during friction stir welding. *Scripta Materialia*. 2008; 58: p. 372-376.
93. Colligan K, Ucock I, McTernan K, Konko PJ, Pickens JR. *Friction stir welding of thick section 5083-H131 and 2195-T8P4 aluminium plates*. 3<sup>rd</sup> International FSW Symposium, Kobe, Japan, 27-28 September, 2001. Retrieved: CD-ROM.
94. Crawford R, Cook GE, Strauss AM, Hartman DA, Stremmer MA. Experimental defect analysis and force prediction simulation of high weld pitch friction stir welding. *Science and Technology of Welding and Joining* 2006; 11(6): p. 657-665.

95. Jones MJ, Heurtier P, Desrayaud C, Montheillet F, Allehaux D, Driver JH. Correlation between microstructure and microhardness in a friction stir welded 2024 aluminium alloy. *Scripta Materialia*. 2005; 52: p. 693-697.
96. Peel M, Steuwer A, Preuss M, Withers PJ. Microstructure, mechanical properties and residual stresses as a function of welding speed in aluminium AA5083 friction stir welds. *Acta Materialia* 2003; 51: p.4791-4801.
97. Krishnan KN. On the formation of onion rings in friction stir welds. *Materials Science Engineering A* 2002; 327: p. 246-251.
98. Amancio-Filho ST, Sheikhi S, Dos Santos JF, Bolfarini C. preliminary study on the microstructure and mechanical properties of dissimilar friction stir welds in aircraft aluminium alloys 2024-T351 and 6056-T4. *Journal of materials Processing technology* 2008; 206: p. 132-142.
99. Attalah MM, Davis CL, Strangwood M. *Microstructure-property development in friction stir welds of Al-Mg alloys*. 8<sup>th</sup> International conference on trends in welding research. Georgia, USA. ASM International; 1-6 June 2008.
100. Khodir SA, Shibayanagi T. Friction stir welding of dissimilar AA2024 and AA7075 aluminium alloys. *Materials Science Engineering B* 2008; 148: p. 82-87.
101. Sato YS, Sugiura Y, Shogi Y, Park SHC, Kokawa H, Ikeda K. *Effect of microstructure on postweld formability in friction stir welded Al alloy* . 7<sup>th</sup> International conference on trends in welding research. Georgia, USA. ASM International; 16-20 May 2005.
102. Yan J, Xu Z, Li Z, Li L, Yang S. Microstructure characteristics and performance of dissimilar welds between magnesium alloy and aluminium formed by friction stirring. *Scripta Materialia* 2005; 53: p. 585-589.

103. Somasekharan AC, Murr LE. Microstructures in friction stir welded dissimilar magnesium alloys and magnesium alloys to 6061-T6 aluminium alloy. *Material Characterisation* 2004; 52: p. 49-52.
104. Chen ZW, Pasang T, Qi Y. Shear flow and formation of nugget zone during friction stir welding of aluminium alloy 5083-O. *Materials Science Engineering A* 2008; 474: p. 312-316.
105. Vural M, Ogor A, Cam G, Ozarpa C. On the friction stir welding of aluminium EN AW 2024-0 and EN AW 5754-H22. *Archives of Materials Science and Engineering* 2007; 28(1): p. 49-54.
106. Cao X, Jahazi M. Effect of welding speed on the quality of friction stir welded butt joints of a magnesium alloy. *Materials and Design* 2009, 30: p. 2033-2042.
107. Leitao C, Leal RM, Rodrigues DM, Loureiro A, Vilaca P. Mechanical behaviour of similar and dissimilar AA5182-H111 and AA6016-T4 thin friction stir welds. *Materials and Design* 2009; 30: p. 101-108.
108. Polar A, Rumiche F, Pareek M, Indacochea JE. *Friction stir welding of copper: metallurgical characterisation and corrosion resistance*. 7<sup>th</sup> International conference on trends in welding research. Georgia, USA. ASM International. 16-20 May 2005.
109. Lim S, Kim S, Lee C, Kim S. Tensile behaviour of friction stir welded Al 6061-T651. *Metallurgical and Materials Transactions A* 2004; 35: p. 2829-2835.
110. Lim S, Kim S, Lee C, Kim S. Tensile behaviour of friction stir welded A356-T6/Al 6061T651 bi-alloy plate. *Metallurgical and Materials Transactions A*. 2004; 35: p. 2837-2843.

111. Ceschini L, Boromei I, Minak G, Morri A, Tarterini F. Effect of friction stir welding on microstructure, tensile and fatigue properties of the AA7005/10% vol. %Al<sub>2</sub>O<sub>3</sub>P composite. *Composites Science and Technology* 2007; 67: p. 605-615.
112. Savolainen K, Mononen J, Saukkonen T, Hänninen H. *A preliminary study on friction stir welding of dissimilar metal joints of copper and aluminium*. 6<sup>th</sup> International FSW symposium. Montreal, Canada. 10-13 October 2006. TWI (UK). Retrieved: CD-ROM.
113. Braunović M, Alexandrov N. Intermetallic compounds at aluminium –to – copper electrical interfaces: effect of temperature and electric current. *IEEE Transactions on Components, Packaging, and Manufacturing Technology – Part A*1994; 17(1): p. 78-85.
114. Massalski TB, Okamoto H, Subramanian PR, Kacprzak, L. *Binary alloy phase diagrams*, ASM International, Ohio, USA; 1990. p:141-143.
115. Barradas S, Guipont V, Molins R, Jeandin M, Arrigoni M, Boustie M, Bolis C, Berthe L, Ducos M. Laser shock flier impact simulation of particle-substrate interactions in cold spray. *Journal of Thermal Spray Technology* 2007; 16:p. 548-556.
116. Enjo T, Ikeuchi K, Akikawa N. Diffusion welding of copper to aluminium. *Transactions of JWRI* 1979; 8:p. 77-84.
117. Rabkin DM, Ryabov VR, Lozovskaya AV, Dovzhenko VA. Preparation and properties of copper-aluminium intermetallic compounds. *Soviet Powder Metallurgy and Metals* 1970; 8:p. 695-700.
118. Kim H, Lee YJ, Koh K, Won, J, Choe S, Lee J, Moon J, Park Y. Effects of Cu/Al intermetallic compound on copper wire and aluminium pad bondability.

- IEEE Transactions on Components and Packaging Technologies* 2003; 26:p. 367-374.
119. Davis JR (ed). *ASM Specialty Handbook Copper and Copper Alloys*. ASM International, Ohio, USA; 2001. p: 370.
120. Lee WB, Schmuecker M, Mercardo UA, Biallas G, Jung S. Interfacial reaction in steel-aluminium joints made by friction stir welding. *Scripta Materialia* 2006; 55: p. 355-358.
121. Kwon YJ, Shigematsu I, Saito N. Dissimilar friction stir welding between magnesium and aluminium alloys. *Materials Letters* 2008; 62: p. 3827-3829.
122. Tanaka T, Morishige T, Hirata T. Comprehensive analysis of joint strength for dissimilar friction stir welds of mild steel to aluminium alloys. *Scripta Materialia* 2009; 61: p. 756-759.
123. Ouyang J, Yarrapareddy E, Kovacevic R. Microstructural evolution in the friction stir welded 6061 aluminium alloy (T6- temper condition) to copper. *Journal of Materials Processing technology* 2006; 172: p. 110-122.
124. Okamura H, Aota K, Satou K, Sakamoto M. *Friction stir welding method and component part welded by the method*. US20030102354A1 (Patent) 2003.
125. Abbasi M, Taheri AK, Salehi MT. Growth rate of intermetallic compounds in Al/ Cu bimetal produced by cold roll welding process. *Journal of Alloys and Compounds* 2001; 319: p. 233 – 241.
126. Ultrasonic Energy Welds Copper to Aluminium. Available from: [http://www.amtechultrasonic.com/articles\\_weldingjournal\\_0197.asp](http://www.amtechultrasonic.com/articles_weldingjournal_0197.asp) [Accessed May 2008].

127. Priem D, Marya SK. Application of magnetic pulse welding for dissimilar aluminium – copper joints. Available from: <http://www.aws.org/conferences/2003>. [Accessed June 2008].
128. Theron M, van Rooyen C, Ivanchev LH. *CW ND: YAG laser welding of dissimilar sheet metals*. Paper #803, National Laser Centre, CSIR.
129. Schmidt M, Weigl M. *Modulated laser spot welding of dissimilar copper-aluminium connections*. Bayerisches Laserzentrum GmbH, Konrad-Zuse Str.2-6, 91052, Germany.
130. Mozhaiskaya TM, Chekanova NT. Structure and properties of welded aluminium-copper joints. *Metal Science and Heat treatment* 1990; 32: p. 938-939.
131. Murr LE, Flores RD, Flores OV, McClure JC, Liu G, Brown D. Friction stir welding: Microstructural characterisation. *Material Resources Innovation* 1998; 1: p. 211-223.
132. Murr LE, Li Y, Flores RD, Trillo EA, McClure JC. Intercalation vortices and related microstructural features in the friction stir welding of dissimilar metals. *Material Resources Innovation* 1998; 2: p. 150-163.
133. I-STIR 4-Axis PDS *Operation manual*. April 2008. MTS Systems Corporation, Minnesota, USA.
134. Dawes, CJ. *Faster and faster – welding speed increase with tool development – one of a series of steps*. (2000) Technical report, TWI Bulletin. In: Mulenga AM. Analysis of weld gap variation on Friction Stir joint integrity. M.Tech dissertation, Nelson Mandela Metropolitan University, Port Elizabeth, South Africa 2008.

- 
135. Longhurst WR. *Force control of Friction Stir Welding*. PhD thesis, Faculty of Engineering, Vanderbilt University Nashville, Tennessee, USA.
136. Dawes CJ, Threadgill PL, Spurgin EJR, Staines DG. Development of the New Friction Stir technique for welding aluminium- Phase II, TWI member report 5651/35/95. Nov 1995. In: *Friction stir welding and processing*. Mishra RS, Mahoney MW (eds.) Materials Park Ohio; ASM International; 2007.
137. Hua T. *Monitoring and intelligent control for complex curvature friction stir welding*. D.Tech thesis. Faculty of Engineering, Nelson Mandela Metropolitan University, Port Elizabeth, South Africa; 2006.
138. Lienert TJ. Microstructure and mechanical properties of friction stir welded titanium alloys. In: *Friction stir welding and processing*. Mishra RS, Mahoney MW (eds.) Materials Park Ohio; ASM International; 2007.
139. Adamowski J, Szkodo M. Friction stir welds of aluminium AW6082-T2. *Journal of Achievements in Materials and manufacturing Engineering*. 2007; Vol 20, Issues 1-2: p.403-406.
140. Barlas Z, Uzun H. Microstructure and mechanical properties of friction stir butt welded dissimilar Cu/CuZn<sub>30</sub> sheets. *Journal of Achievements in Materials and manufacturing Engineering*. 2008; Vol 30, Issue 2: p.182-186.
141. Mashinini, PM. *Process window for friction stir welding of 3 mm Titanium (Ti-6Al-4V)*, M.Tech dissertation, Faculty of Engineering Built Environment and Information Technology, Nelson Mandela Metropolitan University, Port Elizabeth, South Africa. 2010.
142. Cederqvist L, Reynolds AP. Properties of friction stir welding aluminium lap joints. 2<sup>nd</sup> International FSW symposium, Gothenburg, Sweden. 26-28 June 2000. TWI (UK). Retrieved: CD-ROM.

- 
143. Abdollah – Zadeh A, Saeid T, Sazgari B. Microstructural and mechanical properties of friction stir welded aluminium/copper lap Joints. *Journal of Alloys and Compounds* 2008; 460: p. 535-538.
144. Metallographic preparation of aluminium and aluminium alloys. Struers Application notes. 04.2008/62140407. Available from [www.struers.com](http://www.struers.com) [Accessed July 2008].
145. Metallographic preparation of copper and copper alloys. Struers Application notes. 11.07/62140408. Available from [www.struers.com](http://www.struers.com) [Accessed July 2008].
146. Standard test methods for determining average grain size, E 112-96<sup>ε1</sup>, Copyright ©ASM International, USA. 2000.
147. Powder Diffraction Files (PDF-2). International Centre for Diffraction Data, Pennsylvania, USA, release 2002.
148. Standard test method for microindentation hardness of materials, E 384-08a Copyright ©ASM International, USA. 2002.
149. Standard test methods for tension testing of metallic materials, E 8M-01<sup>ε1</sup> Copyright ©ASM International, USA. 2002.
150. Test methods for measuring electrical resistance in non-ferrous materials. ASTM book of standards Vol 02.04. Copyright ©ASM International, USA. 2002.

151. Vilaça P, Quintino L, dos Santos JF, Zettler R, Sheikhi S. Quality assessment of friction stir welding joints via an analytical thermal model, *ISTIR. Materials Science and Engineering A* 2007; 445-446: p. 501-508.
152. Zhang Z, Liu YL, Chen JT. Effect of shoulder size on the temperature rise and the material deformation in friction stir welding. *International journal of Advanced Manufacturing Technology* 2009; 45:p. 889-895.
153. Holman JP. *Heat Transfer*, ninth edition. McGraw-Hill series in Mechanical Engineering. 2002. p. 6
154. Reynolds AP, Lockwood WD, Seidel TU. Processing-property correlation in Friction Stir Welds 2000; *Materials Science Forum, Trans Tech Publications Switzerland*. 531:p.1719-1724.
155. Gould JE, Feng Z. Heat flow model for friction stir welding of aluminium alloys. *Journal of Materials Processing & Manufacturing Science* 1998; 7:p. 185-193.
156. Ryan TP. *Modern engineering statistics*. Wiley-Interscience. 2007. p. 131-135.
157. Ghilani CD, Wolf PR. *Elementary surveying: An introduction to geomatics*. Prentice Hall. 2008. p. 57-61.
158. Saeid T, Abdollah-Zadeh A, Sazgari B. Weldability and mechanical properties of dissimilar aluminium-copper lap joints made by friction stir welding. *Journal of Alloys and Compounds* 2008, doi: 10.1016/j.jallcom.2009.10.127.
159. Blight G. *Geotechnical Engineering for mine waste disposal and management*. CRC press (city) 2009. p. 618.

160. Clifford Matthews (ed). ASME Engineers data book, second edition. ASME New York; 2005. p. 169.
161. Moreno D, Garrett J, Embury JD. A technique for rapid characterisation of intermetallics and interfaces. *Intermetallics* 1999; 7: p. 1001-1009.
162. Greasley P. Quantitative data analysis using SPSS. An introduction for health and social science; Open University Press, McGraw-Hill Education 2008. p. 77-85.
163. Ashenfelter O, Levine PB, Zimmerman DJ. *Statistics and econometrics: Methods and applications*. John Wiley & Sons Incorporations, United States of America. 2003. p. 158-165.
164. Multiple Regressions. Available from:  
<http://www.statsoft.com/textbook/multiple-regression/> [Accessed August 2010].
165. Akinlabi ET, Els-Botes A, Lombard H. *Effect of tool displacement on defect formation in Friction Stir Welding of Aluminium and Copper*. 8<sup>th</sup> International FSW Symposium, Hamburg, Germany. 18-20 May 2010.
166. Dieter GE. *Mechanical metallurgy, SI metric edition*. McGraw-Hill Book Company. 1988. p. 189-190.

## APPENDIX A

### WEIGHT PERCENTAGE CALCULATION OF ALUMINIUM AND COPPER IN INTERMETALLIC COMPOUNDS

The formula used is stated below:

$$\% \text{ Element} = \frac{\text{Atomic weight} \times \text{No. of atoms in compound}}{\text{Total weight of compound}}$$

Note: the atomic weight of Aluminium = 26.98

Atomic weight of Copper = 63.55

#### 1. AlCu

$$\% \text{ Aluminium} = \frac{(26.98)}{(26.98 + 63.55)} \times 100$$

$$\% \text{ Al} = 30\% \text{ and } \% \text{ Cu} = 70\%$$

#### 2. Al<sub>2</sub>Cu

$$\% \text{ Al} = \frac{26.98 \times 2}{(26.98 \times 2) + 63.55} \times 100$$

$$\% \text{ Al} = 46\% \text{ and } \% \text{ Cu} = 54\%$$

#### 3. Al<sub>3</sub>Cu<sub>4</sub>

$$\% \text{ Al} = \frac{26.98 \times 3}{(26.98 \times 3) + (63.55 \times 4)} \times 100$$

$$\% \text{ Al} = 24\% \text{ and } \% \text{ Cu} = 76\%$$

#### 4. Al<sub>4</sub>Cu<sub>9</sub>

$$\% \text{ Al} = \frac{(26.98 \times 4)}{(26.98 \times 4) + (63.55 \times 9)} \times 100$$

$$\% \text{ Al} = 16\% \text{ and } \% \text{ Cu} = 84\%$$

#### 5. AlCu<sub>3</sub>

$$\% \text{ Al} = \frac{(26.98)}{(26.98) + (63.55 \times 3)} \times 100$$

$$\% \text{ Al} = 12\% \text{ and } \% \text{ Cu} = 88\%$$

#### 6. Al<sub>2</sub>Cu<sub>3</sub>

$$\% \text{ Al} = \frac{(26.98 \times 2)}{(26.98 \times 2) + (63.55 \times 3)} \times 100$$

$$\% \text{ Al} = 22\% \text{ and } \% \text{ Cu} = 78\%$$

## APPENDIX B

### B1. THE KEY SUBSYSTEMS OF THE I-STIR PDSFSW PLATFORM

The key subsystems of the I-STIR PDSFSW platform are described briefly below:

**Pin/adapter tooling:** one tool holder is provided to allow for three welding modes which include the adjustable pin, self-reacting pin and fixed pin. Only the fixed pin tool was used in this research work. The tool holder that is shown in Figure B1a provides mechanical innerves for the tool.



Figure B1a: FSW Tool holder<sup>137</sup>

**Machine base:** the machine base acts as the foundation for the I-STIR PDS system.

**Weld head assembly:** the custom weld head assembly attaches the I-STIR PDS pin tool to the rotational drive system.

**Z axis manipulator and self-reacting load table:** the I-STIR PDS is equipped with a z-axis manipulation system and self-reacting load table. The z axis manipulation system allows the weld head to be raised for workpiece set up. The load reaction table limits the magnitude of forces induced on the foundation to the static weight of the I-STIR PDS.

**X axis manipulator:** the I-STIR PDS is equipped with an x-axis manipulation system and hydraulically controlled pitch. The x-axis actuator is used to drive the head assembly along the weld path.

**Y axis manipulator:** the I-STIR PDS is also equipped with a y-axis table. The y-axis actuator is used to drive the weld table  $\pm 305$ mm.

**Pitch axis and pitch adjustment:** the pitch axis is gimbal axis that primarily moves the weld head in the X-Z plane. The forge beam assembly allows pitch ( $\pm 15^\circ$ ) adjustment of the weld head.

**Measurement and control sensors:** the I-STIR PDS is instrumented to accurately measure, control and monitor the key process parameters such as the pin rotation, torque, forge force and traverse loads, displacement, tool cooling flow, and temperature.

**Specimen welding table:** the specimen welding table serves as a 1651 mm long by 1016 mm wide by 92.25 mm high generic clamping surface.

**Hydraulic distribution system:** the hydraulic distribution system is made of the Hydraulic Power Unit (HPU), the Hydraulic Service Manifold (HSM) and the hose distribution. The HPU is an assembly of three separate pump modules and has an internal fluid circulation function that provides the source of hydraulic fluid for cooling the spindle and spindle hydraulic motor. The HSM provides the on / off separation of the machine and the HPU. In addition, the HSM incorporates filtration and ramping up or down of downstream pressure.

**MTS Schema™ VME Digital control system:** An MTS Schema™ VME digital control platform has an interface and control system that enables the operator to conveniently select, control, modify, and record I-STIR PDS processing parameters. A PC serves as the main operator interface.

**Remote station control pendant:** The remote station control pendant is used to manually position each of the machine's axes and also to make trim adjustments during a weld.

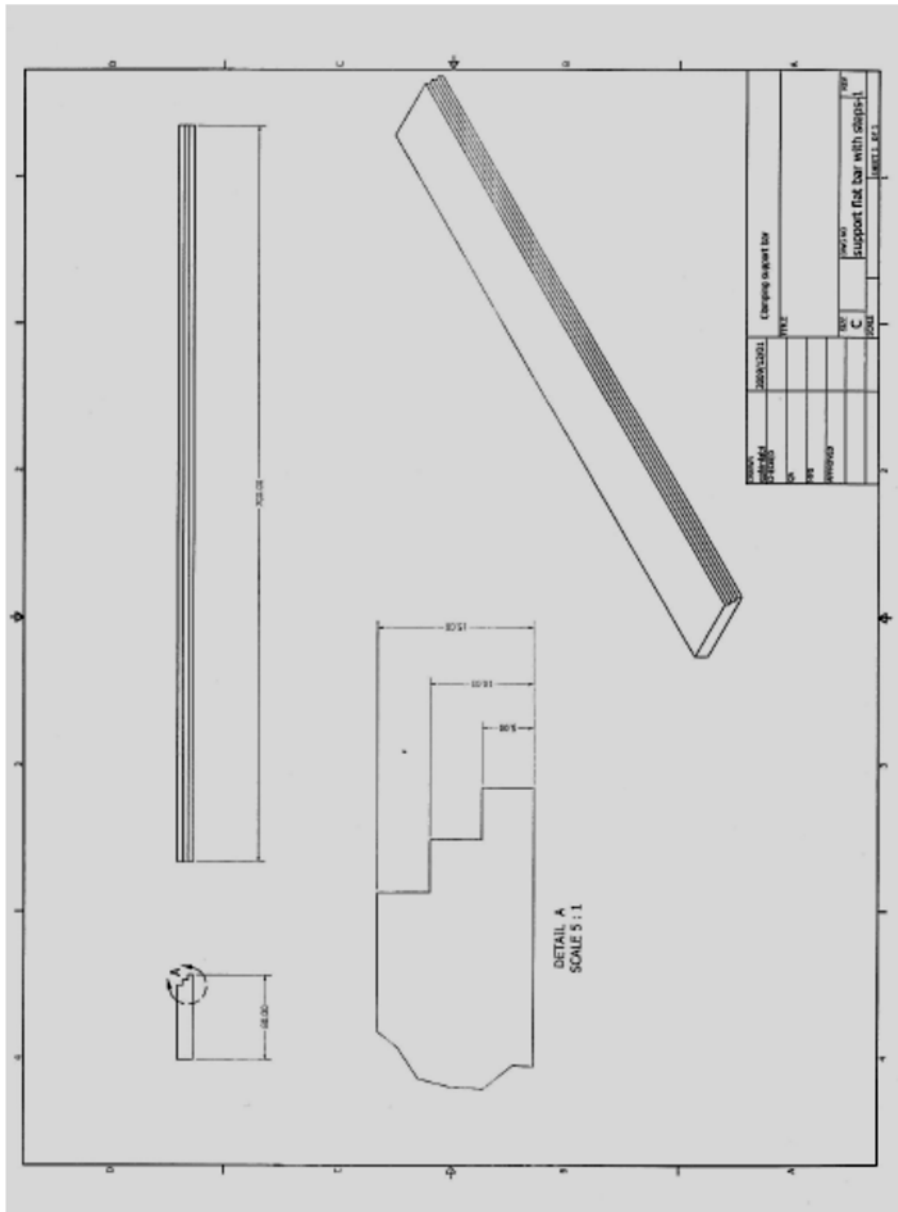
## B2. THE I-STIR PDS FSW SYSTEM SPECIFICATIONS

Table 1 below lists the I-STIR PDS specifications for each system axis.

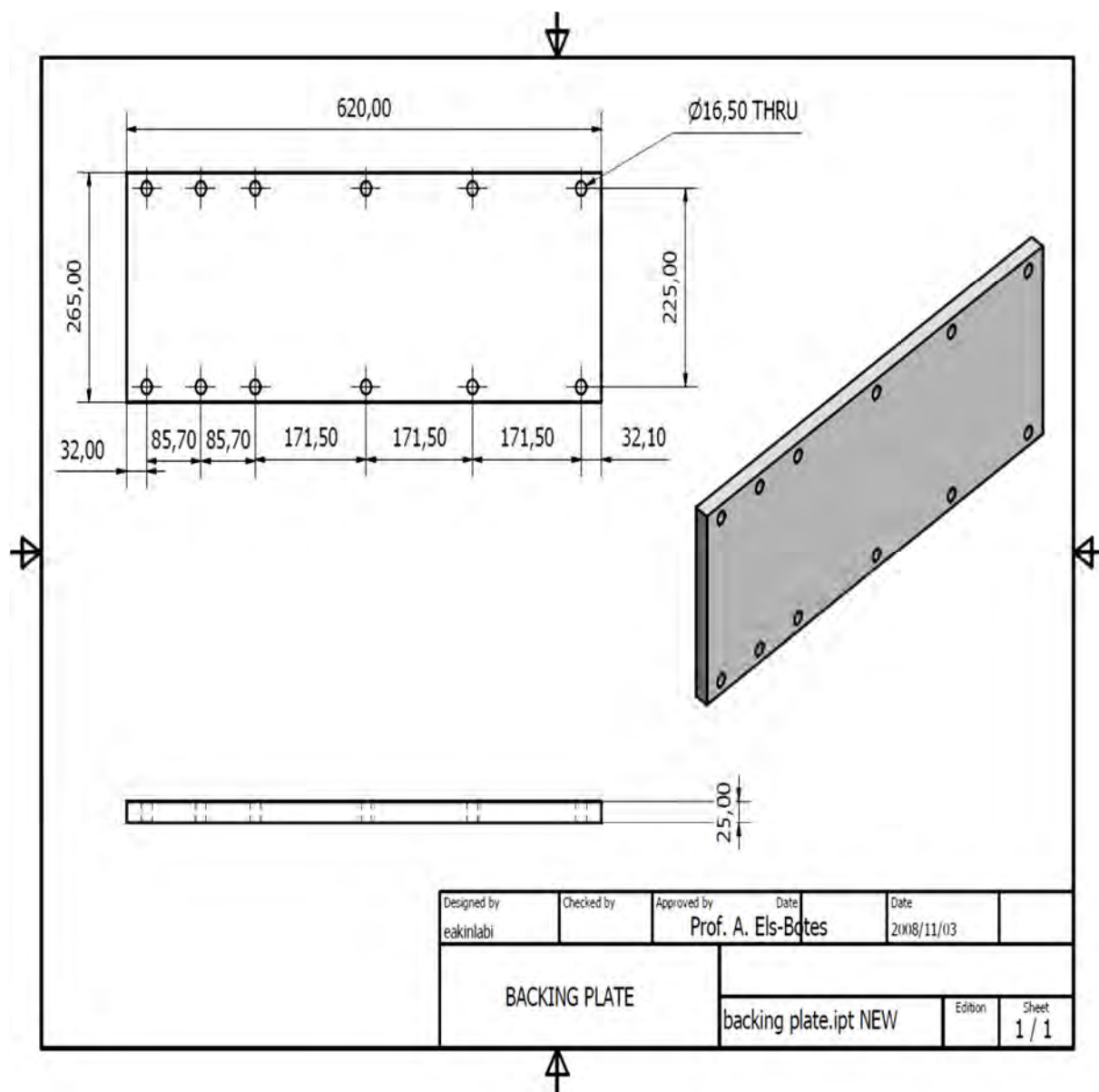
Table 1: System specifications<sup>137</sup>

<b>Axis</b>	<b>Stroke</b>	<b>Speed</b>	<b>Force</b>
X	1041mm stroke, 1524 mm work envelop	0 to 2000 mm/min	0.88 to 66.7 kN
Y	610 mm stroke	0 to 2000 mm/min	0.88 to 36 kN
Z	317.5 mm stroke	2.5 to 1400 mm/min	133 kN tension
Tool rotation	Infinite Clockwise/Counter Clockwise	200 to 2000 rpm (unloaded) 50 to 800 rpm (with gear reducer)	180 Nm  565 Nm (with gear reducer)
Pitch adjustment	$\pm 15^\circ$	0.1 to 300 °/min (unloaded)	0.88 to 66.7 kN
Adjustable pin (optional)	$\pm 15$ mm	2.54 to 1270 mm/min (unloaded)	$\pm 89$ kN

**B3. Support flat bar used for clamping**



**B4. Backing plate**



**B5.****WELD PROGRAM**

#COMMISIONING FSWAL/CU WELD FIXED PIN WELD

COORDS/PART

BREAK/"START FROM PENDANT"

FEEDRATE/RATE	2000	RAMP	2000				
GOTO/0	0	50	-1				
FORGEMOVE/POSITION	5	RATE	500	RAMP	500		
FEEDRATE/RATE	250	RAMP	1000				
GOTO/0	0	0					
FORGEMOVE/TOUCH	0	RATE	25	OVERTRAVEL	35	FORCE	1.2

BREAK/"Touching?"

SPINDLE/RPM	800	RAMP	500				
DELAY/SEC	3						

# Plunge

FORGEMOVE/POSITION	-1.2	RATE	10	RAMP	240	RELATIVE	
DELAY/SEC	10						

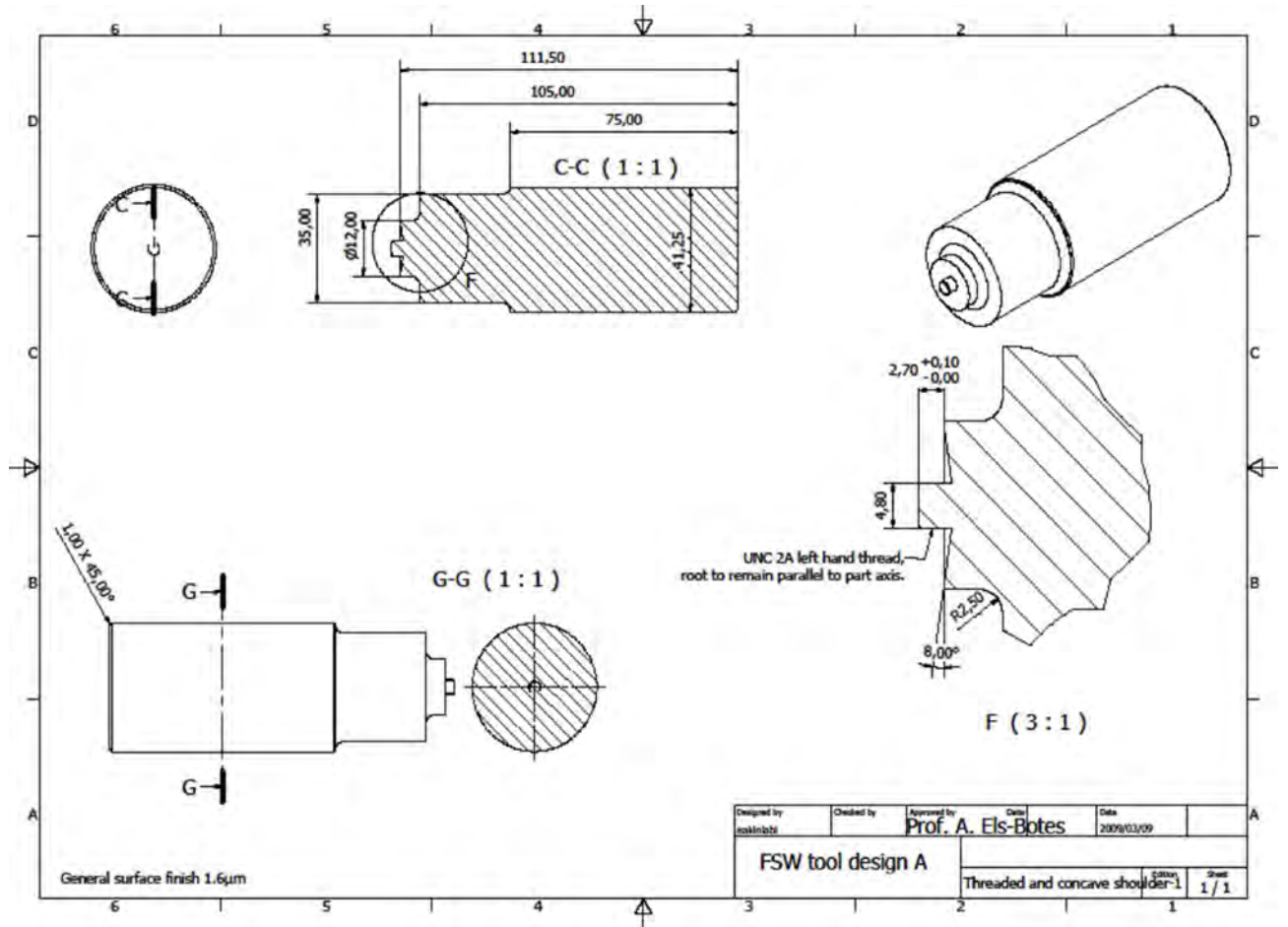
#MOVE 100MM IN POSITION CONTROL

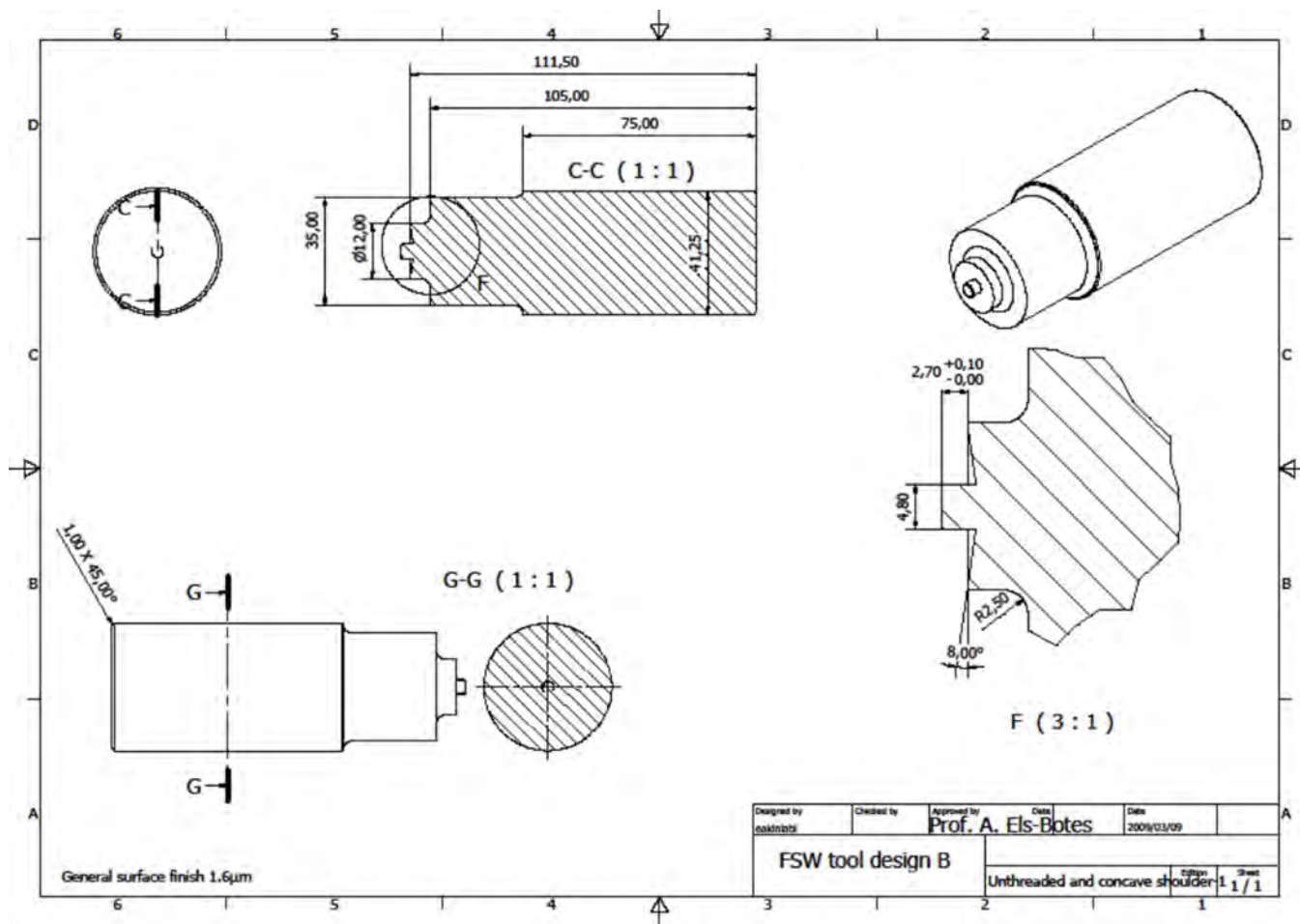
FEEDRATE/RATE	100	ACCEL	1000				
GOTO/200	0	0					

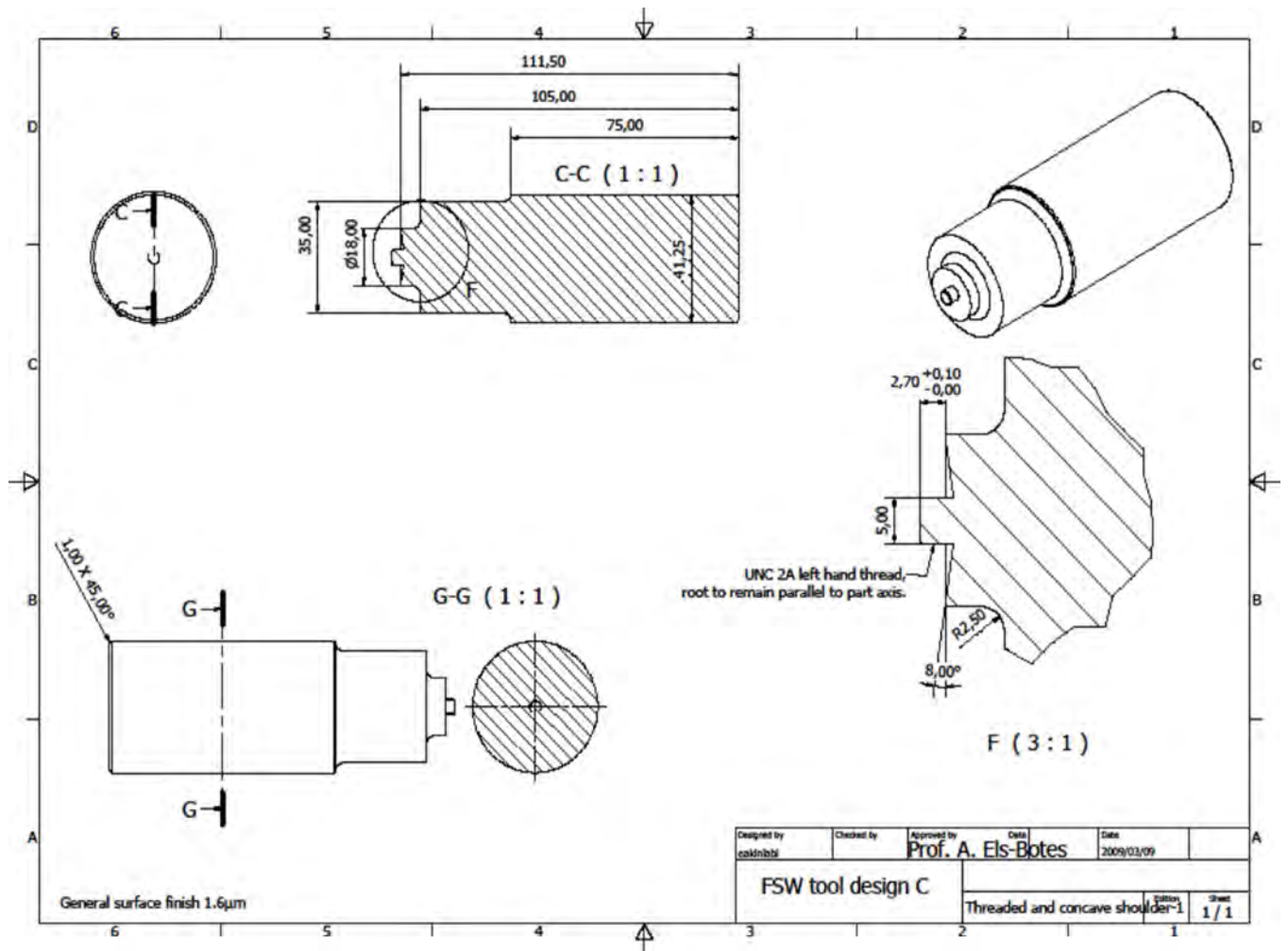
# RETRACT TOOL

FORGEMOVE/POSITION	5	RATE	100	RAMP	200	RELATIVE	
SPINDLE/RPM	0	RAMP	600				

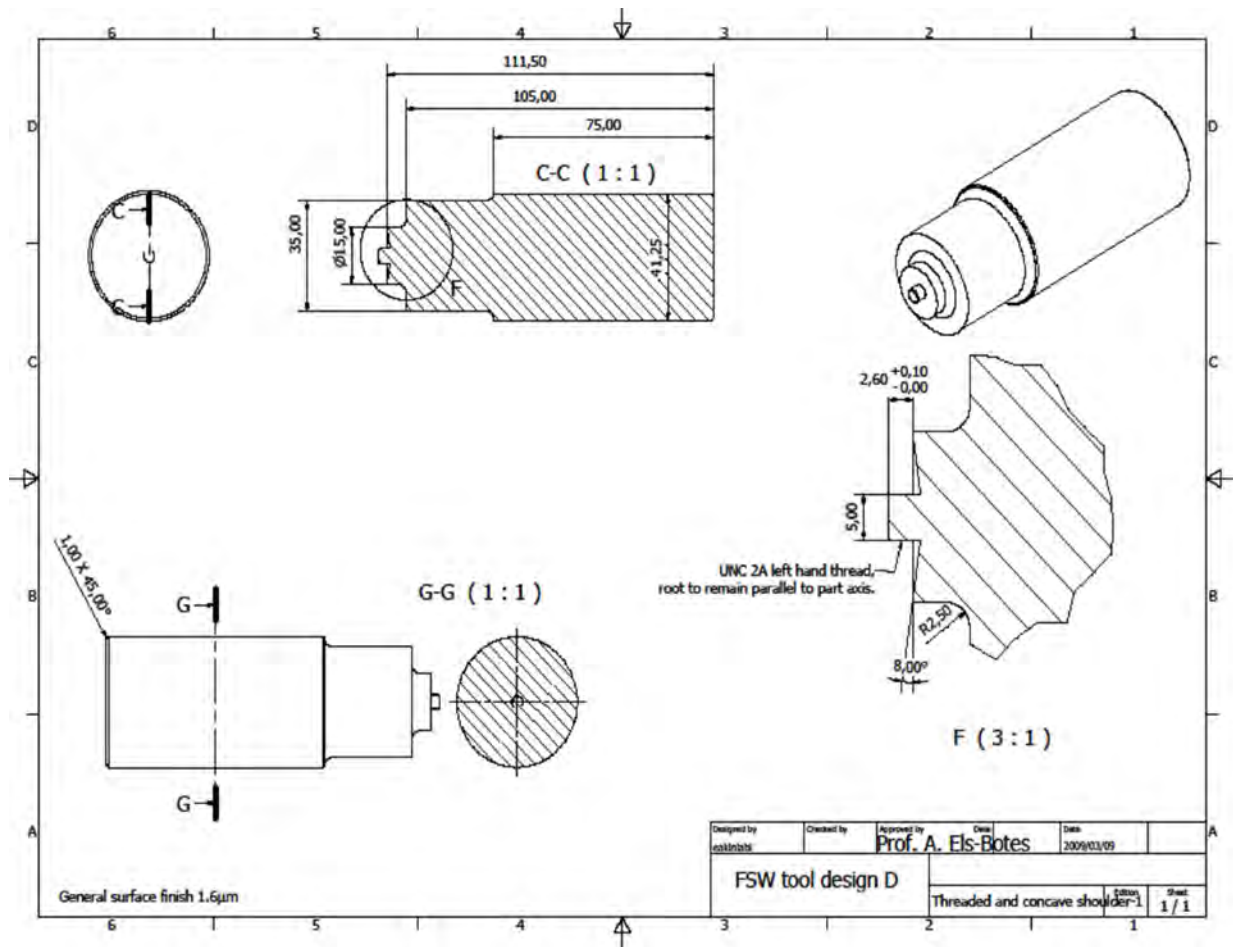
**B6. Tool design drawings for preliminary welds.**

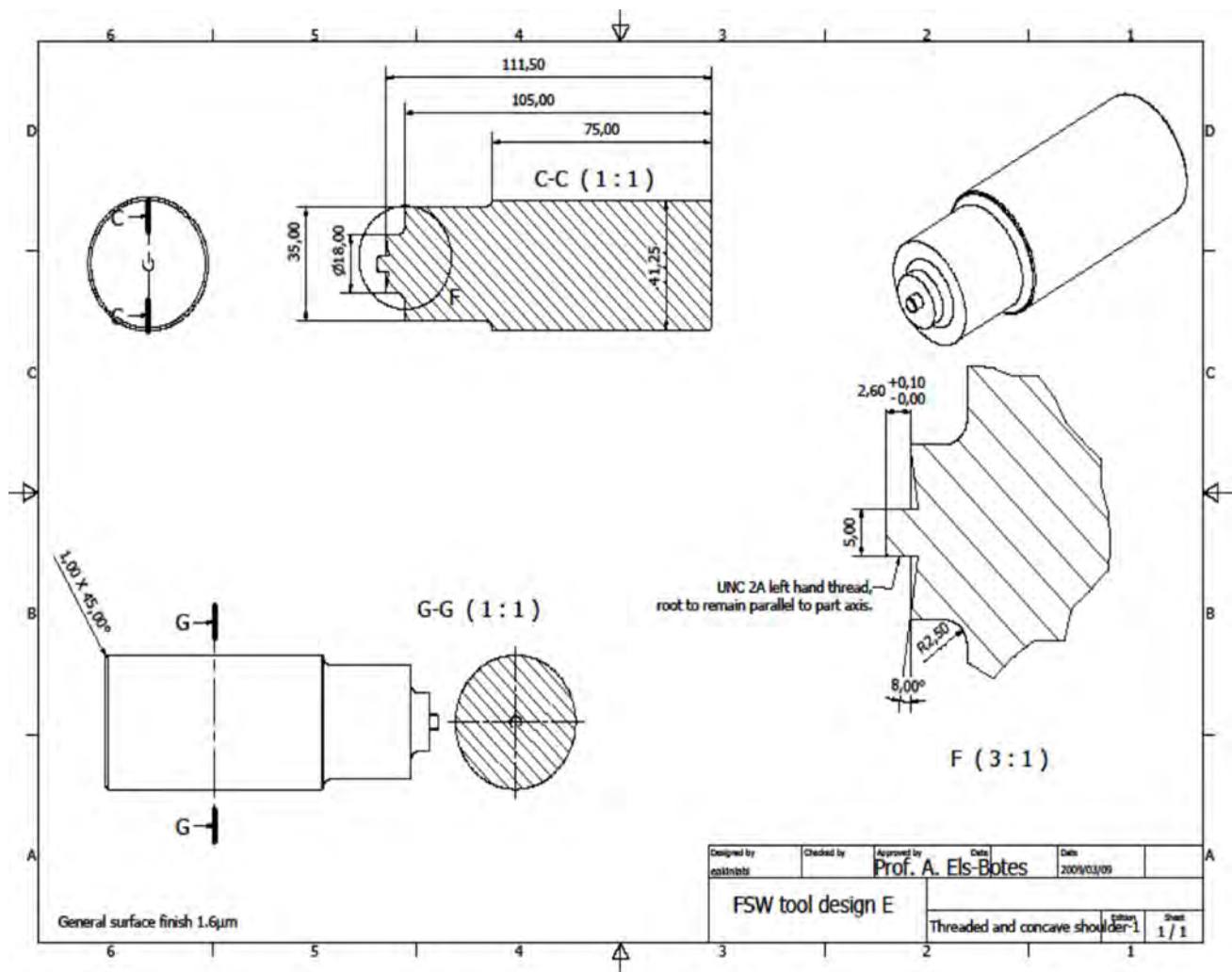


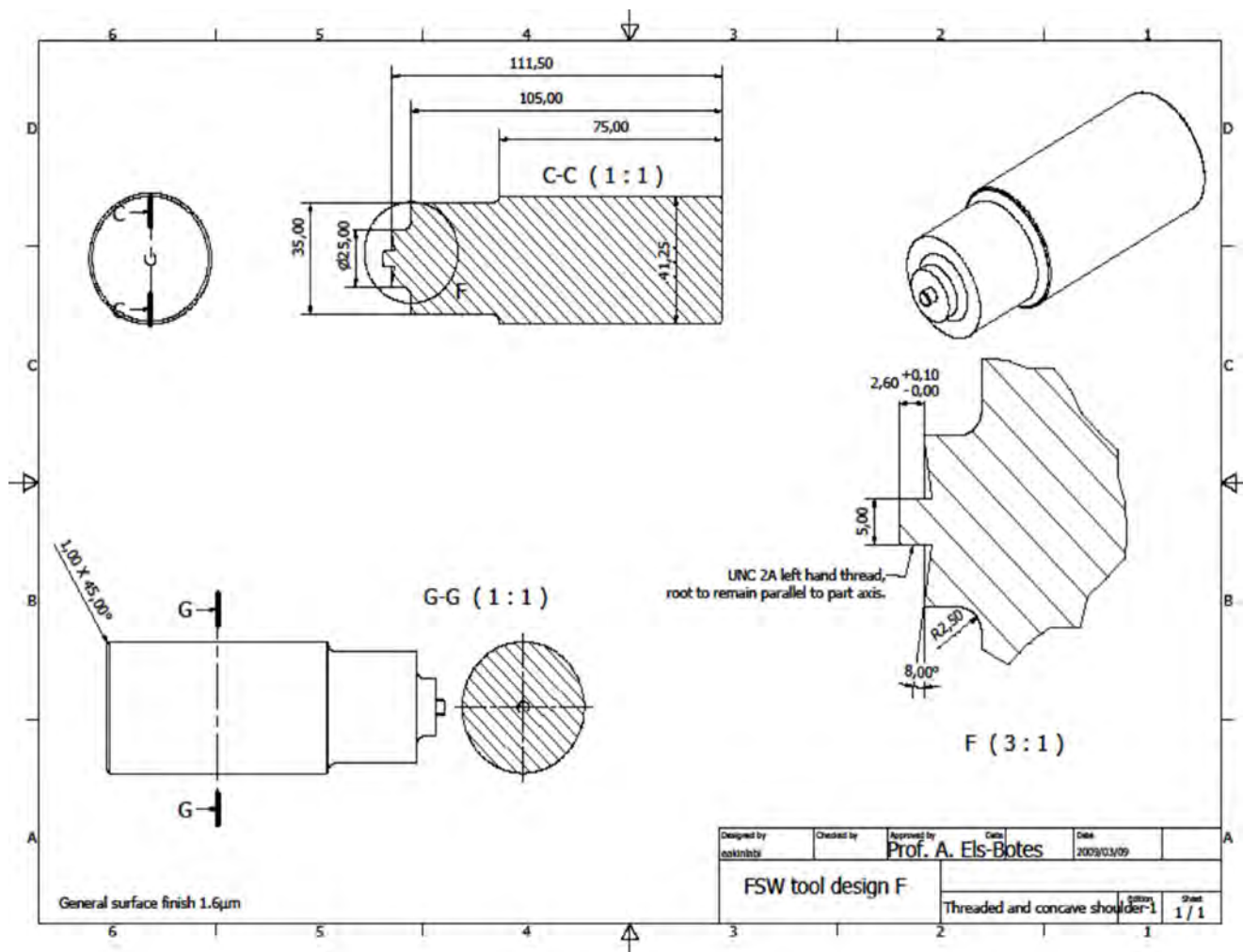




**B7. Tool design drawings for the final weld matrix.**







**B8 Preliminary weld matrix**

Preliminary test matrix								
Weld No	Rotational speed	Traverse speed	Tool displacement	Dwell time	Tool tilt	Plunge depth	Comment	Tool design
1 Al	500	100	Centreline	5	1	2.7	Bead-on-plate Al	A
2 Cu	800	100	Centreline	5	1	2.7	Bead-on-plate Cu	A
1 Al/Cu	800	100	Centreline	5	1	2.7	Wormhole defect	A
2 Al/Cu	600	100	Centreline	5	1	2.7	Wormhole defect	A
3 Al/Cu	950	100	Centreline	5	1	2.7	Wormhole defect	A
4 Al/Cu	1200	100	Centreline	5	1	2.7	Wormhole defect	A
5 Al/Cu	600	300	Centreline	5	1	2.7	Wormhole defect	A
6 Al/Cu	950	300	Centreline	5	1	2.7	Wormhole defect	A
7 Al/Cu	1200	300	Centreline	5	1	2.7	Wormhole defect	A
8 Al/Cu	600	50	Centreline	5	1	2.7	Wormhole defect	B
9 Al/Cu	600	100	Centreline	5	1	2.7	Wormhole defect	B
10 Al/Cu	800	100	Centreline	5	1	2.7	Wormhole defect	B
11 Al/Cu	950	100	Centreline	5	1	2.7	Wormhole defect	B
12 Al/Cu	1200	100	Centreline	5	1	2.7	Wormhole defect	B
13 Al/Cu	600	300	Centreline	5	1	2.7	Wormhole defect	B
14 Al/Cu	800	300	Centreline	5	1	2.7	Wormhole defect	B
15 Al/Cu	950	300	Centreline	5	1	2.7	Wormhole defect	B
16 Al/Cu	1200	300	Centreline	5	1	2.7	Wormhole defect	B
17 Al/Cu	600	50	Centreline	5	1	2.7	No Wormhole defect	C
18	800	50	Centreline	5	1	2.7	No Wormhole defect	C

Al/Cu								
19 Al/Cu	950	50	Centreline	5	1	2.7	No Wormhole defect	C
20 Al/Cu	1200	50	Centreline	5	1	2.7	No Wormhole defect	C
21 Al/Cu	600	150	Centreline	5	1	2.7	No Wormhole defect (Cu on Adv)	C
22 Al/Cu	600	150	Centreline	5	1	2.7	Wormhole defect (Cu on Rtr)	C
23 Al/Cu	600	50	Tool pin in Cu	5	1	2.7	No Wormhole defect	C
24 Al/Cu	950	50	Tool pin in Cu	5	1	2.7	No Wormhole defect	C
25 Al/Cu	1200	50	Tool pin in Cu	5	1	2.7	Wormhole defect	C
26 Al/Cu	600	150	Tool pin in Cu	5	1	2.7	No Wormhole defect	C
27 Al/Cu	950	150	Tool pin in Cu	5	1	2.7	No Wormhole defect	C
28 Al/Cu	1200	150	Tool pin in Cu	5	1	2.7	No Wormhole defect	C
29 Al/Cu	600	300	Tool pin in Cu	5	1	2.7	No Wormhole defect	C
30 Al/Cu	950	300	Tool pin in Cu	5	1	2.7	No Wormhole defect	C
31 Al/Cu	1200	300	Tool pin in Cu	5	1	2.7	Wormhole defect	C
32 Al/Cu	600	50	Tool pin in Al	5	1	2.7	No Wormhole defect	C
33 Al/Cu	950	50	Tool pin in Al	5	1	2.7	No Wormhole defect	C
34 Al/Cu	1200	50	Tool pin in Al	5	1	2.7	No Wormhole defect	C
35 Al/Cu	600	150	Tool pin in Al	5	1	2.7	No Wormhole defect	C
36 Al/Cu	950	150	Tool pin in Al	5	1	2.7	No Wormhole defect	C

37 Al/Cu	1200	150	Tool pin in Al	5	1	2.7	No Wormhole defect	C
38 Al/Cu	600	300	Tool pin in Al	5	1	2.7	No Wormhole defect	C
39 Al/Cu	950	300	Tool pin in Al	5	1	2.7	No Wormhole defect	C
40 Al/Cu	1200	300	Tool pin in Al	5	1	2.7	No Wormhole defect	C
41 Al/Cu	600	50	Tool pin in Al	5	2	2.7	Less flash and no visible defect	C
42 Al/Cu	950	50	Tool pin in Al	5	2	2.7	Less flash and no visible defect	C
43 Al/Cu	1200	50	Tool pin in Al	5	2	2.7	Less flash and no visible defect	C
44 Al/Cu	600	150	Tool pin in Al	5	2	2.7	Less flash and no visible defect	C
45 Al/Cu	950	150	Tool pin in Al	5	2	2.7	Less flash and no visible defect	C
46 Al/Cu	1200	150	Tool pin in Al	5	2	2.7	Less flash and no visible defect	C
47 Al/Cu	600	300	Tool pin in Al	5	2	2.7	Less flash and no visible defect	C
48 Al/Cu	950	300	Tool pin in Al	5	2	2.7	Less flash and no visible defect	C
49 Al/Cu	1200	300	Tool pin in Al	5	2	2.7	Less flash and no visible defect	C
50 Al/Cu	600	50	Tool pin in Al	5	3	2.7	Heavy flash	C
51 Al/Cu	950	50	Tool pin in Al	5	3	2.7	Heavy flash	C
52 Al/Cu	1200	50	Tool pin in Al	5	3	2.7	Heavy flash	C
53 Al/Cu	600	150	Tool pin in Al	5	3	2.7	Heavy flash	C
54 Al/Cu	950	150	Tool pin in Al	5	3	2.7	Heavy flash	C
55 Al/Cu	1200	150	Tool pin in Al	5	3	2.7	Heavy flash	C

Al/Cu								
56 Al/Cu	600	300	Tool pin in Al	5	3	2.7	Heavy flash	C
57 Al/Cu	950	300	Tool pin in Al	5	3	2.7	Heavy flash	C
58 Al/Cu	1200	300	Tool pin in Al	5	3	2.7	Heavy flash	C
59 Al/Cu	600	50	Tool pin in Al	10	2	2.7	Heavy flash	C
60 Al/Cu	950	50	Tool pin in Al	10	2	2.7	Heavy flash	C
61 Al/Cu	1200	50	Tool pin in Al	10	2	2.7	Heavy flash	C
62 Al/Cu	600	50	Tool pin in Al	2	2	2.7	Less flash and no visible defect	C
63 Al/Cu	950	50	Tool pin in Al	2	2	2.7	Less flash and no visible defect	C
64 Al/Cu	1200	50	Tool pin in Al	2	2	2.7	Less flash and no visible defect	C
65 Al/Cu	500	50	Tool pin in Al	2	2	2.7	Excessive vibration on the machine	C
66 Al/Cu	600	50	Tool pin in Al	2	2	2.7	No Wormhole defect (Plates stuck)	C
67 Al/Cu	700	50	Tool pin in Al	2	2	2.6	No Wormhole defect	C
68 Al/Cu	800	50	Tool pin in Al	2	2	2.6	No Wormhole defect	C
69 Al/Cu	900	50	Tool pin in Al	2	2	2.6	No Wormhole defect	C
70 Al/Cu	1200	50	Tool pin in Al	2	2	2.6	No Wormhole defect	C
71 Al/Cu	1500	50	Tool pin in Al	2	2	2.6	Wormhole defect	C
72 Al/Cu	600	150	Tool pin in Al	2	2	2.6	No Wormhole defect	C
73 Al/Cu	950	150	Tool pin in Al	2	2	2.6	No Wormhole defect	C

74 Al/Cu	1200	150	Tool pin in Al	2	2	2.6	No Wormhole defect	C
75 Al/Cu	600	200	Tool pin in Al	2	2	2.6	No Wormhole defect	C
76 Al/Cu	950	200	Tool pin in Al	2	2	2.6	No Wormhole defect	C
77 Al/Cu	1200	200	Tool pin in Al	2	2	2.6	No Wormhole defect	C
78 Al/Cu	600	250	Tool pin in Al	2	2	2.6	No Wormhole defect	C
79 Al/Cu	950	250	Tool pin in Al	2	2	2.6	No Wormhole defect	C
80 Al/Cu	1200	250	Tool pin in Al	2	2	2.6	No Wormhole defect	C
81 Al/Cu	600	300	Tool pin in Al	2	2	2.6	No Wormhole defect	C
82 Al/Cu	950	300	Tool pin in Al	2	2	2.6	No Wormhole defect	C
83 Al/Cu	1200	300	Tool pin in Al	2	2	2.6	No Wormhole defect	C
84 Al/Cu	600	350	Tool pin in Al	2	2	2.6	Wormhole defect	C
85 Al/Cu	950	350	Tool pin in Al	2	2	2.6	Wormhole defect	C
86 Al/Cu	1200	350	Tool pin in Al	2	2	2.6	Wormhole defect	C
87 Al/Cu	600	50	Tool pin in Al	2	2	2.6	No Wormhole defect	C
88 Al/Cu	950	50	Tool pin in Al	2	2	2.6	No Wormhole defect	C
89 Al/Cu	1200	50	Tool pin in Al	2	2	2.6	No Wormhole defect	C

**B9 (a). Chemical analysis of Copper**

01/29/2009 12:54:12 PM

Elements: Concentration

Program: Cu-10-M

Comment: Pure-Cu

Single spark(s)

Sample No: Esther (Cu Plate)

Quality:

Sample Id:

No	Zn %	Pb %	Sn %	P %	Mn %	Fe %	Ni %	Si %	Mg %	Cr %	Te %	As %
1	<0.0012	<0.0003	<0.0001	0.022	<0.0004	<0.0022	<0.0002	<0.0005	0.0001	<0.0003	0.002	<0.0002
2	<0.0012	<0.0003	<0.0001	0.022	<0.0004	<0.0024	<0.0002	<0.0005	0.0001	<0.0003	0.020	<0.0002
3	<0.0012	<0.0003	<0.0001	0.022	<0.0004	<0.0008	<0.0002	<0.0005	0.0001	<0.0003	0.004	<0.0002

No	Sb %	Cd %	Bi %	Ag %	Co %	Al %	S %	Be %	Zr %	Au %	B %	Ti %
1	<0.0005	<0.0002	<0.0018	0.001	0.0019	0.0014	0.0010	<0.0000	0.0011	<0.0005	6E-04	<0.0002
2	<0.0005	<0.0002	<0.0016	0.002	0.0012	0.0010	0.0009	<0.0000	0.0008	<0.0005	<0.0004	<0.0002
3	<0.0005	<0.0002	<0.0036	0.003	0.0013	0.0010	0.0009	<0.0000	0.0008	<0.0005	4E-04	<0.0002

No	Se %	Cu %
1	<0.0002	100.0
2	<0.0002	100.0
3	<0.0002	100.0

**B9 (b). Chemical analysis of Aluminium**

Program: Al-10-M  
 Comment: Al-Global

12000006

05/07/2010 07:30:22 AM  
 Elements: Concentration

Sample No: Esther Al  
 Sample Id:

Quality

	Si %	Fe %	Cu %	Mn %	Mg %	Cr %	Ni %	Zn %	Ti %	Ag %	B %	Ba %
x	0.177	0.324	0.033	0.336	3.03	0.027	0.0019	<0.0010	0.014	<0.001	0.001	<0.0001
	Be %	Bi %	Ca %	Cd %	Ca %	Co %	Ga %	In %	U %	Na %	P %	Pb %
x	0.001	0.0042	0.0007	<0.0001	<0.0016	0.0006	0.0061	<0.0003	<0.0001	0.0017	0.003	<0.0005
	Sb %	Sn %	Sr %	V %	Zr %	Hg %	Al %					
x	<0.0020	0.0027	<0.0001	0.013	0.0007	<0.0020	96.0					

**B10 (a).Material Test Report of Copper**

## Material Test Report of Copper

Chemical  
Analysis

Cu	Zn	Ag	Pb	O	P	Ni	Sn	Ti
99.859	0.0092	0.001	0.0005	0.0001	0.0024	0.0011	0.0041	0.0008

Mechanical  
Test result

	Specification	To	Actual
Hardness Vickers	70	90	75.3

QC Manager  
Bronscor

**B10 (b). Material Test Report of Aluminium**

## Material Test Report of Aluminium - 5754

Chemical  
Analysis

Si	C	Pb	Mg	Cr	Ti	Zn	Al	Si
0.4	0.2	0.8	2.0-3.5	0.3	0.15	0.5	95-96	0.4

Mechanical  
Test result

UTS (MPa) 190-240

%Elongation 13

QC Manager  
Hulett  
Aluminium

**B11. Metallographic sample preparation**

The procedures for metallographic sample preparation employed in this research project are presented in Tables 1 and 2.

Table 1: Procedure for metallographic sample preparation (Grinding)

<b>Step</b>	<b>Plane grinding</b>	<b>Final grinding</b>
Surface	SiC-Paper 320#	MD-Largo
Grit/Suspension	320	DiaPro Largo
Lubricant	Water	
Rpm	150	150
Force (N)	180	180
Time	Until plane	4 minutes

Table 2: Procedure for metallographic sample preparation (Polishing)

<b>Step</b>	<b>Diamond Polishing</b>	<b>Final Polishing</b>
Surface	MD-Mol	OP-Chem
Suspension	DiaPro Mol	OP-S
Rpm	150	150
Force (N)	150	90
Time	3 minutes	1 minute

The etchant used to reveal the microstructure is modified Poulton's reagent, it consists of the following:

30ml HCL, 40ml HNO<sub>3</sub>, 2.5ml HF, 12g CrO<sub>3</sub>, and 42.5ml of H<sub>2</sub>O.

**B12. X- Ray Diffractometer**



X- Ray Diffractometer (Bruker D8 Advance).

**B13. Dimensions of the test specimens**

The initial gauge length of 50 mm was used for all the samples.

T1, T2 and T3 represent the first, second and third sample taken from each weld respectively.

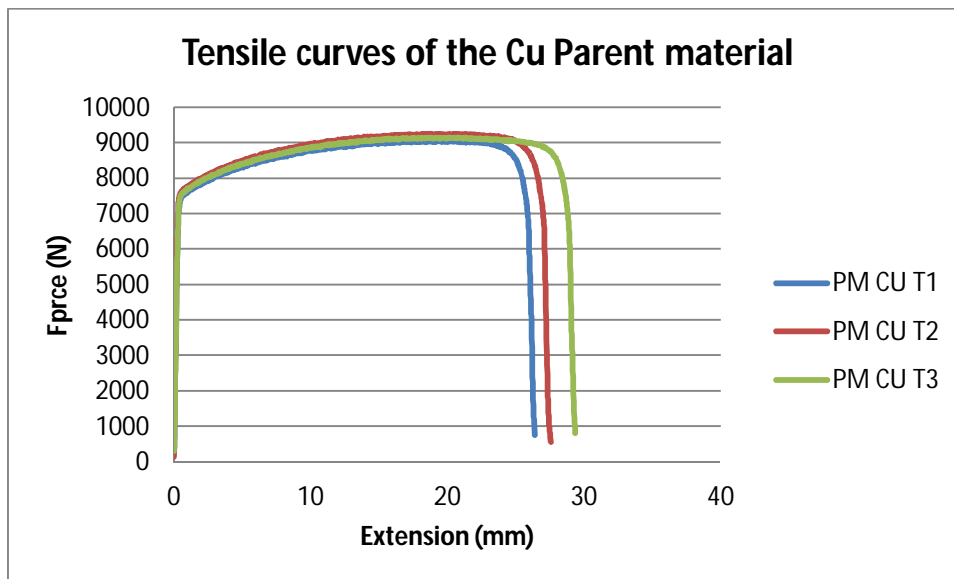
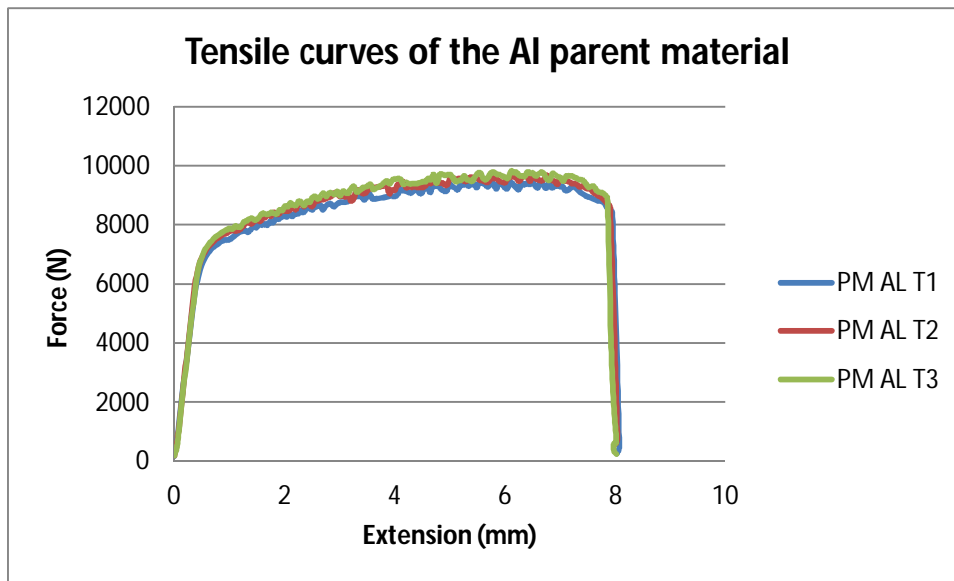
Sample NO.	Spindle speed (rpm)	Feed rate (mm/min)	Thickness (mm)	Width (mm)	Final length (mm)
PM AI T1			2.91	12.18	55.98
PM AL T2			2.92	12.48	55.95
PM AL T3			2.93	12.64	55.84
PM CU T1			3.05	12.28	72.05
PM CU T2			3.00	12.52	72.34
PM CU T3			3.02	12.43	73.28
S15_01 T1	600	50	2.85	12.62	51.00
S15_01 T2	600	50	2.68	12.68	50.50
S15_01 T3	600	50	2.74	12.58	51.50
S15_02 T1	600	150	2.97	12.49	52.25
S15_02 T2	600	150	2.70	12.68	51.50
S15_02 T3	600	150	2.63	12.45	51.80
S15_03 T1	600	300	2.72	12.72	53.80
S15_03 T2	600	300	2.60	12.66	52.75
S15_03 T3	600	300	2.63	12.58	51.86
S15_04 T1	950	50	2.81	12.43	53.50
S15_04 T2	950	50	3.02	12.59	50.58
S15_04 T3	950	50	2.92	12.48	50.76
S15_05 T1	950	150	2.93	12.67	50.95
S15_05 T2	950	150	2.66	12.65	52.85
S15_05 T3	950	150	2.68	12.80	53.63
S15_06 T1	950	300	2.65	12.52	52.85
S15_06 T2	950	300	2.70	12.54	51.76
S15_06 T3	950	300	2.68	12.74	51.10
S15_07 T1	1200	50	2.50	12.69	51.70
S15_07 T2	1200	50	2.52	12.77	50.90

S15_07 T3	1200	50	2.51	12.58	52.05
S15_08 T1	1200	150	2.52	12.46	51.30
S15_08 T2	1200	150	2.55	12.45	51.05
S15_08 T3	1200	150	2.78	12.46	53.65
S15_09 T1	1200	300	2.80	12.48	51.02
S15_09 T2	1200	300	2.76	12.57	51.06
S15_09 T3	1200	300	2.58	12.67	52.50
S18_01 T1	600	50	2.73	12.47	51.50
S18_01 T2	600	50	2.86	12.54	51.25
S18_01 T3	600	50	2.65	12.66	53.30
S18_02 T1	600	150	2.89	12.53	51.80
S18_02 T2	600	150	2.98	12.62	50.70
S18_02 T3	600	150	3.11	12.51	50.65
S18_03 T1	600	300	2.80	12.44	51.48
S18_03 T2	600	300	2.71	12.38	51.40
S18_03 T3	600	300	2.70	12.54	50.95
S18_04 T1	950	50	2.85	12.47	53.95
S18_04 T2	950	50	3.02	12.37	50.58
S18_04 T3	950	50	3.09	12.34	52.90
S18_05 T1	950	150	2.76	12.51	52.10
S18_05 T2	950	150	2.89	12.49	53.05
S18_05 T3	950	150	2.75	12.65	53.93
S18_06 T1	950	300	3.09	12.66	51.98
S18_06 T2	950	300	2.86	12.50	52.65
S18_06 T3	950	300	2.85	12.55	50.93
S18_07 T1	1200	50	2.86	12.43	51.85
S18_07 T2	1200	50	2.64	12.42	51.85
S18_07 T3	1200	50	2.58	12.62	51.50
S18_08 T1	1200	150	2.57	12.59	51.82
S18_08 T2	1200	150	2.88	12.55	52.45
S18_08 T3	1200	150	2.85	12.45	52.85
S18_09 T1	1200	300	2.51	12.49	51.65

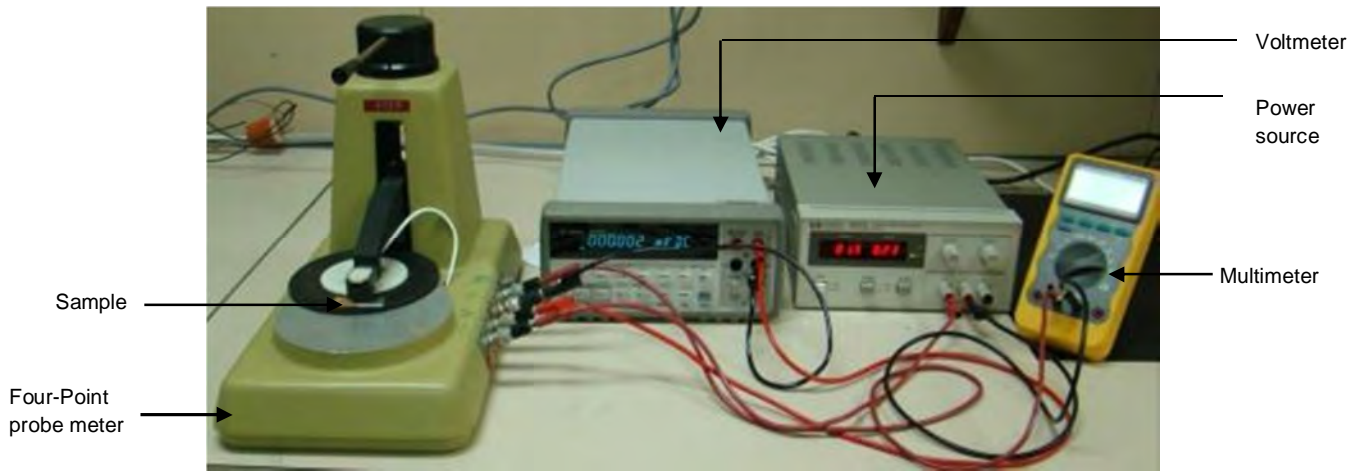
S18_09 T2	1200	300	2.59	12.51	51.02
S18_09 T3	1200	300	2.61	12.63	50.93
S25_01 T1	600	50	3.08	12.60	53.45
S25_01 T2	600	50	2.52	12.53	51.32
S25_01 T3	600	50	2.52	12.70	51.09
S25_02 T1	600	150	2.96	12.47	50.59
S25_02 T2	600	150	3.01	12.51	51.02
S25_02 T3	600	150	3.09	12.70	51.36
S25_03 T1	600	300	2.67	12.82	51.86
S25_03 T2	600	300	2.91	12.70	51.27
S25_03 T3	600	300	2.92	12.69	51.73
S25_04 T1	950	50	2.91	12.46	51.08
S25_04 T2	950	50	2.98	12.79	51.26
S25_04 T3	950	50	2.97	12.54	51.40
S25_05 T1	950	150	2.98	12.46	53.05
S25_05 T2	950	150	2.73	12.69	51.63
S25_05 T3	950	150	2.76	12.48	53.14
S25_06 T1	950	300	2.56	12.64	50.74
S25_06 T2	950	300	2.52	12.57	52.05
S25_06 T3	950	300	2.50	12.70	51.34
S25_07 T1	1200	50	2.63	12.49	52.50
S25_07 T2	1200	50	2.76	12.48	51.39
S25_07 T3	1200	50	2.56	12.47	51.90
S25_08 T1	1200	150	2.84	12.56	50.53
S25_08 T2	1200	150	2.79	12.64	52.80
S25_08 T3	1200	150	2.90	12.60	52.85
S25_09 T1	1200	300	2.66	12.74	50.96
S25_09 T2	1200	300	2.64	12.56	50.86
S25_09 T3	1200	300	2.68	12.57	51.98

**B14. Tensile curves of the parent materials**

The sample dimensions are given in Appendix B13.



**B15. Experimental set-up for electrical resistivity measurement**



Experimental set-up for electrical resistance measurement.

## APPENDIX C

### C1. Macrographs of welds

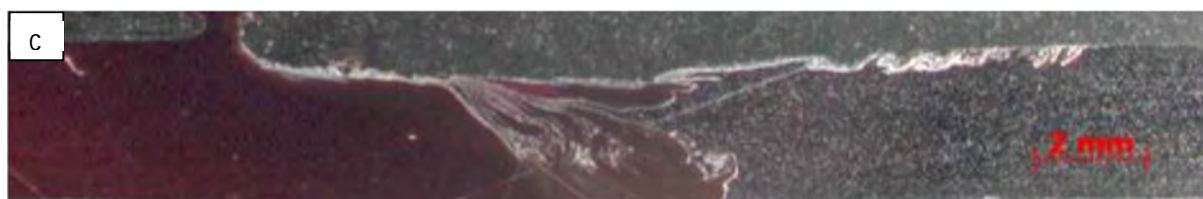
The macrographs of the welds produced using the 15 mm shoulder diameter tools and their corresponding input process parameters are hereby presented.



S15\_01 600 rpm and 50 mm/min



S15\_02 600 rpm and 150 mm/min



S15\_03 600 rpm and 300 mm/min



S15\_04 950 rpm and 50 mm/min



S15\_05 950 rpm and 150 mm/min



S15\_06 950 rpm and 300 mm/min



S15\_07 1200 rpm and 50 mm/min



S15\_08 1200 rpm and 150 mm/min



S15\_09 1200 rpm and 300 mm/min

The macrographs of the welds produced using the 18 mm shoulder diameter tools and their corresponding input process parameters are hereby presented.



S18\_01 600 rpm and 50 mm/min



S18\_02 600 rpm and 150 mm/min



S18\_03 600 rpm and 300 mm/min



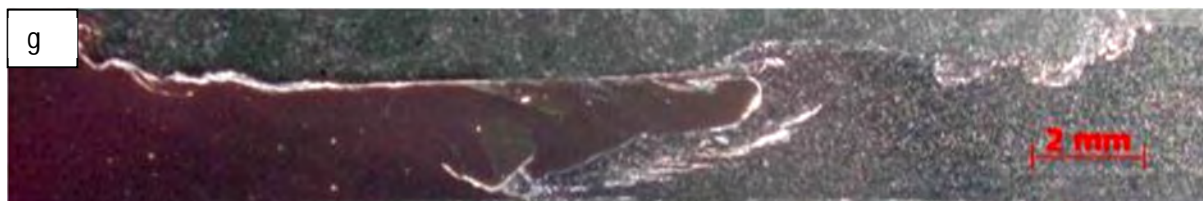
S18\_04 950 rpm and 50 mm/min



S18\_05 950 rpm and 150 mm/min



S18\_06 950 rpm and 300 mm/min



S18\_07 1200 rpm and 50 mm/min

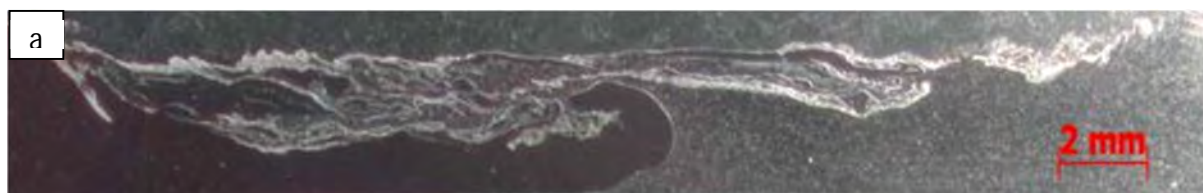


S18\_08 1200 rpm and 150 mm/min



S18\_09 1200 rpm and 300 mm/min

The macrographs of the welds produced using the 25 mm shoulder diameter tools and their corresponding input process parameters are hereby presented.



S25\_01 600 rpm and 50 mm/min



S25\_02 600 rpm and 150 mm/min



S25\_03 600 rpm and 300 mm/min



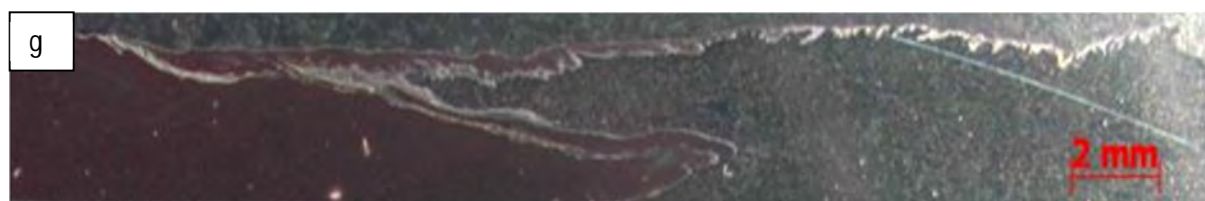
S25\_04 950 rpm and 50 mm/min



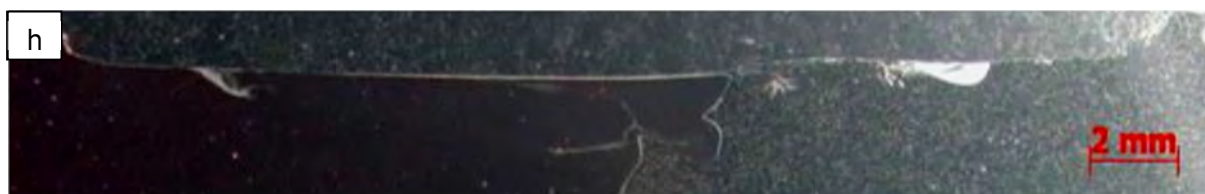
S25\_05 950 rpm and 150 mm/min



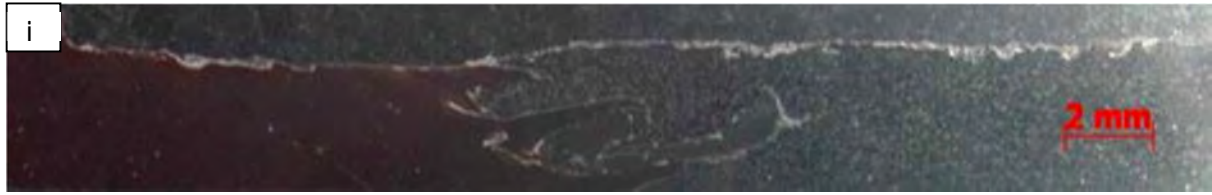
S25\_06 950 rpm and 300 mm/min



S25\_07 1200 rpm and 50 mm/min

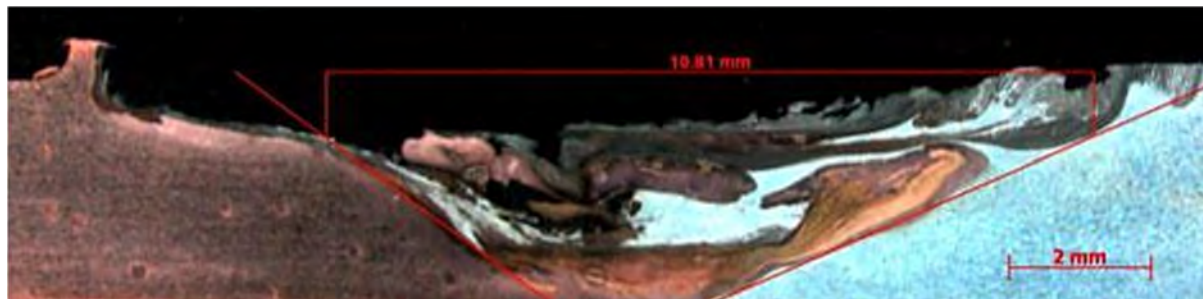


S25\_08 1200 rpm and 150 mm/min

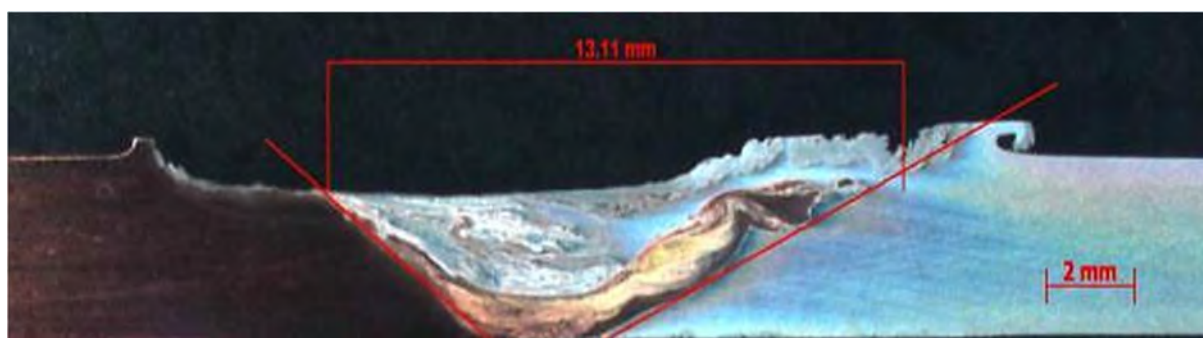


S25\_09 1200 rpm and 300 mm/min

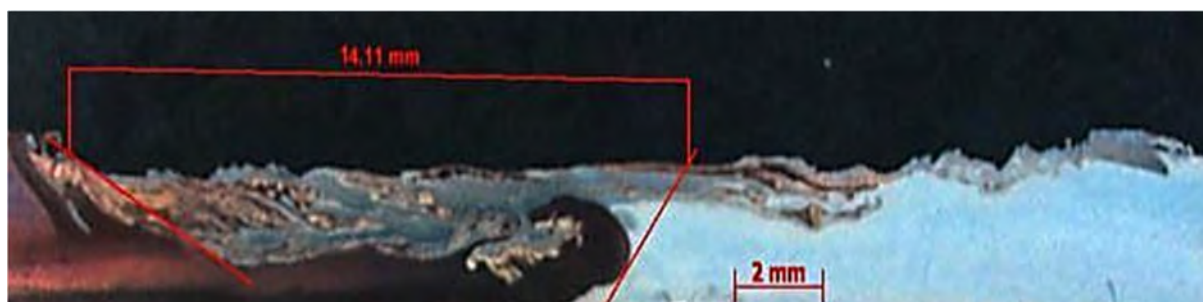
**C2. Macrographs of welds produced at the same input process parameters (600 rpm and 50 mm/min) with the different shoulder diameter tools indicating measurements of the SZ and TMAZ**



S15\_01 produced at 600 rpm and 50 mm/min with the 15 mm shoulder diameter tool



S18\_01 produced at 600 rpm and 50 mm/min with the 18 mm shoulder diameter tool



S25\_01 produced at 600 rpm and 50 mm/min with the 25 mm shoulder diameter tool

### C3. Tensile graphs of welds

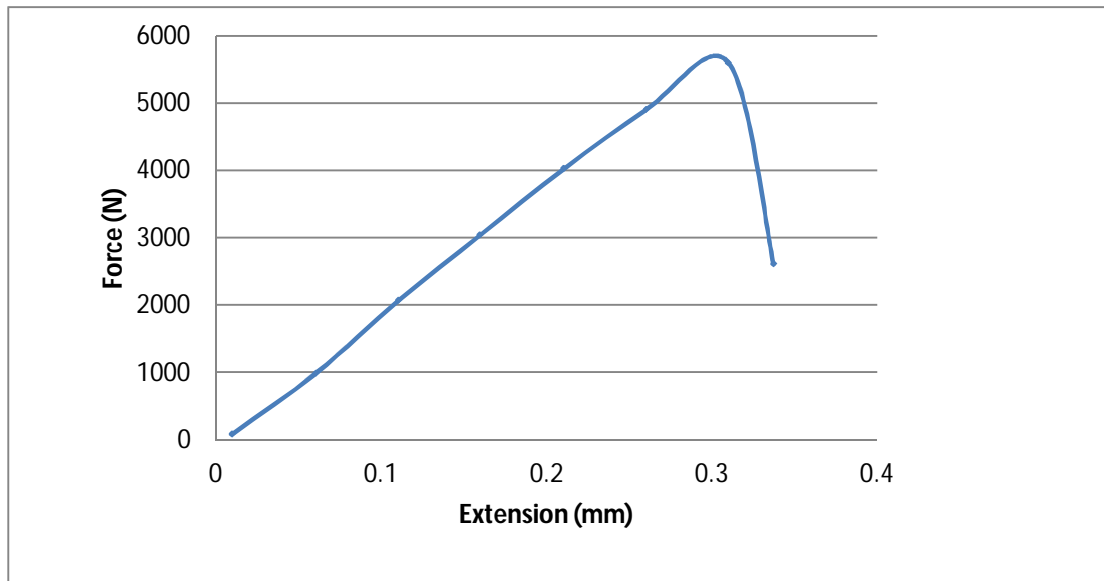


Figure C3i: Tensile behaviour of weld produced at 600 rpm and 50 mm/min with 15 mm shoulder  $\Phi$

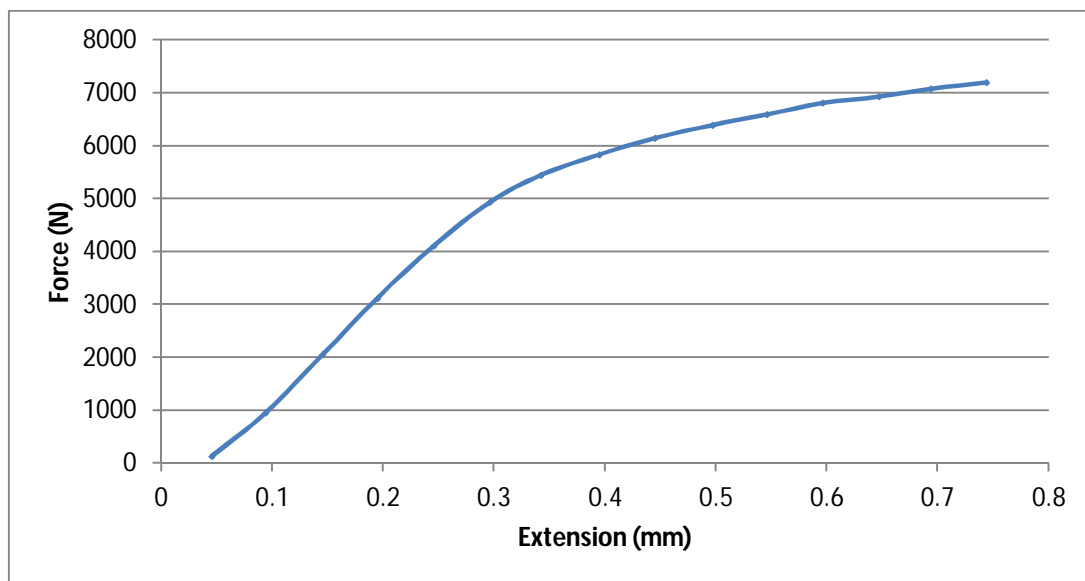


Figure C3ii: Tensile behaviour of weld produced at 600 rpm and 150 mm/min with 15 mm shoulder  $\Phi$

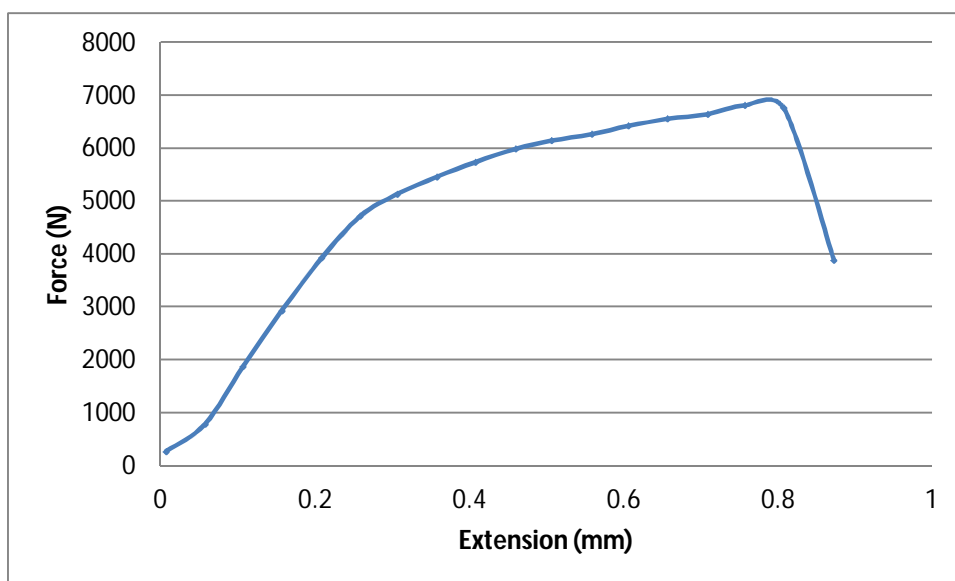


Figure C3iii: Tensile behaviour of weld produced at 600 rpm and 300 mm/min with 15 mm shoulder  $\Phi$

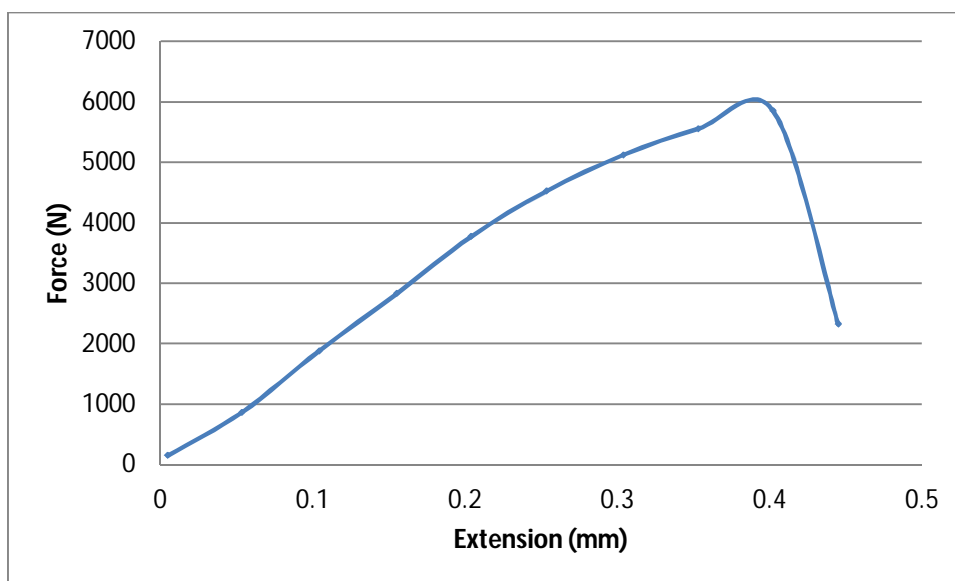


Figure C3iv: Tensile behaviour of weld produced at 950 rpm and 50 mm/min with 15 mm shoulder  $\Phi$

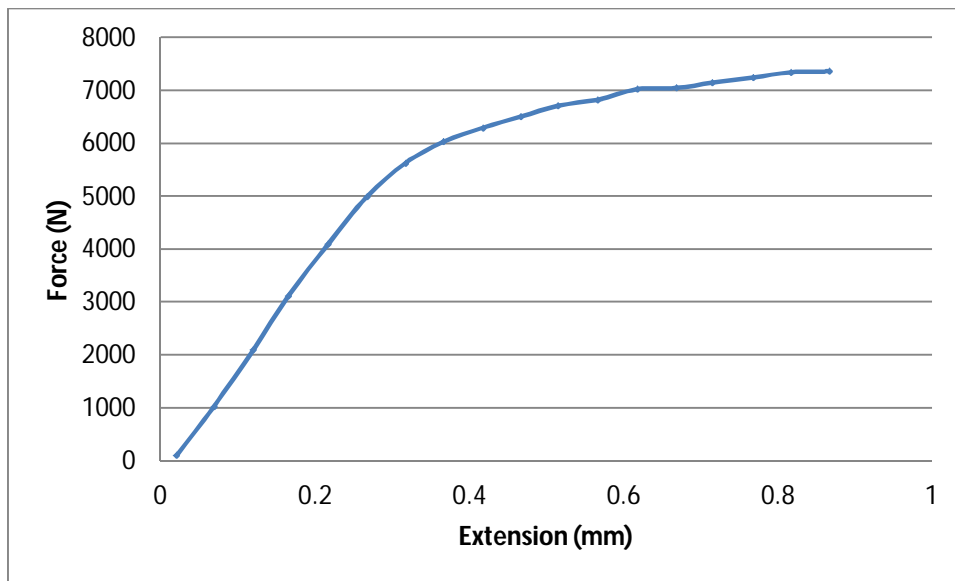


Figure C3v: Tensile behaviour of weld produced at 950 rpm and 150 mm/min with 15 mm shoulder  $\Phi$

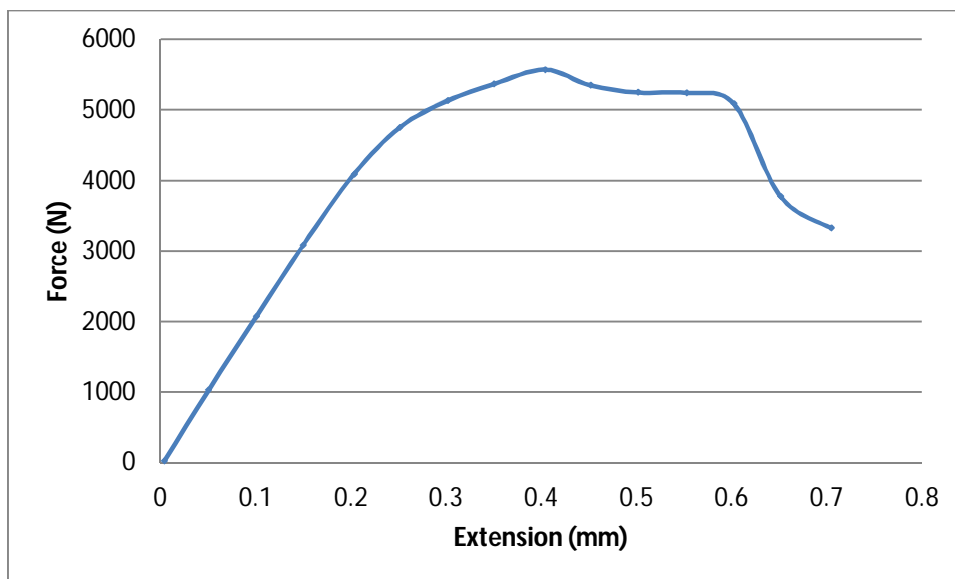


Figure C3vi: Tensile behaviour of weld produced at 950 rpm and 300 mm/min with 15 mm shoulder  $\Phi$

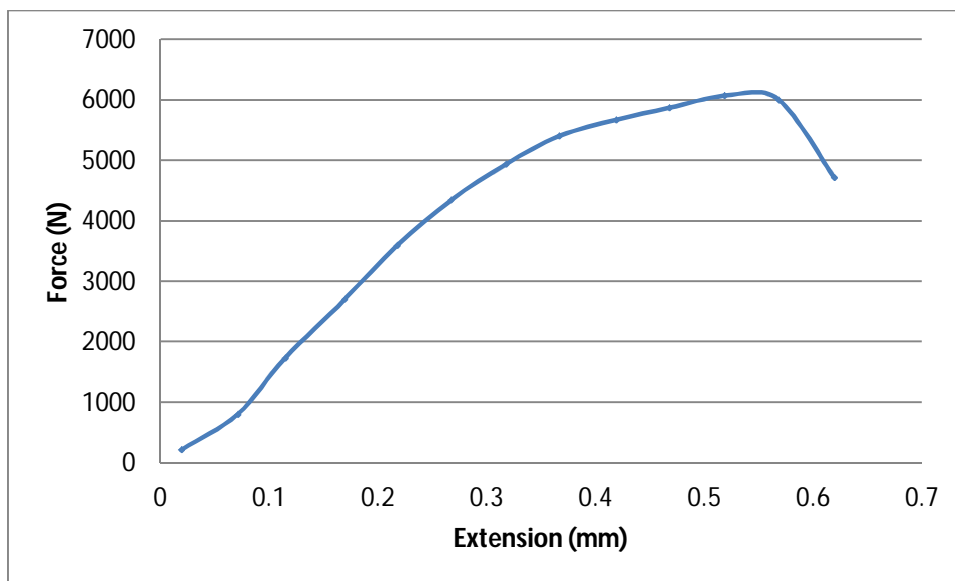


Figure C3vii: Tensile behaviour of weld produced at 1200 rpm and 50 mm/min with 15 mm shoulder  $\Phi$

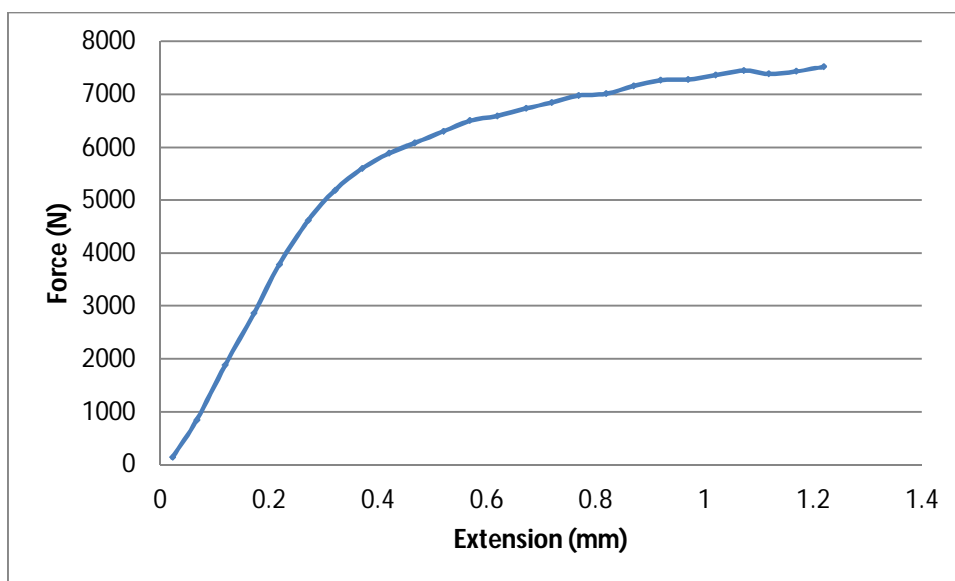


Figure C3viii: Tensile behaviour of weld produced at 1200 rpm and 150 mm/min with 15 mm shoulder  $\Phi$

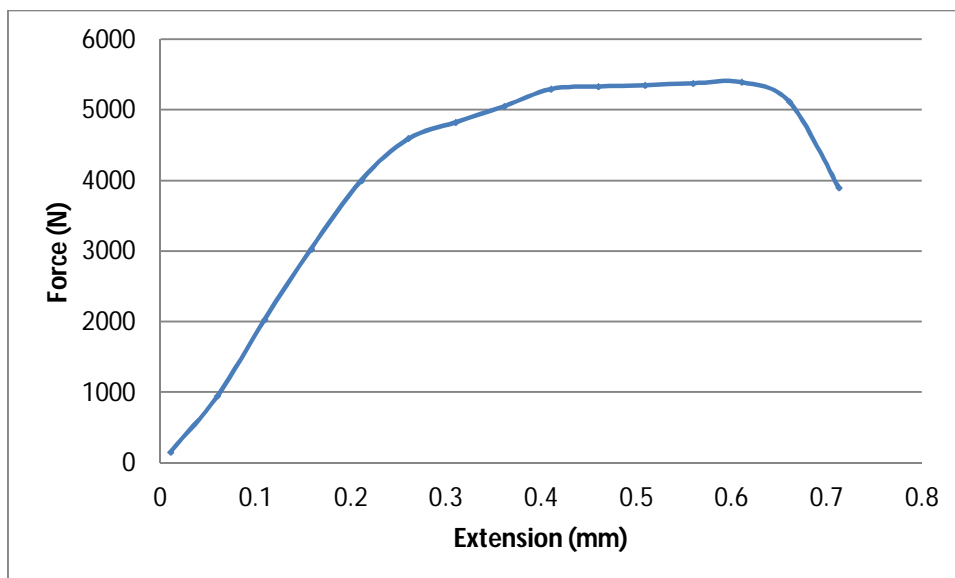


Figure C3ix: Tensile behaviour of weld produced at 1200 rpm and 300 mm/min with 15 mm shoulder  $\Phi$

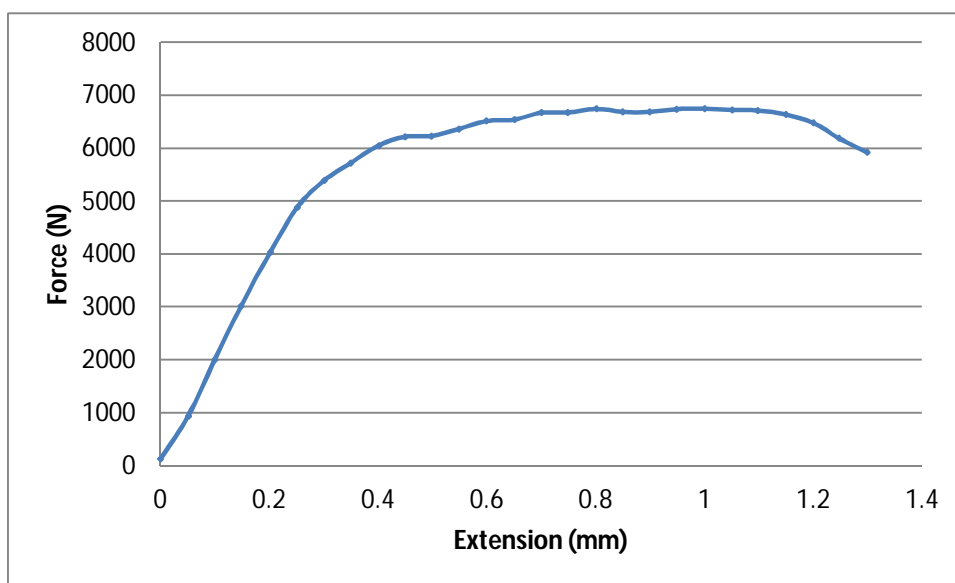


Figure C3x: Tensile behaviour of weld produced at 600 rpm and 50 mm/min with 18 mm shoulder  $\Phi$

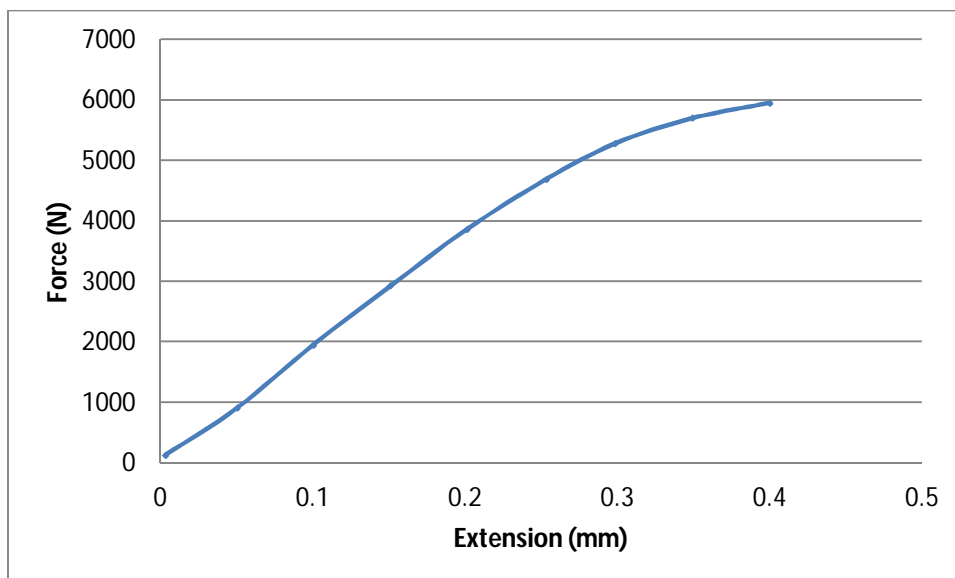


Figure C3xi: Tensile behaviour of weld produced at 600 rpm and 150 mm/min with 18 mm shoulder  $\Phi$

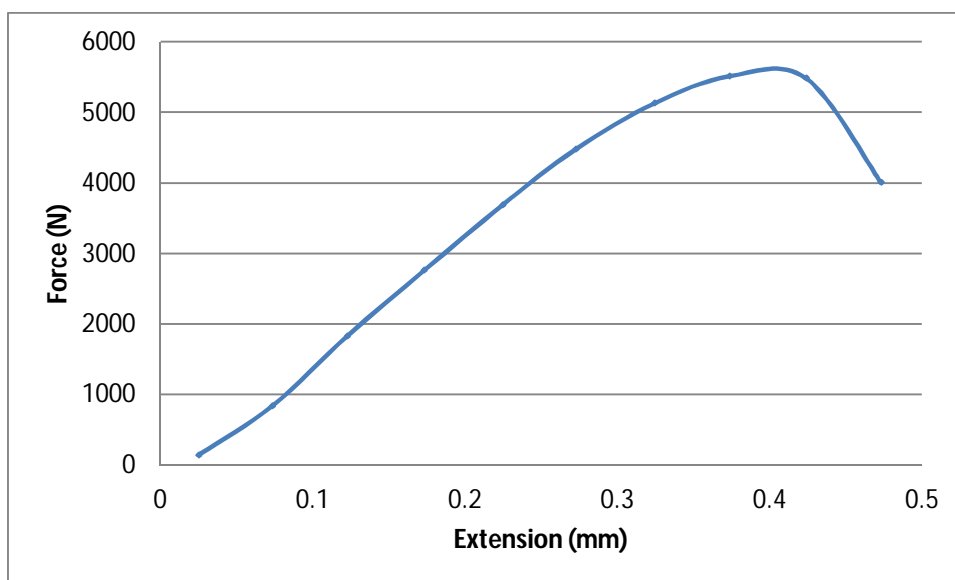


Figure C3xii: Tensile behaviour of weld produced at 600 rpm and 300 mm/min with 18 mm shoulder  $\Phi$

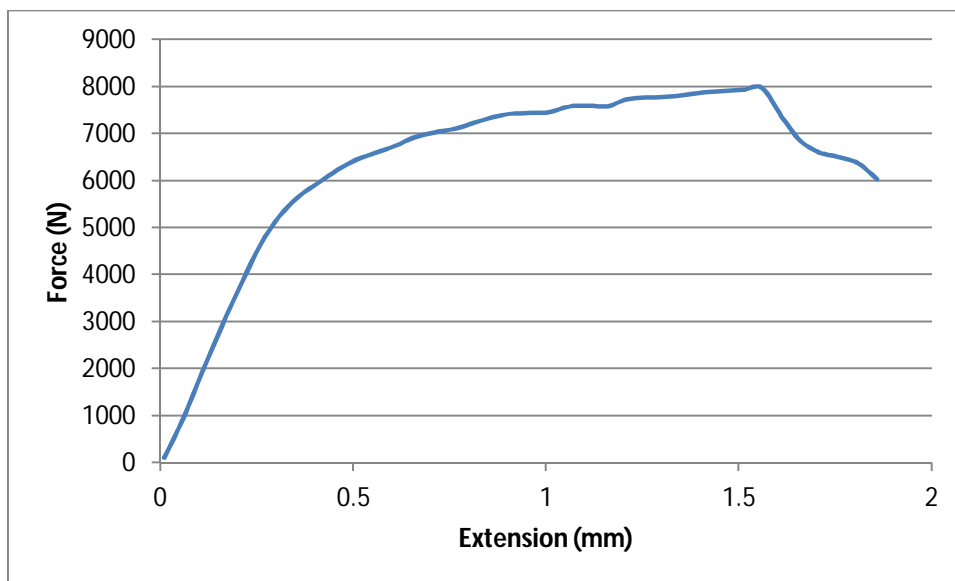


Figure C3xiii: Tensile behaviour of weld produced at 950 rpm and 50 mm/min with 18 mm shoulder  $\Phi$

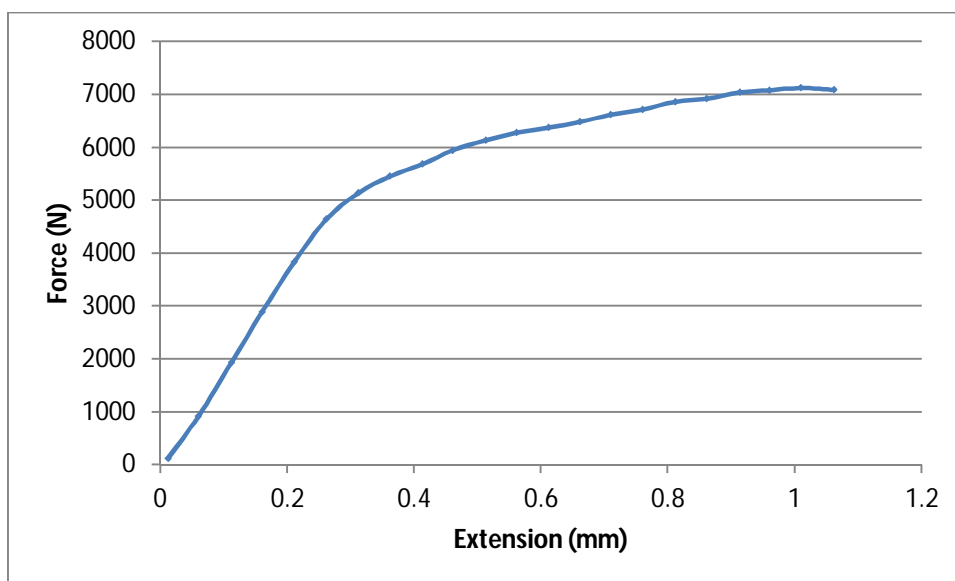


Figure C3xiv: Tensile behaviour of weld produced at 950 rpm and 150 mm/min with 18 mm shoulder  $\Phi$

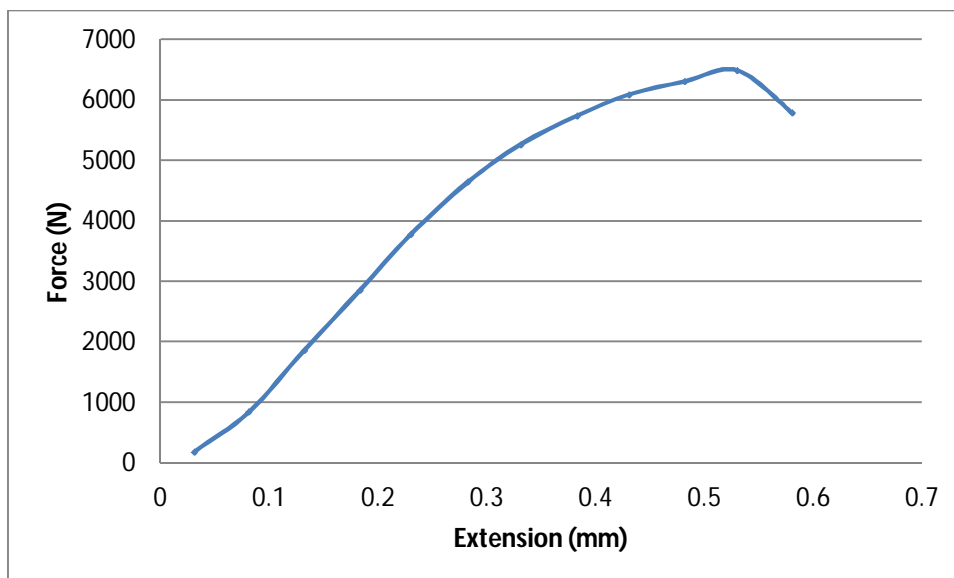


Figure C3xv: Tensile behaviour of weld produced at 950 rpm and 300 mm/min with 18 mm shoulder  $\Phi$

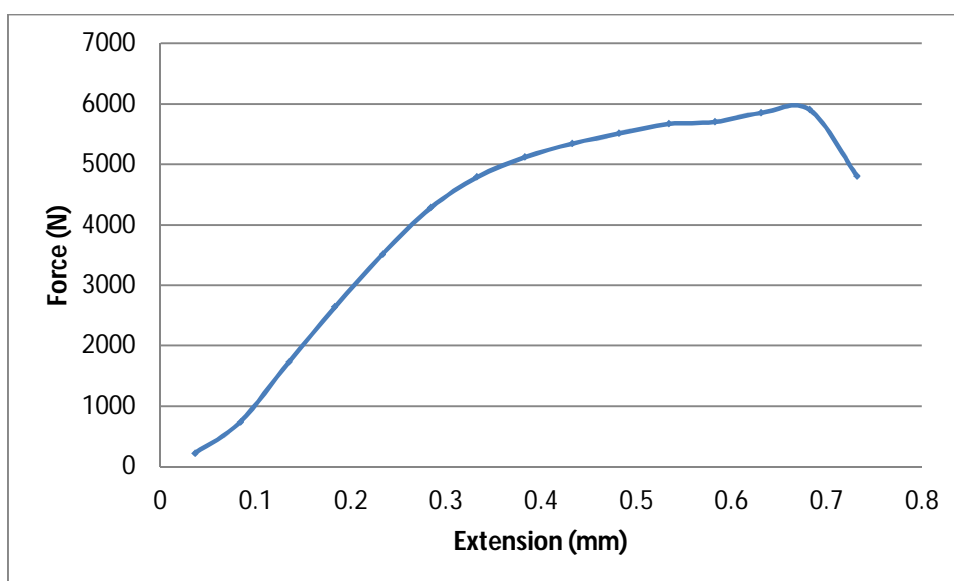


Figure C3xvi: Tensile behaviour of weld produced at 1200 rpm and 50 mm/min with 18 mm shoulder  $\Phi$

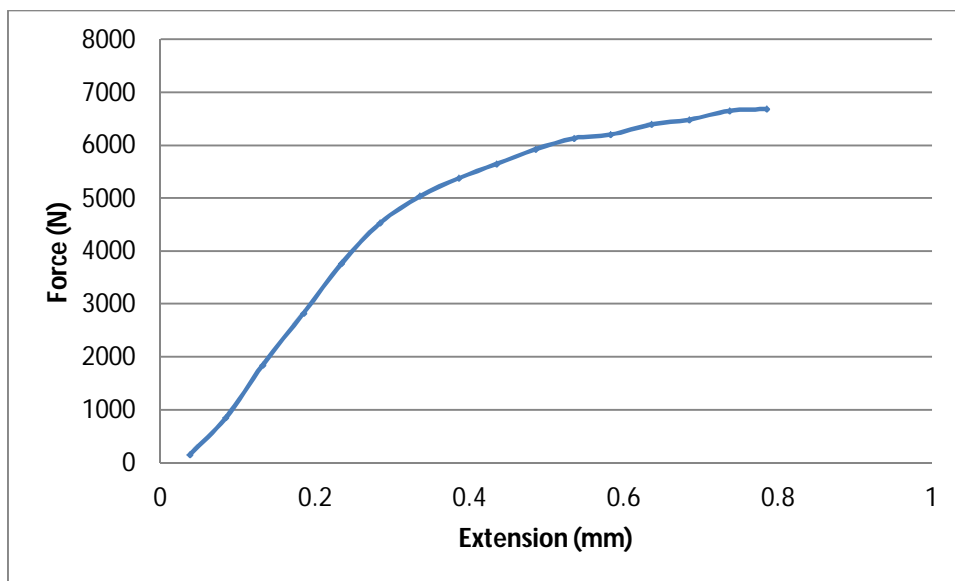


Figure C3xvii: Tensile behaviour of weld produced at 1200 rpm and 150 mm/min with 18 mm shoulder  $\Phi$

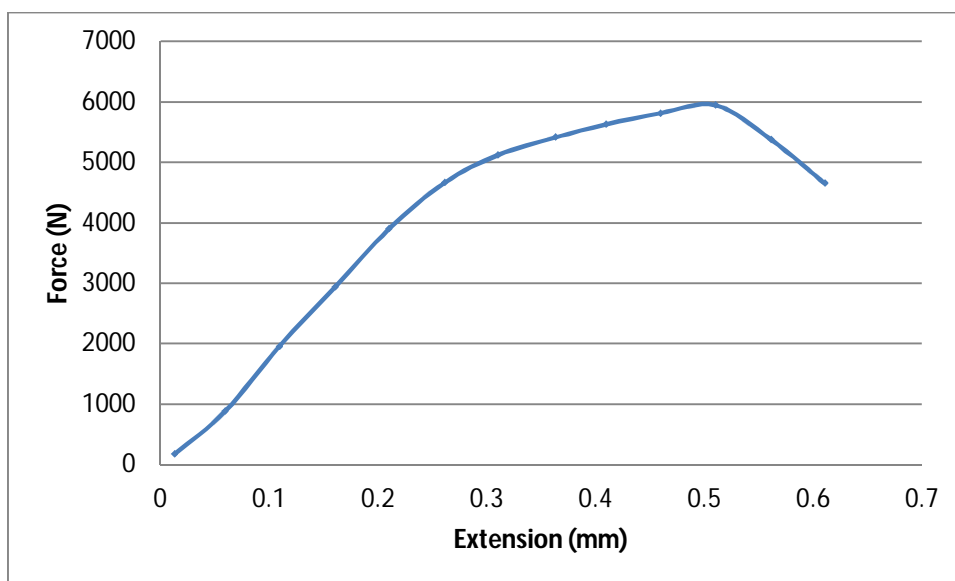


Figure C3xviii: Tensile behaviour of weld produced at 1200 rpm and 300 mm/min with 18 mm shoulder  $\Phi$

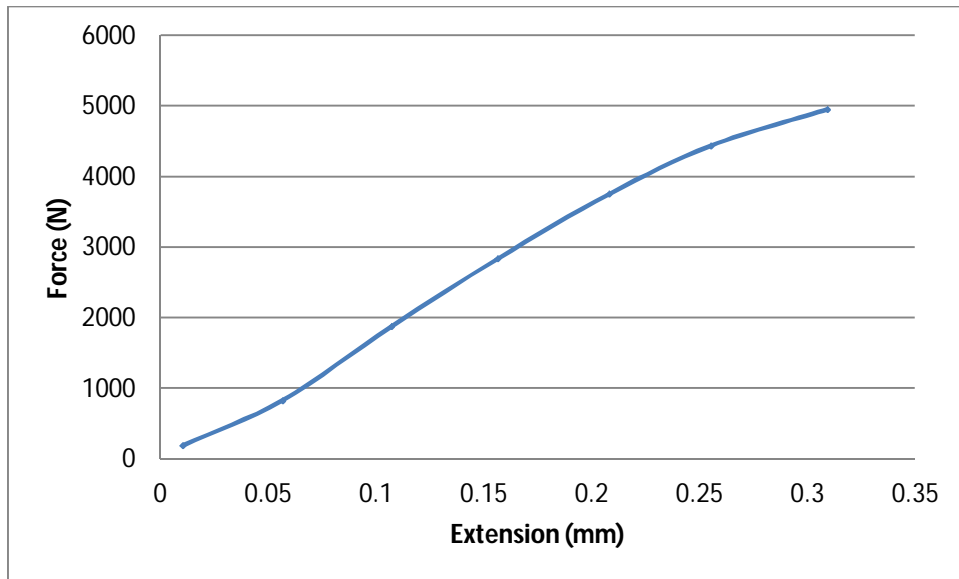


Figure C3xix: Tensile behaviour of weld produced at 600 rpm and 50 mm/min with 25 mm shoulder  $\Phi$

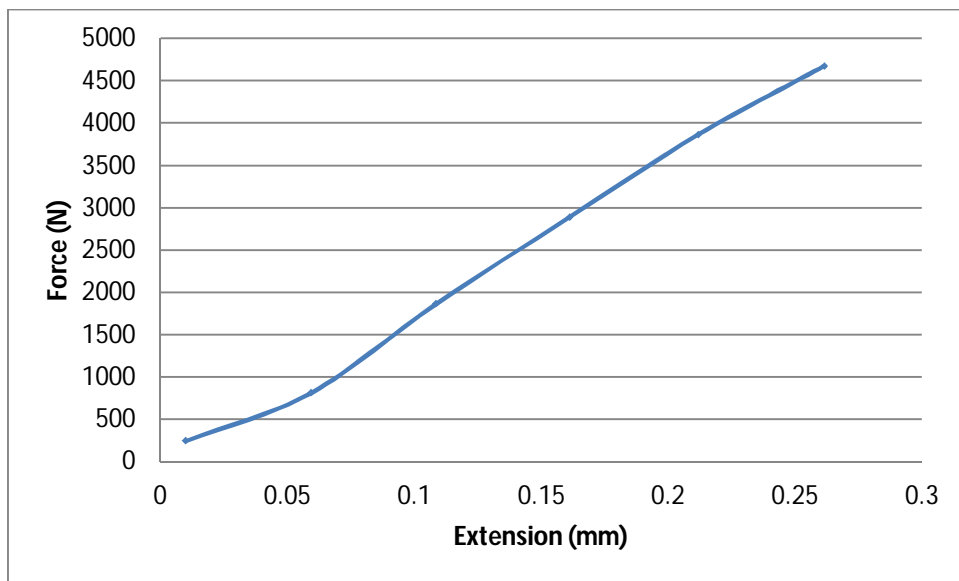


Figure C3xx: Tensile behaviour of weld produced at 600 rpm and 150 mm/min with 25 mm shoulder  $\Phi$

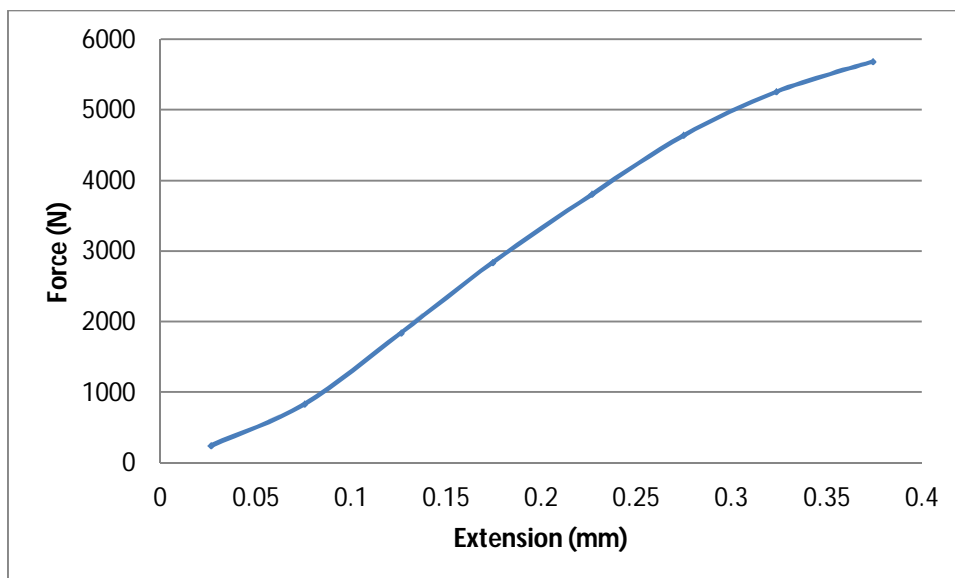


Figure C3xxi: Tensile behaviour of weld produced at 600 rpm and 300 mm/min with 25 mm shoulder  $\Phi$

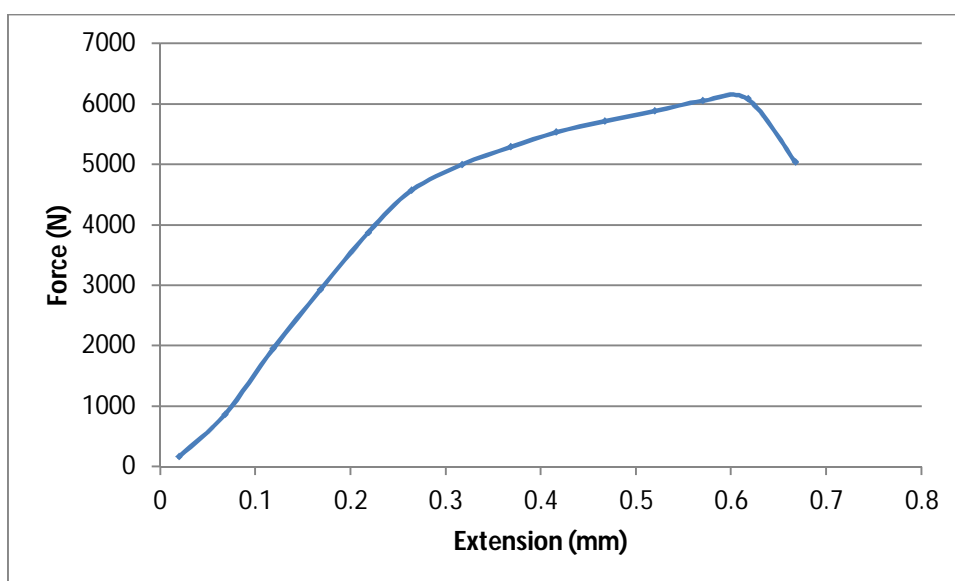


Figure C3xxii: Tensile behaviour of weld produced at 950 rpm and 50 mm/min with 25 mm shoulder  $\Phi$

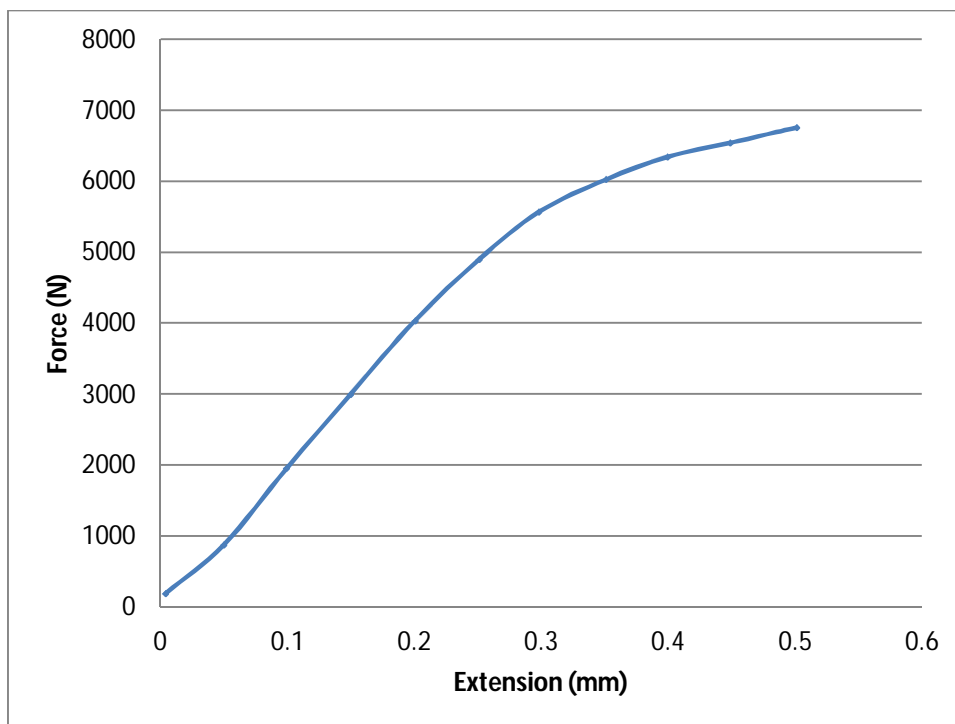


Figure C3xxiii: Tensile behaviour of weld produced at 950 rpm and 150 mm/min with 25 mm shoulder  $\Phi$

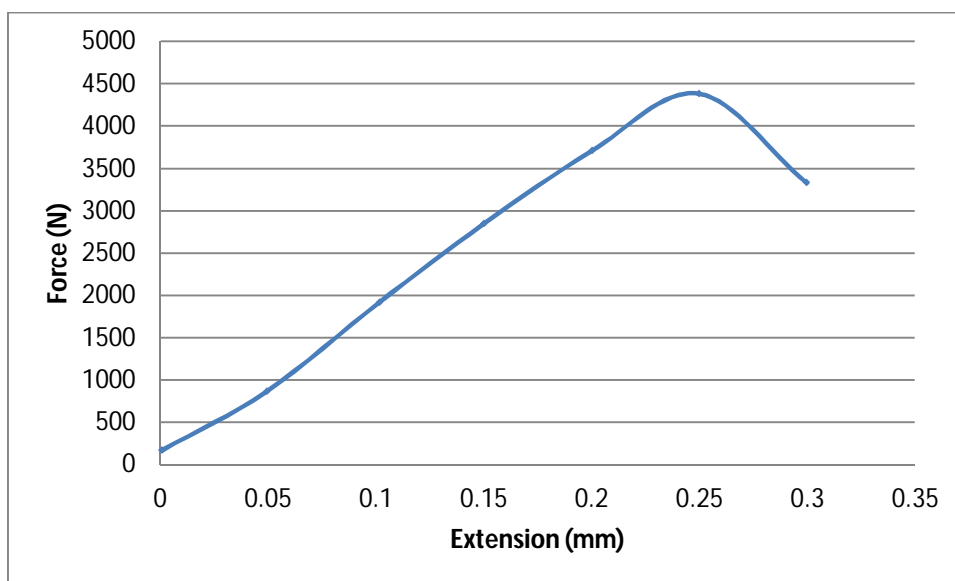


Figure C3xxiv: Tensile behaviour of weld produced at 950 rpm and 300 mm/min with 25 mm shoulder  $\Phi$

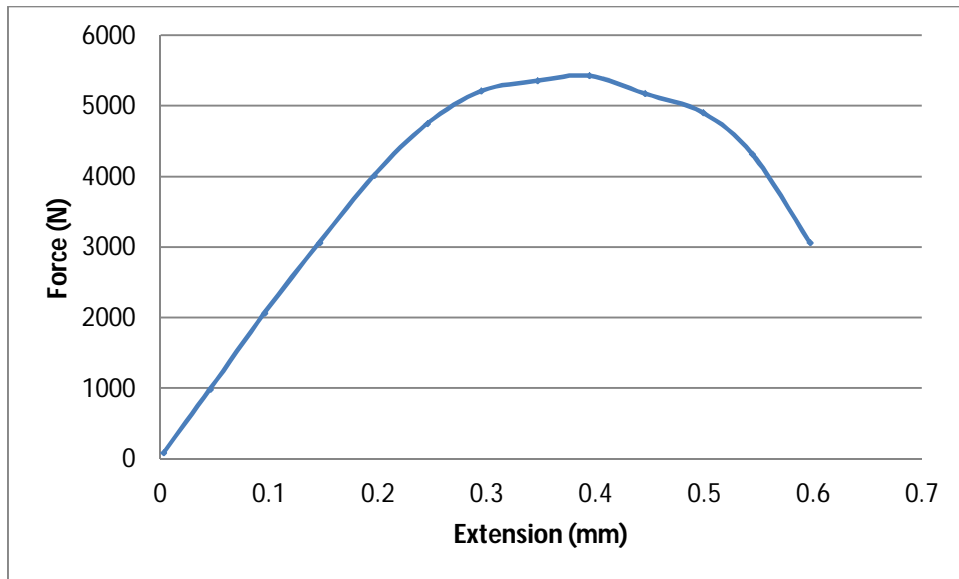


Figure C3xxv: Tensile behaviour of weld produced at 1200 rpm and 50 mm/min with 25 mm shoulder  $\Phi$

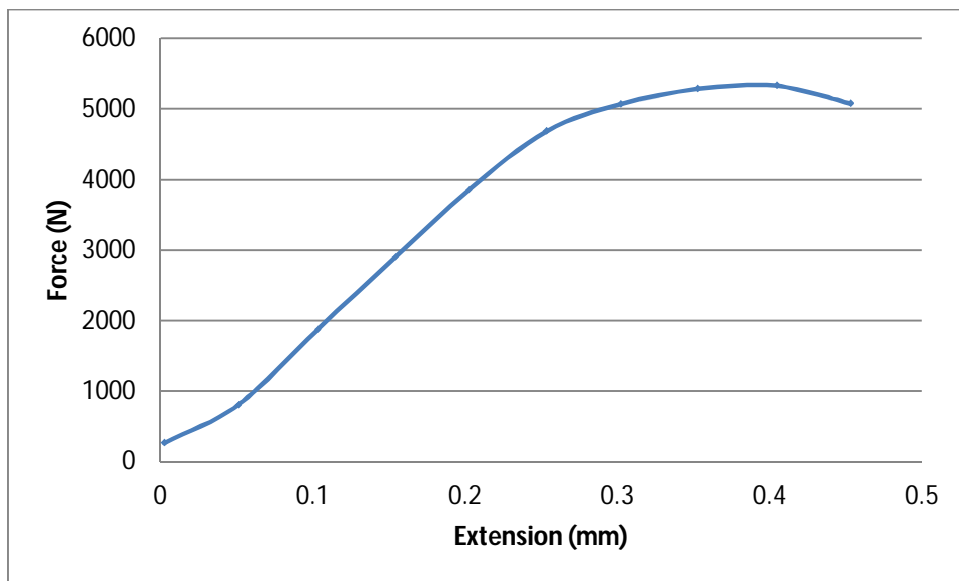


Figure C3xxvi: Tensile behaviour of weld produced at 1200 rpm and 150 mm/min with 25 mm shoulder  $\Phi$

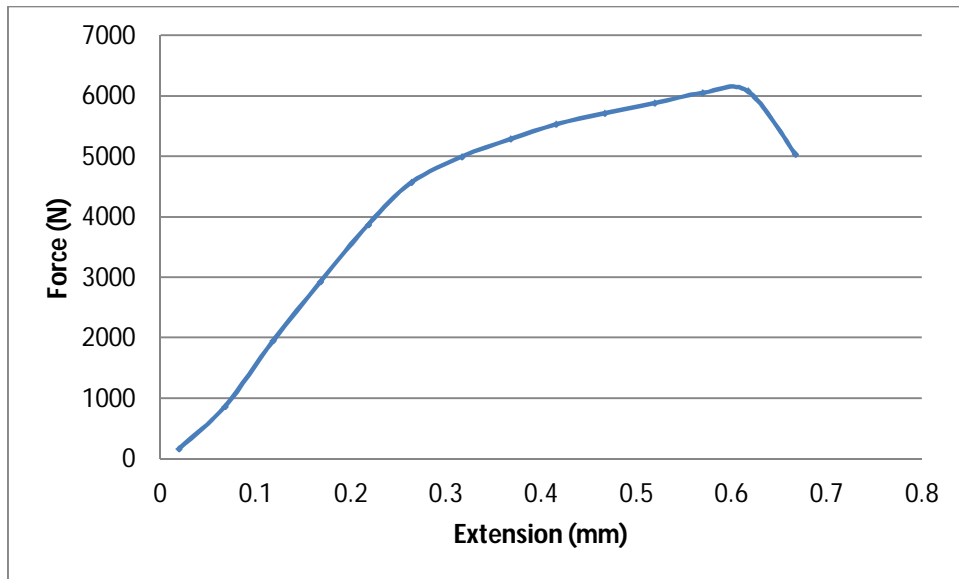


Figure C3xxvii: Tensile behaviour of weld produced at 1200 rpm and 300 mm/min with 25 mm shoulder  $\Phi$

**C4. (a) Fracture locations of tensile samples of welds produced with the 15 mm shoulder diameter tool**

<b>Weld No.</b>	<b>Rotational speed (rpm)</b>	<b>Traverse speed (mm/min)</b>	<b>Tensile sample</b>	<b>Fracture location</b>
S15_01	600	50	T1	TMAZ Cu
S15_01	600	50	T2	TMAZ Cu
S15_01	600	50	T3	TMAZ Cu
S15_02	600	150	T1	TMAZ Cu
S15_02	600	150	T2	TMAZ Cu
S15_02	600	150	T3	TMAZ Cu
S15_03	600	300	T1	TMAZ Al
S15_03	600	300	T2	TMAZ Al
S15_03	600	300	T3	TMAZ Cu
S15_04	950	50	T1	TMAZ Al
S15_04	950	50	T2	TMAZ Cu
S15_04	950	50	T3	TMAZ Cu
S15_05	950	150	T1	TMAZ Al
S15_05	950	150	T2	TMAZ Al
S15_05	950	150	T3	TMAZ Cu
S15_06	950	300	T1	TMAZ Al
S15_06	950	300	T2	TMAZ Cu
S15_06	950	300	T3	TMAZ Cu
S15_07	1200	50	T1	TMAZ Cu
S15_07	1200	50	T2	TMAZ Cu
S15_07	1200	50	T3	TMAZ Cu
S15_08	1200	150	T1	TMAZ Al
S15_08	1200	150	T2	TMAZ Cu
S15_08	1200	150	T3	TMAZ Cu
S15_09	1200	300	T1	TMAZ Cu
S15_09	1200	300	T2	TMAZ Al
S15_09	1200	300	T3	TMAZ Cu

**(b) Fracture locations of tensile samples of welds produced with the 18 mm shoulder diameter tool**

<b>Weld No.</b>	<b>Rotational speed (rpm)</b>	<b>Traverse speed (mm/min)</b>	<b>Tensile sample</b>	<b>Fracture location</b>
S18_01	600	50	T1	TMAZ Cu
S18_01	600	50	T2	TMAZ Cu
S18_01	600	50	T3	TMAZ Cu
S18_02	600	150	T1	TMAZ Al
S18_02	600	150	T2	TMAZ Cu
S18_02	600	150	T3	TMAZ Cu
S18_03	600	300	T1	TMAZ Cu
S18_03	600	300	T2	TMAZ Al
S18_03	600	300	T3	TMAZ Cu
S18_04	950	50	T1	TMAZ Cu
S18_04	950	50	T2	TMAZ Cu
S18_04	950	50	T3	TMAZ Cu
S18_05	950	150	T1	TMAZ Cu
S18_05	950	150	T2	TMAZ Cu
S18_05	950	150	T3	TMAZ Cu
S18_06	950	300	T1	TMAZ Al
S18_06	950	300	T2	TMAZ Cu
S18_06	950	300	T3	TMAZ Al
S18_07	1200	50	T1	TMAZ Al
S18_07	1200	50	T2	TMAZ Al
S18_07	1200	50	T3	TMAZ Cu
S18_08	1200	150	T1	TMAZ Al
S18_08	1200	150	T2	TMAZ Cu
S18_08	1200	150	T3	TMAZ Cu
S18_09	1200	300	T1	TMAZ Cu
S18_09	1200	300	T2	TMAZ Al
S18_09	1200	300	T3	TMAZ Cu

**(c) Fracture locations of tensile samples of welds produced with the 25 mm shoulder diameter tool**

<b>Weld No.</b>	<b>Rotational speed rpm</b>	<b>Traverse speed (mm/min)</b>	<b>Tensile sample</b>	<b>Fracture location</b>
S25_01	600	50	T1	TMAZ Al
S25_01	600	50	T2	TMAZ Cu
S25_01	600	50	T3	TMAZ Cu
S25_02	600	150	T1	TMAZ Al
S25_02	600	150	T2	TMAZ Al
S25_02	600	150	T3	TMAZ Cu
S25_03	600	300	T1	TMAZ Cu
S25_03	600	300	T2	TMAZ Al
S25_03	600	300	T3	TMAZ Cu
S25_04	950	50	T1	TMAZ Al
S25_04	950	50	T2	TMAZ Cu
S25_04	950	50	T3	TMAZ Cu
S25_05	950	150	T1	TMAZ Al
S25_05	950	150	T2	TMAZ Al
S25_05	950	150	T3	TMAZ Cu
S25_06	950	300	T1	TMAZ Al
S25_06	950	300	T2	TMAZ Cu
S25_06	950	300	T3	TMAZ Cu
S25_07	1200	50	T1	TMAZ Cu
S25_07	1200	50	T2	TMAZ Cu
S25_07	1200	50	T3	TMAZ Cu
S25_08	1200	150	T1	TMAZ Cu
S25_08	1200	150	T2	TMAZ Cu
S25_08	1200	150	T3	TMAZ Cu
S25_09	1200	300	T1	TMAZ Al
S25_09	1200	300	T2	TMAZ Al
S25_09	1200	300	T3	TMAZ Cu

**C5. Photo montages of fracture locations due to lack of fusion**



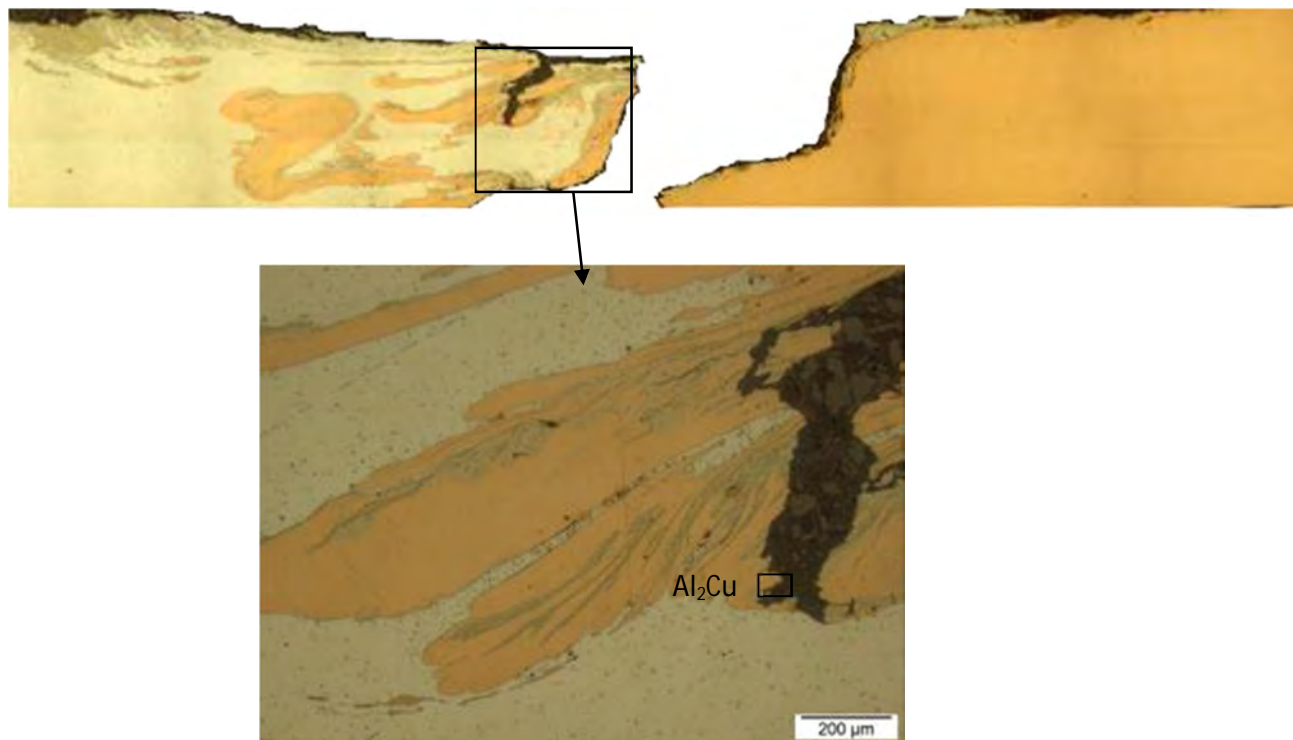
**(b) S18\_07 T1: Fractured surface of weld produced at 1200 rpm and 50 mm/min with the 18 mm shoulder diameter tool**



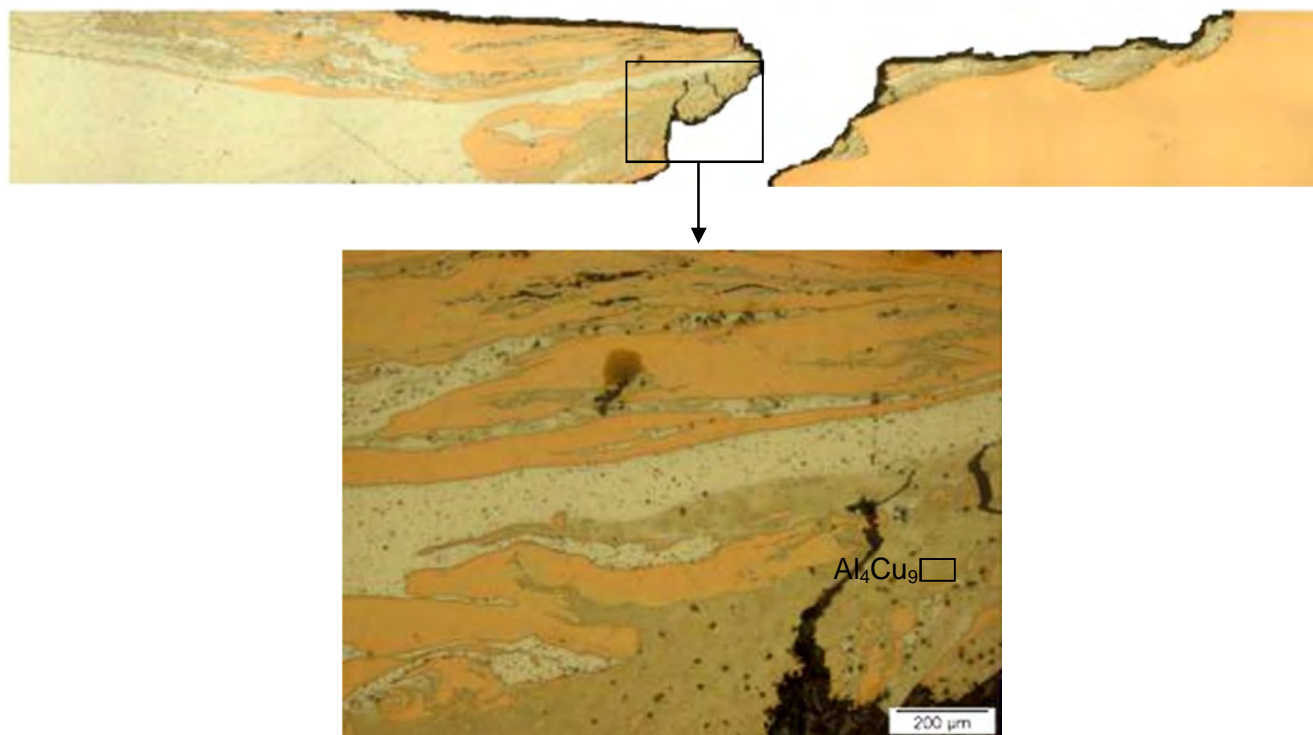
**(c) S25\_06 T1: Fractured surface of weld produced at 950 rpm and 300 mm/min with the 25 mm shoulder diameter tool**



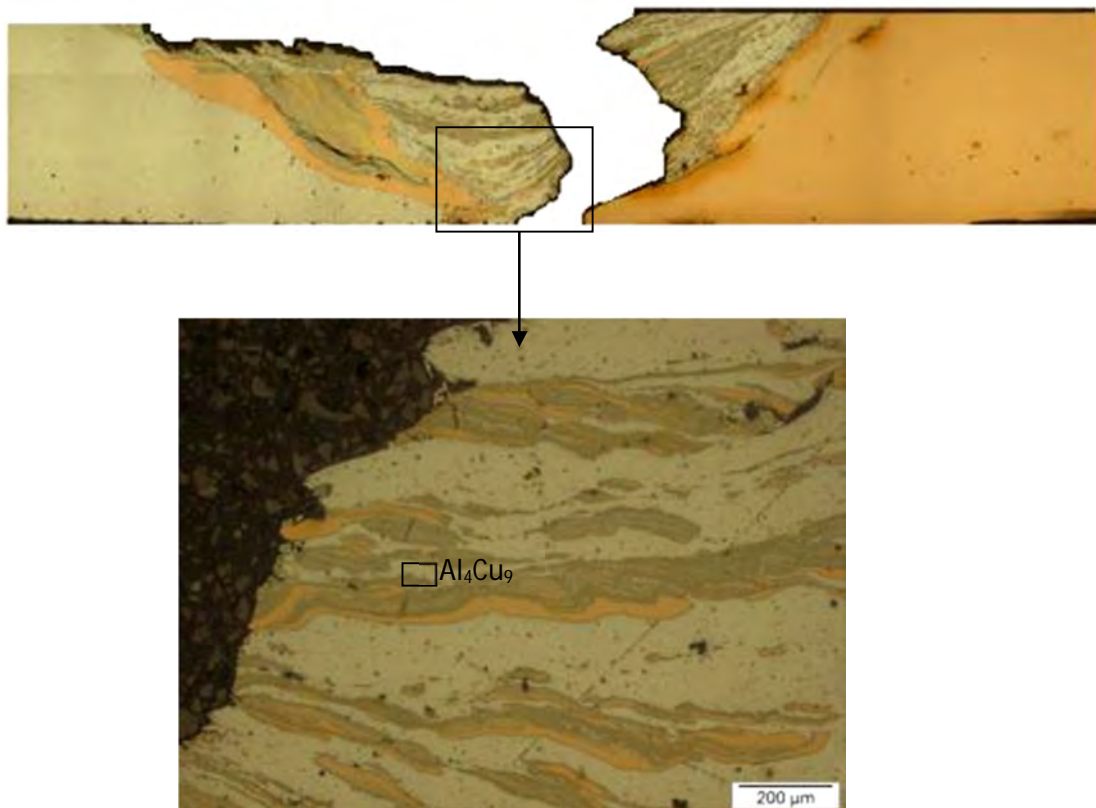
**(d) S25\_09 T1: Fractured surface of weld produced at 1200 rpm and 300 mm/min with the 25 mm shoulder diameter tool**

**C6. Photo montages of fracture locations due to intermetallics**

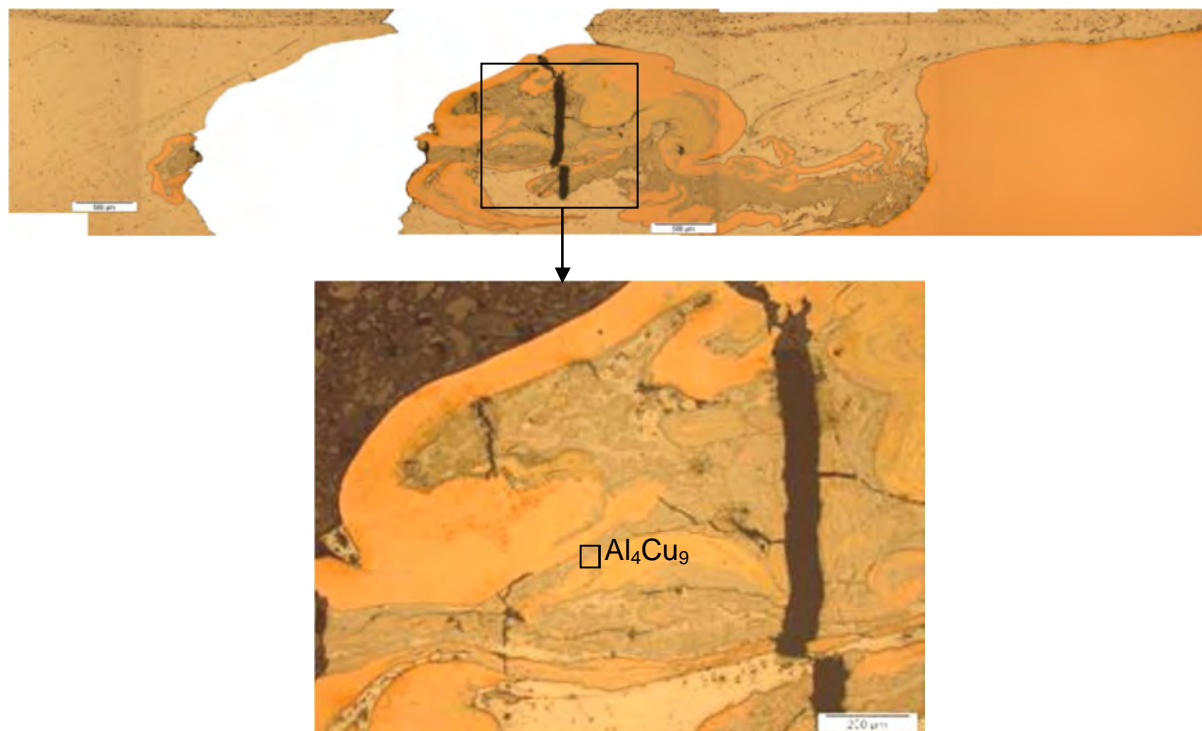
**(a) S15\_01 T2: Fractured surface of weld produced at 600 rpm and 50 mm/min with the 15 mm shoulder diameter tool**



**(b) S15\_04 T2: Fractured surface of weld produced at 950 rpm and 50 mm/min with the 15 mm shoulder diameter tool**

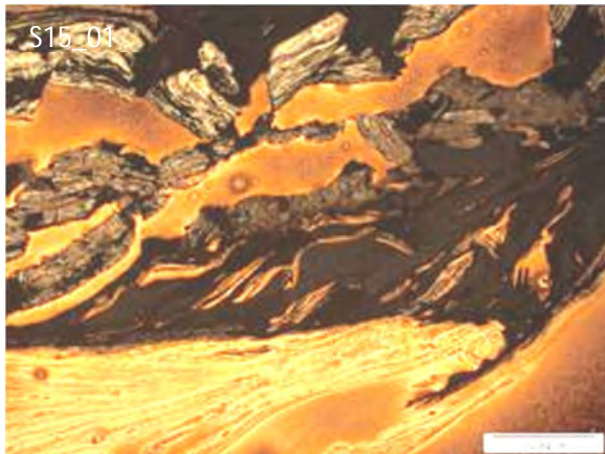


(d) S18\_01 T1: Fractured surface of weld produced at 600 rpm and 50 mm/min with the 18 mm shoulder diameter tool

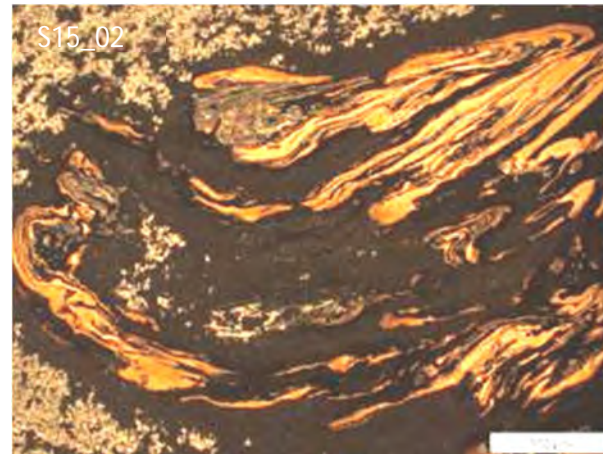


(e) S18\_08 T1: Fractured surface of weld produced at 1200 rpm and 150 mm/min with the 18 mm shoulder diameter tool

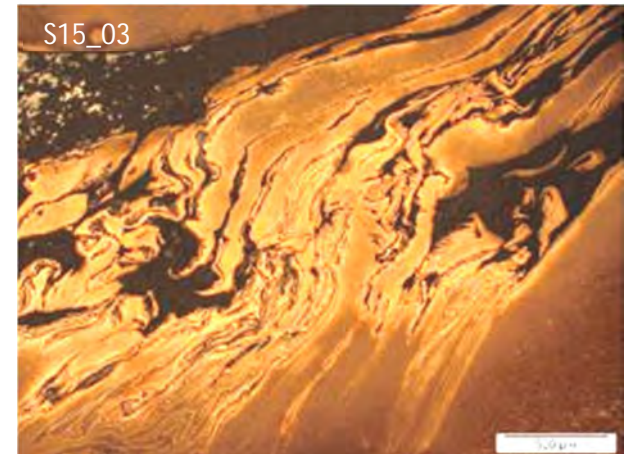
**C7. Etched SZ**



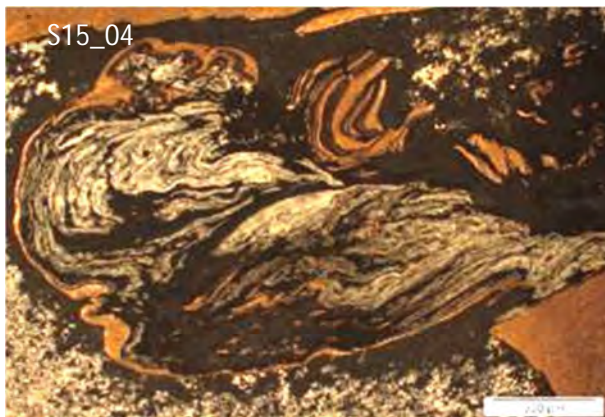
**(a) Produced at 600 rpm and 50 mm/min**



**(b) Produced at 600 rpm and 150 mm/min**



**(c) Produced at 600 rpm and 300 mm/min**



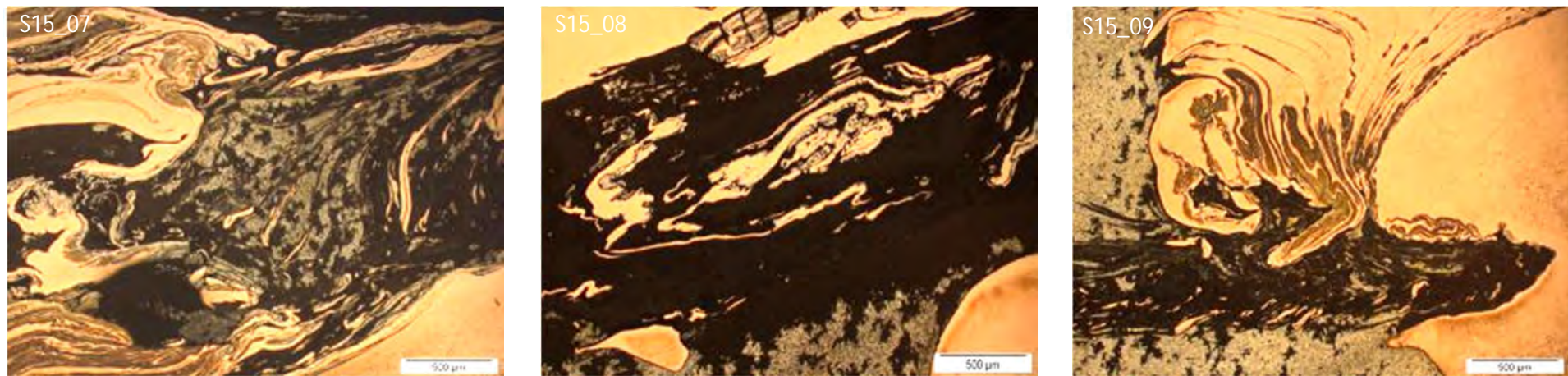
**(d) Produced at 950 rpm and 50mm/min**



**(e) Produced at 950 rpm and 150mm/min**

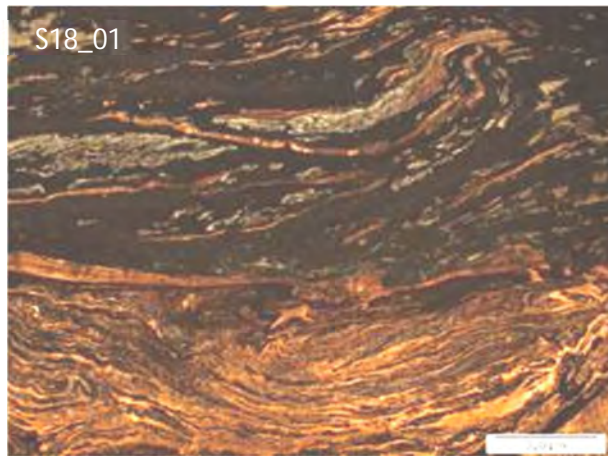


**(f) Produced at 950 rpm and 300mm/min**

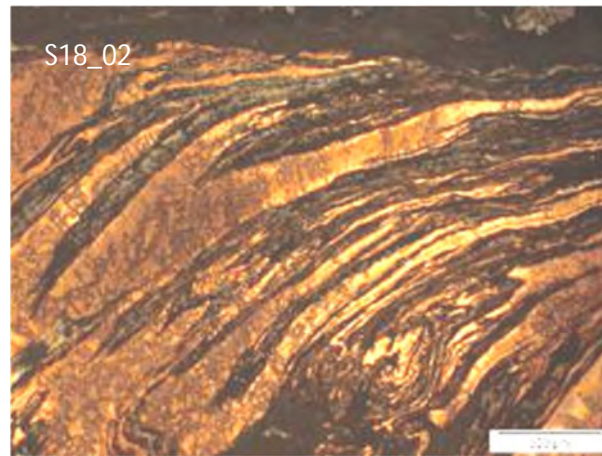


(g) Produced at 1200 rpm and 50 mm/min (h) Produced at 1200 rpm and 150 mm/min (i) Produced at 1200 rpm and 300 mm/min

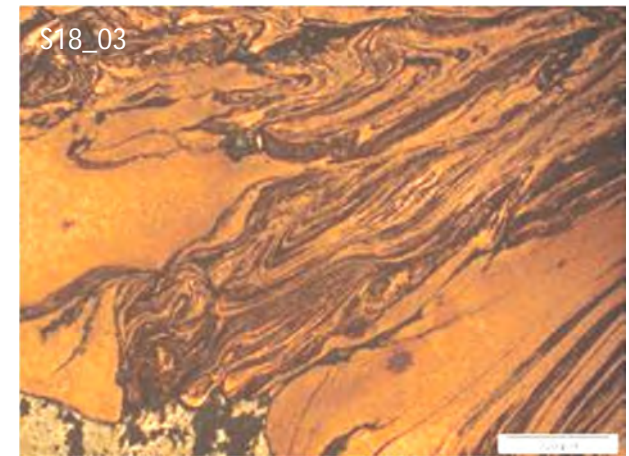
Figure C7: 1. (a-i): Microstructure of stir zones of welds produced with the 15 mm shoulder diameter tool



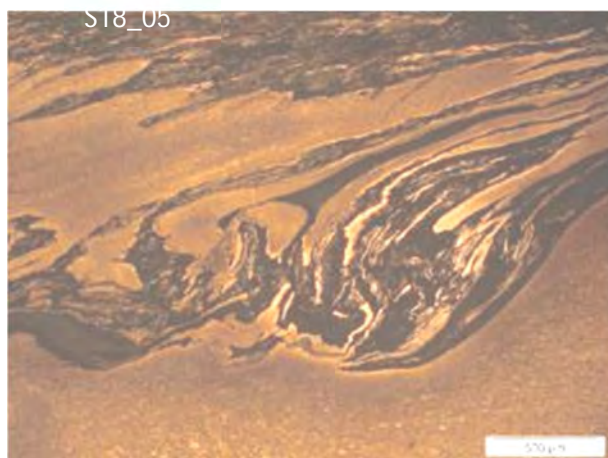
(a) Produced at 600 rpm and 50 mm/min



(b) Produced at 600 rpm and 150 mm/min



(c) Produced at 600 rpm and 300 mm/min



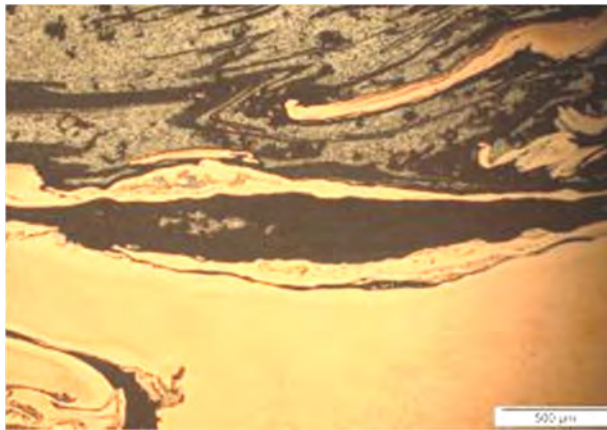
(d) Produced at 950 rpm and 50 mm/min



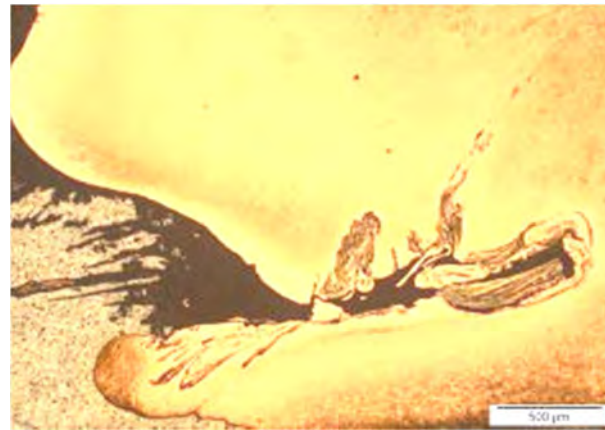
(e) Produced at 950 rpm and 150 mm/min



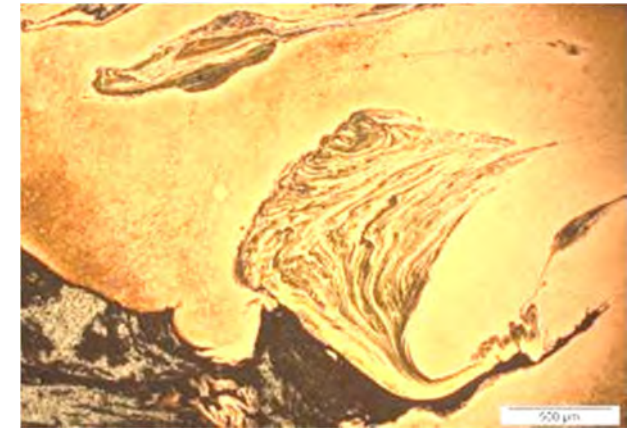
(f) Produced at 950 rpm and 300 mm/min



(g) Produced at 1200 rpm and 50 mm/min

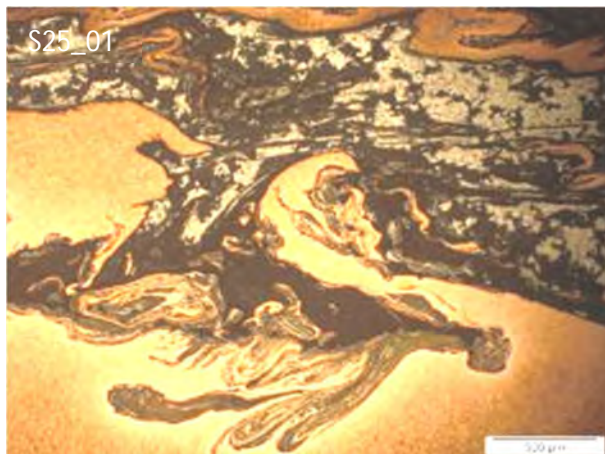


(h) Produced at 1200 rpm and 150 mm/min

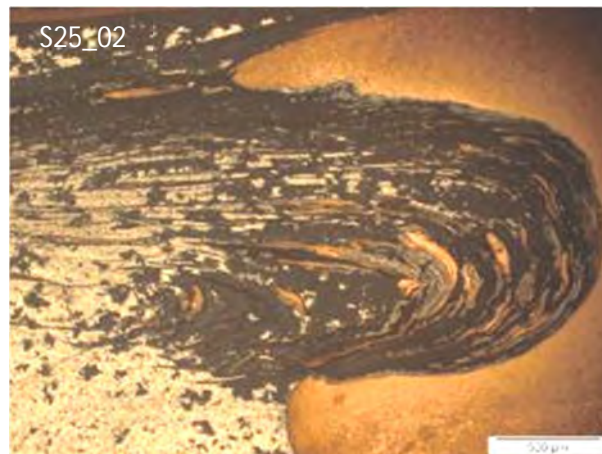


(i) Produced at 1200 rpm and 50 mm/min

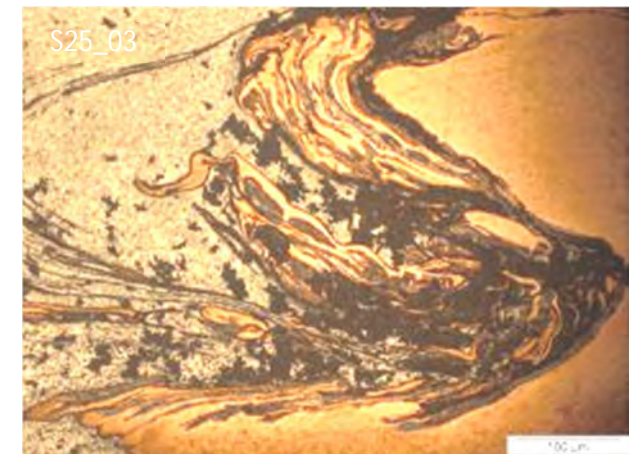
Figure C7 : 2. (a-i): Microstructure of stir zones of welds produced with the 18mm shoulder diameter tool



(a) Produced at 600 rpm and 50 mm/min



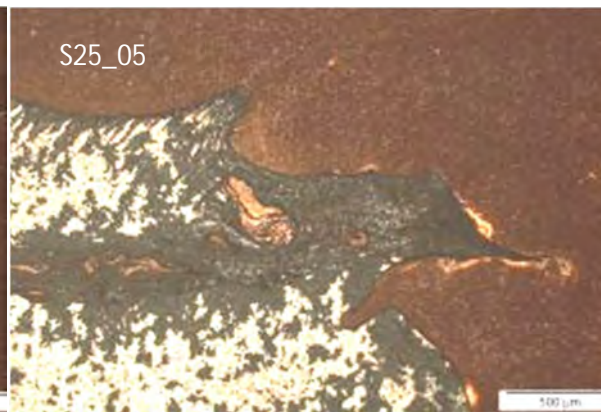
(b) Produced at 600 rpm and 150 mm/min



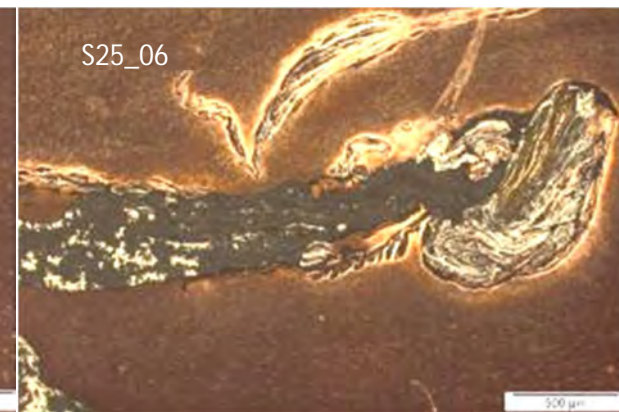
(c) Produced at 600 rpm and 300 mm/min



(d) Produced at 950 rpm and 50 mm/min



(e) Produced at 950 rpm and 150 mm/min



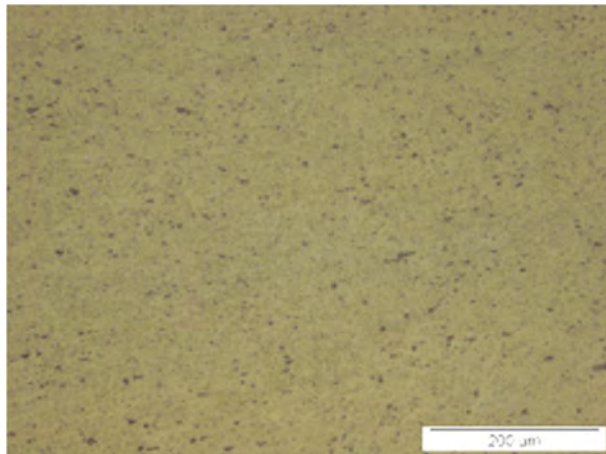
(f) Produced at 950 rpm 300 mm/min



(g) Produced at 1200 rpm and 50 mm/min (h) Produced at 1200 rpm and 150 mm/min (i) Produced at 1200 rpm 300 mm/min

Figure C7 : 3. (a-i): Microstructure of stir zones of welds produced with the 25 mm shoulder diameter tool

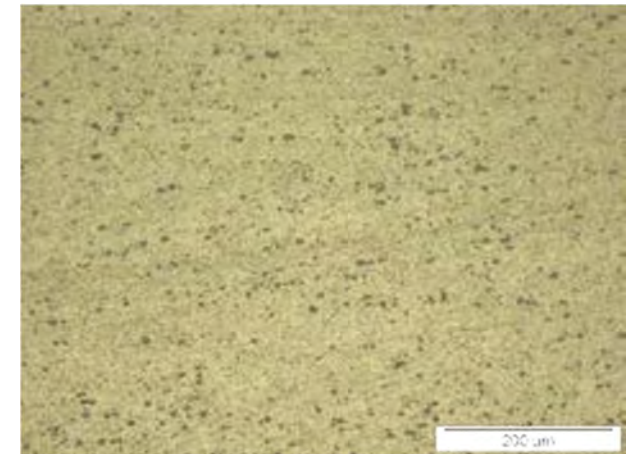
**C8. Etched TMAZ**



(a) TMAZ Al produced with 15 mm  $\Phi$

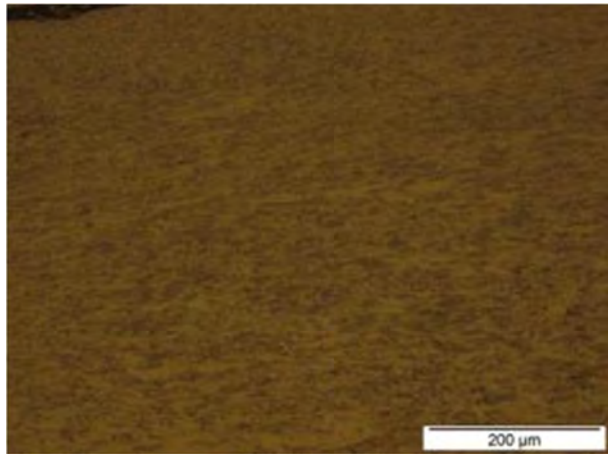


(b) TMAZ Al produced with 18 mm  $\Phi$



(c) TMAZ Al produced with 25 mm  $\Phi$

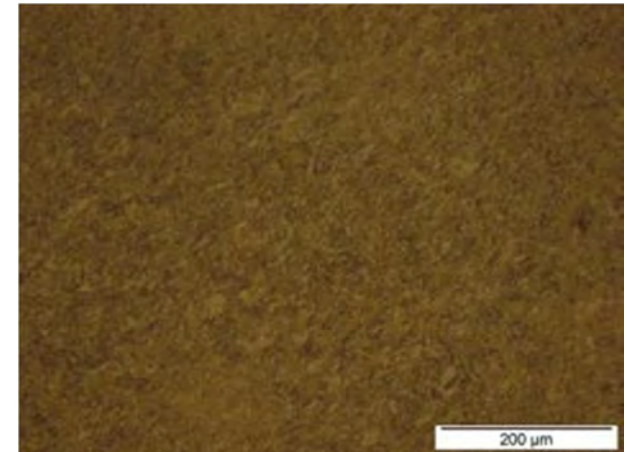
**Figure C8 :1. (a-c): Microstructure of the TMAZ of Al in welds produced with the 15, 18 and 25 mm shoulder diameter tools respectively**



(a) TMAZ Cu produced with 15 mm  $\Phi$



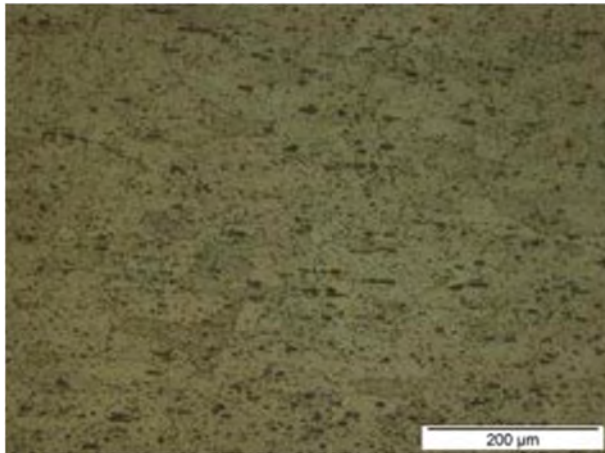
(b) TMAZ Cu produced with 18 mm  $\Phi$



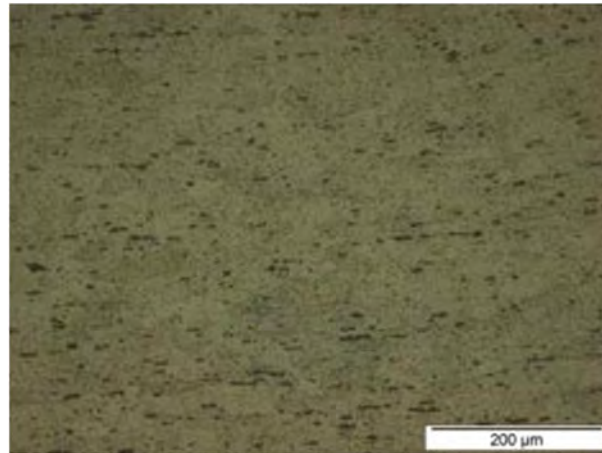
(c) TMAZ Cu produced with 25 mm  $\Phi$

C8:2. (a-c): Microstructure of the TMAZ of Cu in welds produced with the 15, 18 and 25 mm shoulder diameter tools respectively

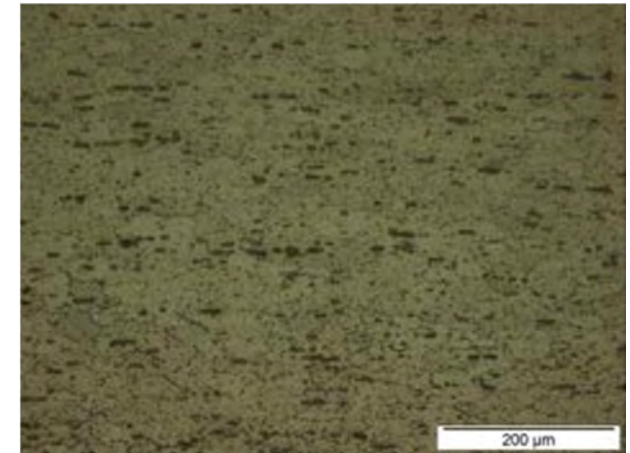
**C9. Etched HAZ**



**(a) HAZ Al produced with 15 mm  $\Phi$**

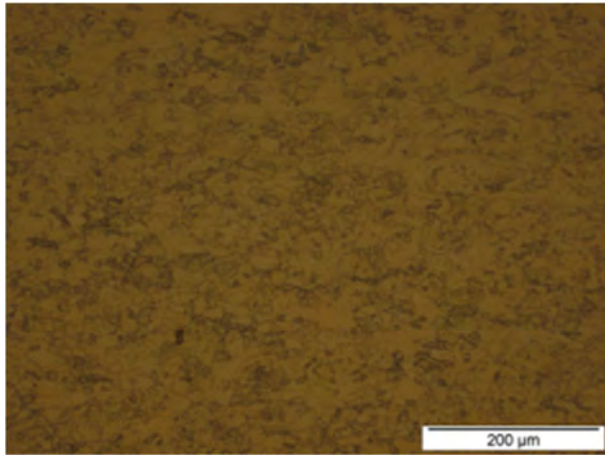


**(b) HAZ Al produced with 18 mm  $\Phi$**

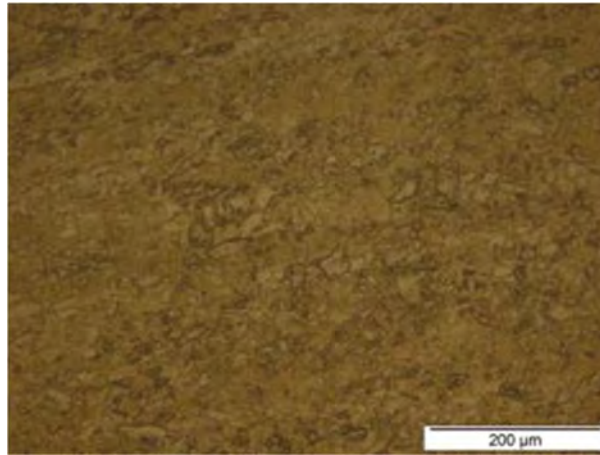


**(c) HAZ Al produced with 25 mm  $\Phi$**

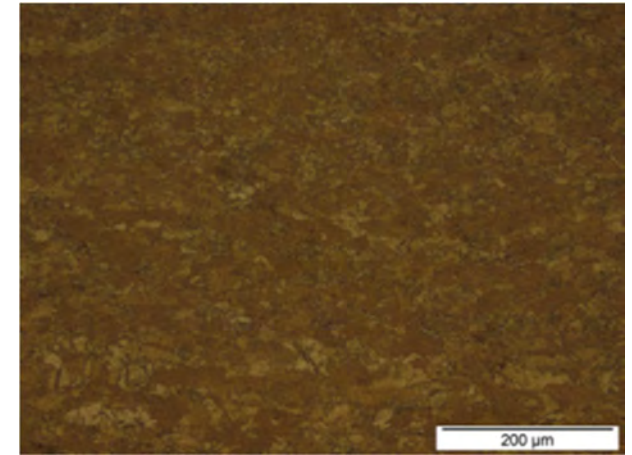
**C9: 1. (a-c): Microstructure of the HAZ of Al in welds produced with the 15, 18 and 25 mm shoulder diameter tools respectively**



(a) HAZ Cu produced with 15 mm  $\Phi$



(b) HAZ Cu produced with 18 mm  $\Phi$



(c) HAZ Cu produced with 25 mm  $\Phi$

**C9: 2. (a-c): Microstructure of the HAZ of Cu in welds produced with the 15, 18 and 25 mm shoulder diameter tools respectively**

Typical onion ring structure observed as semi-circular rings were observed in the SZ of welds S15\_04 (produced at 950 rpm and 50 mm/min), S15\_05 (produced at 950 rpm and 150 mm/min) and S15\_08 (produced at 1200 rpm and 150mm/min) with the 15 mm shoulder diameter tool; S18\_01 (produced at 600 rpm and 50 mm/min), S18\_04 (produced at 950 rpm and 50 mm/min, S18\_05 (produced at 950 rpm and 150 mm/min and S18\_07 (produced at 1200 rpm and 150 mm/min) with the 18 mm shoulder diameter tool; S25\_02 (produced at 600 rpm and 150 mm/min) and S25\_09 (produced at 1200 rpm and 300 mm/min) produced with the 25 mm shoulder diameter tool. It should be noted that most of these welds were produced at traverse speeds of 50 and 150 mm/min which is an indication that lower feed rates can be used to produce good welds.

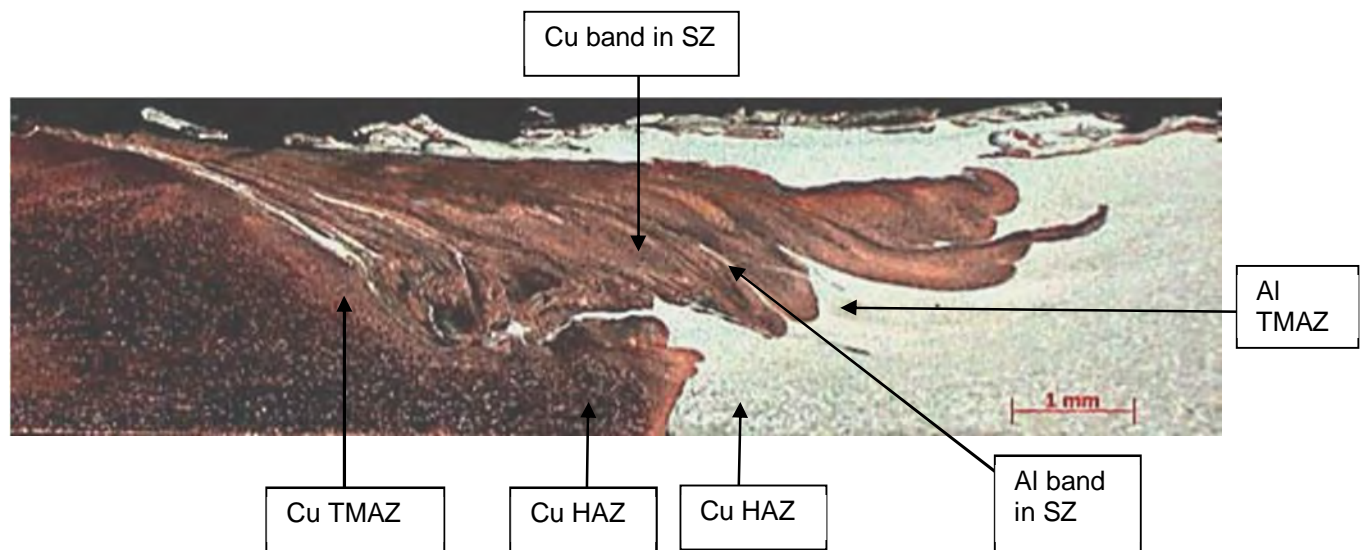
**C10. Grain size measurements**

Figure C10a: Sample S18\_04 used for the grain size measurement

It was observed that the HAZ in this representative sample is narrow; this is expected because the thermal diffusivity for both metals is high<sup>152</sup> ( $0.809$  and  $1.128\text{cm}^2\text{s}^{-1}$  for aluminium and copper respectively), therefore the cooling rate is high and the HAZ should be relatively small.

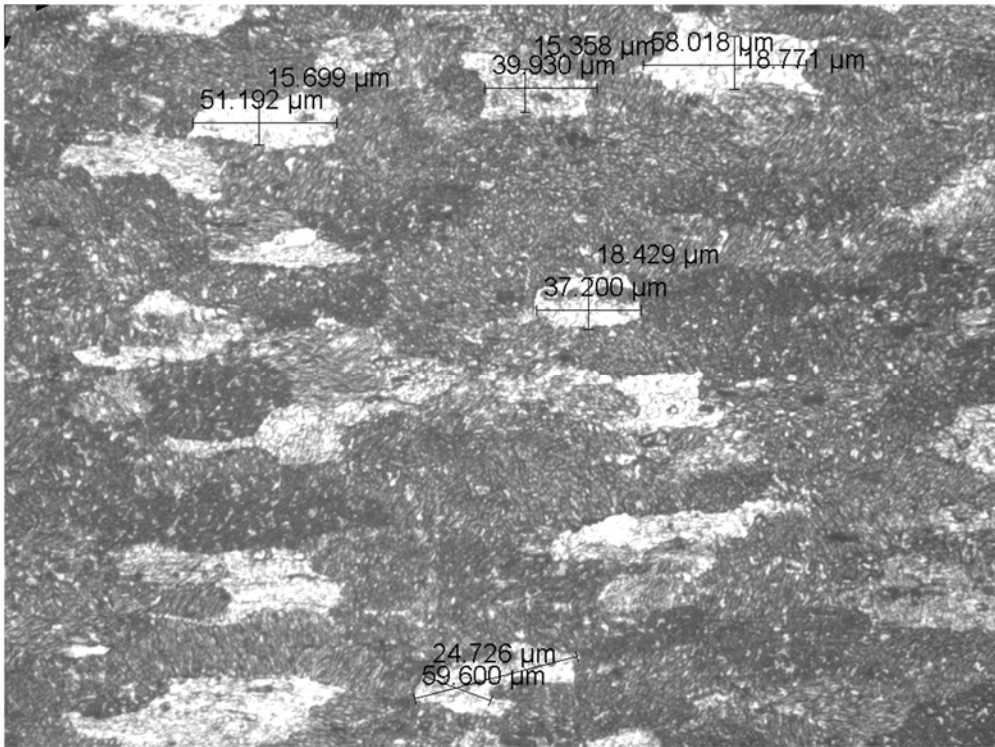


Figure C10b: Microstructure of PM Al indicating the grain measurements (x400)

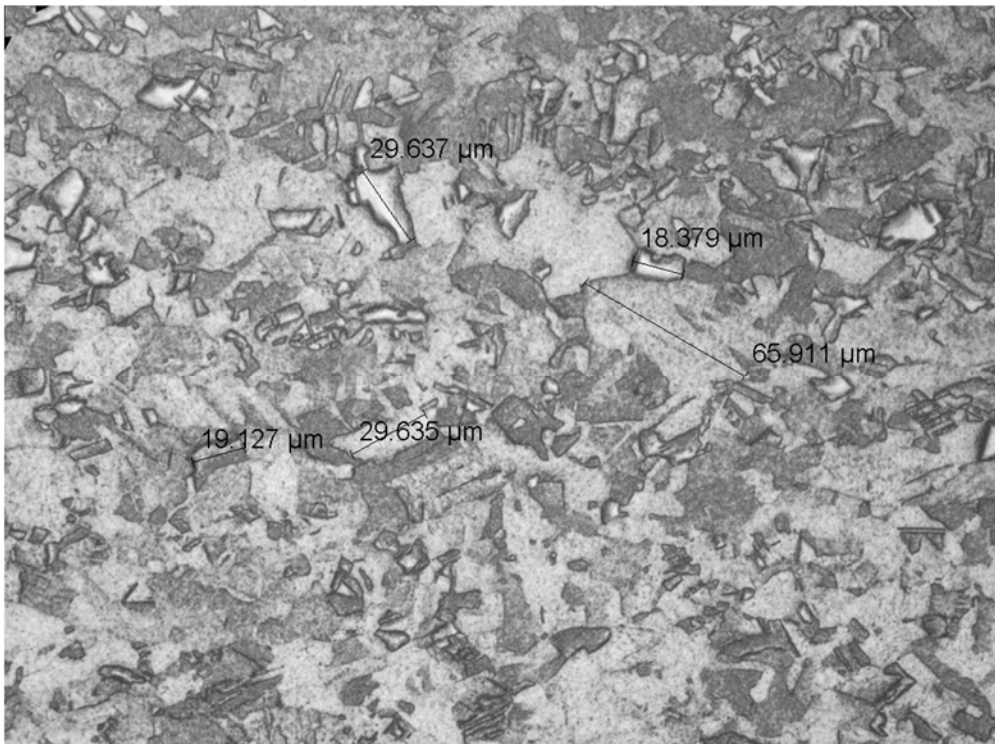


Figure C10c: Microstructure of PM Cu indicating the grain measurements (x400)

## C11. Microhardness profiles

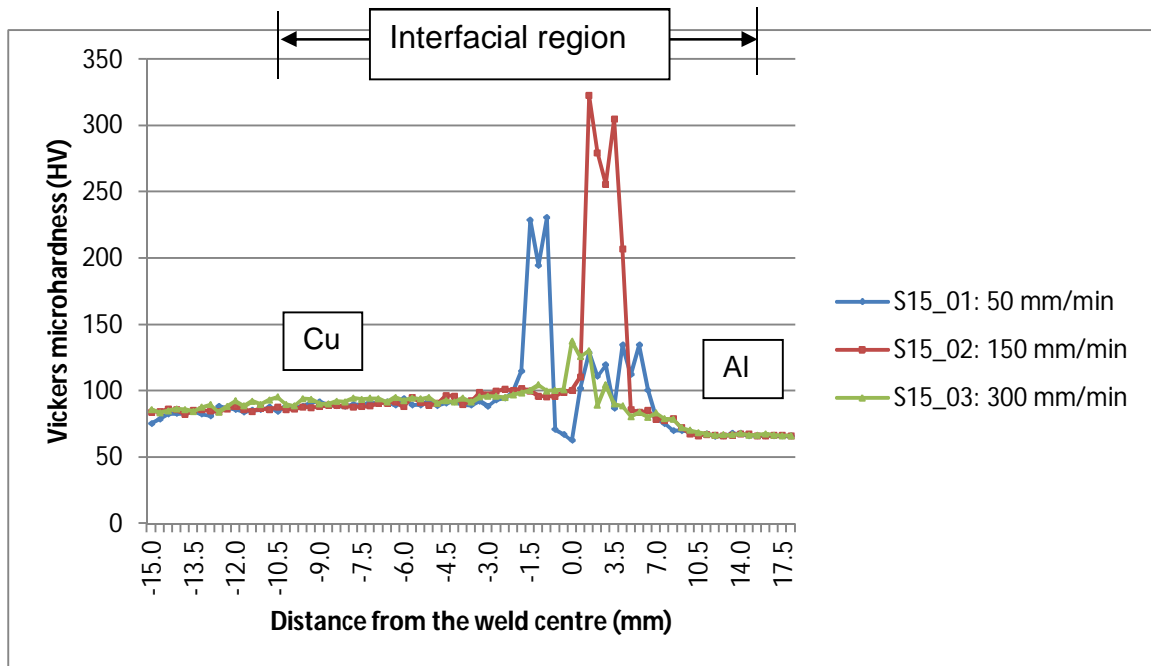


Figure C11a: Microhardness profiles of welds produced at a constant rotational speed of 600 rpm with the 15 mm shoulder diameter tool

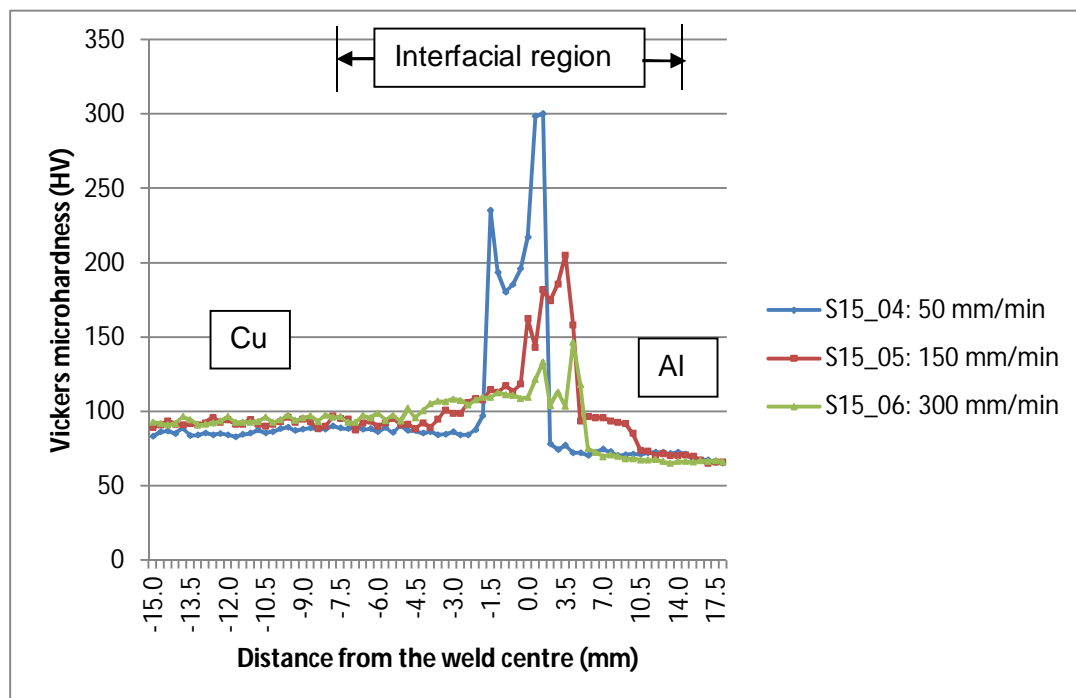


Figure C11b: Microhardness profiles of welds produced at a constant rotational speed of 950 rpm with the 15 mm shoulder diameter tool.

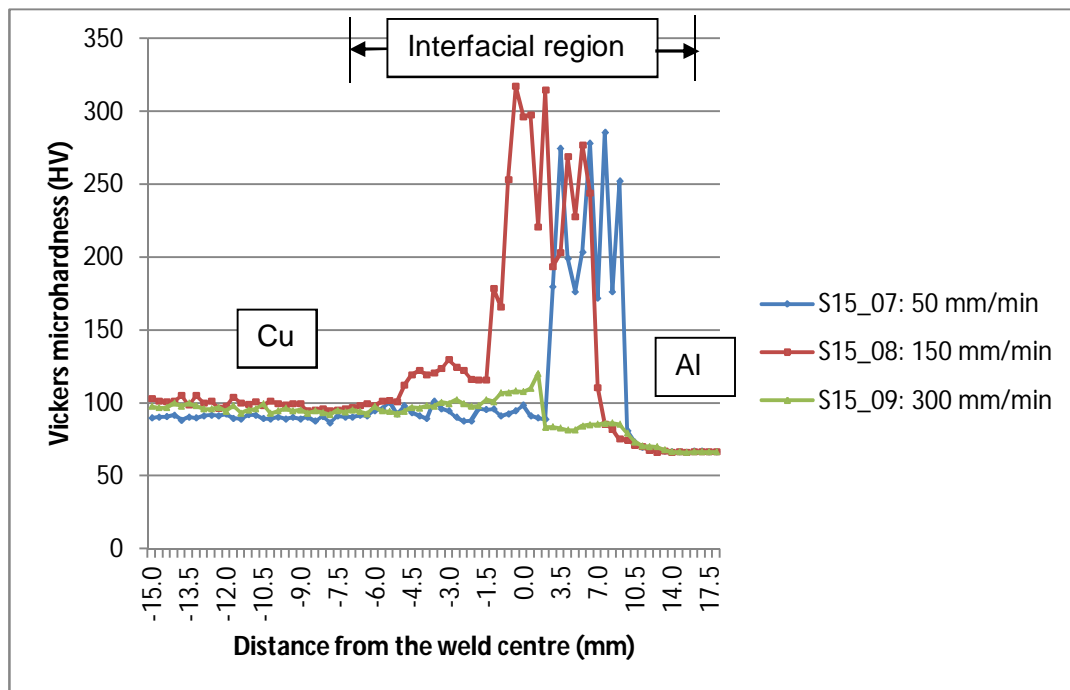


Figure C11c: Microhardness profiles of welds produced at a constant rotational speed of 1200 rpm with the 15 mm shoulder diameter tool.

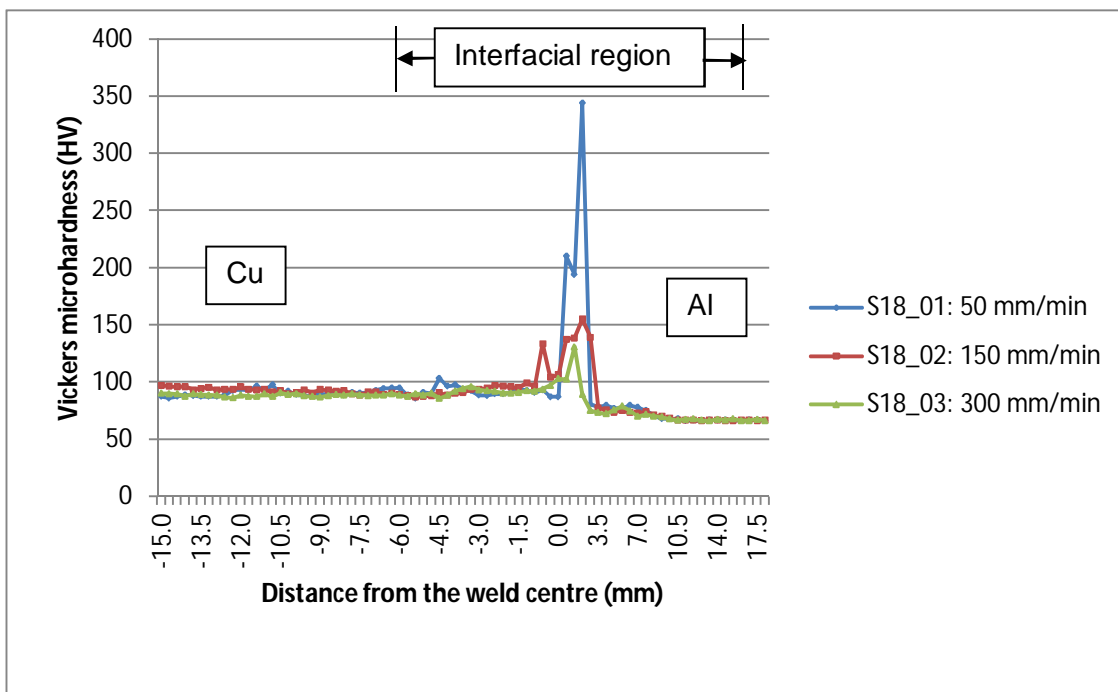


Figure C11d: Microhardness profiles of welds produced at a constant rotational speed of 600 rpm with the 18 mm shoulder diameter tool.

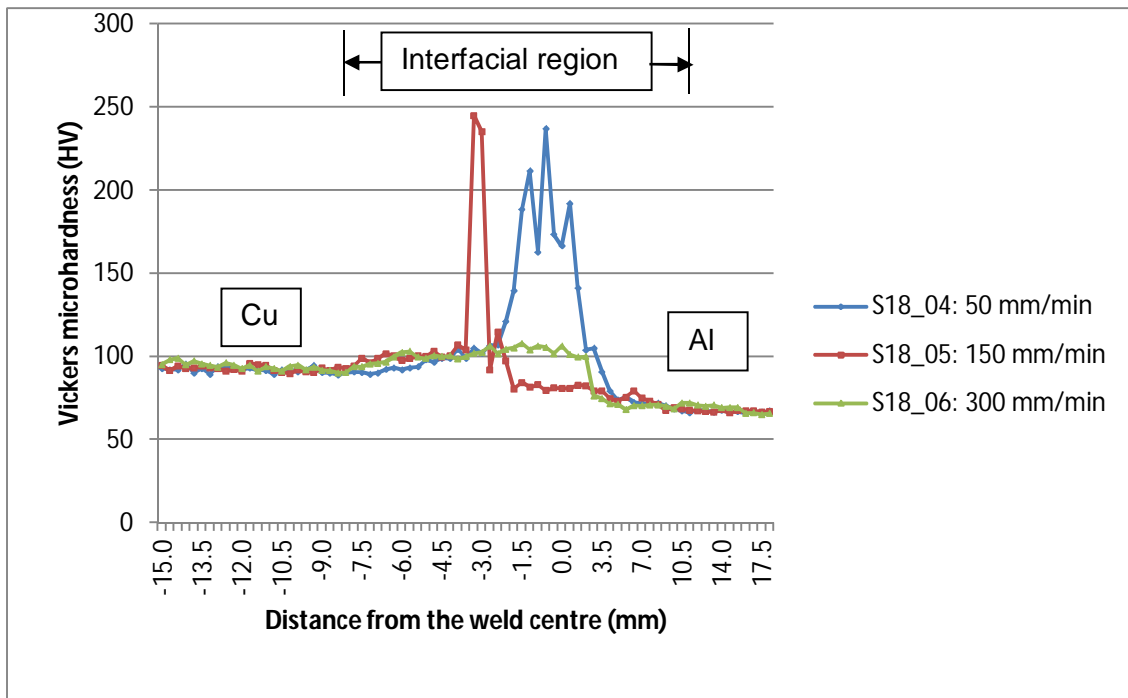


Figure C11e: Microhardness profiles of welds produced at a constant rotational speed of 950 rpm with the 18 mm shoulder diameter tool

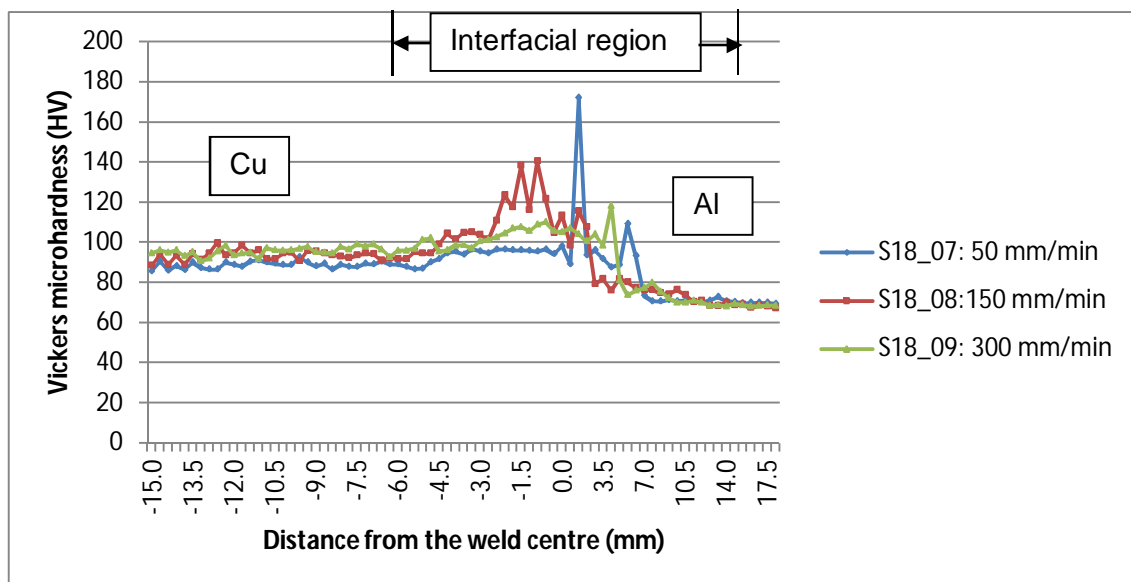


Figure C11f: Microhardness profiles of welds produced at a constant rotational speed of 1200 rpm with the 18 mm shoulder diameter tool

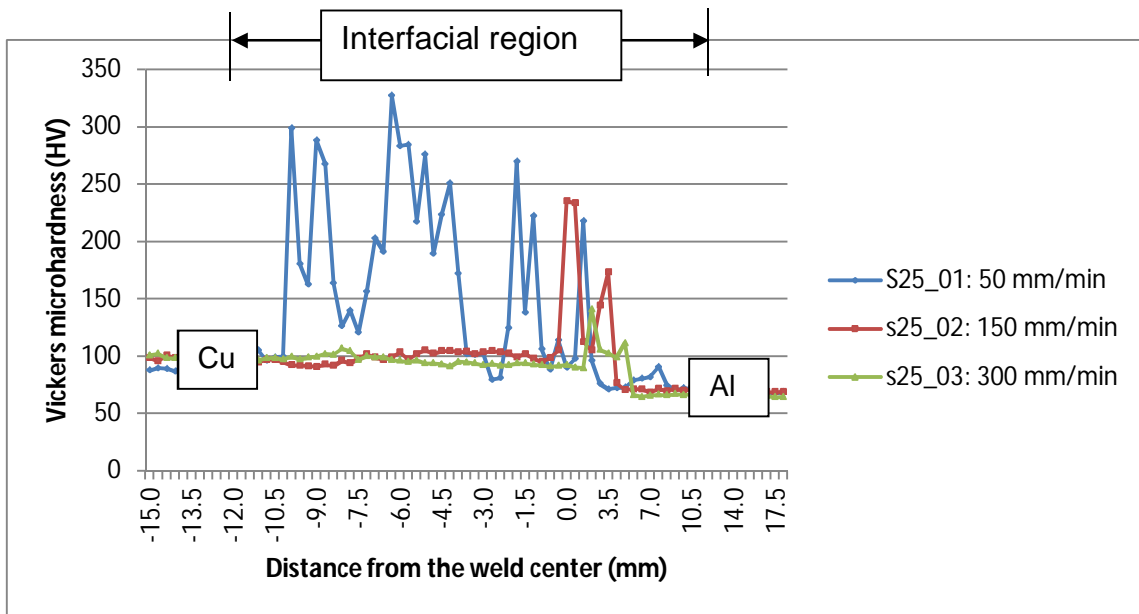


Figure C11g: Microhardness profiles of welds produced at a constant rotational speed of 600 rpm with the 25 mm shoulder diameter tool

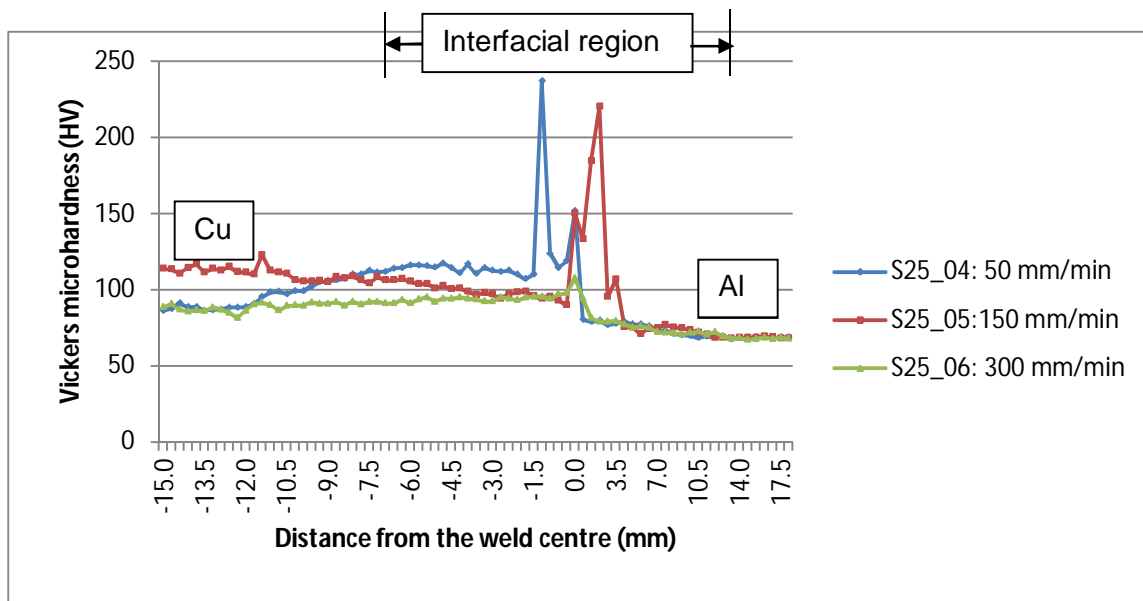


Figure C11h: Microhardness profiles of welds produced at a constant rotational speed of 950 rpm with the 25 mm shoulder diameter tool

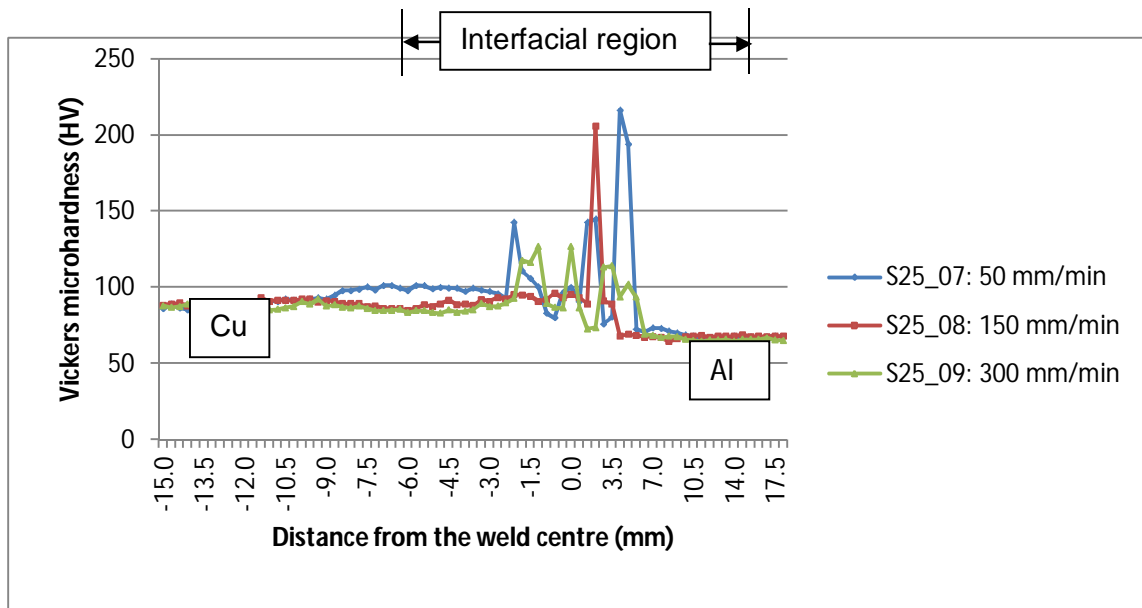


Figure C11i: Microhardness profiles of welds produced at a constant rotational speed of 1200 rpm with the 25 mm shoulder diameter tool.

**C12. Data Files for intermetallic compounds of Al-Cu.**

\*data for ICSD #1625

Copyright ©2004 by Fachinformationszentrum Karlsruhe, and the U.S. Secretary of Commerce on behalf of the United States. All rights reserved.

Coll Code 1625

Rec Date 1980/01/01

Mod Date 1999/11/30

Chem Name Aluminium Copper (4/9) - Gamma

Structured Cu<sub>9</sub>Al<sub>4</sub>

Sum Al<sub>4</sub> Cu<sub>9</sub>

ANX N4O9

D(calc) 6.84

Title Crystal perfection in a non-centrosymmetric alloy. Refinement and test of twinning of the gamma-Cu<sub>9</sub>Al<sub>4</sub> structure

Author(s) Arnberg, L.; Westman, S.

Reference Acta Crystallographica A (24,1968-38,1982)  
(1978), 34, 399-404

Unit Cell 8.7068(3) 8.7068(3) 8.7068(3) 90. 90. 90.

Vol 660.05

Z 4

Space Group P -4 3 m

SG Number 215

Cryst Sys cubic

Pearson cP52

Wyckoff i2 g f e4

R Value 0.024

Red Cell P 8.706 8.706 8.706 90 90 90 660.048

Trans Red 1.000 0.000 0.000 / 0.000 1.000 0.000 / 0.000 0.000 1.000

Comments xy(Cu<sub>6</sub>) was given as 0 0, PDF 24-3

The structure has been assigned a PDF number: 24-3

At least one temperature factor is implausible or meaningless but agrees with the value given in the paper.

The coordinates given in the paper contain an error. The

values in the database have been corrected.

Atom #	OX	SITE	x	y	z	SOF	H
Al 1	+0	4 e	0.1157(6)	0.1157(6)	0.1157(6)	1.	0
Cu 1	+0	4 e	-.1704(4)	-.1704(4)	-.1704(4)	1.	0
Cu 2	+0	6 f	0	0	0.3553(5)	1.	0
Cu 3	+0	12 i	0.3153(2)	0.3153(2)	0.0322(3)	1.	0
Cu 4	+0	4 e	0.6066(3)	0.6066(3)	0.6066(3)	1.	0
Cu 5	+0	4 e	0.3253(4)	0.3253(4)	0.3253(4)	1.	0
Cu 6	+0	6 g	0.5	0.5	0.8549(5)	1.	0
Al 2	+0	12 i	0.8113(4)	0.8113(4)	0.5332(6)	1.	0

Lbl	Type	Beta11	Beta22	Beta33	Beta12	Beta13	Beta23
Al1	Al0+	0.0019(4)	0.0019(4)	0.0019(4)	0.0008(7)	0.0008(7)	0.0008(7)
Cu1	Cu0+	0.0022(2)	0.0022(2)	0.0022(2)	0.0005(3)	0.0005(3)	0.0005(3)
Cu2	Cu0+	0.0023(3)	0.0023(3)	0.0025(6)	0.0006(5)	0	0
Cu3	Cu0+	0.0041(3)	0	0.0032(5)	-.0004(3)	-.0010(2)	0
Cu4	Cu0+	0.0044(3)	0.0044(3)	0.0044(3)	0.0014(4)	0.0014(4)	0.0014(4)
Cu5	Cu0+	0.0023(2)	0.0023(2)	0.0023(2)	0.0000(3)	0.0000(3)	0.0000(3)
Cu6	Cu0+	0.0035(3)	0.0035(3)	0.0013(6)	0.0008(5)	0	0
Al2	Al0+	0.0032(5)	0	0.0020(9)	0.0004(6)	-.0001(4)	0

\*end for ICSD #1625

\*data for ICSD #40332

Copyright ©2004 by Fachinformationszentrum Karlsruhe, and the U.S. Secretary of Commerce on behalf of the United States. All rights reserved.

Coll Code 40332

Rec Date 1999/11/30

Mod Date 2003/04/01

Chem Name Aluminum Copper (1/1)

Structured Al Cu

Sum Al1 Cu1

ANX NO

Min Name Cupalite

D(calc) 5.36

Title Crystal structure of Cu<sub>3</sub>Al<sub>2</sub>+ (h) and Cu Al (r)

Author(s) El-Boragy, M.;Szepan, R.;Schubert, K.

Reference Journal of the Less-Common Metals  
(1972), 29, 133-140

ZapiskiVsesoyuznogoMineralogicheskogoObshchestva  
(1985), 114, 90-100

Unit Cell 9.889 4.105 6.913 90. 89.996 90.

Vol 280.63

Z 10

Space Group I 1 2/m 1

SG Number 12

Cryst Sys monoclinic

Pearson mS20

Wyckoff i4 c a

R Value 0.19

Red Cell I 4.105 6.372 6.372 65.696 71.211 71.210 140.314

Trans Red 0.000 -1.000 0.000 / 0.500 -0.500 -0.500 / 0.500 -0.500 0.500

Comments Transformed from C2/m with a=12.055, beta=55.04 grd  
PDF 39-1371, 88-1713

Mineral from Khatyr massif, Koryakmts., Kamchatka, Russia,  
(2nd ref., Razin et al., with 12 at% Zn for Cu) has  
c=10.04, b=4.16, a=6.95, D=5.12, CsCl-type with vacancies

Stable below 833 K

Compound with mineral name: Cupalite

The structure has been assigned a PDF number: 39-1371

Calculated density unusual but tolerable.

At least one temperature factor missing in the paper.

Atom #	OX	SITE	x	y	z	SOF	H
Cu 1	+0	2 a	0	0	1.	0	
Cu 2	+0	4 i	0.256	0	0.016	1.	0
Cu 3	+0	4 i	0.109	0	0.337	1.	0
Al 1	+0	2 c	0	0.5	0.5	1.	0

---

Al 2 +0 4 i 0.155 0 0.698 1. 0  
Al 3 +0 4 i 0.382 0 0.395 1. 0  
\*end for ICSD #40332

\*data for ICSD #42517

CopyRight ©2004 by Fachinformationszentrum Karlsruhe, and the U.S. Secretary of  
Commerce on behalf of the United States. All rights reserved.

Coll Code 42517

Rec Date 2000/07/15

Mod Date 2003/04/01

Chem Name Aluminium Copper (2/1)

Structured Al<sub>2</sub> Cu

Sum Al<sub>2</sub> Cu<sub>1</sub>

ANX NO<sub>2</sub>

Min Name Khatyrkite

D(calc) 4.35

Title Refinement of the crystal structure of tetragonal Al<sub>2</sub> Cu

Author(s) Meetsma, A.; de Boer, J.L.; vanSmaalen, S.

Reference Journal of Solid State Chemistry  
(1989), 83, 370-372

Unit Cell 6.067(1) 6.067(1) 4.877(1) 90. 90. 90.

Vol 179.52

Z 4

Space Group I 4/m c m

SG Number 140

Cryst Sys tetragonal

Pearson tI12

Wyckoff h a

R Value 0.032

Red Cell I 4.877 4.934 4.934 75.865 60.385 60.385 89.757

Trans Red 0.000 0.000 1.000 / -0.500 -0.500 0.500 / 0.500 -0.500 0.500

Comments Compound with mineral name: Khatyrkite

The structure has been assigned a PDF number: 25-12

Atom #	OX	SITE	x	y	z	SOF	H
Al 1	+0	8 h	0.1581(6)	0.6581(6)	0	1.	0
Cu 1	+0	4 a	0	0	0.25	1.	0

\*end for ICSD #42517

\*data for ICSD #57667

Copyright ©2004 by Fachinformationszentrum Karlsruhe, and the U.S. Secretary of Commerce on behalf of the United States. All rights reserved.

Coll Code 57667

Rec Date 2003/10/01

Chem Name Aluminium Copper (2/3.4) - Epsilon

Structured Al<sub>2</sub> Cu<sub>3.4</sub>

Sum Al<sub>2</sub> Cu<sub>3.4</sub>

ANX N<sub>2</sub>O<sub>3</sub>

D(calc) 5.95

Title Kristallstruktur von Cu Al<sub>3</sub> (h) und Cu Al (r)

Author(s) El-Boragy, M.;Szepan, R.;Schubert, K.

Reference Journal of the Less-Common Metals  
(1972), 29, 133-140

Unit Cell 4.146(1) 4.146 5.063(3) 90. 90. 120.

Vol 75.37

Z 1

Space Group P 63/m m c

SG Number 194

Cryst Sys hexagonal

Pearson hP5

Wyckoff d c a

Red Cell P 4.146 4.146 5.063 90 90 120 75.37

Trans Red 1.000 0.000 0.000 / 0.000 1.000 0.000 / 0.000 0.000 1.000

Comments Total SOF on at least one site differs from unity (SOF < 0.997 resp. SOF > 1.003)

The structure has been assigned a PDF number: 26-15

Temperature in Kelvin: 903

X-ray diffraction (powder)

No R value given in the paper.

At least one temperature factor missing in the paper.

Atom #	OX	SITE	x	y	z	SOF	H
Al 1	+0	2 c	0.3333	0.6667	0.25	1.	0
Cu 1	+0	2 a	0	0	0	1.	0
Cu 2	+0	2 d	0.3333	0.6667	0.75	0.7	0

\*end for ICSD #57667

\*data for ICSD #57668

CopyRight ©2004 by Fachinformationszentrum Karlsruhe, and the U.S. Secretary of Commerce on behalf of the United States. All rights reserved.

Coll Code 57668

Rec Date 2003/10/01

Chem Name Aluminium Copper (3/2)

Structured Al<sub>3</sub> Cu<sub>2</sub>

Sum Al<sub>3</sub> Cu<sub>2</sub>

ANX N<sub>2</sub>O<sub>3</sub>

D(calc) 4.64

Title A metastable phase Al<sub>3</sub> Cu<sub>2</sub>

Author(s) Ramachandrarao, P.;Laridjani, M.

Reference Journal of Materials Science

(1974), 9, 434-437

Unit Cell 4.106(1) 4.106 5.094(3) 90. 90. 120.

Vol 74.38

Z 1

Space Group P -3 m 1

SG Number 164

Cryst Sys trigonal/rhombohedral

Pearson hP5

Wyckoff d2 a

Red Cell P 4.106 4.106 5.094 90 90 120 74.375

Trans Red 1.000 0.000 0.000 / 0.000 1.000 0.000 / 0.000 0.000 1.000

Comments Metastable, splat quenched

X-ray diffraction (powder)

No R value given in the paper.

Atom #	OX	SITE	x	y	z	SOF	H
Al 1	+0	1 a	0	0	0	1.	0
Al 2	+0	2 d	0.3333	0.6667	0.352	1.	0
Cu 2	+0	2 d	0.3333	0.6667	0.851	1.	0

\*end for ICSD #57668

## C13. Diffractograms of Al-Cu joint interfaces

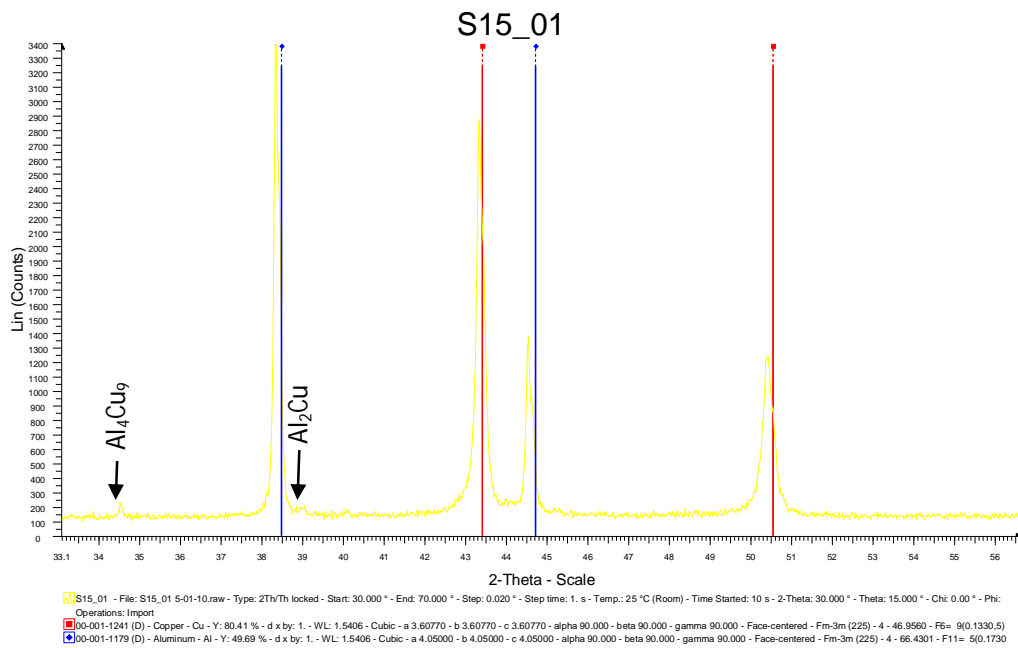


Figure C13i: PDF diffractogram of a weld produced with the 15 mm shoulder diameter tool at 600 rpm and 50 mm/min.

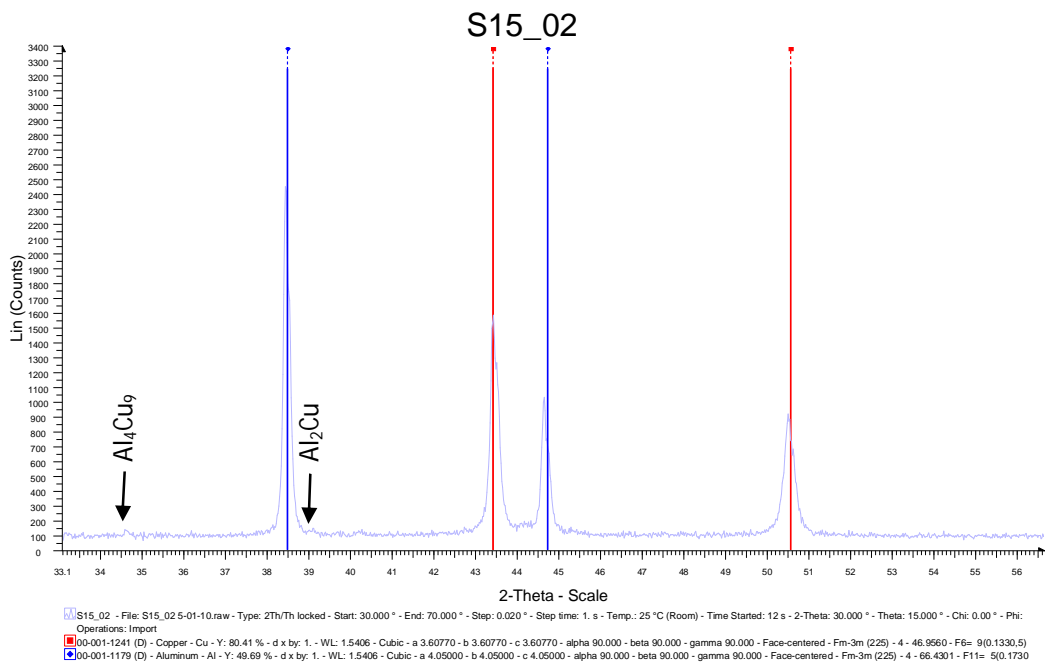


Figure C13ii: PDF diffractogram of a weld produced with the 15 mm shoulder diameter tool at 600 rpm and 150 mm/min.

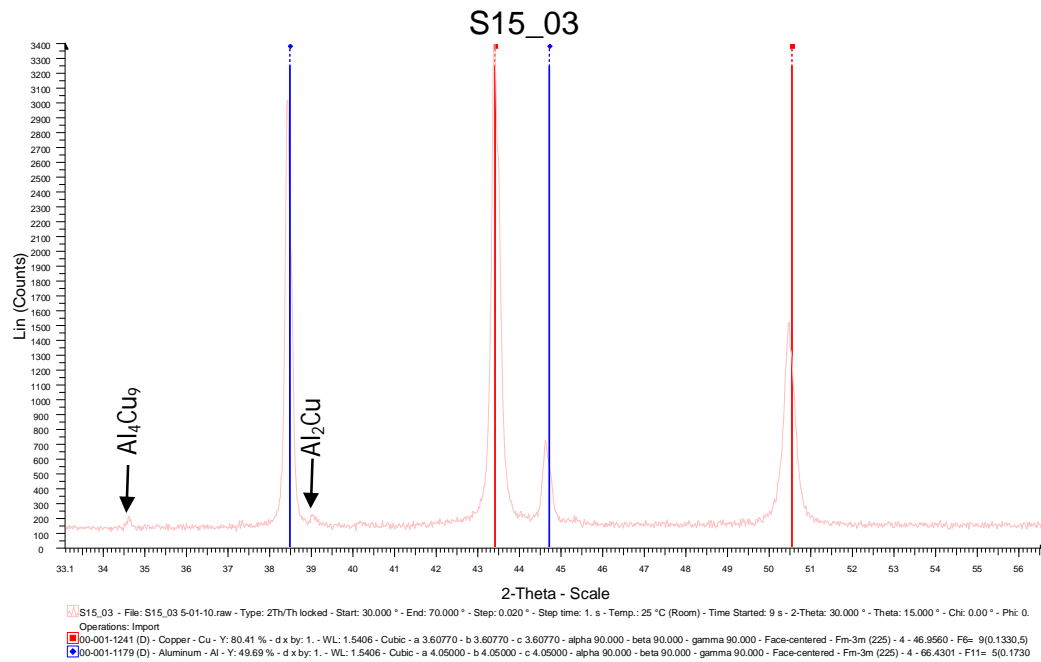


Figure C13iii: PDF diffractogram of a weld produced with the 15 mm shoulder diameter tool at 600 rpm and 300 mm/min.

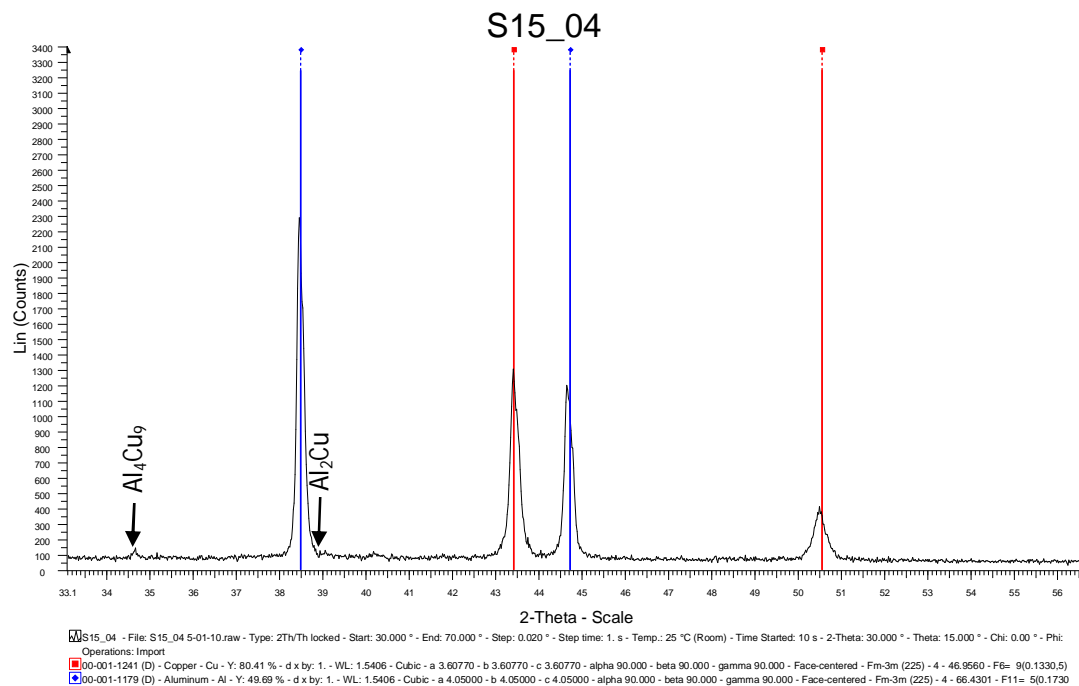


Figure C13iv: PDF diffractogram of a weld produced with the 15 mm shoulder diameter tool at 950 rpm and 50 mm/min.

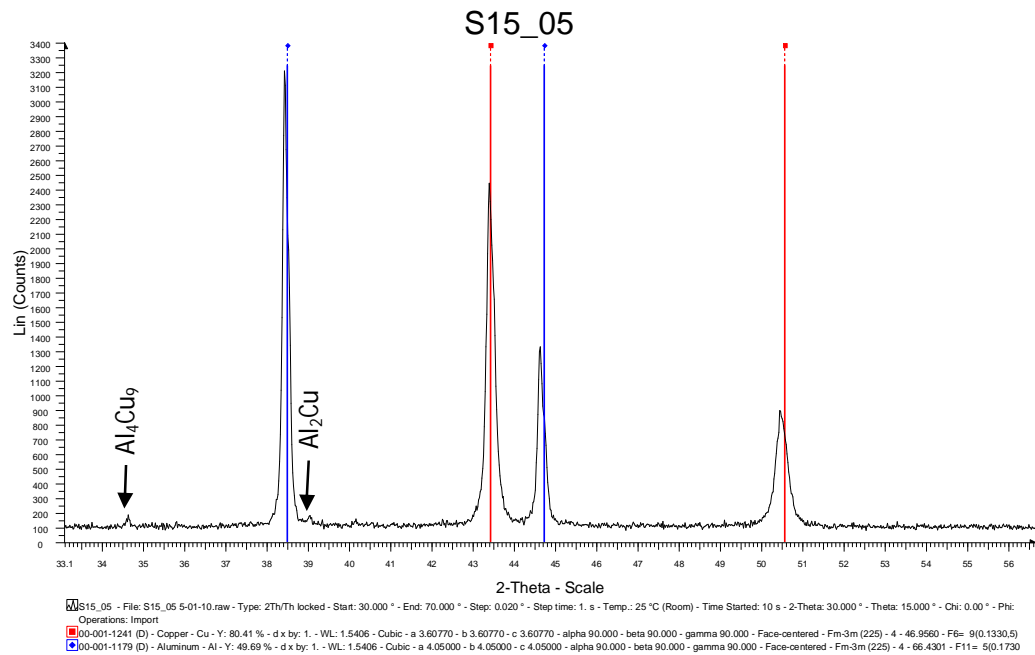


Figure C13v: PDF diffractogram of a weld produced with the 15 mm shoulder diameter tool at 950 rpm and 150 mm/min.

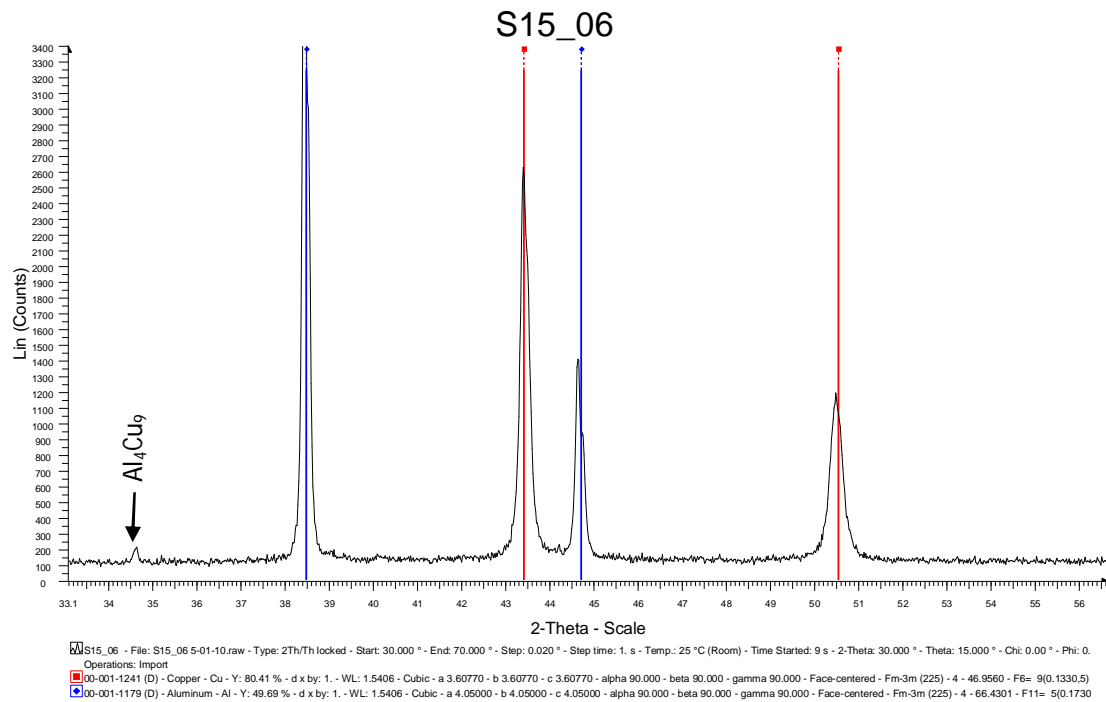


Figure C13vi: PDF diffractogram of a weld produced with the 15 mm shoulder diameter tool at 950 rpm and 300 mm/min.

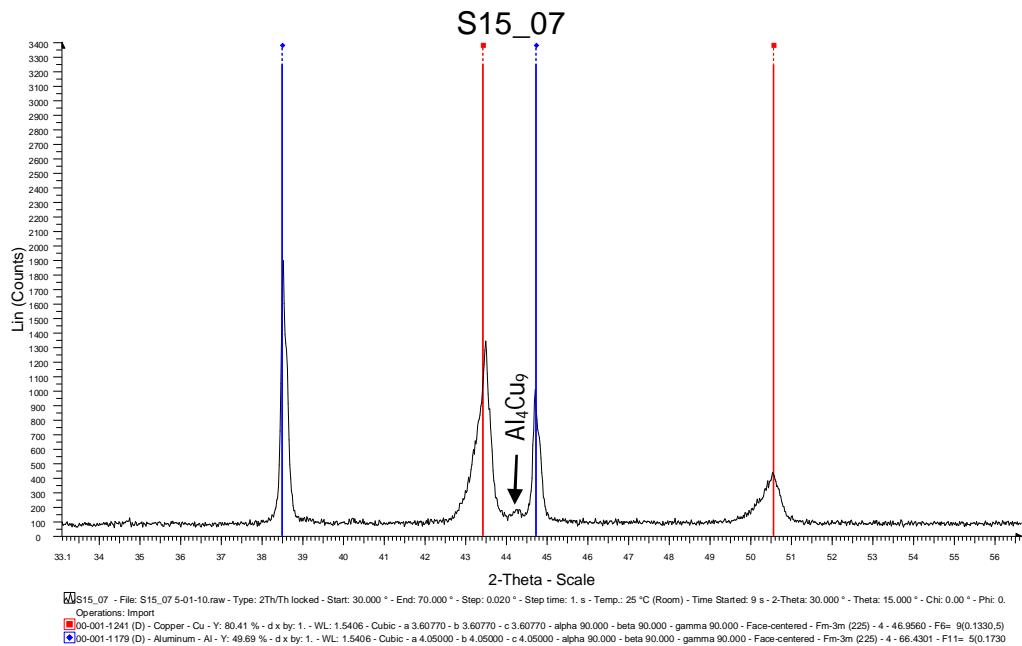


Figure C13vii: PDF diffractogram of a weld produced with the 15 mm shoulder diameter tool at 1200 rpm and 50 mm/min.

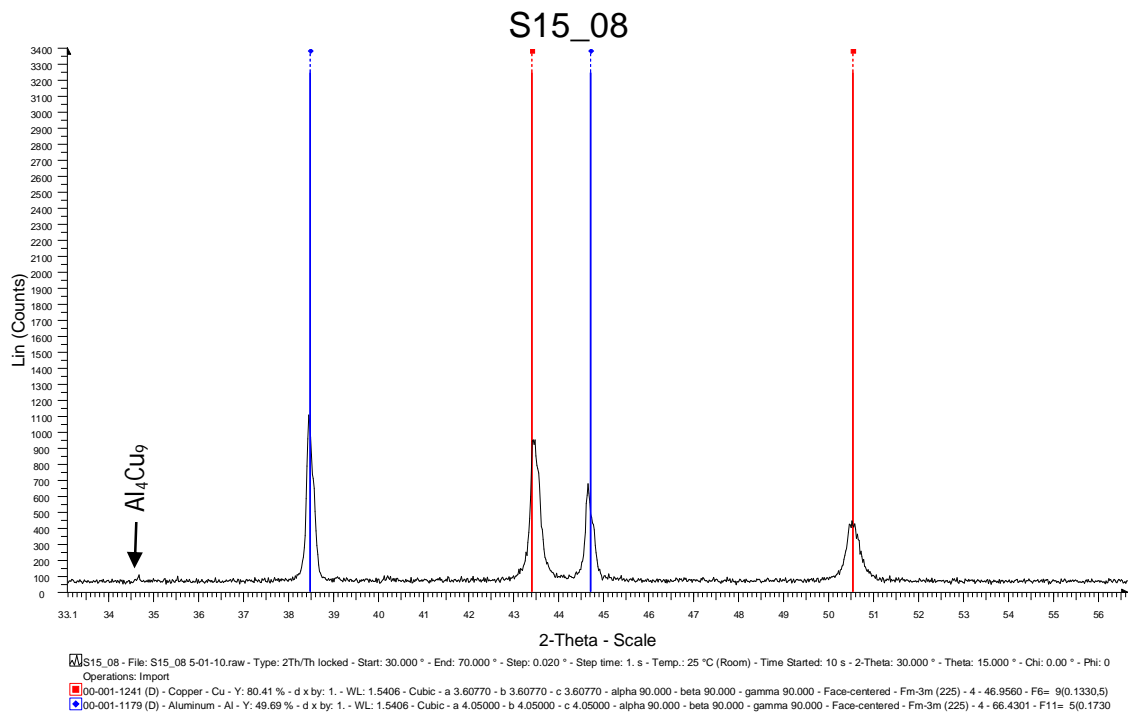


Figure C13viii: PDF diffractogram of a weld produced with the 15 mm shoulder diameter tool at 1200 rpm and 150 mm/min.

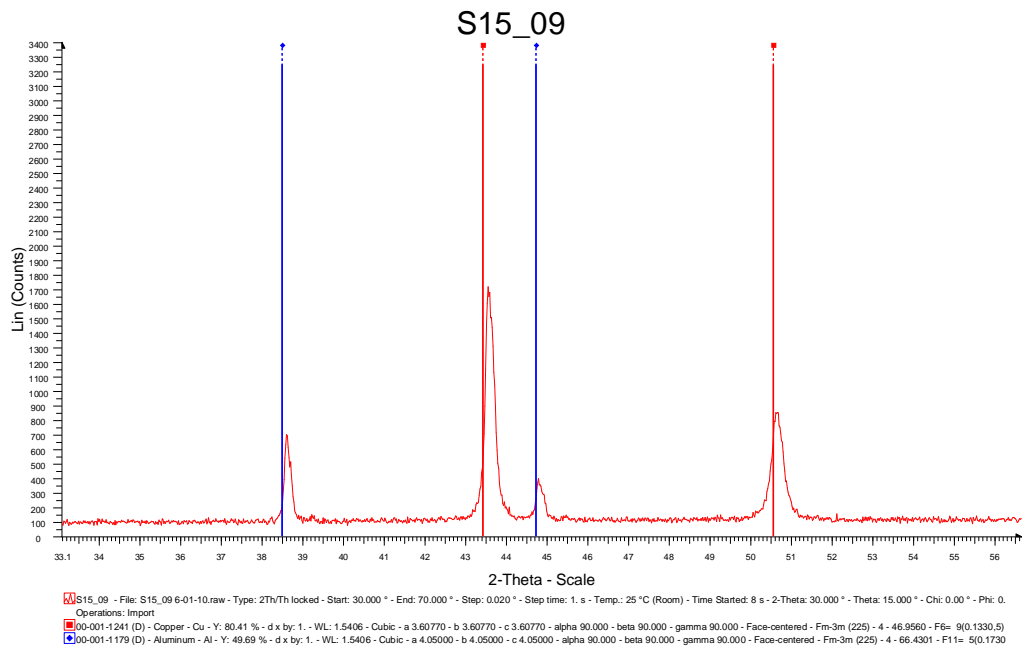


Figure C13ix: PDF diffractogram of a weld produced with the 15 mm shoulder diameter tool at 1200 rpm and 300 mm/min.

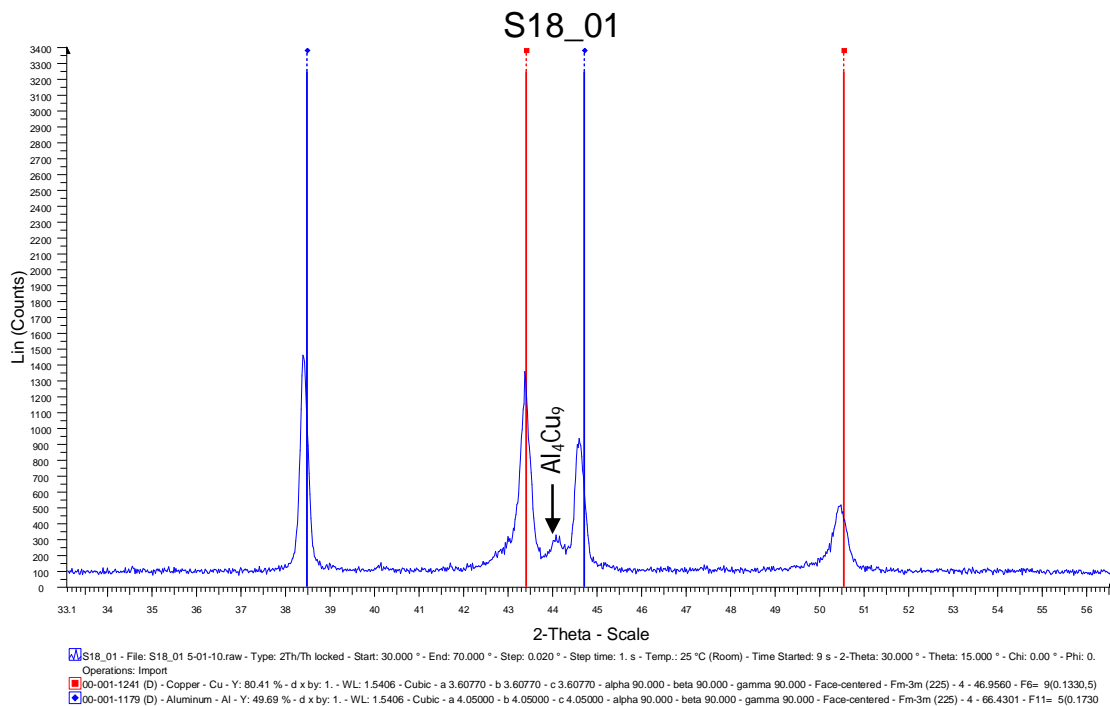


Figure C13x: PDF diffractogram of a weld produced with the 18 mm shoulder diameter tool at 600 rpm and 50 mm/min.

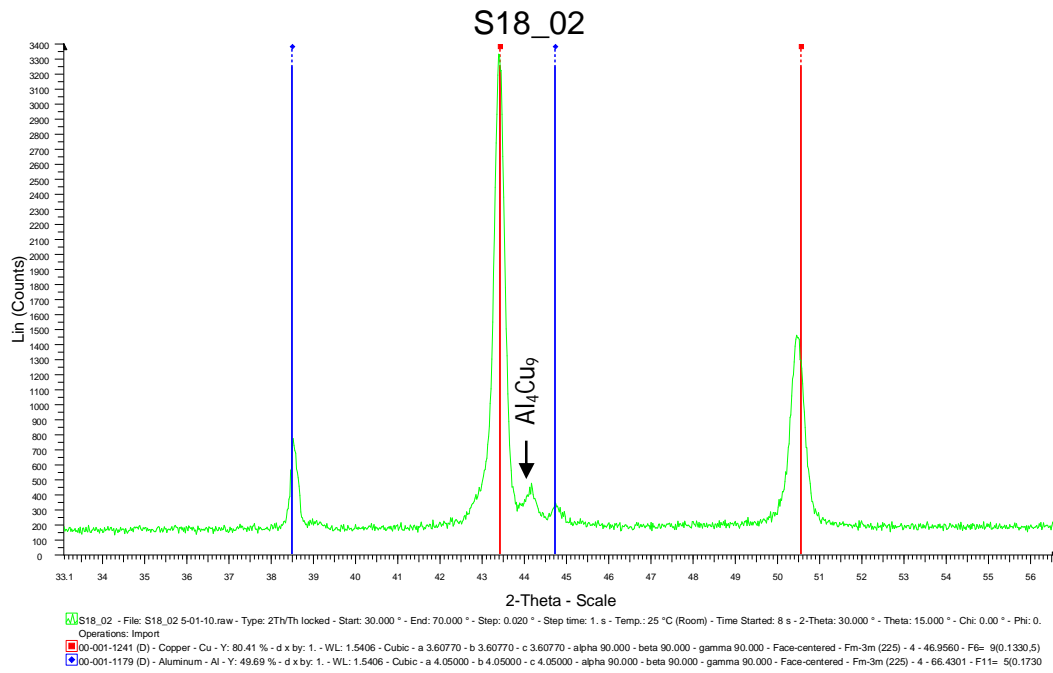


Figure C13xi: PDF diffractogram of a weld produced with the 18 mm shoulder diameter tool at 600 rpm and 150 mm/min.

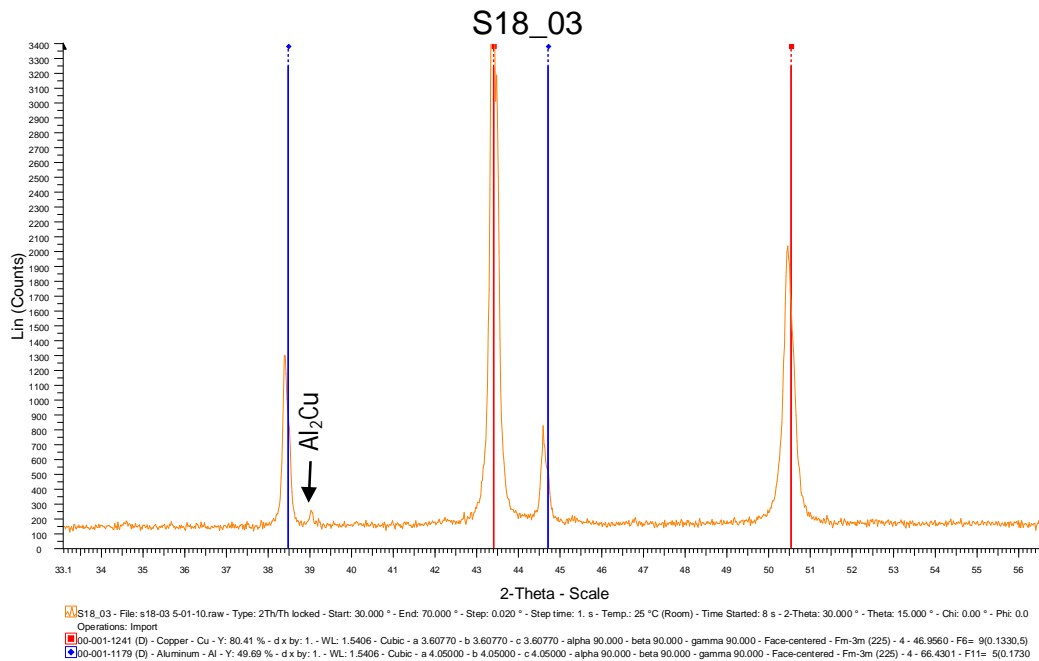


Figure C13xii: PDF diffractogram of a weld produced with the 18 mm shoulder diameter tool at 600 rpm and 300 mm/min.

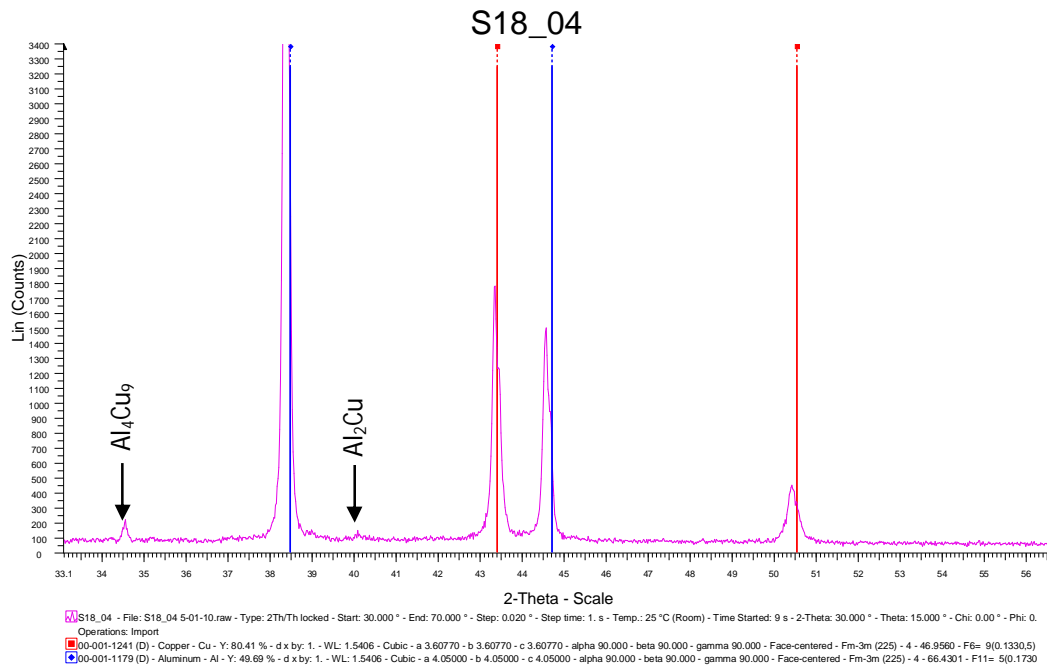


Figure C13xiii: PDF diffractogram of a weld produced with the 18 mm shoulder diameter tool at 950 rpm and 50 mm/min.

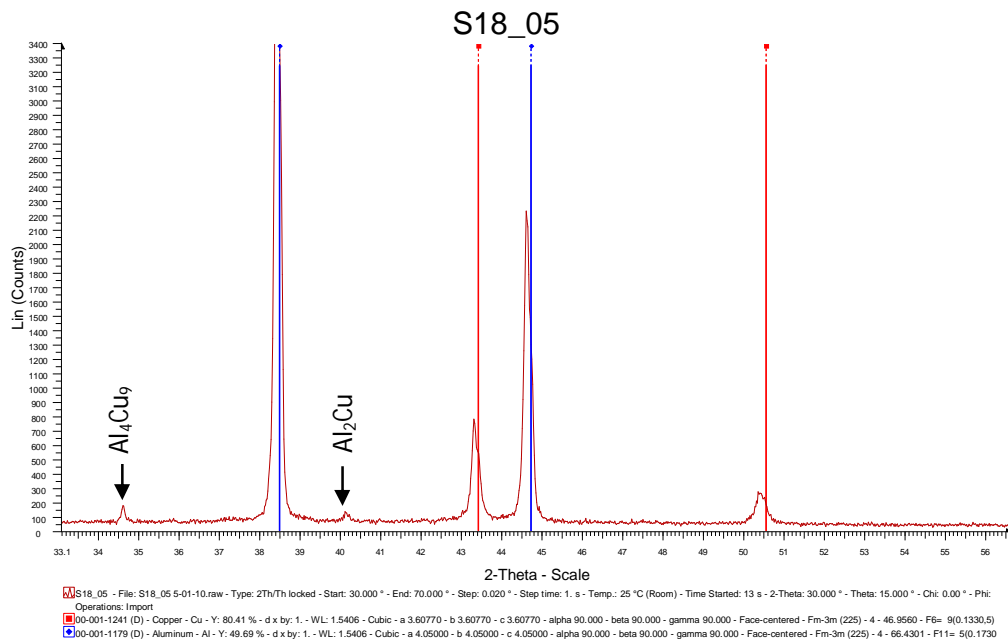


Figure C13xiv: PDF diffractogram of a weld produced with the 18 mm shoulder diameter tool at 950 rpm and 150 mm/min.

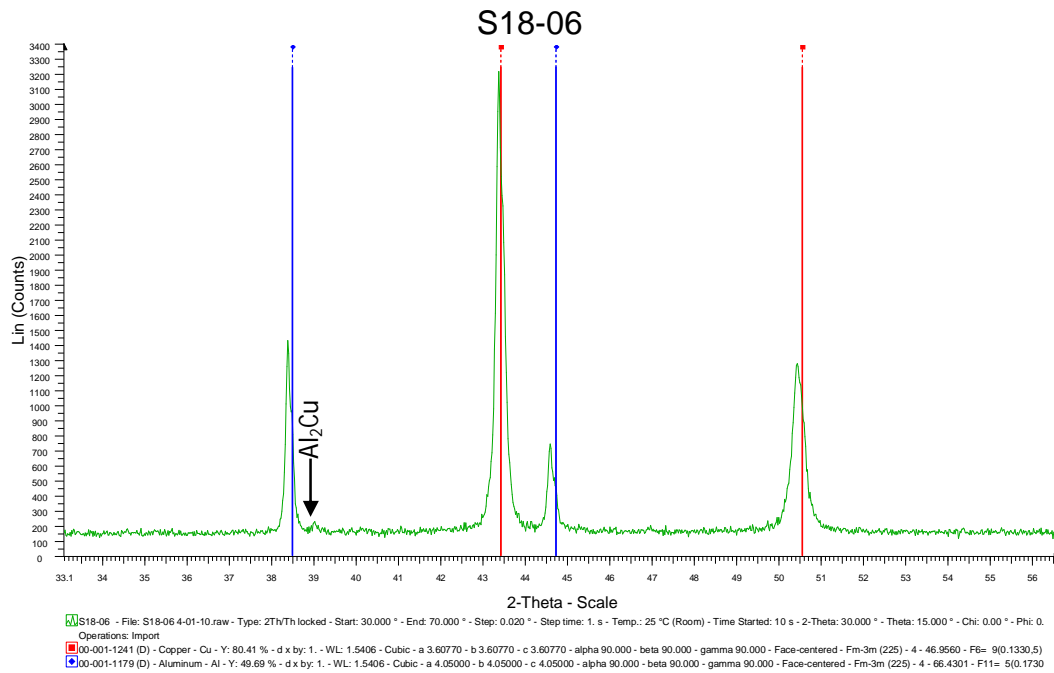


Figure C13xv: PDF diffractogram of a weld produced with the 18 mm shoulder diameter tool at 950 rpm and 300 mm/min.

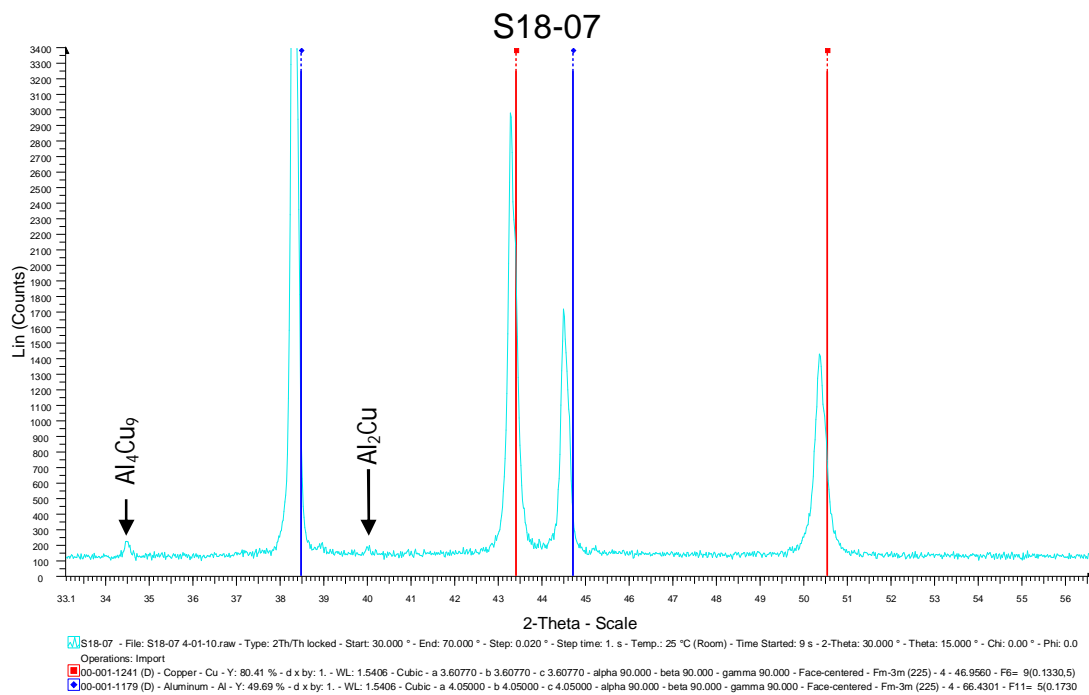


Figure C13xvi: PDF diffractogram of a weld produced with the 18 mm shoulder diameter tool at 1200 rpm and 50 mm/min.

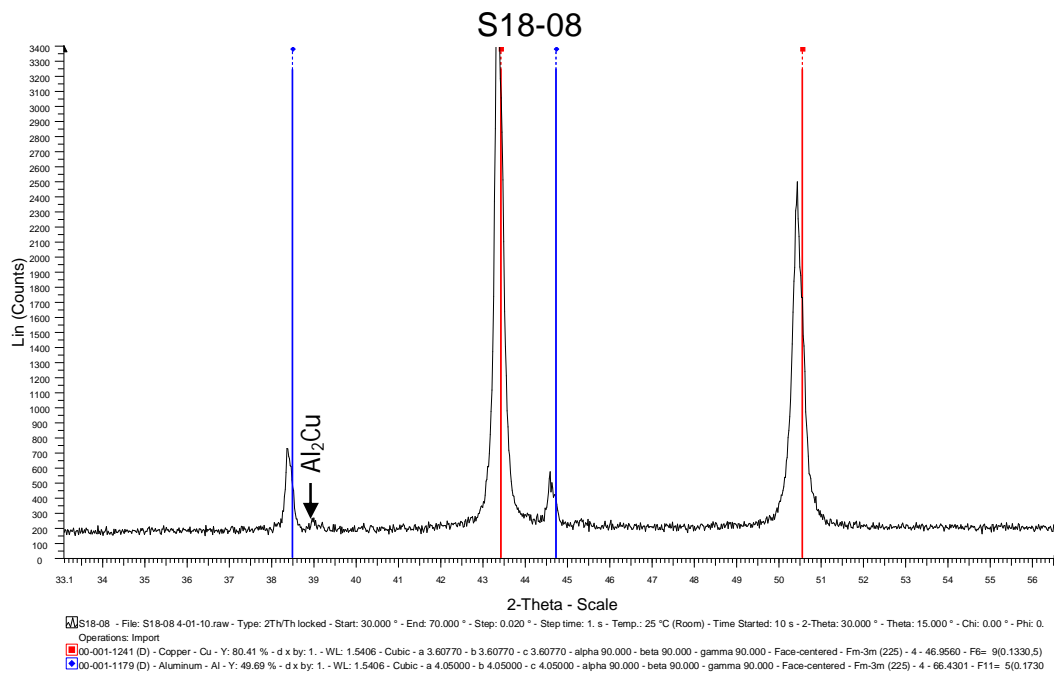


Figure C13xvii: PDF diffractogram of a weld produced with the 18 mm shoulder diameter tool at 1200 rpm and 150 mm/min.

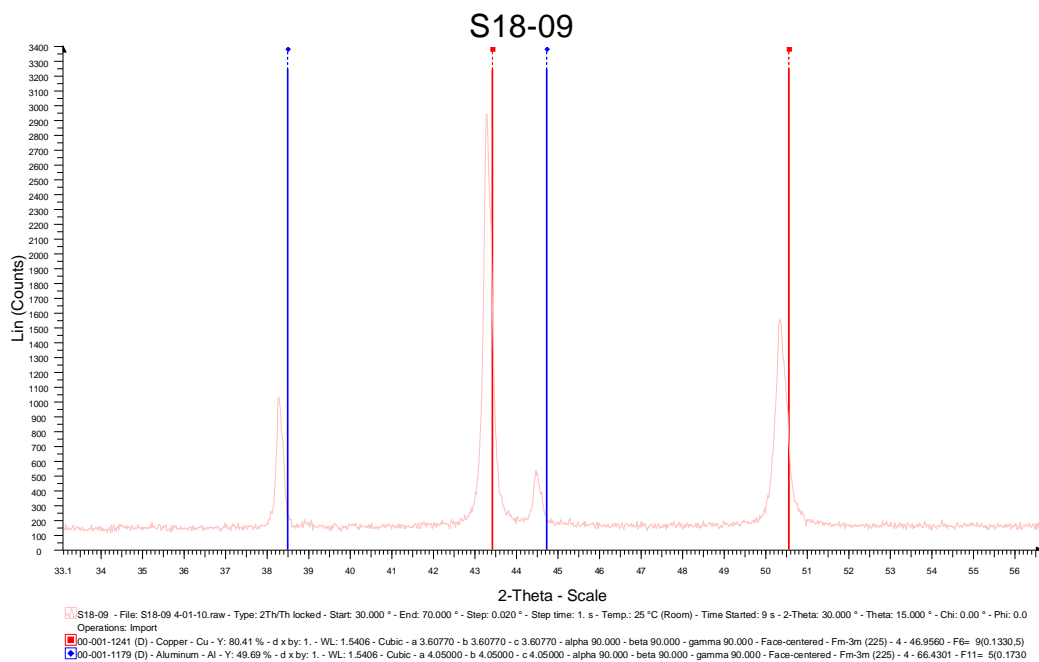


Figure C13xviii: PDF diffractogram of a weld produced with the 18 mm shoulder diameter tool at 1200 rpm and 300 mm/min.

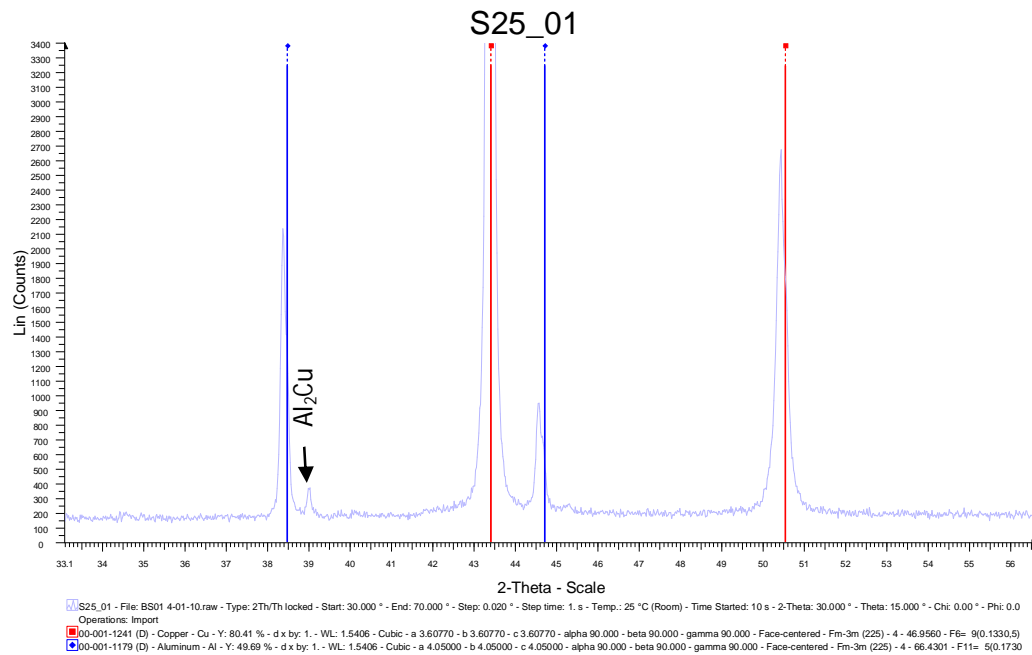


Figure C13xix: PDF diffractogram of a weld produced with the 25 mm shoulder diameter tool at 600 rpm and 50 mm/min.

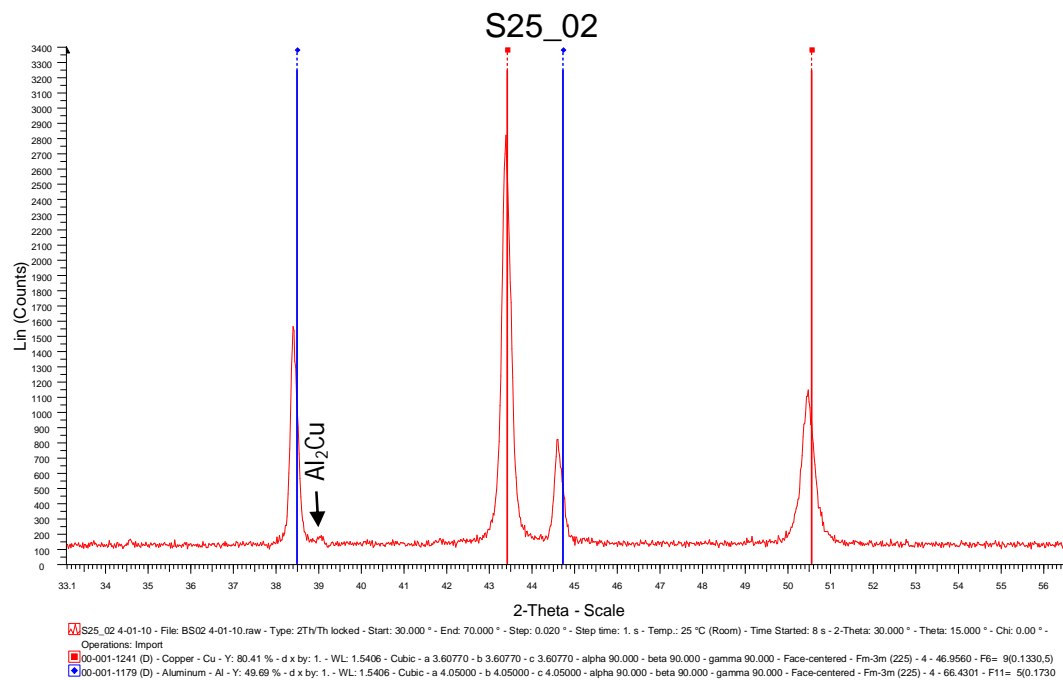


Figure C13xx: PDF diffractogram of a weld produced with the 25 mm shoulder diameter tool at 600 rpm and 150 mm/min.

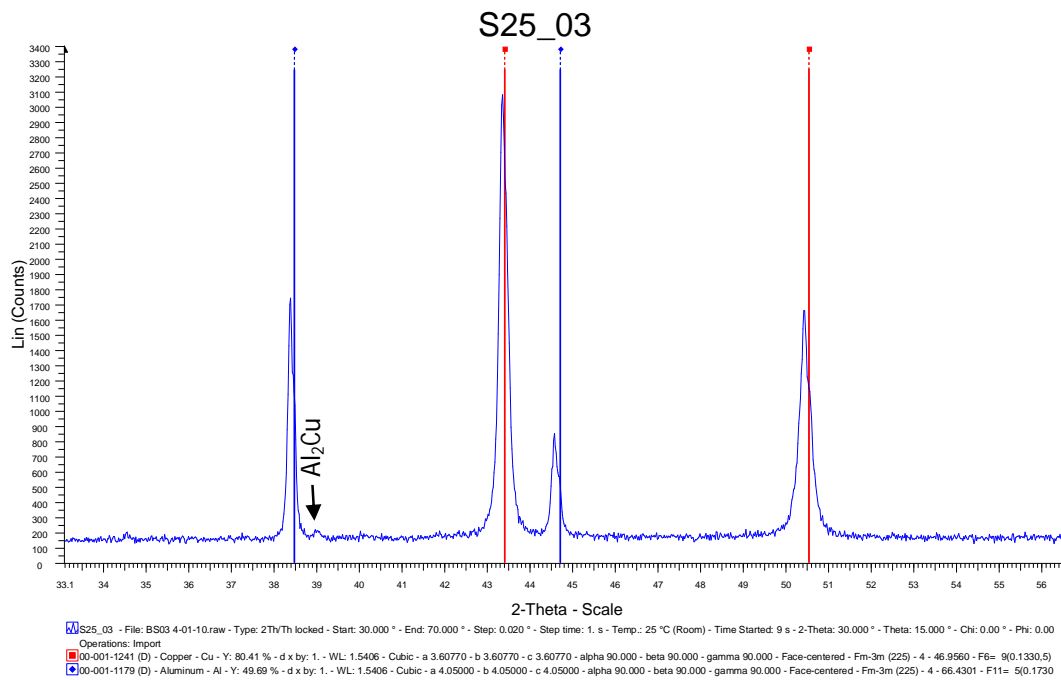


Figure C13xxi: PDF diffractogram of a weld produced with the 25 mm shoulder diameter tool at 600 rpm and 300 mm/min.

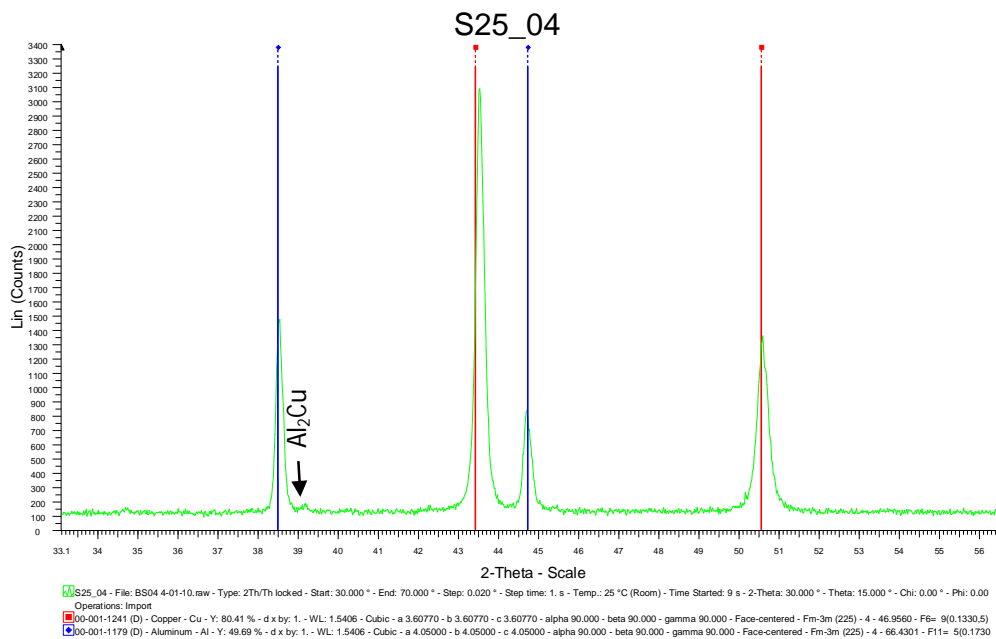


Figure C13xxii: PDF diffractogram of a weld produced with the 25 mm shoulder diameter tool at 950 rpm and 50 mm/min.

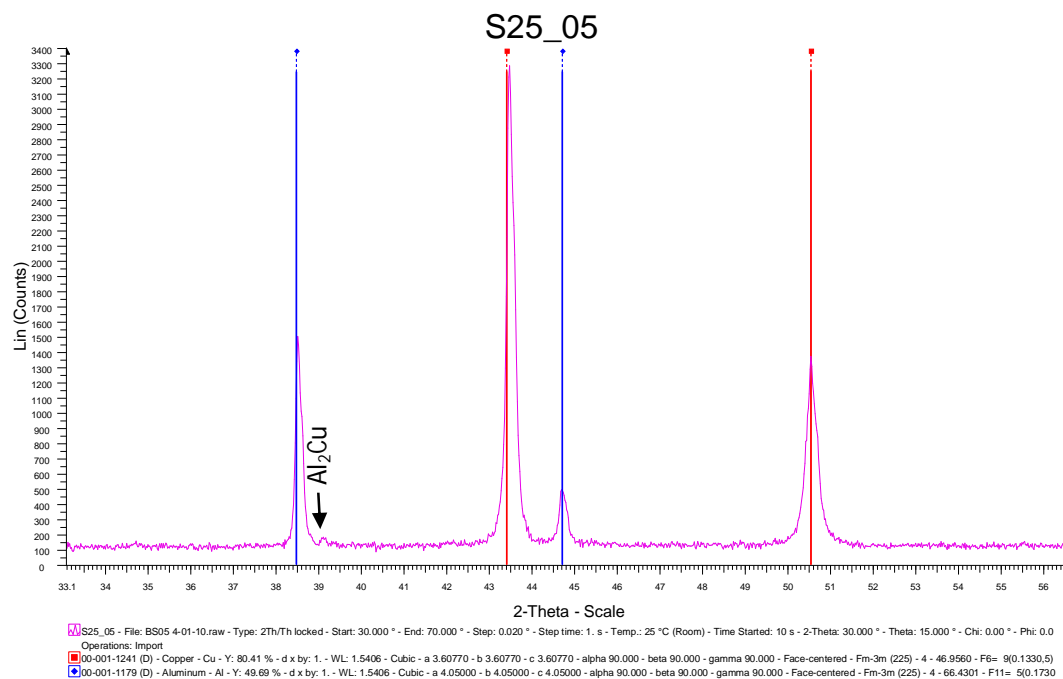


Figure C13xxiii: PDF diffractogram of a weld produced with the 25 mm shoulder diameter tool at 950 rpm and 150 mm/min.

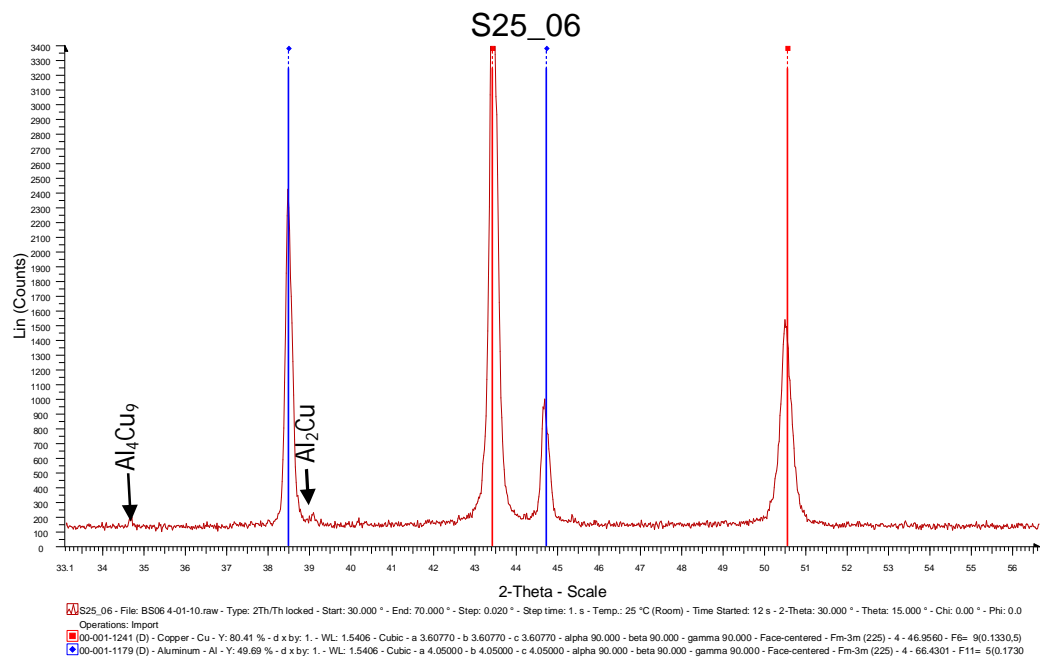


Figure C13xxiv: PDF diffractogram of a weld produced with the 25 mm shoulder diameter tool at 950 rpm and 300 mm/min.

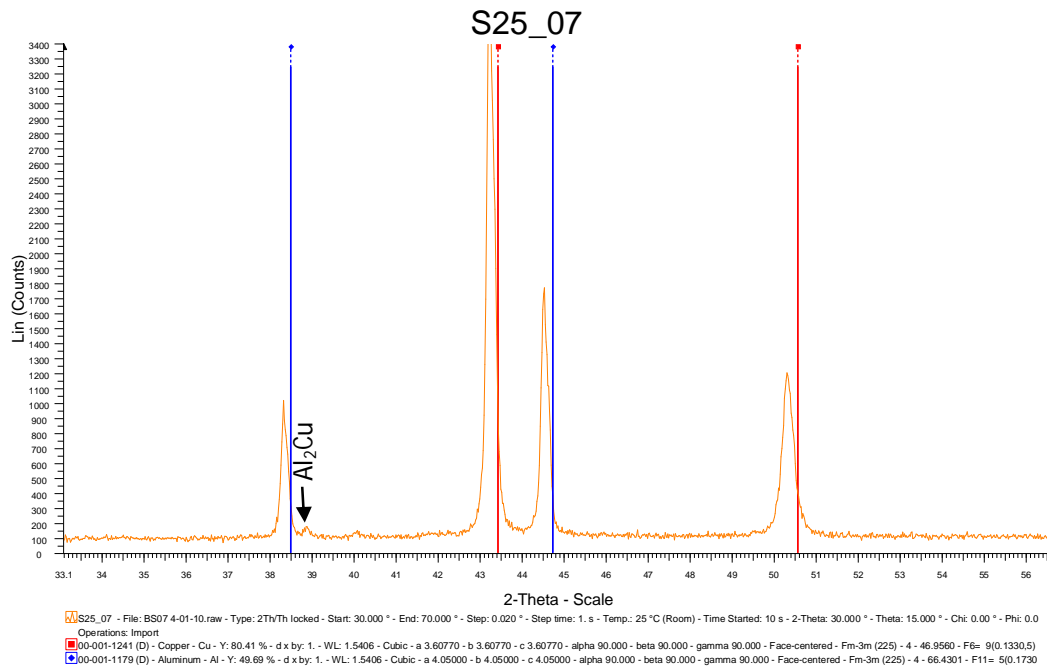


Figure C13xxv: PDF diffractogram of a weld produced with the 25 mm shoulder diameter tool at 1200 rpm and 50 mm/min.

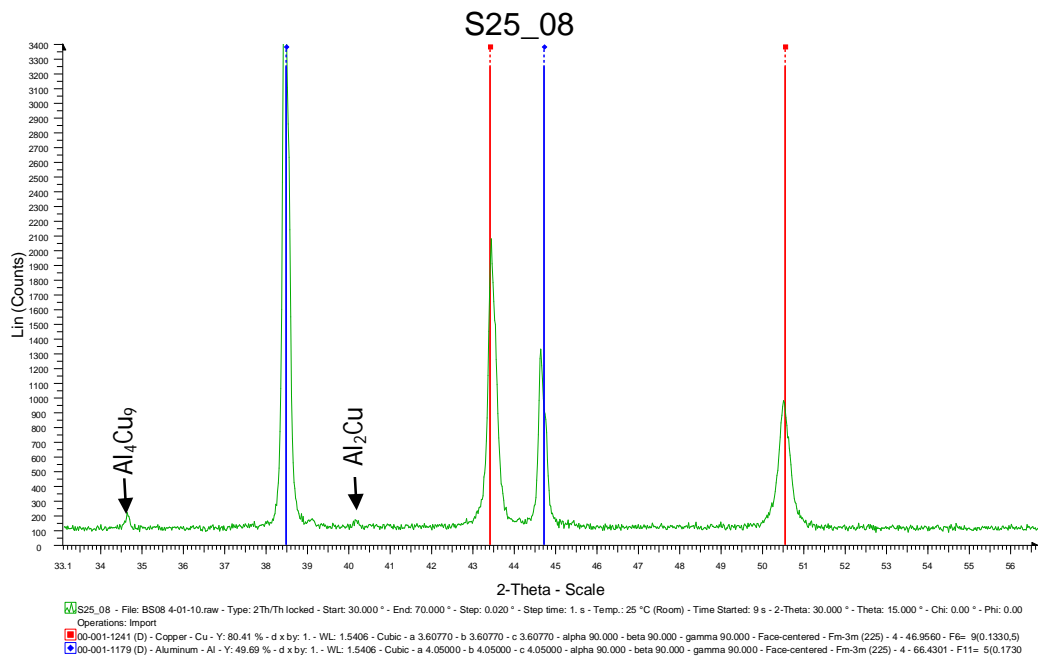


Figure C13xxvi: PDF diffractogram of a weld produced with the 25 mm shoulder diameter tool at 1200 rpm and 150 mm/min.

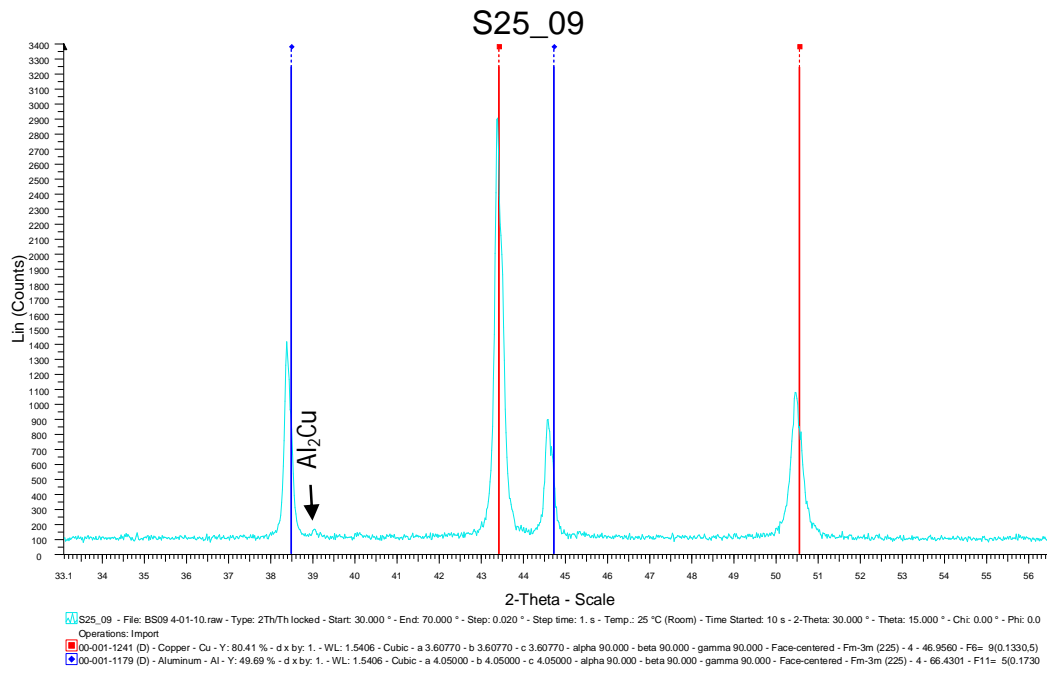


Figure C13xxvii: PDF diffractogram of a weld produced with the 25 mm shoulder diameter tool at 1200 rpm and 300 mm/min.

## C14. Multiple regression analysis

All Groups Regression Summary for Dependent Variable: Torque (FSW.st R= .69102833 R <sup>2</sup> = .47752015 Adjusted R <sup>2</sup> = .40937060 F(3,23)=7.0069 p<.00163 Std.Error of estimate: 5.1625						
N=27	b*	Std.Err. of b*	b	Std.Err. of b	t(23)	p-value
Intercept			25.63624	7.302470	3.51063	0.001879
Spindle speed	-0.497827	0.287223	-0.01334	0.007694	-1.73324	0.096441
Feed rate	0.518966	0.581321	0.03330	0.037298	0.89274	0.381244
Interaction	-0.088097	0.630646	-0.00001	0.000039	-0.13969	0.890118

All Groups Regression Summary for Dependent Variable: Heat input (KJ/mm R= .82208830 R <sup>2</sup> = .67582917 Adjusted R <sup>2</sup> = .63354602 F(3,23)=15.983 p<.00001 Std.Error of estimate: .30771						
N=27	b*	Std.Err. of b*	b	Std.Err. of b	t(23)	p-value
Intercept			1.13653501	0.435263	2.61114	0.015615
Feed rate (mm/min)	-0.713276	0.457898	#####	0.002223	-1.55772	0.132954
Spindle speed (rpm)	0.164103	0.226241	0.00033264	0.000459	0.72535	0.475555
Interaction	-0.111709	0.496750	#####	0.000002	-0.22488	0.824059

All Groups Regression Summary for Dependent Variable: UTS (MPa) R= .25719362 R <sup>2</sup> = .06614856 Adjusted R <sup>2</sup> = .02976474 F(3,77)=1.8181 p<.15087 Std.Error of estimate: 34.727						
N=81	b*	Std.Err. of b*	b	Std.Err. of b	t(77)	p-value
Intercept			146.9909	28.36040	5.182963	0.000002
Spindle speed (rpm)	0.193336	0.209866	0.0275	0.02988	0.921239	0.359803
Feed rate (mm/min)	0.149707	0.424755	0.0511	0.14485	0.352455	0.725460
Interaction	-0.431213	0.460796	-0.0001	0.00015	-0.935801	0.352301

All Groups Regression Summary for Dependent Variable: Electrical resistivity (micro-Ohm) R= .87822639 R <sup>2</sup> = .77128160 Adjusted R <sup>2</sup> = .74144876 F(3,23)=25.853 p<.00000 Std.Error of estimate: .00212						
N=27	b*	Std.Err. of b*	b	Std.Err. of b	t(23)	p-value
Intercept			0.10151956	0.003001	33.82694	0.000000
Feed rate (mm/min)	-0.683878	0.384620	-0.00002725	0.000015	-1.77806	0.088619
Spindle speed (rpm)	0.048753	0.190035	0.00000081	0.000003	0.25655	0.799811
Interaction	-0.215820	0.417255	-0.00000001	0.000000	-0.51724	0.609930

Regression Summary for Dependent Variable: UTS R= .33838268 R <sup>2</sup> = .11450284 Adjusted R <sup>2</sup> = .06789772 F(4,76)=2.4569 p<.05267 Std.Error of estimate: 33.830						
N=81	b*	Std.Err. of b*	b	Std.Err. of b	t(76)	p-value
Intercept			194.6103	15.66224	12.42544	0.000000
Fx	0.345354	0.245328	10.8737	7.72427	1.40772	0.163290
Fy	0.310125	0.172126	24.9234	13.83301	1.80173	0.075553
Fz	-0.700086	0.297301	-3.0675	1.30267	-2.35481	0.021115
Torque	-0.094367	0.171304	-0.4985	0.90496	-0.55088	0.583333

### UTS regressions

All Groups Regression Summary for Dependent Variable: UTS (MPa) R= .25719362 R <sup>2</sup> = .06614856 Adjusted R <sup>2</sup> = .02976474 F(3,77)=1.8181 p<.15087 Std.Error of estimate: 34.727						
N=81	b*	Std.Err. of b*	b	Std.Err. of b	t(77)	p-value
Intercept			146.9909	28.36040	5.182963	0.000002
Spindle speed (rpm)	0.193336	0.209866	0.0275	0.02988	0.921239	0.359803
Feed rate (mm/min)	0.149707	0.424755	0.0511	0.14485	0.352455	0.725460
Interaction	-0.431213	0.460796	-0.0001	0.00015	-0.935801	0.352301

Weld grp=S15 Regression Summary for Dependent Variable: UTS (MPa) R= .36330898 R <sup>2</sup> = .13199342 Adjusted R <sup>2</sup> = .01877517 F(3,23)=1.1658 p<.34425 Std.Error of estimate: 36.966						
N=27	b*	Std.Err. of b*	b	Std.Err. of b	t(23)	p-value
Intercept			104.8399	52.28929	2.00500	0.056871
Spindle speed (rpm)	0.39669	0.370208	0.0590	0.05509	1.07152	0.295049
Feed rate (mm/min)	1.27735	0.749278	0.4553	0.26707	1.70478	0.101709
Interaction	-1.38909	0.812854	-0.0005	0.00028	-1.70891	0.100930

Weld grp=S18 Regression Summary for Dependent Variable: UTS (MPa) R= .66695742 R <sup>2</sup> = .44483220 Adjusted R <sup>2</sup> = .37241901 F(3,23)=6.1430 p<.00318 Std.Error of estimate: 24.965						
N=27	b*	Std.Err. of b*	b	Std.Err. of b	t(23)	p-value
Intercept			149.9145	35.31313	4.245292	0.000306
Spindle speed (rpm)	0.458551	0.296071	0.0576	0.03721	1.548788	0.135084
Feed rate (mm/min)	-0.278349	0.599230	-0.0838	0.18036	-0.464512	0.646648
Interaction	-0.332452	0.650074	-0.0001	0.00019	-0.511406	0.613941

Weld grp=S25 Regression Summary for Dependent Variable: UTS (MPa) R= .32382549 R <sup>2</sup> = .10486295 Adjusted R <sup>2</sup> = ----- F(3,23)=.89813 p<.45717 Std.Error of estimate: 29.866						
N=27	b*	Std.Err. of b*	b	Std.Err. of b	t(23)	p-value
Intercept			186.2182	42.24610	4.40794	0.000204
Spindle speed (rpm)	-0.287809	0.375949	-0.0341	0.04451	-0.76555	0.451727
Feed rate (mm/min)	-0.769989	0.760897	-0.2184	0.21577	-1.01195	0.322091
Interaction	0.543151	0.825459	0.0001	0.00023	0.65800	0.517071

### % Elongation regressions

All Groups Regression Summary for Dependent Variable: % Elongation R= .15224355 R <sup>2</sup> = .02317810 Adjusted R <sup>2</sup> = ----- F(3,77)=.60902 p<.61116 Std.Error of estimate: 1.8688						
N=81	b*	Std.Err. of b*	b	Std.Err. of b	t(77)	p-value
Intercept			1.903292	1.526184	1.24709	0.216144
Spindle speed (rpm)	0.262944	0.214640	0.001970	0.001608	1.22505	0.224292
Feed rate (mm/min)	0.468397	0.434418	0.008405	0.007795	1.07822	0.284303
Interaction	-0.581726	0.471278	-0.000010	0.000008	-1.23436	0.220823

Weld grp=S15 Regression Summary for Dependent Variable: % Elongation R= .42491450 R <sup>2</sup> = .18055233 Adjusted R <sup>2</sup> = .07366785 F(3,23)=1.6892 p<.19712 Std.Error of estimate: 1.9442						
N=27	b*	Std.Err. of b*	b	Std.Err. of b	t(23)	p-value
Intercept			-0.529788	2.750056	-0.19265	0.848927
Spindle speed (rpm)	0.46074	0.359703	0.003711	0.002897	1.28089	0.212998
Feed rate (mm/min)	1.48030	0.728018	0.028560	0.014046	2.03333	0.053716
Interaction	-1.36819	0.789790	-0.000026	0.000015	-1.73235	0.096603

Weld grp=S18 Regression Summary for Dependent Variable: % Elongation R= .34212297 R <sup>2</sup> = .11704813 Adjusted R <sup>2</sup> = .00188049 F(3,23)=1.0163 p<.40355 Std.Error of estimate: 1.9179						
N=27	b*	Std.Err. of b*	b	Std.Err. of b	t(23)	p-value
Intercept			3.416152	2.712878	1.259235	0.220576
Spindle speed (rpm)	0.179956	0.373381	0.001378	0.002858	0.481963	0.634387
Feed rate (mm/min)	-0.286837	0.755701	-0.005259	0.013856	-0.379564	0.707751
Interaction	-0.006327	0.819822	-0.000000	0.000015	-0.007718	0.993909

Weld grp=S25 Regression Summary for Dependent Variable: % Elongation R= .17072077 R <sup>2</sup> = .02914558 Adjusted R <sup>2</sup> = ----- F(3,23)=.23016 p<.87443 Std.Error of estimate: 1.6881						
N=27	b*	Std.Err. of b*	b	Std.Err. of b	t(23)	p-value
Intercept			2.823512	2.387869	1.182440	0.249111
Spindle speed (rpm)	0.127714	0.391526	0.000821	0.002516	0.326196	0.747226
Feed rate (mm/min)	0.124322	0.792425	0.001913	0.012196	0.156888	0.876702
Interaction	-0.311986	0.859663	-0.000005	0.000013	-0.362917	0.719981

### Electrical resistivity regressions

All Groups Regression Summary for Dependent Variable: Electrical resistivity (micro-Ohr) R= .87822639 R <sup>2</sup> = .77128160 Adjusted R <sup>2</sup> = .74144876 F(3,23)=25.853 p<.00000 Std.Error of estimate: .00212						
N=27	b*	Std.Err. of b*	b	Std.Err. of b	t(23)	p-value
Intercept			0.10151956	0.003001	33.82694	0.000000
Feed rate (mm/min)	-0.683878	0.384620	-0.00002725	0.000015	-1.77806	0.088619
Spindle speed (rpm)	0.048753	0.190035	0.00000081	0.000003	0.25655	0.799811
Interaction	-0.215820	0.417255	-0.00000001	0.000000	-0.51724	0.609930

Shoulder Diameter=15 Regression Summary for Dependent Variable: Electrical resistivity (micro-Ohr) R= .96072011 R <sup>2</sup> = .92298312 Adjusted R <sup>2</sup> = .87677300 F(3,5)=19.974 p<.00326 Std.Error of estimate: .00140						
N=9	b*	Std.Err. of b*	b	Std.Err. of b	t(5)	p-value
Intercept			0.10347996	0.003440	30.07957	0.000001
Feed rate (mm/min)	-1.34788	0.478689	-0.00004948	0.000018	-2.81578	0.037293
Spindle speed (rpm)	-0.04915	0.236513	-0.00000075	0.000004	-0.20782	0.843571
Interaction	0.45104	0.519305	0.00000002	0.000000	0.86854	0.424817

Shoulder Diameter=18 Regression Summary for Dependent Variable: Electrical resistivity (micro-Ohr) R= .84683514 R <sup>2</sup> = .71712975 Adjusted R <sup>2</sup> = .54740760 F(3,5)=4.2253 p<.07739 Std.Error of estimate: .00325						
N=9	b*	Std.Err. of b*	b	Std.Err. of b	t(5)	p-value
Intercept			0.10071222	0.007952	12.66444	0.000055
Feed rate (mm/min)	-0.212558	0.917390	-0.00000941	0.000041	-0.23170	0.825956
Spindle speed (rpm)	0.045974	0.453269	0.00000085	0.000008	0.10143	0.923152
Interaction	-0.664782	0.995230	-0.00000003	0.000000	-0.66797	0.533744

Shoulder Diameter=25 Regression Summary for Dependent Variable: Electrical resistivity (micro-Ohr) R= .94232701 R <sup>2</sup> = .88798019 Adjusted R <sup>2</sup> = .82076830 F(3,5)=13.212 p<.00821 Std.Error of estimate: .00169						
N=9	b*	Std.Err. of b*	b	Std.Err. of b	t(5)	p-value
Intercept			0.10036649	0.004142	24.23287	0.000002
Feed rate (mm/min)	-0.624348	0.577308	-0.00002288	0.000021	-1.08148	0.328861
Spindle speed (rpm)	0.152761	0.285240	0.00000234	0.000004	0.53555	0.615221
Interaction	-0.352775	0.626293	-0.00000001	0.000000	-0.56327	0.597570

### Heat input regressions

All Groups Regression Summary for Dependent Variable: Heat input (KJ/mm) R= .82208830 R <sup>2</sup> = .67582917 Adjusted R <sup>2</sup> = .63354602 F(3,23)=15.983 p<.00001 Std.Error of estimate: .30771						
N=27	b*	Std.Err. of b*	b	Std.Err. of b	t(23)	p-value
Intercept			1.13653501	0.435263	2.61114	0.015615
Feed rate (mm/min)	-0.713276	0.457898	#####	0.002223	-1.55772	0.132954
Spindle speed (rpm)	0.164103	0.226241	0.00033264	0.000459	0.72535	0.475555
Interaction	-0.111709	0.496750	#####	0.000002	-0.22488	0.824059

Shoulder Diameter=15 Regression Summary for Dependent Variable: Heat input (KJ/mm) R= .91198751 R <sup>2</sup> = .83172123 Adjusted R <sup>2</sup> = .73075396 F(3,5)=8.2375 p<.02219 Std.Error of estimate: .18338						
N=9	b*	Std.Err. of b*	b	Std.Err. of b	t(5)	p-value
Intercept			1.11937808	0.449287	2.49146	0.055063
Feed rate (mm/min)	-0.988012	0.707579	#####	0.002295	-1.39633	0.221440
Spindle speed (rpm)	-0.026511	0.349605	#####	0.000473	-0.07583	0.942495
Interaction	0.085681	0.767617	0.00000027	0.000002	0.11162	0.915467

Shoulder Diameter=18 Regression Summary for Dependent Variable: Heat input (KJ/mm) R= .90804380 R <sup>2</sup> = .82454354 Adjusted R <sup>2</sup> = .71926967 F(3,5)=7.8324 p<.02456 Std.Error of estimate: .25034						
N=9	b*	Std.Err. of b*	b	Std.Err. of b	t(5)	p-value
Intercept			0.95837880	0.613330	1.562583	0.178911
Feed rate (mm/min)	-0.600304	0.722512	#####	0.003133	-0.830858	0.443906
Spindle speed (rpm)	0.248486	0.356983	0.00044981	0.000646	0.696072	0.517405
Interaction	-0.332853	0.783817	#####	0.000003	-0.424657	0.688740

Shoulder Diameter=25 Regression Summary for Dependent Variable: Heat input (KJ/mm) R= .91394620 R <sup>2</sup> = .83529765 Adjusted R <sup>2</sup> = .73647624 F(3,5)=8.4526 p<.02106 Std.Error of estimate: .31468						
N=9	b*	Std.Err. of b*	b	Std.Err. of b	t(5)	p-value
Intercept			1.33184814	0.770975	1.72749	0.144659
Feed rate (mm/min)	-0.814551	0.700019	#####	0.003938	-1.16361	0.297085
Spindle speed (rpm)	0.248666	0.345870	0.00058401	0.000812	0.71896	0.504354
Interaction	-0.082090	0.759416	#####	0.000004	-0.10810	0.918123

**(Fx) regressions**

All Groups Regression Summary for Dependent Variable: Fx (FSW.sta) R= .59081325 R <sup>2</sup> = .34906030 Adjusted R <sup>2</sup> = .26415512 F(3,23)=4.1112 p<.01791 Std.Error of estimate: .96683						
N=27	b*	Std.Err. of b*	b	Std.Err. of b	t(23)	p-value
Intercept			2.27342824	1.367602	1.662346	0.110014
Spindle speed	-0.024840	0.320593	-0.00011164	0.001441	-0.077481	0.938911
Feed rate	0.603520	0.648861	0.00649698	0.006985	0.930123	0.361968
Interaction	-0.015184	0.703917	-0.00000016	0.000007	-0.021571	0.982976

Weld grp=S15 Regression Summary for Dependent Variable: Fx (FSW.sta) R= .80668964 R <sup>2</sup> = .65074817 Adjusted R <sup>2</sup> = .44119708 F(3,5)=3.1054 p<.12707 Std.Error of estimate: .82101						
N=9	b*	Std.Err. of b*	b	Std.Err. of b	t(5)	p-value
Intercept			0.689944	2.011505	0.34300	0.745550
Spindle speed	0.20536	0.503654	0.000864	0.002119	0.40773	0.700340
Feed rate	1.74183	1.019365	0.017555	0.010274	1.70874	0.148197
Interaction	-1.14812	1.105858	-0.000011	0.000011	-1.03822	0.346745

Weld grp=S18 Regression Summary for Dependent Variable: Fx (FSW.sta) R= .70694351 R <sup>2</sup> = .49976913 Adjusted R <sup>2</sup> = .19963061 F(3,5)=1.6651 p<.28809 Std.Error of estimate: .62437						
N=9	b*	Std.Err. of b*	b	Std.Err. of b	t(5)	p-value
Intercept			2.593779	1.529731	1.695578	0.150734
Spindle speed	-0.141092	0.602765	-0.000377	0.001612	-0.234074	0.824210
Feed rate	1.040599	1.219960	0.006664	0.007813	0.852978	0.432623
Interaction	-0.475613	1.323473	-0.000003	0.000008	-0.359367	0.733999

Weld grp=S25 Regression Summary for Dependent Variable: Fx (FSW.sta) R= .93598760 R <sup>2</sup> = .87607278 Adjusted R <sup>2</sup> = .80171645 F(3,5)=11.782 p<.01051 Std.Error of estimate: .47882						
N=9	b*	Std.Err. of b*	b	Std.Err. of b	t(5)	p-value
Intercept			3.536562	1.173126	3.014647	0.029597
Spindle speed	-0.199473	0.300017	-0.000822	0.001236	-0.664872	0.535565
Feed rate	-0.479232	0.607217	-0.004729	0.005992	-0.789227	0.465739
Interaction	1.431672	0.658739	0.000014	0.000006	2.173353	0.081796

### Fy regressions

All Groups Regression Summary for Dependent Variable: Fy (FSW.sta) R= .37373728 R <sup>2</sup> = .13967955 Adjusted R <sup>2</sup> = .02746384 F(3,23)=1.2447 p<.31647 Std.Error of estimate: .43546						
N=27	b*	Std.Err. of b*	b	Std.Err. of b	t(23)	p-value
Intercept			-1.15890228	0.615969	-1.88143	0.072631
Spindle speed	0.408497	0.368565	0.00071930	0.000649	1.10835	0.279168
Feed rate	0.322985	0.745953	0.00136220	0.003146	0.43298	0.669061
Interaction	-0.186433	0.809247	-0.00000076	0.000003	-0.23038	0.819834

Weld grp=S15 Regression Summary for Dependent Variable: Fy (FSW.sta) R= .17736059 R <sup>2</sup> = .03145678 Adjusted R <sup>2</sup> = ----- F(3,5)=.05413 p<.98159 Std.Error of estimate: .44123						
N=9	b*	Std.Err. of b*	b	Std.Err. of b	t(5)	p-value
Intercept			-0.89409681	1.081035	-0.827075	0.445857
Spindle speed	0.086242	0.838730	0.00011712	0.001139	0.102825	0.922099
Feed rate	0.408358	1.697539	0.00132823	0.005521	0.240559	0.819449
Interaction	-0.275088	1.841575	-0.00000087	0.000006	-0.149377	0.887095

Weld grp=S18 Regression Summary for Dependent Variable: Fy (FSW.sta) R= .90919572 R <sup>2</sup> = .82663685 Adjusted R <sup>2</sup> = .72261896 F(3,5)=7.9471 p<.02386 Std.Error of estimate: .18237						
N=9	b*	Std.Err. of b*	b	Std.Err. of b	t(5)	p-value
Intercept			#####	0.446808	-4.47585	0.006544
Spindle speed	1.00577	0.354847	0.00133431	0.000471	2.83438	0.036486
Feed rate	1.92265	0.718189	0.00610935	0.002282	2.67709	0.043973
Interaction	-1.37002	0.779127	#####	0.000002	-1.75841	0.139008

Weld grp=S25 Regression Summary for Dependent Variable: Fy (FSW.sta) R= .81126072 R <sup>2</sup> = .65814396 Adjusted R <sup>2</sup> = .45303033 F(3,5)=3.2087 p<.12088 Std.Error of estimate: .29790						
N=9	b*	Std.Err. of b*	b	Std.Err. of b	t(5)	p-value
Intercept			-0.58276695	0.729870	-0.798453	0.460833
Spindle speed	0.457787	0.498293	0.00070648	0.000769	0.918711	0.400396
Feed rate	-0.906559	1.008514	-0.00335098	0.003728	-0.898906	0.409901
Interaction	0.781636	1.094086	0.00000281	0.000004	0.714419	0.506925

**(Fz) regressions**

All Groups Regression Summary for Dependent Variable: Fz (FSW.sta) R= .42911434 R <sup>2</sup> = .18413912 Adjusted R <sup>2</sup> = .07772248 F(3,23)=1.7304 p<.18871 Std.Error of estimate: 7.7779						
N=27	b*	Std.Err. of b*	b	Std.Err. of b	t(23)	p-value
Intercept			15.00016	11.00199	1.363404	0.185953
Spindle speed	-0.096366	0.358915	-0.00311	0.01159	-0.268492	0.790714
Feed rate	-0.152684	0.726423	-0.01181	0.05619	-0.210186	0.835374
Interaction	0.599400	0.788059	0.00005	0.00006	0.760602	0.454622

Weld grp=S15 Regression Summary for Dependent Variable: Fz (FSW.sta) R= .91389153 R <sup>2</sup> = .83519774 Adjusted R <sup>2</sup> = .73631638 F(3,5)=8.4465 p<.02109 Std.Error of estimate: 1.7458						
N=9	b*	Std.Err. of b*	b	Std.Err. of b	t(5)	p-value
Intercept			9.796311	4.277167	2.290374	0.070616
Spindle speed	-0.187632	0.345975	-0.002444	0.004506	-0.542330	0.610879
Feed rate	1.303142	0.700232	0.040655	0.021846	1.861015	0.121812
Interaction	-0.554250	0.759646	-0.000017	0.000023	-0.729616	0.498356

Weld grp=S18 Regression Summary for Dependent Variable: Fz (FSW.sta) R= .98346619 R <sup>2</sup> = .96720574 Adjusted R <sup>2</sup> = .94752919 F(3,5)=49.155 p<.00039 Std.Error of estimate: .64932						
N=9	b*	Std.Err. of b*	b	Std.Err. of b	t(5)	p-value
Intercept			6.857012	1.590855	4.31027	0.007641
Spindle speed	0.348961	0.154334	0.003790	0.001676	2.26107	0.073253
Feed rate	1.731319	0.312363	0.045036	0.008125	5.54266	0.002624
Interaction	-0.864813	0.338867	-0.000022	0.000009	-2.55208	0.051137

Weld grp=S25 Regression Summary for Dependent Variable: Fz (FSW.sta) R= .85039914 R <sup>2</sup> = .72317869 Adjusted R <sup>2</sup> = .55708591 F(3,5)=4.3541 p<.07352 Std.Error of estimate: 6.1483						
N=9	b*	Std.Err. of b*	b	Std.Err. of b	t(5)	p-value
Intercept			28.34714	15.06365	1.88182	0.118598
Spindle speed	-0.30181	0.448397	-0.01068	0.01587	-0.67309	0.530739
Feed rate	-1.42873	0.907528	-0.12112	0.07694	-1.57431	0.176231
Interaction	2.11009	0.984532	0.00017	0.00008	2.14325	0.084968

### Torque regressions

All Groups Regression Summary for Dependent Variable: Torque (FSW.sta) R= .69102833 R <sup>2</sup> = .47752015 Adjusted R <sup>2</sup> = .40937060 F(3,23)=7.0069 p<.00163 Std.Error of estimate: 5.1625						
N=27	b*	Std.Err. of b*	b	Std.Err. of b	t(23)	p-value
Intercept			<b>25.63624</b>	<b>7.302470</b>	<b>3.51063</b>	<b>0.001879</b>
Spindle speed	-0.497827	0.287223	-0.01334	0.007694	-1.73324	0.096441
Feed rate	0.518966	0.581321	0.03330	0.037298	0.89274	0.381244
Interaction	-0.088097	0.630646	-0.00001	0.000039	-0.13969	0.890118

Weld grp=S15 Regression Summary for Dependent Variable: Torque (FSW.sta) R= .91762383 R <sup>2</sup> = .84203349 Adjusted R <sup>2</sup> = .74725358 F(3,5)=8.8841 p<.01903 Std.Error of estimate: 2.8380						
N=9	b*	Std.Err. of b*	b	Std.Err. of b	t(5)	p-value
Intercept			<b>21.31243</b>	<b>6.953224</b>	<b>3.06511</b>	<b>0.027939</b>
Spindle speed	-0.555293	0.338723	-0.01201	0.007326	-1.63937	0.162061
Feed rate	0.981329	0.685556	0.05084	0.035514	1.43144	0.211722
Interaction	-0.594237	0.743725	-0.00003	0.000037	-0.79900	0.460543

Weld grp=S18 Regression Summary for Dependent Variable: Torque (FSW.sta) R= .97773566 R <sup>2</sup> = .95596702 Adjusted R <sup>2</sup> = .92954724 F(3,5)=36.184 p<.00082 Std.Error of estimate: 1.2712						
N=9	b*	Std.Err. of b*	b	Std.Err. of b	t(5)	p-value
Intercept			<b>21.65899</b>	<b>3.114535</b>	<b>6.95416</b>	<b>0.000945</b>
Spindle speed	<b>-0.534317</b>	<b>0.178835</b>	<b>-0.00980</b>	<b>0.003281</b>	<b>-2.98777</b>	<b>0.030525</b>
Feed rate	<b>1.159286</b>	<b>0.361951</b>	<b>0.05095</b>	<b>0.015908</b>	<b>3.20288</b>	<b>0.023918</b>
Interaction	-0.741139	0.392662	-0.00003	0.000017	-1.88747	0.117742

Weld grp=S25 Regression Summary for Dependent Variable: Torque (FSW.st R= .89765883 R <sup>2</sup> = .80579137 Adjusted R <sup>2</sup> = .68926619 F(3,5)=6.9152 p<.03142 Std.Error of estimate: 3.2671						
N=9	b*	Std.Err. of b*	b	Std.Err. of b	t(5)	p-value
Intercept			33.93732	8.004398	4.23983	0.008171
Spindle speed	-0.810161	0.375575	-0.01819	0.008433	-2.15712	0.083490
Feed rate	-0.035237	0.760142	-0.00190	0.040883	-0.04636	0.964821
Interaction	0.862708	0.824639	0.00005	0.000043	1.04616	0.343401

## C15. Analysis of Variance plot

Analysis of Variance (ANOVA) is a statistical tool used to test for significant differences between means. This is done by quantifying the variability in a data set. The deviations from the mean of values are squared before summation; this sum is a useful measure of variability which will increase with a greater scatter of data points around the mean. This quantity is referred to as a *Sum of Squares* (SS).

The results of the analysis of variance of the data obtained for UTS and percentage elongation of the weld samples are hereby presented. Marked effects are significant at  $P < 0.05000$ .

Effect	All Groups Univariate Tests of Significance for UTS Sigma-restricted parameterization Effective hypothesis decomposition				
	SS	Degr. of Freedom	MS	F	p
Intercept	2045536	1	2045536	1837.593	0.000000
Spindle speed	2447	2	1223	1.099	0.338689
Feed rate	6727	2	3363	3.021	0.054951
Spindle speed*Feed rate	10113	4	2528	2.271	0.069819
Error	80148	72	1113		

Effect	Weld grp=S15 Univariate Tests of Significance for UTS Sigma-restricted parameterization Effective hypothesis decomposition				
	SS	Degr. of Freedom	MS	F	p
Intercept	703090.7	1	703090.7	588.8532	0.000000
Spindle speed	734.7	2	367.4	0.3077	0.738940
Feed rate	6940.5	2	3470.3	2.9064	0.080566
Spindle speed*Feed rate	7041.0	4	1760.3	1.4743	0.251384
Error	21492.0	18	1194.0		

Weld grp=S18 Univariate Tests of Significance for UTS Sigma-restricted parameterization Effective hypothesis decomposition					
Effect	SS	Degr. of Freedom	MS	F	p
Intercept	816756.1	1	816756.1	1356.404	0.000000
Spindle speed	3635.9	2	1817.9	3.019	0.074019
Feed rate	8624.3	2	4312.1	7.161	0.005151
Spindle speed*Feed rate	2721.0	4	680.3	1.130	0.373787
Error	10838.7	18	602.1		

Weld grp=S25 Univariate Tests of Significance for UTS Sigma-restricted parameterization Effective hypothesis decomposition					
Effect	SS	Degr. of Freedom	MS	F	p
Intercept	540176.3	1	540176.3	773.2351	0.000000
Spindle speed	2968.2	2	1484.1	2.1244	0.148485
Feed rate	1996.2	2	998.1	1.4287	0.265518
Spindle speed*Feed rate	5379.6	4	1344.9	1.9251	0.149891
Error	12574.7	18	698.6		

All Groups Univariate Tests of Significance for % Elongation Sigma-restricted parameterization Effective hypothesis decomposition					
Effect	SS	Degr. of Freedom	MS	F	p
Intercept	1027.131	1	1027.131	325.8236	0.000000
Spindle speed (rpm)	13.410	2	6.705	2.1269	0.126634
Feed rate (mm/min)	5.943	2	2.971	0.9425	0.394389
Spindle speed (rpm)*Feed rate (mm/min)	28.962	4	7.241	2.2968	0.067254
Error	226.974	72	3.152		

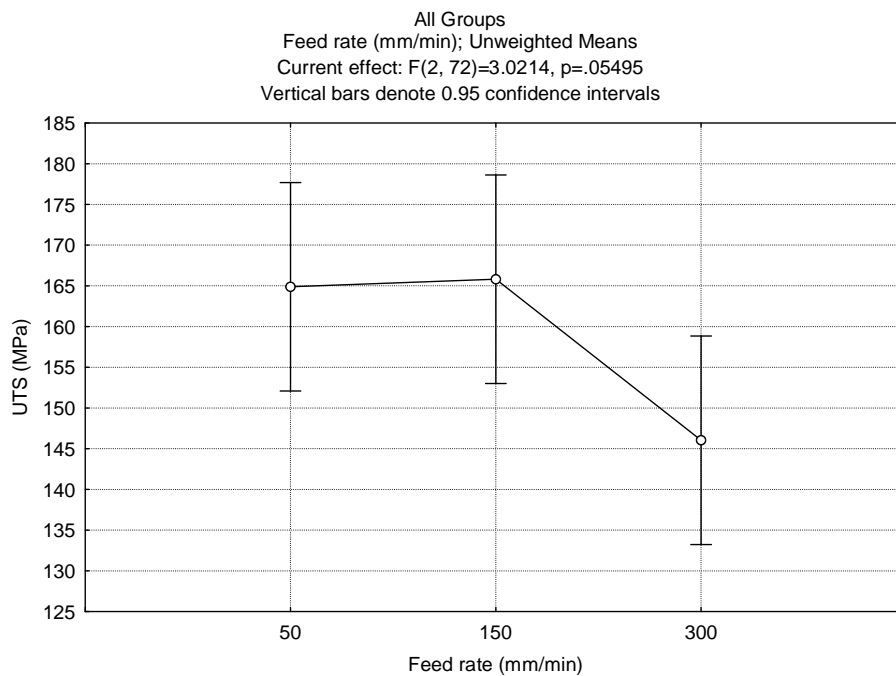
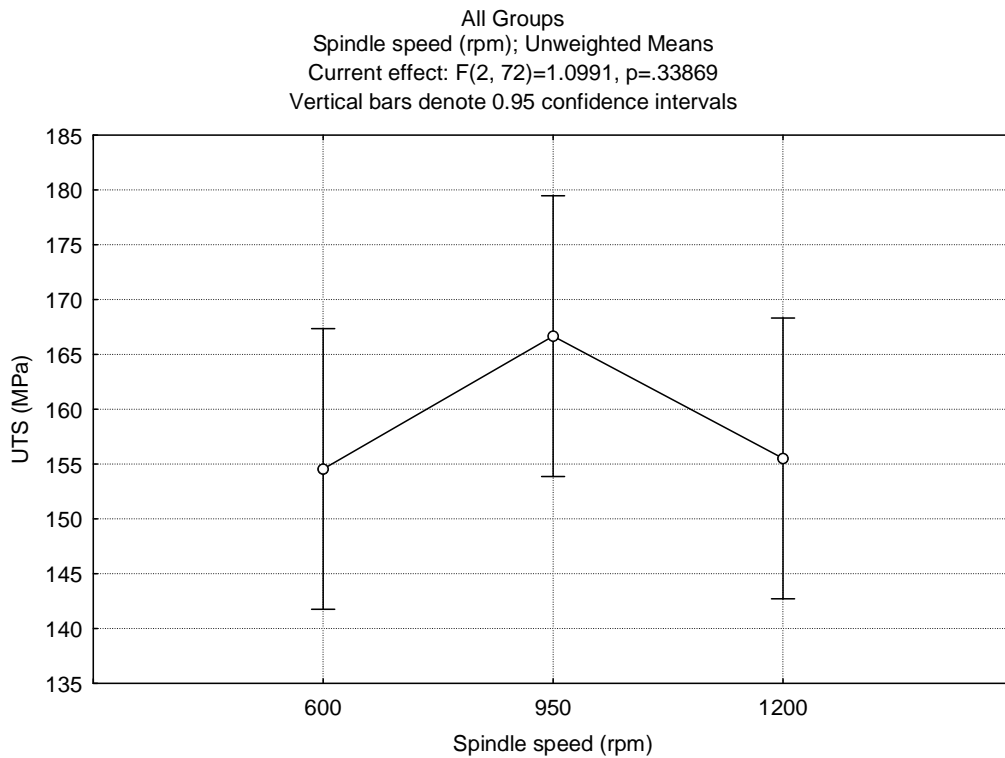
Weld grp=S15 Univariate Tests of Significance for % Elongation Sigma-restricted parameterization Effective hypothesis decomposition					
Effect	SS	Degr. of Freedom	MS	F	p
Intercept	372.7445	1	372.7445	85.50145	0.000000
Spindle speed (rpm)	1.7312	2	0.8656	0.19855	0.821687
Feed rate (mm/min)	12.0025	2	6.0012	1.37659	0.277774
Spindle speed (rpm)*Feed rate (mm/min)	13.8834	4	3.4708	0.79615	0.543098
Error	78.4712	18	4.3595		

Effect	Weld grp=S18 Univariate Tests of Significance for % Elongation Sigma-restricted parameterization Effective hypothesis decomposition				
	SS	Degr. of Freedom	MS	F	p
Intercept	386.8459	1	386.8459	128.7420	0.000000
Spindle speed (rpm)	19.2585	2	9.6293	3.2046	0.064486
Feed rate (mm/min)	10.6719	2	5.3359	1.7758	0.197761
Spindle speed (rpm)*Feed rate (mm/min)	11.7970	4	2.9493	0.9815	0.442287
Error	54.0867	18	3.0048		

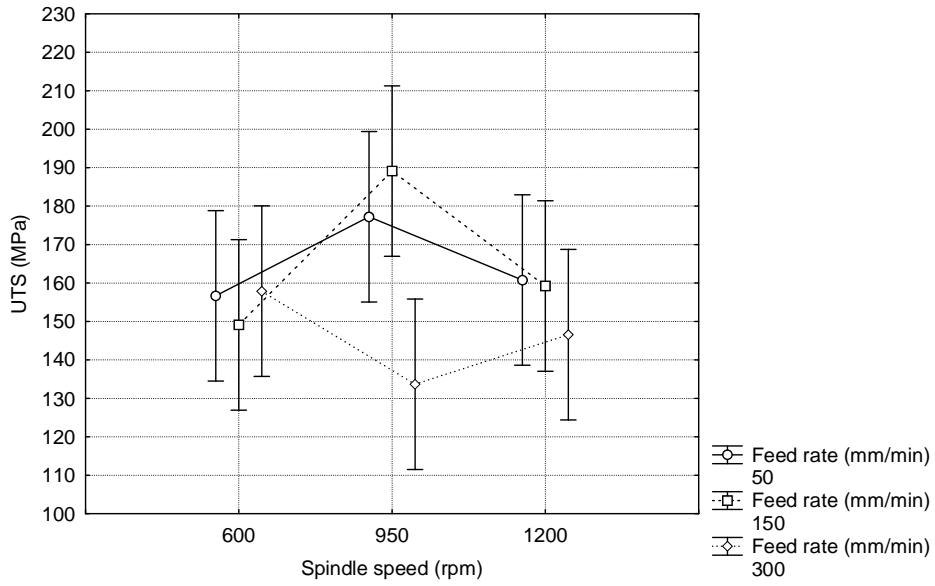
Effect	Weld grp=S25 Univariate Tests of Significance for UTS Sigma-restricted parameterization Effective hypothesis decomposition				
	SS	Degr. of Freedom	MS	F	p
Intercept	540176.3	1	540176.3	773.2351	0.000000
Spindle speed	2968.2	2	1484.1	2.1244	0.148485
Feed rate	1996.2	2	998.1	1.4287	0.265518
Spindle speed*Feed rate	5379.6	4	1344.9	1.9251	0.149891
Error	12574.7	18	698.6		

The intercepts will not be interpreted since they merely indicate that the average of the dependent variable differ significantly from zero. A few noticeable effects are observed where the p-value is not less than 0.05 but only marginally bigger. In one case, namely the effect of feed rate on UTS of welds produced with the 18 mm shoulder diameter tool, the p-value is 0.005151 ( $< 0.05000$ ). Therefore, it can be interpreted that the feed rate significantly influence the UTS of welds produced with this shoulder diameter tool, which further confirm that the 18 mm shoulder diameter tool is the most appropriate compared to other tools employed.

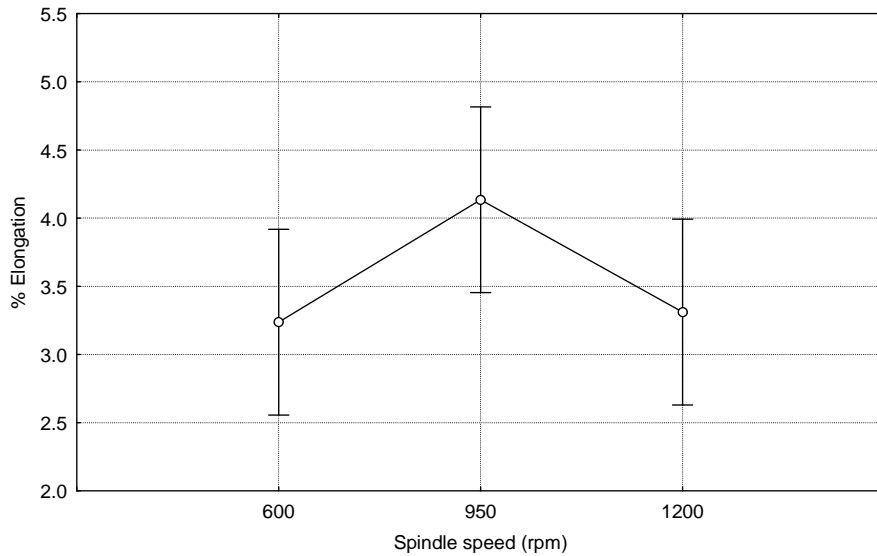
The ANOVA plots of the results of the entire weld groups are hereby presented.

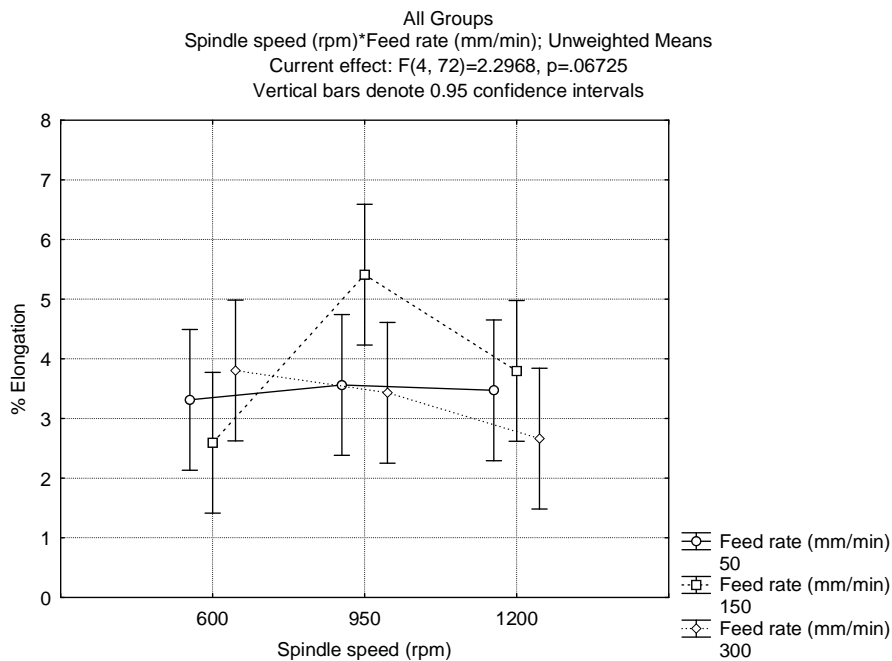
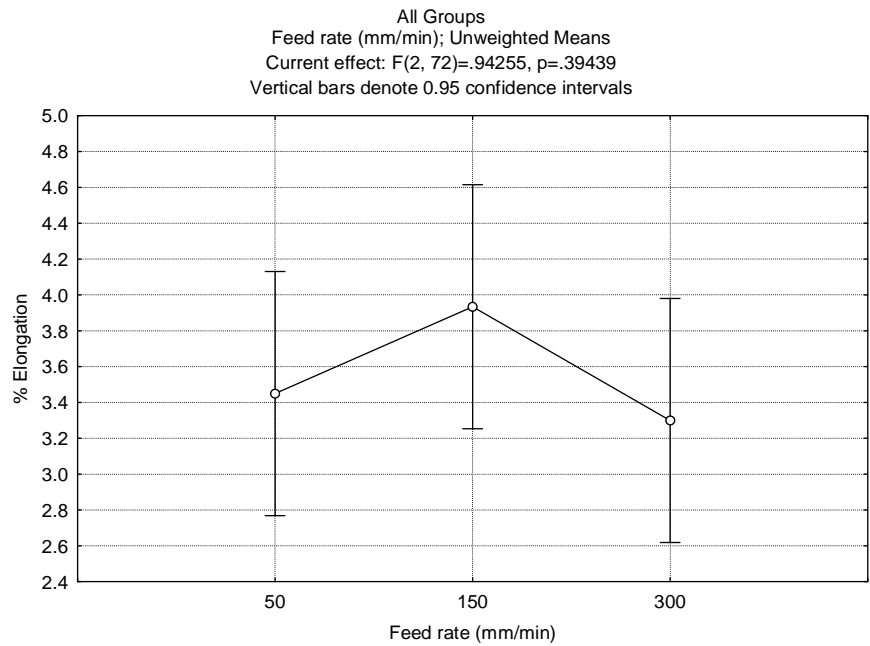


All Groups  
 Spindle speed (rpm)\*Feed rate (mm/min); Unweighted Means  
 Current effect:  $F(4, 72)=2.2713, p=.06982$   
 Vertical bars denote 0.95 confidence intervals

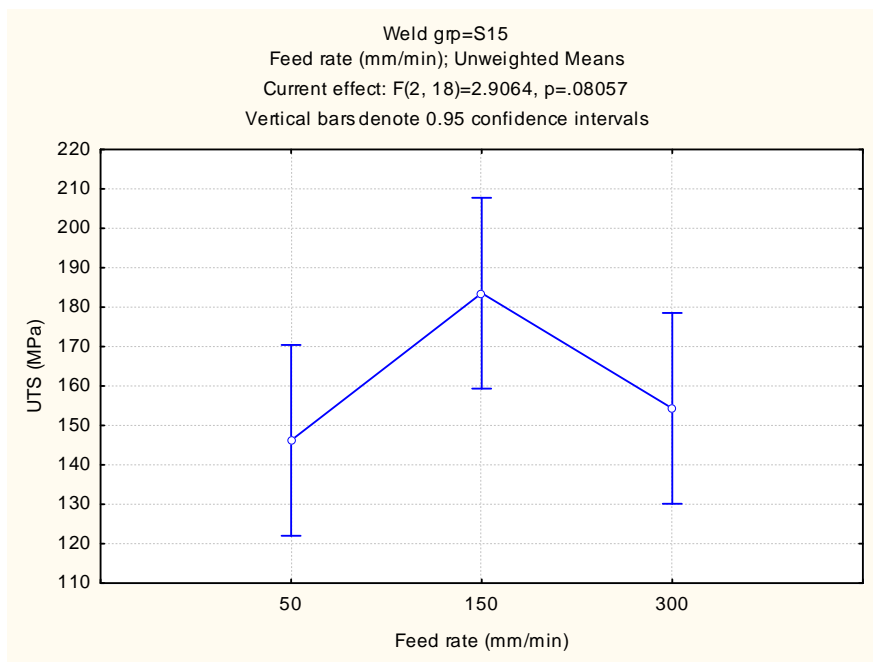
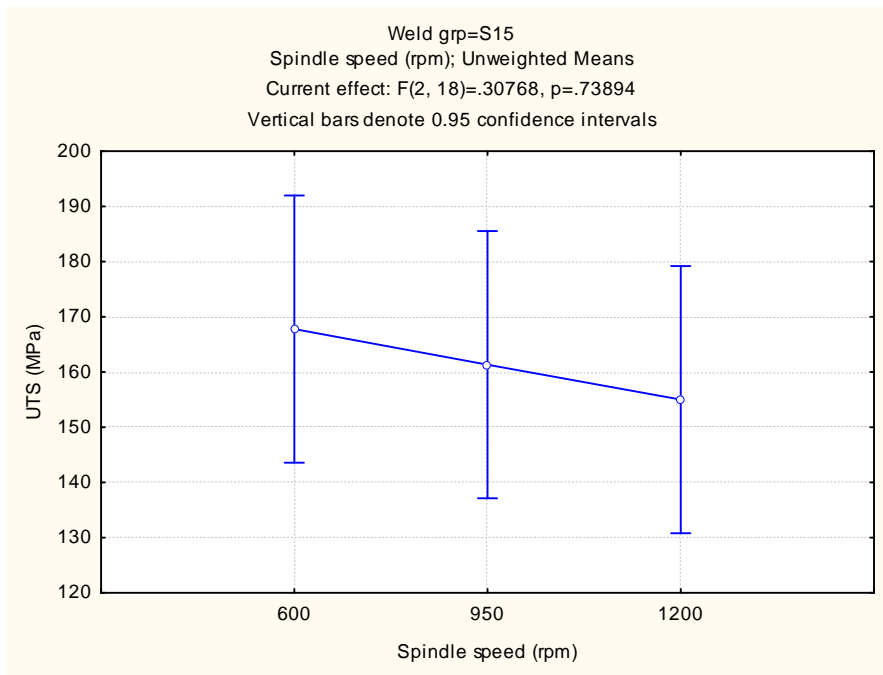


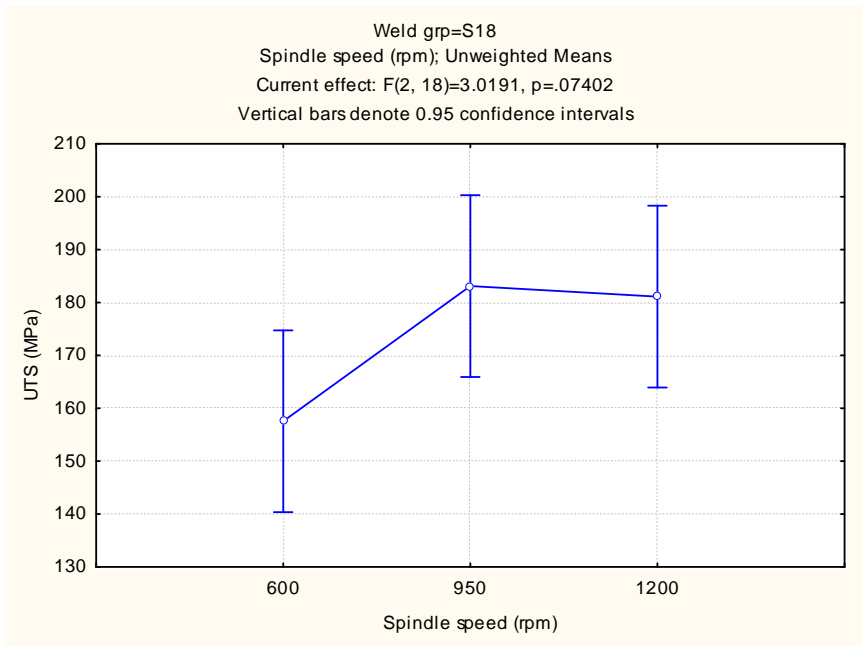
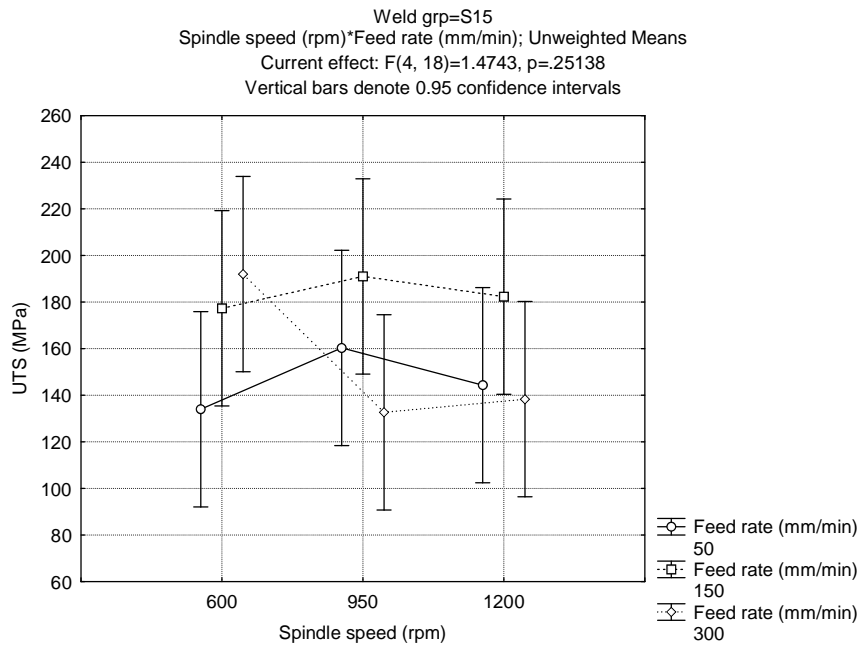
All Groups  
 Spindle speed (rpm); Unweighted Means  
 Current effect:  $F(2, 72)=2.1269, p=.12663$   
 Vertical bars denote 0.95 confidence intervals

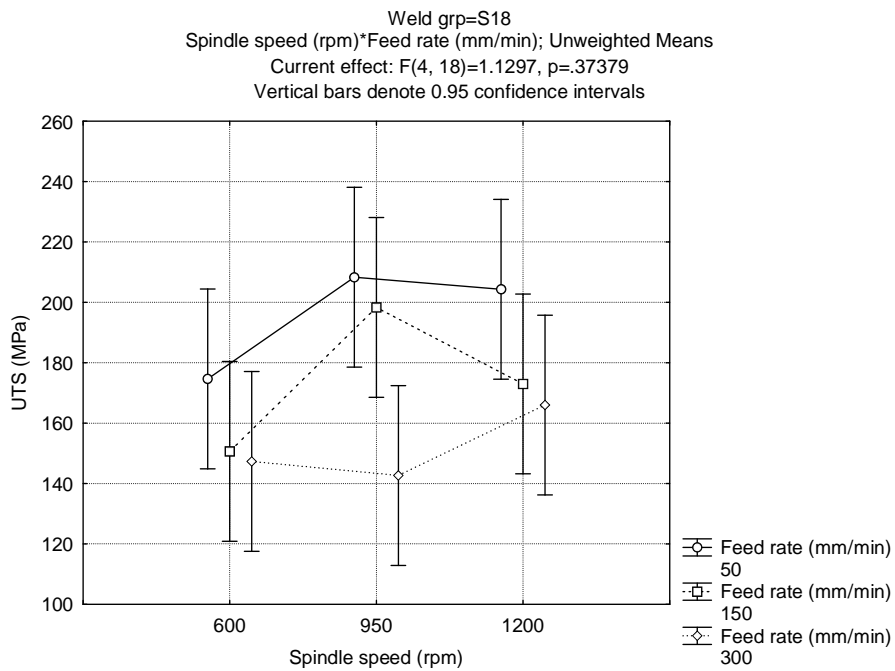
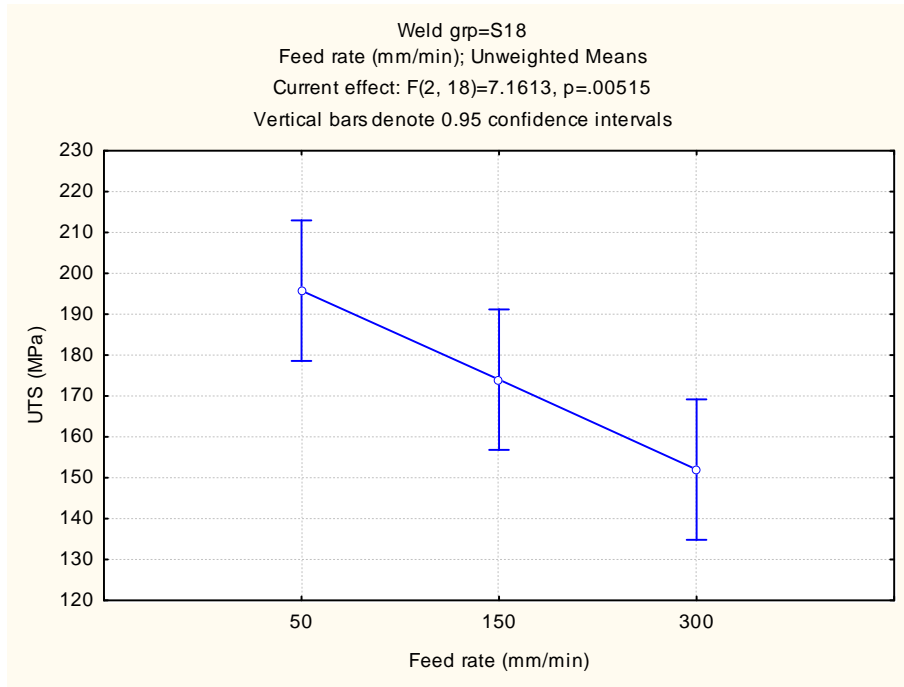


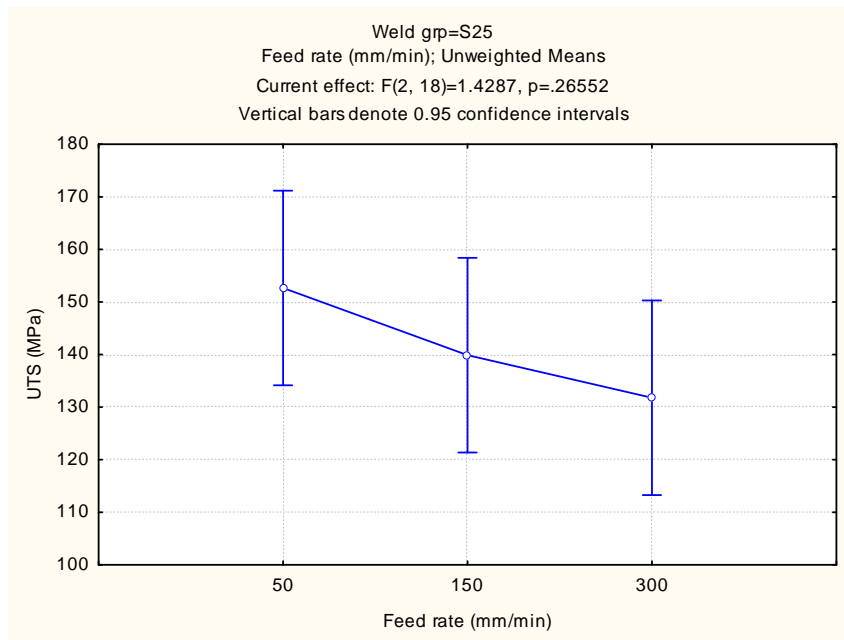
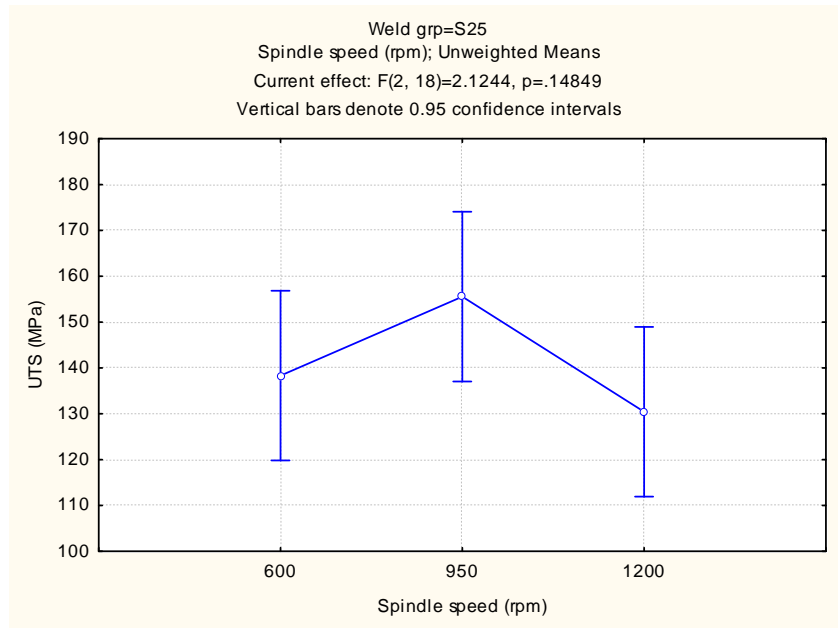


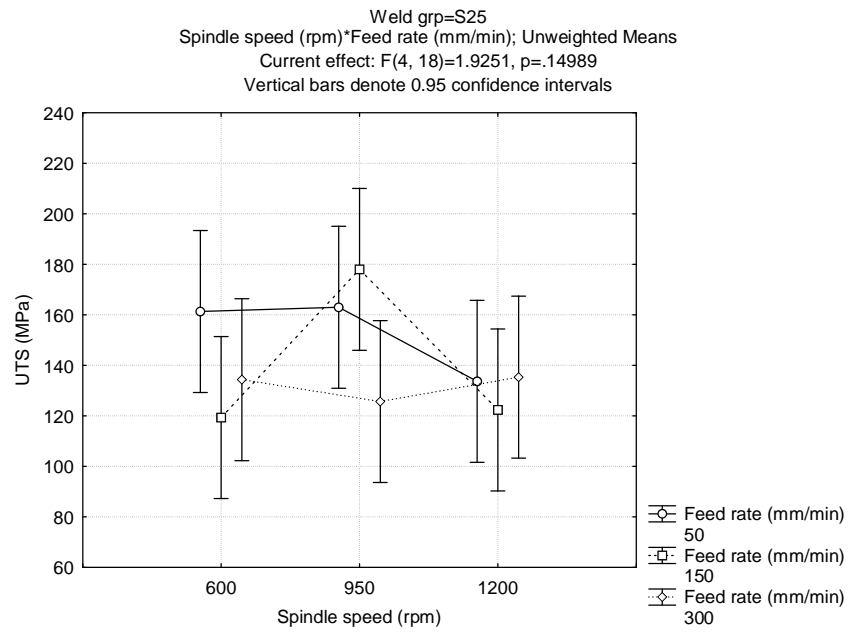
Trends apparent from the graphical representations of the ANOVA results of the tensile data as shown above is that the UTS and the percentage elongation of all the welds produced irrespective of the shoulder diameter are higher at 950 rpm compared to 600 and 1200 rpm. This is an indication that the most appropriate spindle speed to produce a good weld is at medium spindle speed of 950 rpm. Also, it was observed that the UTS decrease as the feed rate increases from 50 to 300 mm/min.



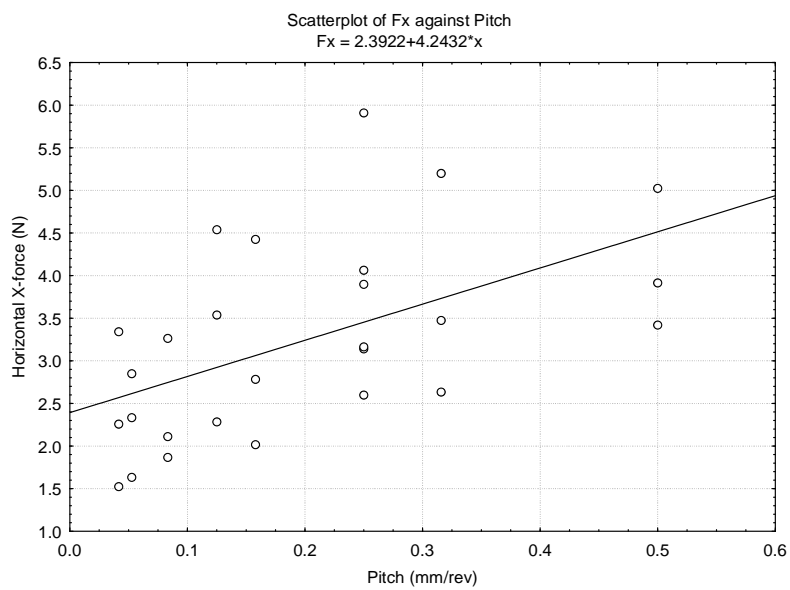
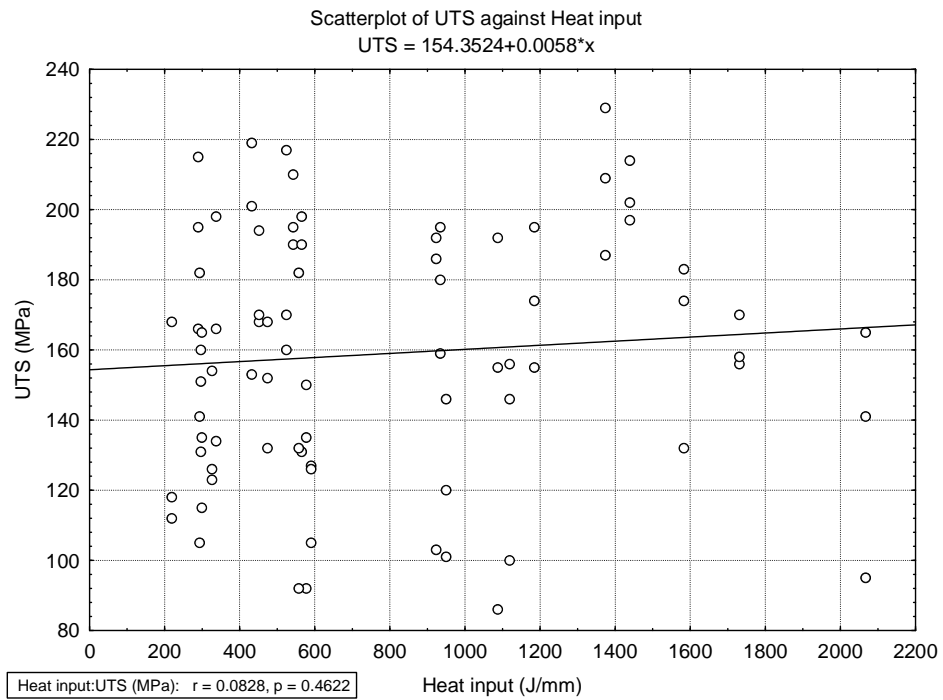


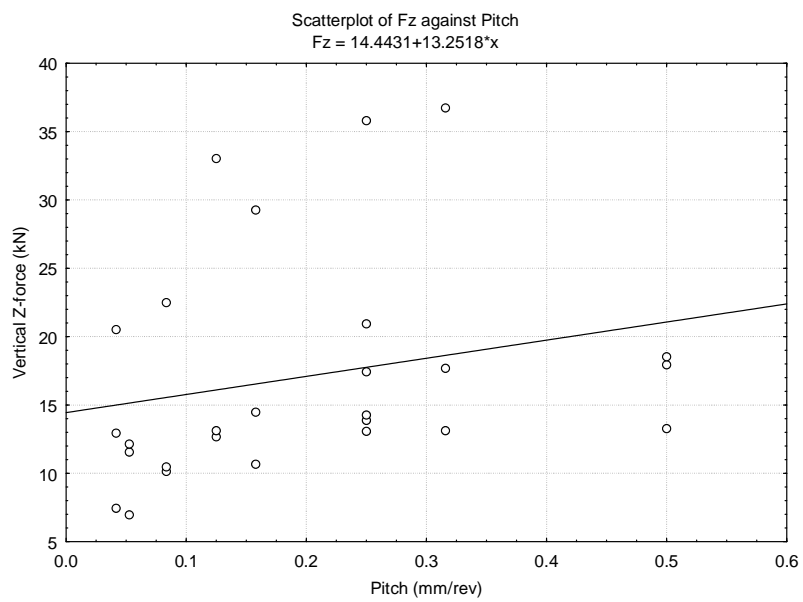
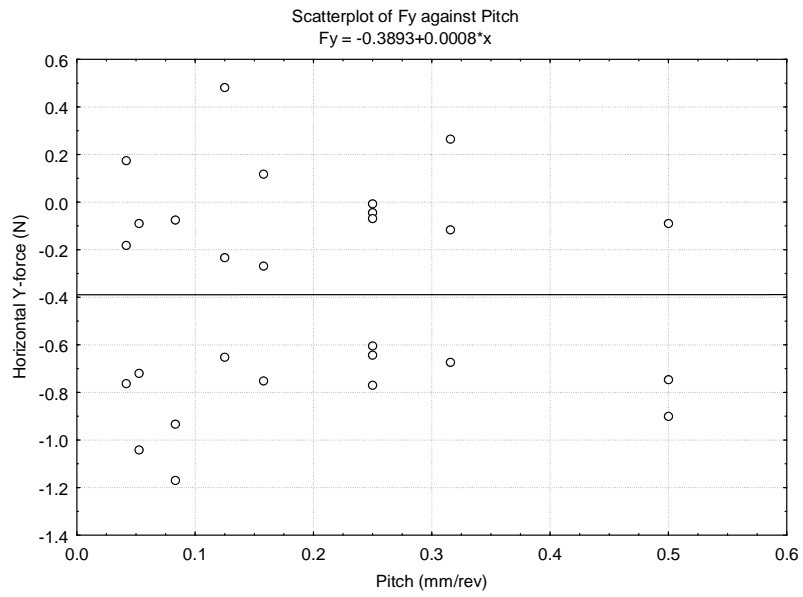


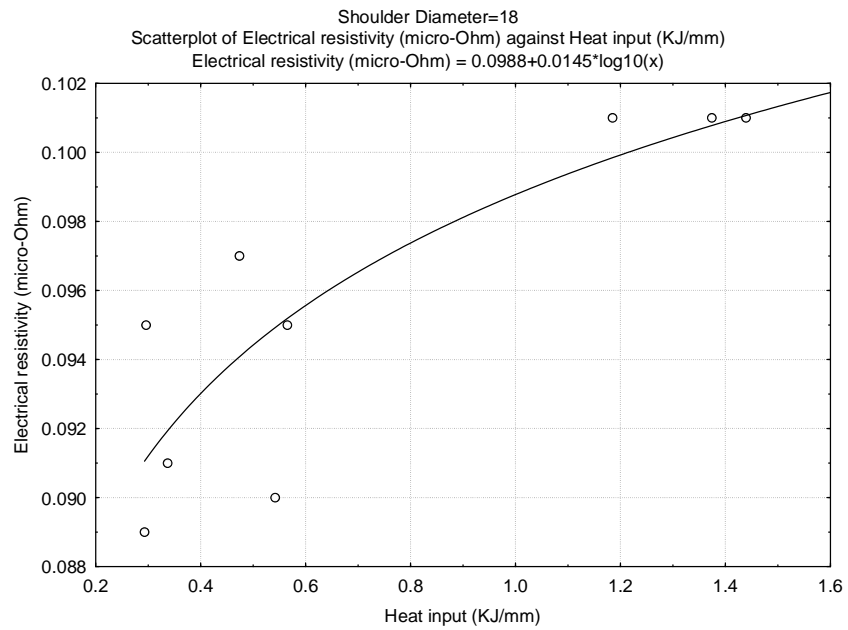
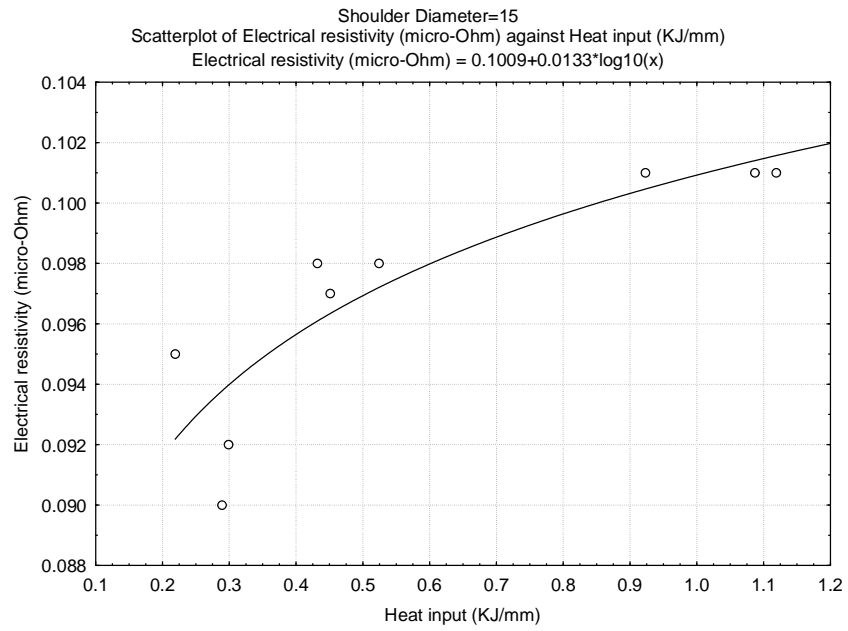


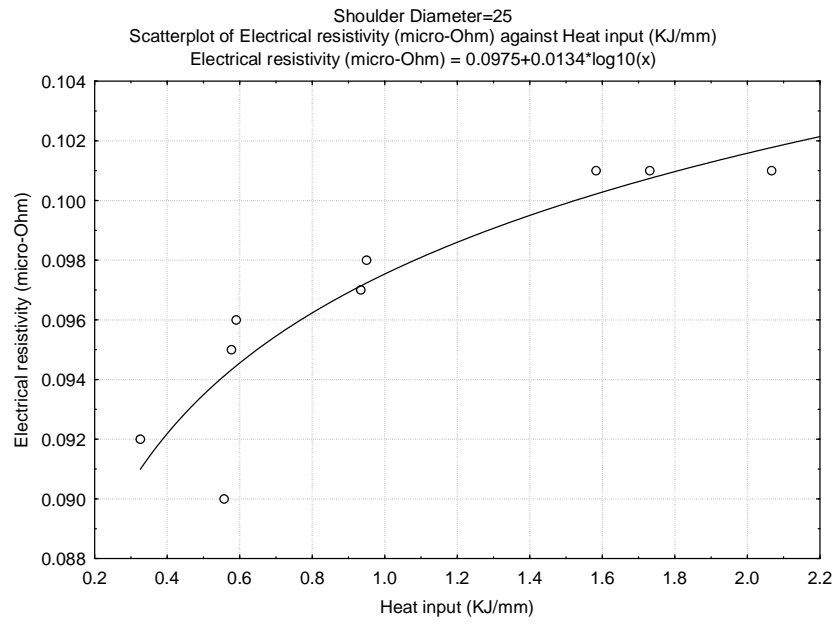


C16. Scatter plots

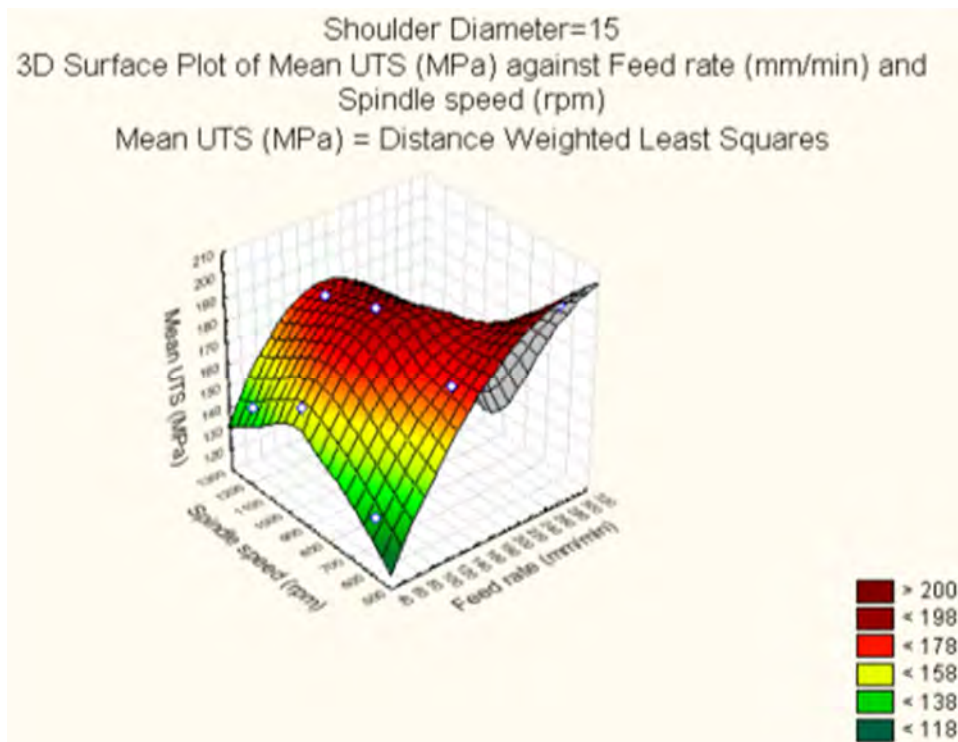
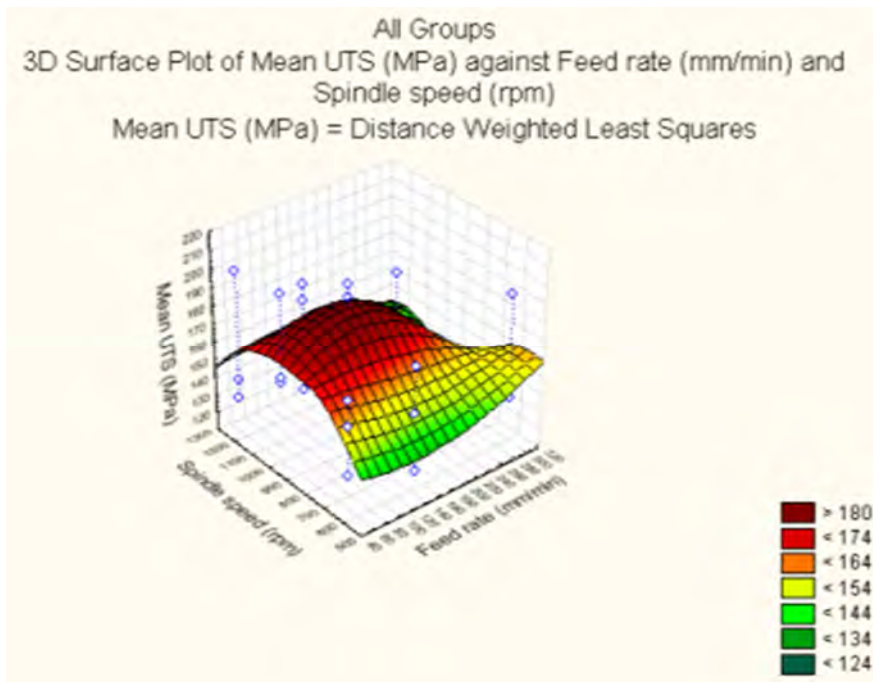


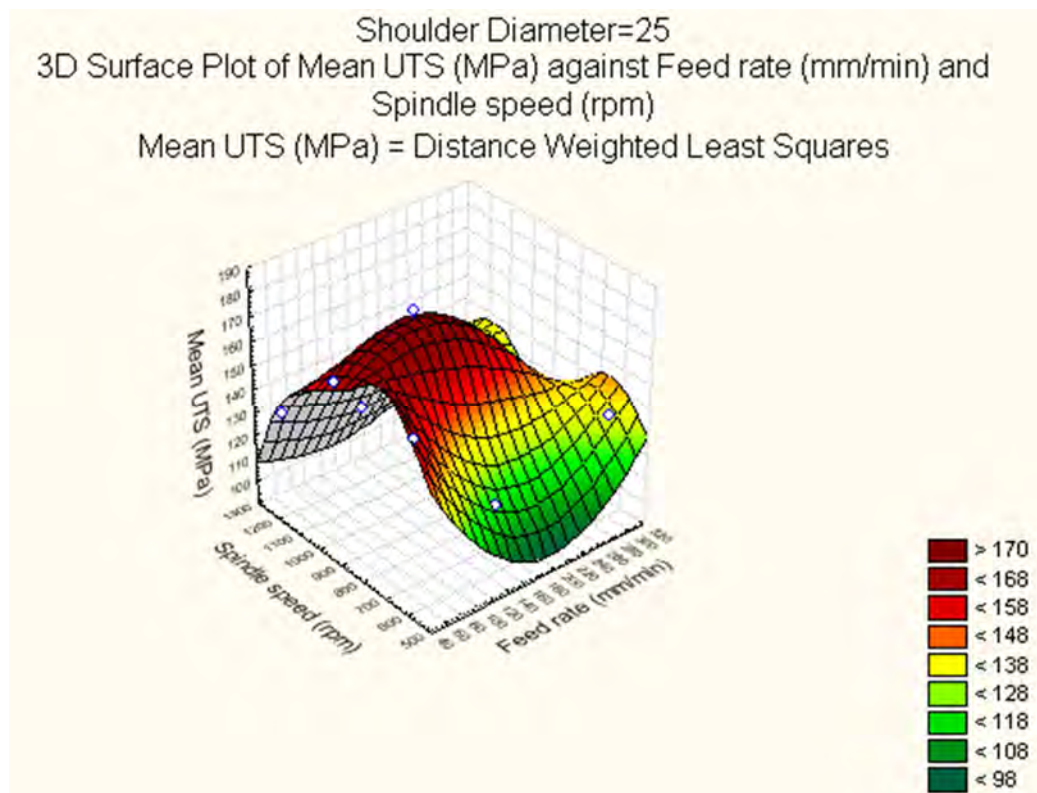
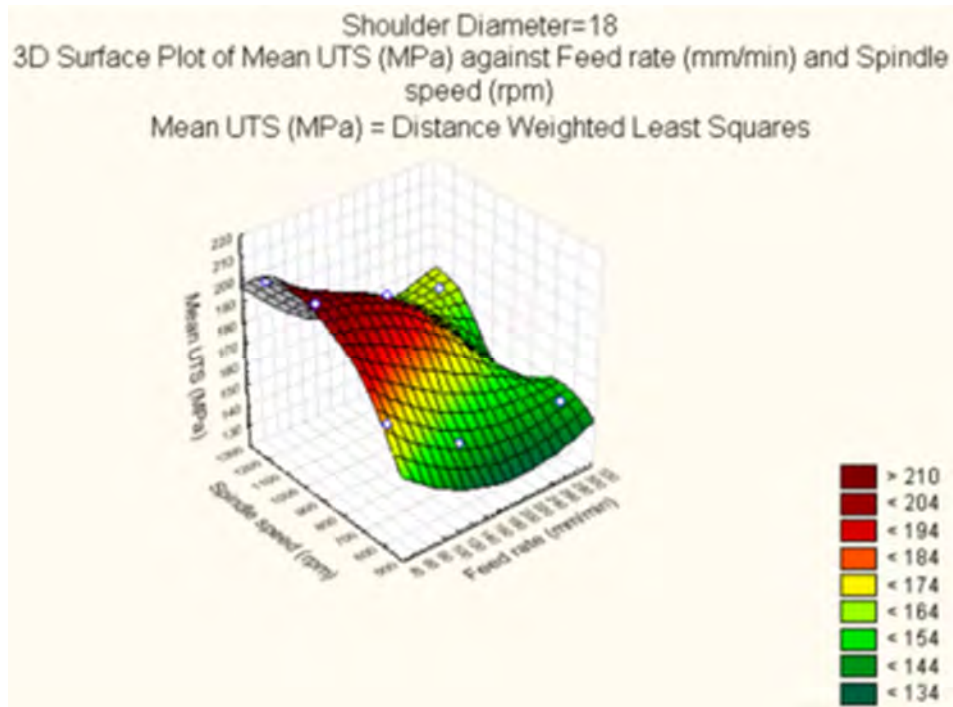


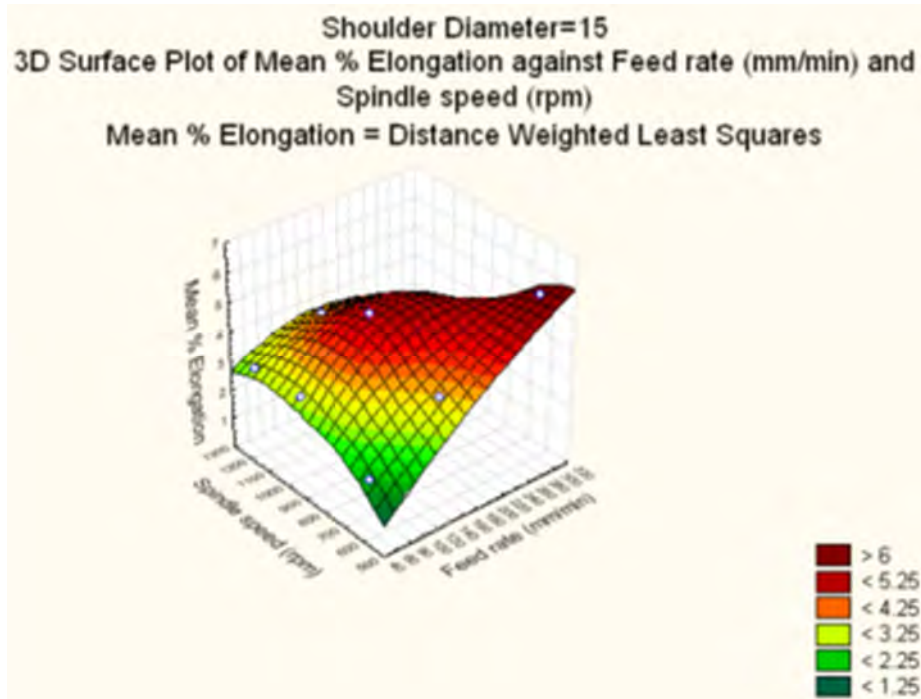
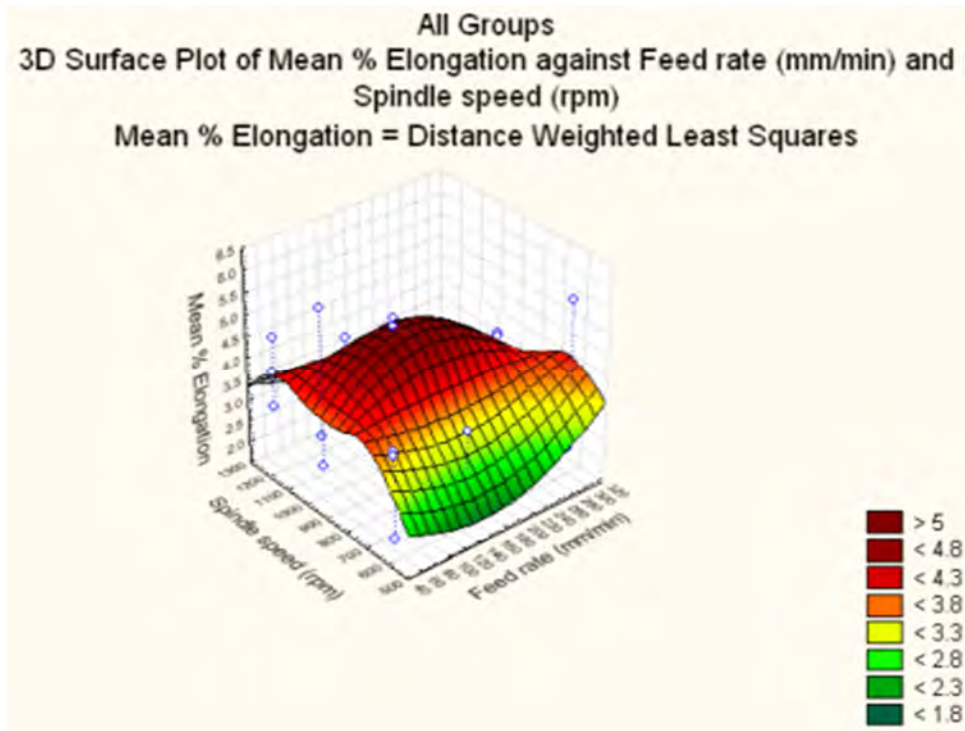


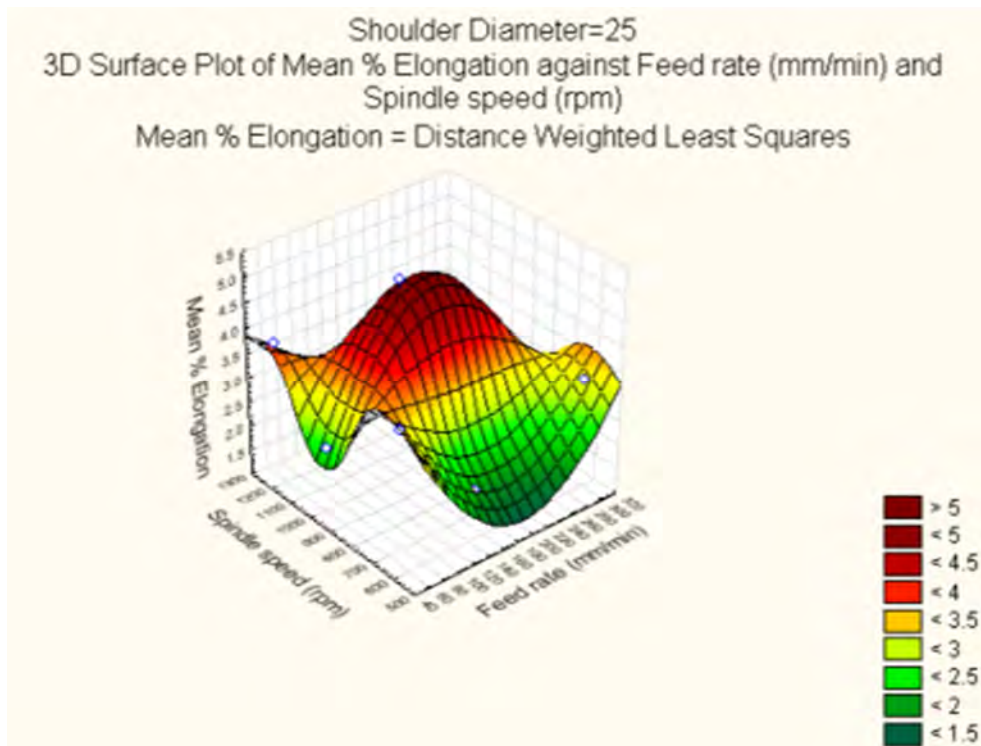
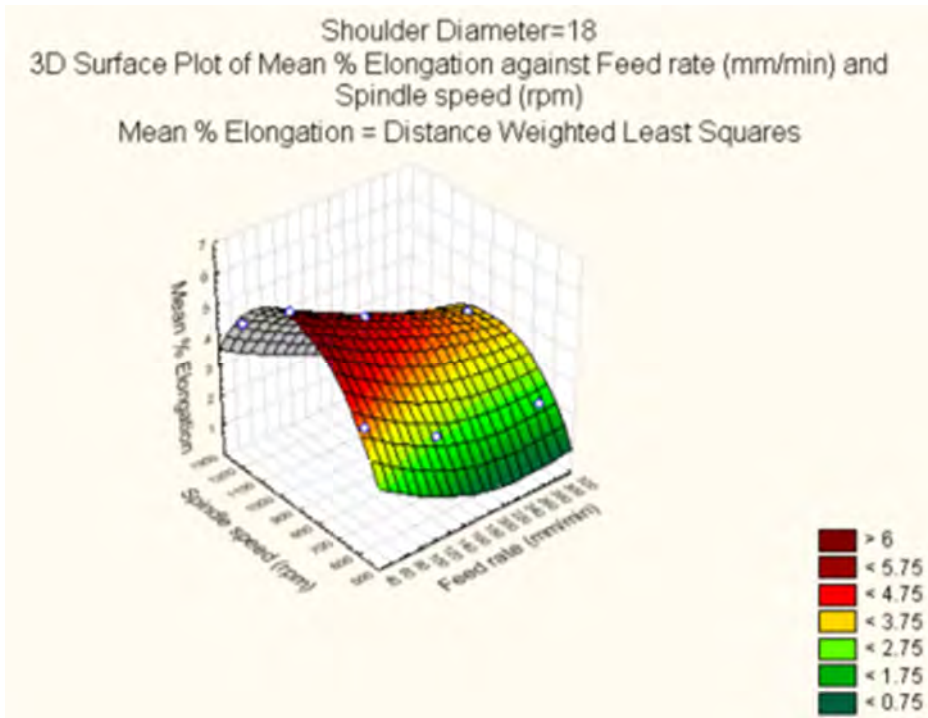


## C17. Surface plots









---

**APPENDIX D – PUBLICATIONS**  
**EFFECT OF TOOL DISPLACEMENT ON DEFECT FORMATION IN FRICTION**  
**STIR WELDING OF ALUMINIUM AND COPPER**

Esther T. Akinlabi, Annelize Els-Botes and Hannalie Lombard

Mechanical Engineering Department, Nelson Mandela Metropolitan University, P. O.  
Box 77000, Summerstrand, Port Elizabeth, South Africa. 6031.

[esther.akinlabi@nmmu.ac.za](mailto:esther.akinlabi@nmmu.ac.za)

**ABSTRACT**

The present study focuses on the effect of tool pin displacement on defect formation in Friction Stir Welding (FSW) of 5052 Aluminium Alloy (AA) and C11000 Copper (Cu). Friction stir welds in butt joint configurations were made by varying the traverse speed and rotational speed while other parameters were kept constant with the tool pin plunged first in Cu, secondly at the weld joint (centreline) and lastly in AA. This paper reports welds made at 1200 rpm and 150 mm/min. Welds produced with the tool pin plunged in Cu and at the weld centre line resulted in wormhole formation. Good top weld surface appearances were achieved with the tool pin plunged in aluminium. Examination of metallographic cross sections of the weld produced with the tool pin plunged in aluminium showed that metallurgical bonding and mixing of both Cu and AA were achieved at the joint interface. Higher Vickers microhardness values were measured in the interfacial region of the weld. Fracture locations of tensile samples were characterized for the weld made with the tool pin plunged in aluminium. It was observed that tensile specimens fractured in the different regions of the fusion line between Aluminium and the Stir Zone (SZ) and in the region of the Thermo Mechanically Affected Zone (TMAZ). The maximum force applied to these tensile samples varied between 4475 N and 6686 N for samples taken at different locations along the length of the weld.

## 1.0 INTRODUCTION

Friction Stir Welding (FSW) is a solid – state joining technique invented and patented by The Welding Institute (TWI) UK in 1991 for butt and lap welding of ferrous and non-ferrous metals and plastics (1). Currently, there is great interest in joining magnesium, steel, titanium and copper to aluminium alloys. The vast need for joining dissimilar materials has opened great opportunity for industrial applications of complex functions such as the joining of aluminium superstructures to steel-hulled ships; combined properties of materials and weight reduction as used in the power generation, petrochemical, nuclear and electrical/electronic industries, and for enabling multi-material design methodologies and low cost fabrication processes (2). Therefore, the availability of a sound joining technique for dissimilar materials is desirable. Generally, the weldability of dissimilar materials is determined by their crystal structures, compositional solubility and rate of diffusion in their liquid and solid states (3); in addition to this, the position of the tool during FSW of dissimilar materials is found to be of importance to produce defect-free welds.

Diffusion of both materials in the weld joint line often results in the formation of intermetallic phases, the majority of which are hard and brittle and are thus detrimental to the mechanical strength, ductility and resistivity of the joint (4). FSW of dissimilar materials has enormous challenges when compared to welding similar materials; this is due to the difference in physical, chemical, mechanical, and thermal properties of the materials being welded. The quality of welds produced by FSW is influenced by a number of process variables which include: tool design, tool rotation and travel speeds, tool plunge depth and tilt angle, welding gap, thickness mismatch and plate thickness variation. Successful, reproducible welds may be produced by operating within process windows (5). Some of the questions that need further investigation in FSW of aluminium to copper are which material should be at the advancing or the retreating side and should the tool pin be displaced to produce a defect-free weld? Reports on tool displacement in dissimilar materials, aluminium and copper in particular are limited. From review of literature on FSW of aluminium and copper (4, 6-10), only Savolainen et al. (4) reported on tool displacement that better welds were produced when the tool pin is displaced to the copper side. The aim of

the present study is to determine the optimum tool displacement position in FSW of aluminium and copper.

## **2.0 EXPERIMENTAL PROCEDURES**

Friction stir butt welds were produced on 600 mm X 120 mm X 3.175 mm thick sheets of 5052 AA and C11000 Cu with an I-STIR PDS FSW platform. The Cu sheet is classified as commercially pure with an average Ultimate Tensile strength of 243MPa and the AA had an Ultimate Tensile Strength of 262MPa. The Cu sheet was placed at the advancing side (AS) and the AA at the retreating side (RS) during welding. The surfaces of both sheets were cleaned with acetone before welding. The tool was made from H13 tool steel and had a shoulder diameter of 18 mm, pin diameter of 5 mm and 2.6 mm pin length; the features of the tool were a threaded pin with a concave shoulder. The welds were produced at 1200 rpm and 150 mm/min, other parameters kept constant were the tool tilt angle at 2°, the dwell time at 5 seconds and the plunge depth was 2.65 mm. All welds were sectioned for microstructure evaluation at 50 mm of the weld length. The AA was etched with Flick's reagent and the Cu was etched with a solution of 100 ml water and 10 g ammonium peroxydisulphate. The cross-section microstructures of the weld zones were observed using an Olympus PMG3 optical microscope. Vickers microhardness profiles were measured at 1.5 mm below the top surface along the cross sections of the welds using a Matsuzawa MHT2 microhardness tester while applying a 200 gf for a dwell time of 10 seconds. The tensile tests were conducted using a servo-hydraulic Instron 8801 tensile machine according to ASTM E8.

## **3.0 RESULTS AND DISCUSSION**

### **3.1 Visual observation**

Top surface appearances of the welds produced at 1200 rpm and 150 mm/min are presented in Figure 1 a-c. Welds made with the tool pin plunged in Cu and at the centreline had a wormhole defect as shown in Figure 1a and b. The wormhole defect in the weld made with the tool pin plunged in Cu occurred about midway of the weld length while the wormhole in the weld made with pin at the centreline occurs throughout the entire weld length. The weld made with the tool pin plunged in Al has

good top surface appearance as shown in Figure 1c. The positions of the tensile samples designated as T1, T2 and T3 respectively were cut as indicated in Figure 1c. Label M in Figure 1c represents the position of cross section examined for microstructure and microhardness profiling.

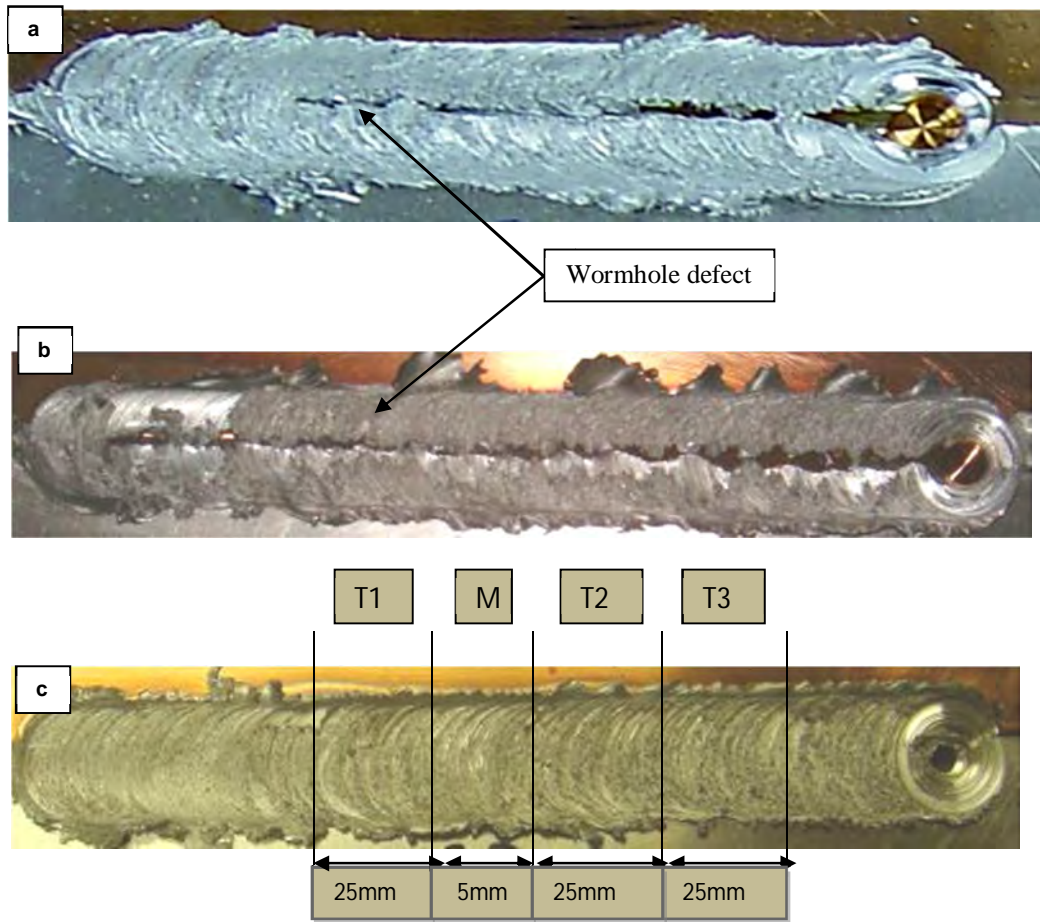


Figure 1: Welds produced at 1200 rpm and 150 mm/min (a) tool pin in Cu (b) tool pin at weld centreline (c) tool pin in Al

### 3.2 Tensile Results

The maximum tensile forces, shown in Table 1, increased for tensile samples T1, T2 and T3 respectively. Samples T2 and T3 have higher maximum forces possibly as a result of preferred welding conditions leading to increased metallurgical bonding. A difference of 2211.3 N was observed between the tensile force for samples T1 and T3.

Table 1: Maximum load measured during tensile tests of samples T1, T2 and T3.

Tensile sample	Maximum applied load (N)
T1	4475
T2	6495
T3	6686

Note that no tensile samples were produced for the welds with the tool pin plunged in Copper and at the weld centre line because of the presence of the wormhole defect. Figure 2 a-c show the fracture locations of tensile samples T1, T2 and T3 respectively taken from the weld produced at 1200 rpm and 150 mm/min with the tool pin plunged in the aluminium alloy. The fracture location of sample T1 occurred in the weld fusion line of Al on the retreating side, while for samples T2 and T3, the fractures occurred through the TMAZ/SZ. The difference in the fracture location of T1 may be due to the fact that the T1 sample was taken first and may perhaps be as a result of unstable welding conditions, although the sample was taken 25 mm away from the weld start position.

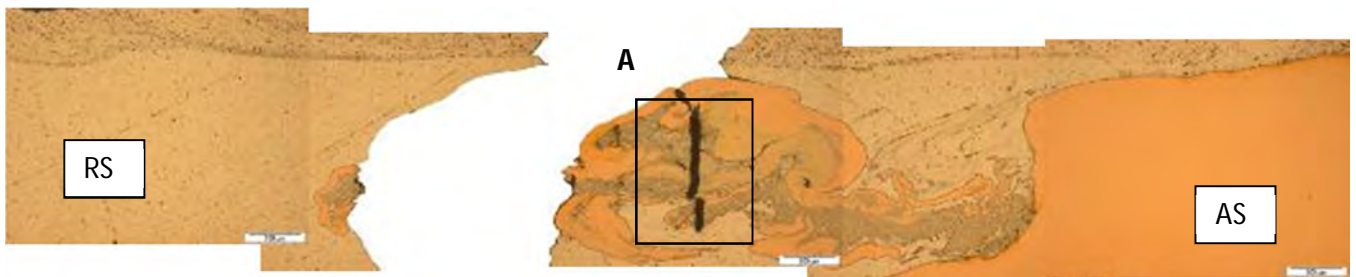


Figure 2a: Fracture location of tensile sample, T1 (x50).

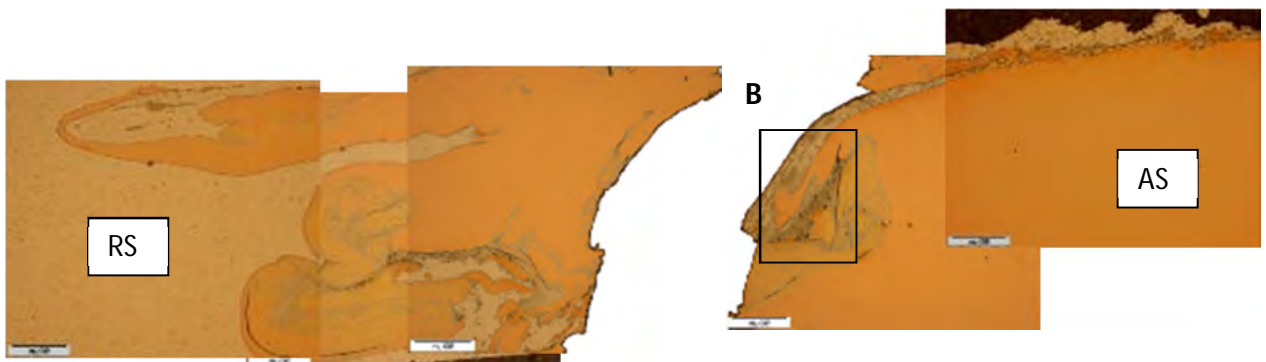


Figure 2b: Fracture location of tensile sample, T2 (x50).

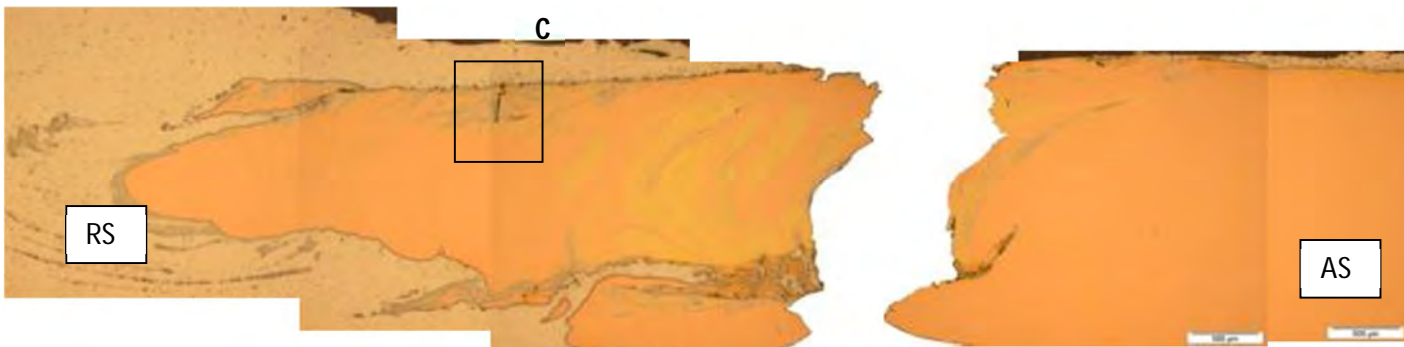


Figure 2c: Fracture location of tensile sample, T3 (x50)

Micrographs at higher magnification of the three fracture regions designated as A, B and C in Figure 2 (a)-(c) indicated the presence of secondary cracks lying perpendicular to the direction of applied load. Secondary cracks also follow flow lines along regions that are rich in aluminium. Since the fracture seemed to follow the flow lines of the aluminium rich phase, it is important to determine the length of weld required in order to obtain stable weld conditions, especially when weld strength is a major consideration.

Position T1 shows clear flow lines with aluminium rich phases and copper rich phases whereas sample T3 shows a more even distribution of alloy in the Stir Zone/Weld Nugget. This indicates that the weld conditions were more stable at a position (length) corresponding to sample T3.

Energy Dispersive Spectroscopy (EDS) of the phases in sample A, shown in Figure 3a, revealed the presence of two intermetallic phases viz:  $\text{Al}_2\text{Cu}$  and  $\text{Al}_4\text{Cu}_9$ . These intermetallic phases are brittle in nature and would therefore rather fracture than plastically deform which explains the presence of secondary cracks in the region of the fracture. The  $\text{Al}_2\text{Cu}$  phase has an average hardness of 367 HV whereas the  $\text{Al}_4\text{Cu}_9$  phase had an average hardness of 222 HV.

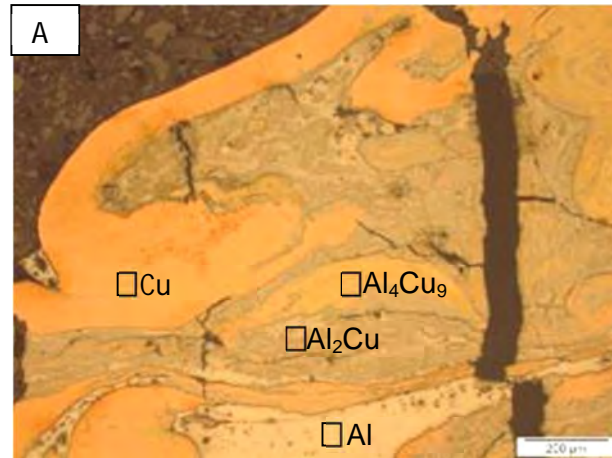


Figure 3a: Fracture location of tensile sample, T1 (x100).

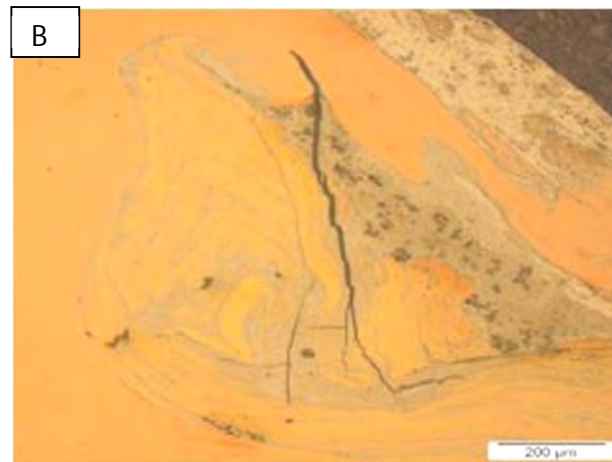


Figure 3b: Fracture location of tensile sample, T2 (x100).



Figure 3c: Fracture location of tensile sample, T3 (x100).

### 3.3 Microhardness

The microhardness profile of the FSW joint produced at 1200 rpm and 150 mm/min with the tool pin plunged in aluminium is presented in Figure 4. The Vickers microhardness values of the parent materials - AA and Cu are HV 28 and HV 89 respectively. It was observed that higher Vickers microhardness values were measured in the interfacial region previously occupied by the tool pin and the shoulder in the welds; this can be attributed to recrystallized grains in these areas resulting from plastic deformation.

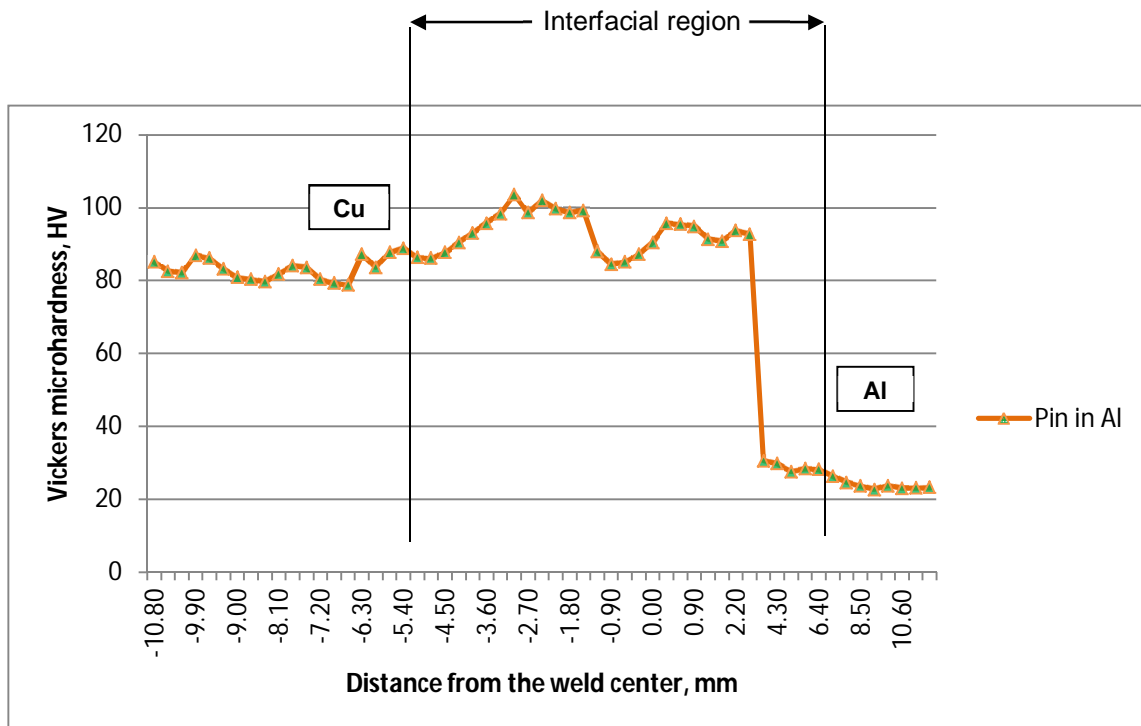


Figure 4. Microhardness profile through the cross section of a weld produced at 1200rpm and 150 mm/min with the tool pin plunged in aluminium.

### 4.0 CONCLUSIONS

The following findings/conclusions can be made:

1. FSW joints between 5052 AA and C11000 Cu in butt configurations were successfully produced when plunging the tool pin in aluminium.

2. The pin in aluminium configuration resulted in a good top surface appearance with no wormhole defect.
3. Microhardness evaluation showed that higher Vickers microhardness values were measured in the interfacial region (which is the positions previously occupied by the tool pin and the shoulder in all the welds).
4. A difference of 2211.3 N was observed between the maximum tensile force for samples T1 and T3. Position T1 shows clear flow lines with aluminium rich phases and copper rich phases whereas sample T3 shows a more even distribution of alloy in the Stir Zone/weld nugget. This indicates the weld conditions were more stable at a position (length) corresponding to sample T3.
5. Since the fracture seemed to follow the flow lines of the aluminium rich phase, it is important to determine the length of weld required in order to obtain stable weld conditions, especially when weld strength is a major consideration.

## 5.0 ACKNOWLEDGEMENTS

The authors wish to thank Dr. T. Hua and Mr L. Von Wielligh for operating the FSW platform, Mr G. C. Erasmus for assistance in the Metallurgy lab, the National Research Foundation (NRF) South Africa and Automotive Components Technology Station (ACTS) of NMMU for financial support.

## REFERENCES

1. Thomas WM, Nicholas ED, Needham JC, Murch MG, Temple-Smith P and Dawes CJ. Improvements relating to Friction Stir Welding. European Patent Specification 0615 480 B1, 1991. In: Mishra RS, Mahoney MW. (ed.) Friction Stir Welding and Processing. Materials Park Ohio, ASM International, 2007.
2. Lee WB, Schmuecker M, Mercardo UA, Biallas G, Jung S. Interfacial reaction in steel-aluminium joints made by friction stir welding. *Scripta Materialia* 2006; 55: pp. 355-358.

3. American Welding Society, Welding Handbook Welding Processes, part 2 volume 3 Ninth Edition Miami: American Welding Society; 2007.
4. Savolainen K, Mononen J, Saukkonen T and Hänninen H. A preliminary study on friction stir welding of dissimilar metal joints of copper and aluminium. 6<sup>th</sup> International FSW symposium. 2006. Montreal, Canada. 10-13 October. TWI (UK). Retrieved: CD-ROM.
5. Record JH, Covington JL, Nelson TW, Sorensen CD and Webb BW. Fundamental characterization of friction stir welding. 2004. 5<sup>th</sup> International FSW symposium Metz, France. 14-16 September. TWI (UK). Retrieved: CD-ROM.
6. Murr LE, Li Y, Flores RD, Trillo EA and McClure JC. Intercalation vortices and related microstructural features in the friction stir welding of dissimilar metals. *Material Resources Innovation* 1998, (2), 150-163.
7. Elrefaey A, Takahashi M and Ikeuchi K. Preliminary investigation of friction stir welding aluminium/copper lap joints. *Welding in the World*, 2005, 49, 93–101.
8. Ouyang J, Yarrapareddy E and Kovacevic R. Microstructural evolution in the friction stir welded 6061 aluminium alloy (T6- temper condition) to copper. *Journal of Materials Processing Technology*, 2006, 172, 110-122.
9. Abdollah – Zadeh A, Saeid T and Sazgari B. Microstructural and mechanical properties of friction stir welded aluminium/copper lap Joints. *Journal of Alloys and Compounds*, 2008, 460, 535-538.
10. Liu P, Shi Q, Wang W, Wang X and Zhang Z. Microstructure and XRD analysis of FSW joints for copper T2/aluminium 5A06 dissimilar materials. *Materials Letters*. 2008, 62, 4106- 4108.

## **Effect of Travel speed on Joint properties of Dissimilar Metal Friction Stir Welds**

Esther T. Akinlabi<sup>1</sup>, Annelize Els-Botes<sup>2</sup>, Patrick J. McGrath<sup>2</sup>

<sup>1</sup>Doctoral Candidate, Department of Mechanical Engineering, Nelson Mandela Metropolitan  
University, P.O. Box 77000, Summerstrand, Port Elizabeth, South Africa. 6031.

Corresponding author email: [esther.akinlabi@nmmu.ac.za](mailto:esther.akinlabi@nmmu.ac.za)

<sup>2</sup>Associate Professor, Department of Mechanical Engineering, Nelson Mandela Metropolitan  
University, P.O. Box 77000, Summerstrand, Port Elizabeth, South Africa. 6031.

### **ABSTRACT**

This paper reports the effect of traverse speed on joint properties of dissimilar metal friction stir welds between aluminium and copper sheets. Welds in butt joint configurations were produced between 5754 Aluminium Alloy (AA) and C11000 Copper (Cu). The welds were produced at a constant rotational speed of 950 rpm and the traverse speed was varied between 50 and 300 mm/min while all other parameters were kept constant. Microstructural evaluation of the welds revealed that at a constant rotational speed and varying the traverse speed, better mixing of both metals and metallurgical bonding were improved at the lowest traverse speed. The average Ultimate Tensile Strength of the welds decreased as the welding speed increased. Higher Vickers microhardness values were measured at the Thermo-Mechanically Affected Zones (TMAZ) and Stir Zones (SZ) of the welds due to dynamic recrystallization and also due to the presence of intermetallic compounds formed in the joint regions. Unlike with similar metal welds which showed a smooth force feedback curve, it was found that a significant variation in force feedback data was obtained for dissimilar metal welds.

**KEYWORDS:** Dissimilar metal; Friction Stir Welding; Macrostructure; Process parameters.

### **1.1 INTRODUCTION**

Friction Stir Welding (FSW) is a solid-state joining technique invented and patented by The Welding Institute (TWI) UK in 1991 for butt and lap welding of ferrous and non-ferrous metals and plastics (Thomas *et al.* 1991). Although FSW gives high quality welds, proper use of the process and control of a number of process parameters is needed to achieve this (Kumar and Kailas, 2008). Process parameters such as tool design, input welding parameters, joint configuration, tool displacement, forces acting on the tool during the welding process and the heat input into the weld during the

process, are found to exert significant effect on the material flow and temperature distribution (Record *et al.* 2004; Akinlabi *et al.* 2010), thereby influencing the microstructural evolution and mechanical properties of the joints.

Most research work reported on process-property relationship in FSW is carried out on aluminium alloys (Reynolds *et al.* 2000; Shukla and Baeslack, 2005). However, there have been recent reports on FSW of aluminium and copper (Elrefaey *et al.* 2005; Liu *et al.* 2008); although, the focus has been on microstructural evaluation. In this report, defect-free welds of dissimilar friction stir welds of aluminium and copper were produced and characterised through microstructural evaluation, tensile testing and microhardness profiling. As part of our effort to relate the process parameters to the resulting properties of the welds, the effect of the traverse speed on the joint properties of the welds were studied. The force feedback obtained was also compared to that of a butt weld using similar materials.

## **1.2 EXPERIMENTAL PROCEDURE**

The parent materials used in the research study were 5754 Aluminium Alloy (AA) and C11000 Copper (Cu). The Ultimate Tensile Strength of the AA was 266 MPa and that of Cu was 244 MPa. The dimensions of the test samples were 600 mm x 120 mm x 3.175 mm. The surfaces of both sheets were cleaned with acetone before the welding procedure. Cu was placed at the advancing side and the tool pin was plunged in the AA. Friction Stir welds were produced using position control on an Intelligent Stir Welding for Industry and Research Process Development System (I-STIR PDS) platform at a constant rotational speed of 950 rpm and the welding speed at 50, 150 and 300 mm/min. The tool was machined from H13 tool steel and hardened to 52 HRC having a shoulder diameter of 18 mm, pin diameter 5 mm, and a pin length of 2.6mm. The features on the tool were cylindrical threaded pin and a concave shoulder. For microstructural evaluation, samples were cut at 50 mm length from the start of the weld in a transverse direction. The aluminium side was etched with Flicks reagent and the Cu was etched with a solution of 25 ml distilled water, 25 ml ammonia water and 15 ml hydrogen peroxide 3% in order to reveal the microstructure. The Vickers microhardness profiles were measured using an FM-ARS 9000 automatic indenter according to ASTM 384. The measurements were made along the cross-sections of the welds at 1.5 mm below the surface with a load of 200g and a dwell time of 15 seconds. The tensile samples were cut perpendicularly to the weld direction and the tests were conducted using a servo-hydraulic Instron 8801 tensile machine according to ASTM E8 standard.

### 1.3 RESULTS AND DISCUSSION

#### 1.3.1 FSW data and force feedback

The weld data captured during the welding process are presented in Table 1. The output process parameters viz; the advancing force ( $F_x$ ), the vertical downward force ( $F_z$ ) and the torque ( $T$ ) presented are average values obtained between 30 mm and 130 mm of weld length. The heat input was calculated using equation (1), where  $Q$  (J/mm) is the heat input,  $\eta$  the efficiency factor (0.9 for Al and Cu),  $\omega$  (rpm) the rotational speed,  $T$  (Nm) is the response torque and  $f$  (mm/min) the feed rate (traverse speed).

$$Q = \eta \frac{2\pi\omega T}{f} \quad (1)$$

**Table 1:** FSW data

Weld No.	Rotational speed, $\omega$ (rpm)	Feed rate, $f$ (mm/min)	Advancing force, $F_x$ (kN)	Vertical downward force, $F_z$ (kN)	Torque (Nm)	Resultant Heat input, $Q$ (J/mm)
W01	950	50	2.85	11.6	12.8	1375
W02	950	150	3.12	14.5	15.2	543
W03	950	300	3.47	16.7	17.4	293

It was observed that the advancing force  $F_x$ , the vertical downward force  $F_z$ , and the torque  $T$  increases as the heat input to the welds  $Q$ , decreases. Analysis of forces acting during the FSW process was conducted by Vilaça *et al.* (2007); in which the downward vertical force was related to the mechanical power delivered by the tool into the plates. It was reported that both the advancing force and torque, and consequently, the total mechanical power delivered by the tool into the parts being welded, increase with an increase in the vertical downward force. Further observation of the force feedback showed a significant variation of the forces during the welding process compared to those obtained for butt welds of single alloys. Figure 1(a) and (b) illustrate the force feedback plots for Al-Cu produced at 950 rpm and 50 mm/min; and a butt weld of Titanium (Ti-6Al-4V) produced at 950 rpm and 55 mm/min by Mashinini (2010).

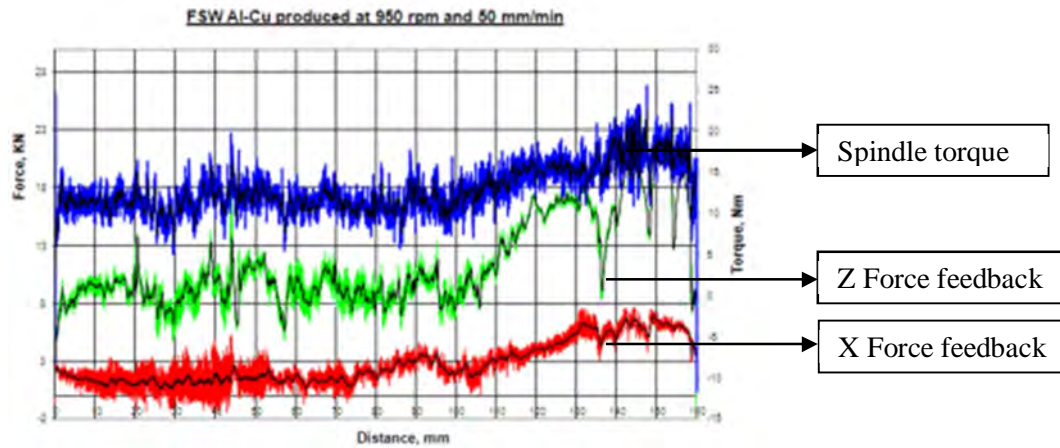


Figure 1(a): Force feedback of FSW Al-Cu produced at 950 rpm and 50 mm/min.

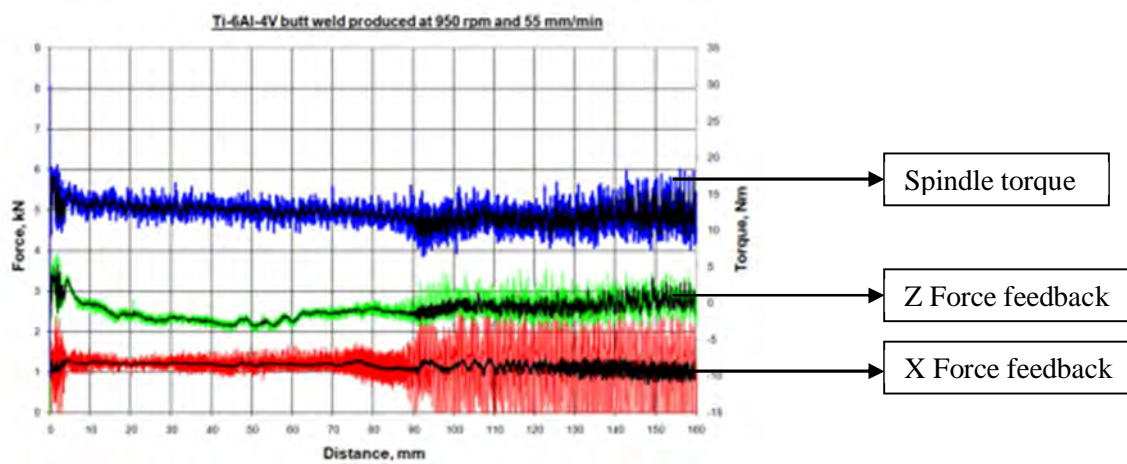


Figure 1(b): Force feedback of FSW Ti-6Al-4V produced at 950 rpm and 55 mm/min (Mashinini, 2010).

Further work is on-going to attempt to quantify the amount of the variation of forces during the welding process and also to identify possible means to achieve a smooth curve (preferred).

### 1.3.2 Optical macrographs

Figures 2 (a), (b) and (c) present macrostructures (through the cross-section) of the welds produced at 950 rpm and at 50, 150 and 300 mm/min respectively.



Figure 2(a): FSW produced at 950 rpm and 50 mm/min



**Figure 2(b):** FSW produced at 950 rpm and 150 mm/min



**Figure 2(c):** FSW produced at 950 rpm and 300 mm/min

It was observed that improved mixing of both metals was achieved at the lowest travel speed of 50 mm/min (Figure 2a), which was produced at a low downward force, ( $F_z$ ) and high heat input compared to the remaining welds produced. The Stir Zone (SZ) of the welds produced at 50 mm/min and 150 mm/min are characterised by mixture layers of aluminium and copper. This observation agrees with Liu *et al.* (2008) on macro appearance of welds produced between aluminium and copper. At a high transverse speed of 300 mm/min (Figure 2c), the vertical downward force is high but the heat input to the weld was low as shown in Table 1; the macrostructure was characterized by ‘openings’ in the Copper, which were filled with the Aluminium Alloy during the welding process as indicated by the arrow. This can be attributed to the fast movement of the tool at this speed; and as a result, the frictional heat generated was not high enough to achieve coalescence and proper mixing of both metals during the welding process.

### 1.3.3 Microhardness profiling

The microhardness profiles of the three welds are shown in Figure 3. The measurements were taken at 1.5 mm below the top surface. The average Vickers microhardness values of the parent materials – Aluminium Alloy (AA) and Copper (Cu) are HV 60 and HV 95 respectively.

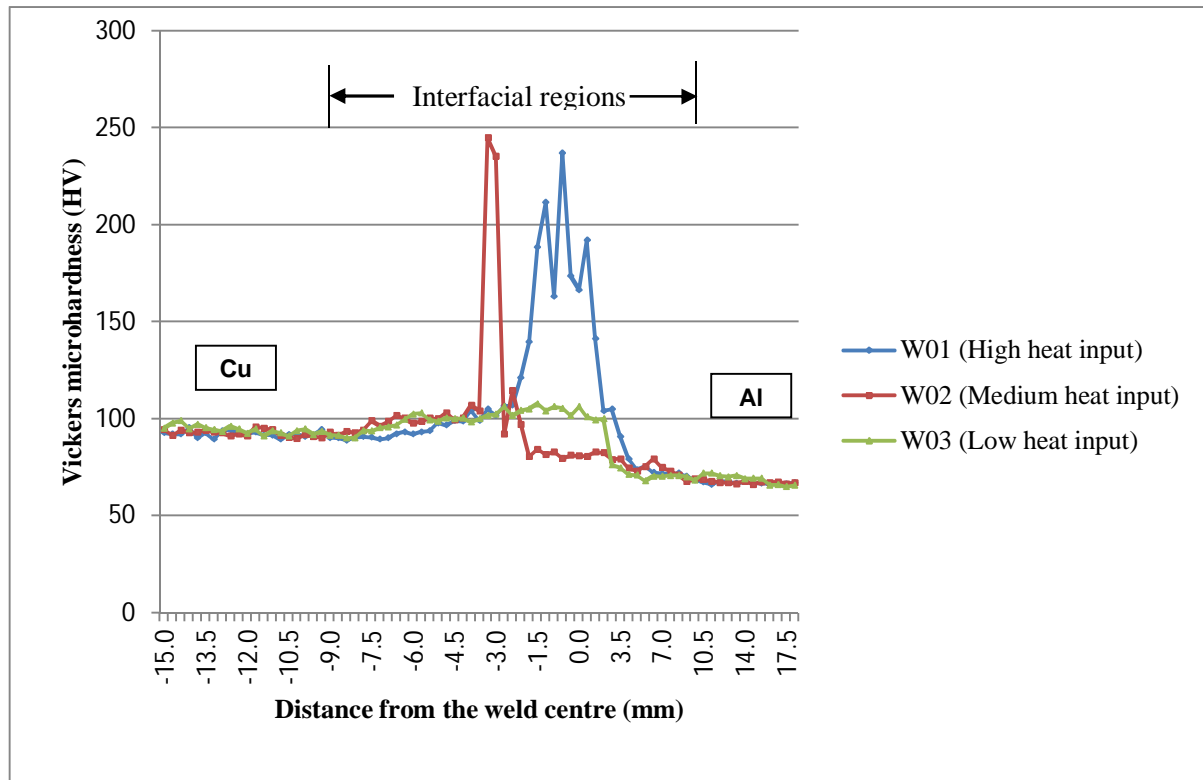


**Figure 3:** Microhardness profiles of welds produced at a constant rotational speed of 950 rpm with varied traverse speeds.

It was observed that higher Vickers microhardness values were measured in the Thermo-Mechanically Affected Zones (TMAZ) and the Stir Zones (SZ) of both metals which are regions previously occupied by the tool pin and the shoulder during the welding process. These regions are referred to as interfacial regions. The increase in the microhardness values at the interfacial regions can be attributed to dynamic recrystallization that has occurred during the welding process and also due to the presence of intermetallic compounds. Due to the variations in the macrostructures as presented in Figure 2(a) to (c), it was observed that the peaks in Figure 3 are distributed according to the positions of the intermetallics in the welds.

Energy Dispersive Spectroscopy (EDS) was conducted on the joint interface region of the weld produced at 950 rpm and 50 mm/min to investigate the presence of intermetallic compounds. It was observed that the high peaks correspond to AlCu intermetallic compound as shown in Figure 4.

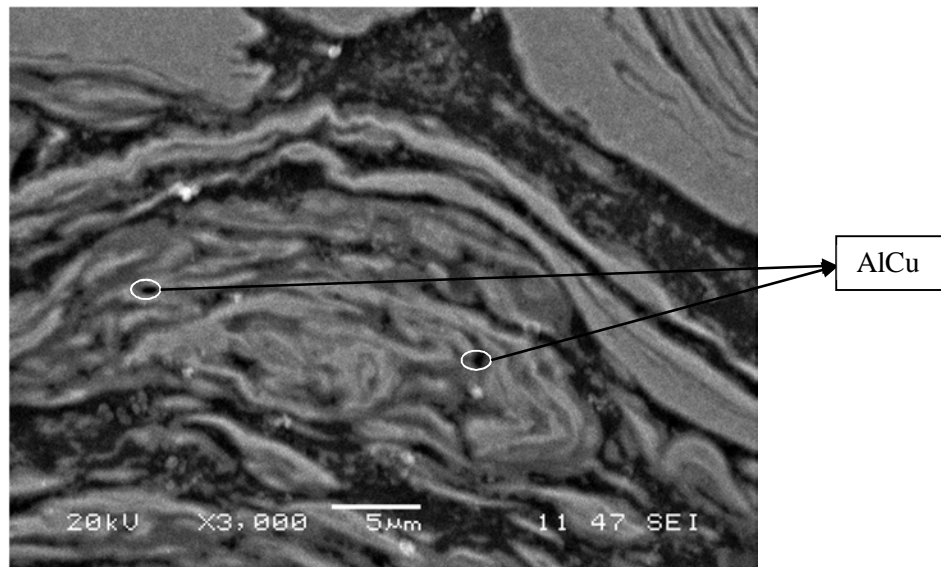


**Figure 4:** Joint interface of W01 (high heat input) produced at 950 rpm and 50 mm/min.

#### 1.3.4 Tensile results

The average Ultimate Tensile Strength of the parent materials and the welds are presented in Table 2. The tensile samples were taken from different positions along the welds and are designated as T1, T2 and T3 corresponding to the first, second and third samples respectively. The trend observed was that at a constant rotational speed, the tensile strengths of the welds decreased as the traverse speed increased from 50 to 300 mm/min respectively. This observation can be related to the heat input into the weld which is higher at low traverse speed as presented in Table 1.

**Table 2:** UTS of the parent materials and the welds

Samples	T1	T2	T3	Average UTS
PM AL	266	266.1	266.4	266
PM CU	243	246	243	244
W01	229	187	209	208
W02	195	190	210	198
W03	141	182	105	143

The highest tensile strength was obtained from the joint produced at low travel speed and can be attributed to the observations on the macrostructures of the welds. It was observed that coalescence and bonding of both metals are better achieved at the lowest travel speed. This trend observed in the tensile results agrees with the explanation given by Cederqvist and Reynolds (2000). It was reported that colder welds produced at high travel speed has less vertical transport of material during the FSW

process and therefore influences the mixing of both metals during welding and consequently influences the tensile strength of the welds.

#### 1.4 CONCLUSION

Dissimilar friction stir welds between 5754 Aluminium Alloy and C11000 Copper were successfully produced. Material characterisation of the welds revealed that good process-property relationship exists in FSW of Al and Cu (based on the UTS). Microstructural evaluation revealed that at a constant rotational speed, improved metallurgical bonding and mixing of both metals were achieved at the lowest traverse speed due to low downward vertical force and high heat input. Higher Vickers microhardness were measured at the interfacial regions due to dynamic recrystallization and the presence of intermetallics. The average Ultimate Tensile Strength of the welds decreased as the welding speed increased. Analysis of the FSW forces acting during the welding procedure revealed that the advancing force ( $F_x$ ) the torque (T) and consequently the heat input to the welds (Q) increased as the vertical downward force increased.

#### 1.5 ACKNOWLEDGEMENTS

The authors wish to thank Dr. T. Hua and Mr L. Von Wielligh for operating the FSW platform, Mr G. Erasmus for assistance in the Metallurgy lab; the National Research Foundation (NRF) South Africa and Automotive Components Technology Station (ACTS) of NMMU for financial support.

#### 1.6 REFERENCES

- Akinlabi, E.T., Els-Botes, A. and Lombard, H., 2010 *Effect of tool displacement on defect formation in friction stir welding of aluminium and copper*. In *Proceedings of the 8<sup>th</sup> International Friction Stir Welding Symposium, Hamburg, Germany*.
- Cederqvist, L, and Reynolds, A.P., 2000 Properties of friction stir welding aluminium lap joints. In *Proceedings of the 2<sup>nd</sup> International Friction Stir Welding Symposium, Gothenburg, Sweden*.
- Elrefaey, A., Takahashi, M. and Ikeuchi K., 2005 *Preliminary investigation of friction stir welding aluminium/copper lap joints*. *Welding in the World* Vol. 49, 93-101.
- Kumar, K and Kailas, S.V., 2008 *The role of friction stir welding tool on material flow and weld formation*. *Materials Science and Engineering A* Vol. 485, 367- 374.
- Liu, P., Shi, Q., Wang, W., Wang, X. and Zhang Z., 2008 *Microstructure and XRD analysis of FSW Joints for copper T2/aluminium 5A06 dissimilar materials*. *Materials letters* Vol. 62, 4106-4108
- Mashinini, P.M., 2010. *Process window for friction stir welding of 3 mm Titanium (Ti-6Al-4V)*,

2<sup>nd</sup> International Conference on Advances in Engineering and Technology (AET),  
Uganda. January 30 – February 1, 2011

*M.Tech dissertation. Faculty of Engineering Built Environment and Information Technology,  
Nelson Mandela Metropolitan University, Port Elizabeth, South Africa.*

Record, J.H., Covington, J.L., Nelson, T.W., Sorensen, C.D and Webb, B.W., 2004 *Fundamental  
characterization of friction stir welding. In Proceedings of the 5<sup>th</sup> International Friction Stir  
Welding Symposium, Metz, France.*

Reynolds, A.P., Lockwood, W.D. and Seidel, T.U., 2000 *Processing-property correlation in friction  
stir welds. Materials Science Forum ISSN0255-5476.*

Shukla, A.K. and Baeslack, W.A., 2005 *Process-property relationship and microstructure evolution  
In friction stir welded thin sheet 2024-T3 aluminium alloy. In Proceedings of the 7<sup>th</sup>  
International conference on trends in welding research. Georgia, USA.*

Thomas, W. M., Nicholas, E.D., Needham, J.C., Murch, M.G., Templesmith, P. and Dawes, C.J.,  
1991 *Friction Stir Welding. International Patent Application, G.B.9125978.8 (Patent).*In  
*Friction Stir Welding and Processing.* Edited by Mishra RS, Mahoney MW (Materials Park  
Ohio, ASM International).

Vilaça, P., Quintino, L., dos Santos, J.F., Zettler, R. and Sheikhi, S., 2007 *Quality assessment of  
friction stir welding joints via an analytical thermal model, iSTIR. Materials Science and  
Engineering A Vol. 445-446, 501-508.*